THE ROLE OF VARIABLE CRACKING ON AGRICHEMICAL TRANSPORT AT THE MISSOURI MSEA SITE USING THE ROOT ZONE WATER QUALITY MODEL

A Thesis

presented to

the Faculty of the Graduate School

University of Missouri-Columbia

In Partial Fulfillment

of the Requirements for the Degree

Master of Science

By

YOUXIU HUA

Dr. R. Lee Peyton Thesis Supervisor

December 1995

The undersigned, appointed by the Dean of the Graduate Faculty, have examined a thesis entitled

THE ROLE OF VARIABLE CRACKING ON AGRICHEMICAL TRANSPORT AT THE MISSOURI MSEA SITE USING THE ROOT ZONE WATER QUALITY MODEL

Presented by

YOUXIU HUA

a candidate for the degree of

MASTER OF SCIENCE

and hereby certify that in their opinion it is worthy of acceptance.

L M

Charles W. Lees 12/7/95

Stephen H. Anderson

ACKNOWLEDGEMENTS

This material is based upon work supported by the Cooperative State Research Service, U.S. Department of Agriculture, under Agreement No. CSRS 91-34214-6012. However, any opinions, findings, conclusions, or recommendations expressed in this thesis are those of the author and do not necessarily reflect the view of the U.S. Department of Agriculture.

The author gratefully acknowledges financial and administrative support from the Department of Civil Engineering (University of Missouri-Columbia), and the Cooperative State Research Service, U.S. Department of Agriculture. The author also gratefully acknowledges help from the following individuals for their contribution during the course of this study. Assistance with running the RZWQM was provided by Fessehaie Ghidey, a Senior Research Scientist of the Department of Agricultural Engineering, University of Missouri-Columbia, and Ken Rojas, a Hydrologist and Programmer of the RZWQM in Great Plains System Research Unit of USDA. Assistance in data acquisition and study direction was provided by Jonathan Baer, a Research Associate of the Department of Soil and Atmospheric Science, University of Missouri-Columbia, and Dr. Stephen Anderson, Associate Professor of the Department of Soil and Atmospheric

Science, University of Missouri-Columbia. This project was under the general supervision of Dr. R. Lee Peyton, Associate Professor of the Department of Civil Engineering, University of Missouri-Columbia.

TABLE OF CONTENTS

LIST OF FIGURES

LIST OF TABLES

CHAPTER 1

INTRODUCTION

1.1 Literature Review

In many materials fracturing occurs over a wide range of scales (Korvin, 1989). One particular type of fracturing is polygonal fracturing due to shrinkage of the material. Clay is a kind of material which can develop polygonal fracturing. When clay is drying, its volume decreases resulting in tensional forces which act equally in all directions of the horizontal surface. It is this tensional force that causes cracks to develop in clay soil. On the other hand, when clay is wetting, the cracks that have been developed during drying close.

In order to determine the shrinkage of soils, the simultaneous measurement of water content changes and volume changes is needed. It is convenient and economic to take clods and small cores to conduct shrinkage studies. These kind of studies has been carried out by Tempany (1917), Haines (1923), Lauritzen and Stewart (1941), Johnston and Hill (1944), Stirk (1954), Holmes (1955), Reeve and Hall (1978), Newman and Thomasson (1979), Yule and Ritchie (1980a), Reeve et al. (1980), Chan (1982), Jayawardane and Greachen (1987) and Dasog et al. (1988). However, it is more useful and accurate to measure the shrinkage of large undisturbed clay soil cores using lysimeters (Yule and Ritchie, 1980b, Bronswijk, 1991).

Field studies on swelling and shrinkage of clay soils by measuring the subsidence of the soil surface were conducted by Yaalon and Kalmar (1972). Woodruff (1936), Aitchison and Holmes (1953), Jamison and Thompson (1967), Bronswijk (1991) and Baer and Anderson (1993) installed benchmarks at several depths in the soil and measured vertical shrinkage and swelling. By using the method of Bronswijk (1991), the volume of cracks in the soil profile can be found.

Soil cracking can be seen in many agricultural soils. It can cause ground water pollution from agricultural chemicals because it causes preferential flow. However, preferential flow due to soil cracking has not been studied much (Anderson, 1995).

Preferred pathways in high clay content soils which shrink and swell with water content are believed to be a primary route for the movement and accumulation of pollutants deep within the profile and close to the groundwater table. Groundwater contamination by pesticides and fertilizers has raised public concern about drinking water quality and safety (Hallberg, 1986). The discovery of widely-used atrazine and alachlor in surveys of groundwater and public drinking water (Berteau and Spath, 1986; Cohen, 1986; EPA, 1988; Hance, 1987; Helling and Gish, 1986) was unexpected in light of previous studies of herbicide physio-chemical characteristics (e.g., water solubility), persistence in surface soil, and leaching into the rooting zone using soil cores (Harris et al., 1969; Helling et al., 1988; Isensee et al., 1988; Lavy et al., 1973; Moorman and Harper, 1989). Herbicides have contaminated a very large volume of groundwater. However, some soils or watersheds are not subject to groundwater contamination by herbicides because the hydrogeologic setting of farmland and environmental variables make some sites less susceptible to groundwater contamination (Rao et al., 1985).

1.2 The Missouri Management System Evaluation Area (MSEA)

The Missouri Management System Evaluation Area (MSEA) is located in the 28-square-mile Goodwater Creek watershed in northern Boone and western Audrain counties of central Missouri (Figure 1.1). The site differs from the other midwest MSEA sites in that very heavy claypan soils are predominant throughout the watershed and region. In Illinois, Missouri, Indiana, Ohio, Kansas, and Oklahoma there are about 16,000 square miles of claypan soils. In addition, there are over 60,000 square miles of glacial soils

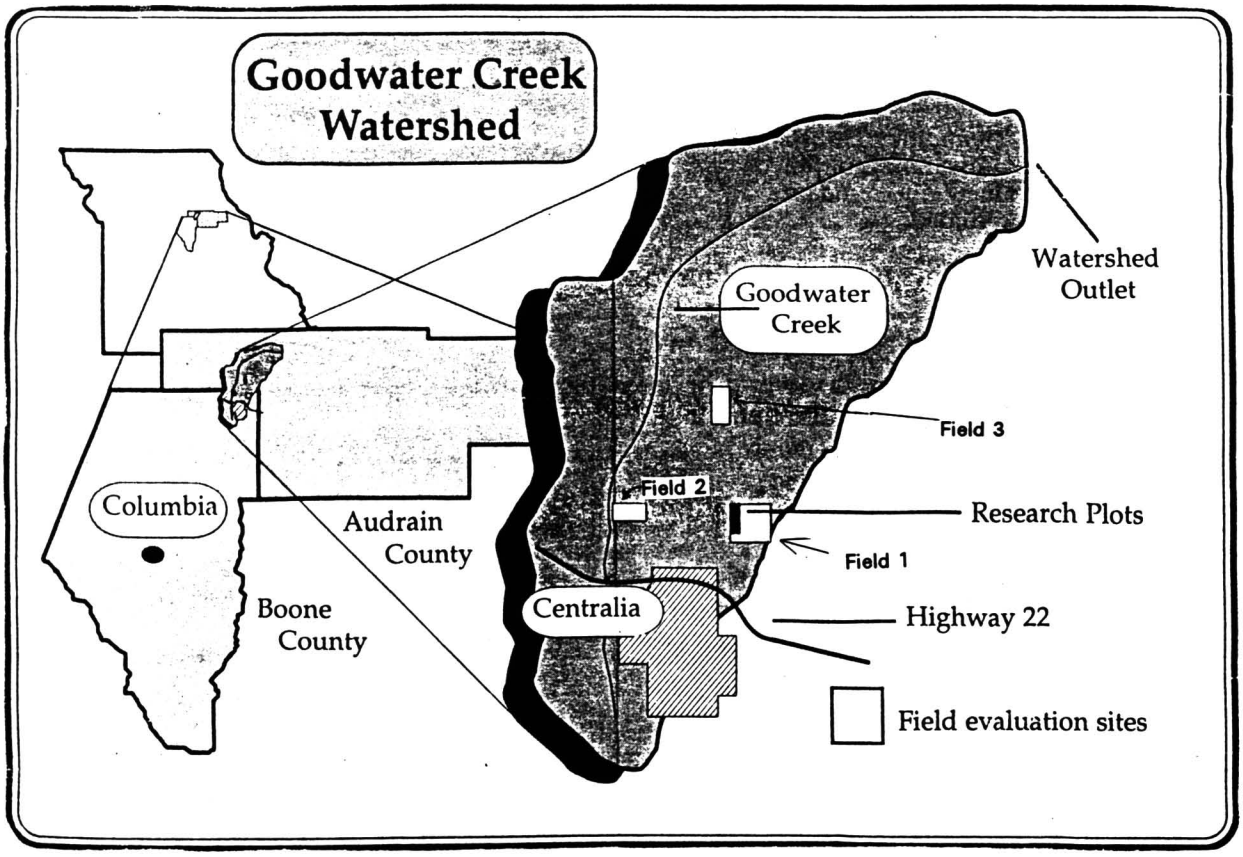

Figure 1.1 Goodwater creek watershed and Research plots (Map drawn by Scott Killpack).

having a large clay content in the central part of the United States (Kelly, 1992). Claypans have very low intrinsic permeabilities. However, macropores are formed in claypans from shrinkage cracks and biologic activity. Two of the Missouri MSEA objectives are to measure how conventional farming systems affect surface and groundwater quality and to study the processes responsible for the fate and transport of nutrients and agrichemicals in the soil and water.

1.3 The Objective of This Study

There are several computer models that simulate water movement through swelling and shrinking soils. One of them is FLOCR (FLOw in CRacking soils) (Oostindie, 1992). FLOCR simulates one-dimensional vertical water flow through the soil

matrix and through the shrinkage cracks in an unsaturated clay soil profile. The model can be used to calculate the water balance, cracking and subsidence of clay soils. However, FLOCR does not simulate chemical and biological processes in the root zone.

Another of the computer models is the Root Zone Water Quality Model (RZWQM) which has been developed over the last eight years by a team of scientists of the Agricultural Research Service of United States Department of Agriculture (USDA-ARS). The newest version of the RZWQM (version 3.0) were released in May 1995. The RZWQM can simulate the movement of water, nutrients and pesticides over and through the root zone of a unit area. Also, the RZWQM can simulate preferential flow, but the cracks specified in the RZWQM cannot be changed during the entire simulation period.

Among agrichemicals, nitrate-nitrogen, atrazine and alachlor are chosen in this study because of their great usage in agriculture practices and pollution problems related to the usage. Twenty to 25 percent of farmstead wells in northern Missouri have nitrate concentrations greater than the Missouri drinking-water standard of 10 milligrams per liter as nitrogen (N) (Sievers and Fulhage, 1989). Atrazine and alachlor have been used extensively for the past decade throughout the Corn Belt (USDA, 1990). Eighty-six percent of the corn acreage in Missouri was treated with atrazine and/or alachlor in 1989 (USDA, 1990). Atrazine is moderately persistent in soil and water and was detected in groundwater elsewhere in the Corn Belt (Berteau and Spath, 1986; Cohen, 1986; Hance, 1987; Helling and Gish, 1986).

Therefore, the objective of this study is to evaluate the effects of variable cracking on the transportation of agricultural chemicals at the Missouri MSEA site using the Root Zone Water Quality Model (The version of the RZWQM used in this thesis is version 3.0). To reach this goal, the following tasks have to be conducted: (1) revising the RZWQM to accommodate variable cracks; (2) calibrating the RZWQM to the Missouri MSEA site;

(3) quantifying cracking at the Missouri MSEA site; (4) using the cracking data in the RZWQM; (5) predicting the effects of cracking on water content, nitrate-nitrogen, atrazine and alachlor transport by using the revised RZWQM; and, (6) analyzing the simulation results.

CHAPTER 2

THE ROOT ZONE WATER QUALITY MODEL

2.1 The Outline of the RZWQM

The RZWQM consists of six scientific subsystems or processes that define the simulation program, a Datafile Generator Program, and an Output Report Generator. The following is a brief description of the scientific processes, whereas a detailed description can be found in the technical documentation of the RZWQM version 1.0 (USDA-ARS, 1992a). The Datafile and Output Report Generators can be found in the user's manual of the RZWQM version 3.0 (USDA-ARS, 1995).

2.2 The General Functions of the RZWQM

The RZWQM simulates the transport of water, nutrients, and pesticides over and through the root zone of a unit area. It is primarily a one-dimensional vertical model designed to simulate the environment at a chosen point (unit area) in a field; it does not consider spatial variability. It also considers some surface and subsurface features including slope, orientation, and microtopography. In the RZWQM, measures of the micro- and macro-porosity differentiate between flow rates through the soil matrix. Chemical, nutrient, and pesticide processes are modeled in detail. A crop growth model simulates plant size and yield in existing environmental stress. Management processes impose controls on other processes through the depth of tillage, the time of irrigation and other management practices.

2.3 Six Processes in the RZWQM

There are six general processes in the RZWQM. They are physical processes, plant growth processes, soil chemical processes, nutrient processes, pesticide processes, and management processes.

Physical processes include Green and Ampt infiltration, chemical transport during infiltration, transfer of chemicals to runoff during rainfall, water and chemical flow through macropore pathways and their absorption by the wall of pathways, soil hydraulic properties estimated from bulk density and 1/3, or 1/10 bar water content, heat flow, evapotranspiration, root water uptake, soil water redistribution, and chemical movement during redistribution.

Plant growth processes include carbon dioxide assimilation, carbon allocation, dark respiration, periodic tissue loss, plant mortality, root growth through the soil profile, water and nutrient uptake, and transpiration.

Soil chemical processes consist of bicarbonate buffering, dissolution and precipitation of calcium carbonate, gypsum, and aluminum hydroxide, ion exchange and solution chemistry of ion pair complexes.

The nutrient processes simulate carbon and nitrogen transformations within the soil profile. Given initial levels of soil humus, crop residues, other organics, nitrate and ammonium concentrations as well as the amount of nutrient applied and apply time, the model can predict the amount of mineralization, nitrification, immobilization, denitrification, and volatilization of appropriate nitrogen.

Pesticide processes define the transformations and degradation of pesticides on plant surfaces, plant residue surfaces, the soil surface and in a given volume of soil. The model can simulate the amount of pesticide reaching the soil surface and the amount adsorbed by and moving through each soil layer.

Management processes consist of tillage practices, irrigation, planting densities and timing, harvest operation and the impact of these practices on surface roughness, soil bulk density, micro- and macroporosity, and soil moisture conditions.

2.4 The Structure of the Computer Program

In order to revise the program, its structure has to be understood. The source code of the RZWQM (version 3.0) written in FORTRAN is included in 15 files in which there are 36,813 lines. In these 15 files, there are 185 subroutines, 36 functions and 4 externals (See Appendix A). The call tree of the program of the RZWQM can be found in Appendix B. To run program RZWQM, seven data files have to be fed (USDA-ARS, 1995).

2.5 The Limitation of the RZWQM

As pointed out in Chapter one, one limitation of the RZWQM is that the cracks specified in the RZWQM cannot be changed during the entire simulation period. In fact, cracks are changing with soil water content which is changing with time. Another limitation is that cracks cannot be specified in the top layer of a profile. In a claypan field, one can see many cracks on the soil surface. One scheme to overcome this limitation is to assume a thin artificial layer on the top of a claypan profile. However, the thickness of the first layer must be greater than two cm thick and the horizon thicknesses must be integer numbers according to the rules for numerical layer formation in the technical documentation of the RZWQM. Thus, the thinnest thickness which can be assumed for the first layer is three centimeters. For the first layer, one can assume some cylindrical pores. Therefore, an alternative scheme is to set the maximum flow-rate capacity (K_{mac}) of existing cracks to the maximum flow-rate capacity of assumed cylindrical pores. By

using Poiseuille's law and assuming gravity flow (unit hydraulic head gradient), for cylindrical holes, K_{mac} is:

$$K_{mac} = \frac{N\rho g\pi r_p^4}{8\eta} = \frac{P_{mac}\rho g r_p^2}{8\eta} \quad (ms^{-1}) \tag{2.1}$$

For planar cracks, K_{mac} is:

$$K_{mac} = \frac{L\rho g d^3}{12\eta} = \frac{P_{mac}\rho g d^2}{12\eta} \quad (ms^{-1}) \tag{2.2}$$

where: ρ = the density [FT^2/L^4]

g = the gravitational constant [L/T^2]

r_p = the radius of cylindrical holes [L]

d = the width of planar cracks [L]

η = the dynamic viscosity of water [FT/L^2]

N = the number of pores per unit area

L = the total length of cracks per unit area [L]

P_{mac} = the macroporosity as fraction of soil volume [L^3/L^3].

Equating the two K_{mac}s, we have:

$$r_p = \sqrt{\frac{2}{3}} \cdot d \tag{2.3}$$

Also, the radius of cylindrical pores is constant in RZWQM during a simulation period, and some work has to be done in order to make the radius of cylindrical pores change with water content or time.

2.6 Two Schemes to Revise the RZWQM

There are two schemes to revise the RZWQM. One is to use the water content calculated by the RZWQM to calculate the crack width with time assuming a reasonable crack length. Another is to input crack volume over area vs. time directly to calculate the

crack width with time. For the first layer, the radius of cylindrical pores will be gained using Equation 2.3 under the assumption that the macroporosity of the first layer is equal to that of the second layer. The revised part of the RZWQM can be found in Appendix C.

CHAPTER 3

QUANTIFYING CRACKING AT THE MISSOURI MSEA SITE

3.1 Research Plots and Soil Classification

In the Missouri MSEA project, in order to do various research, three fields and thirty plots were chosen (Figure 1.1). A watershed divide separates Field 1 from thirty plots which are west of Field 1 (Figure 3.1). In this thesis, Plot 13, nest 2 (in the middler of Plot 13) is chosen to run the RZWQM because it is near the center of the plots and more data are available from this site. Each plot is 18.29 meters wide and 190.50 meters long. The slope of the plots are different at different sites. At the summit position, slope is about 1-2% and soil is eroded away. At the middle of the plots, slope is about 1-3% and soil is eroded away also. At the foot position, slope is about 0-1% and soil is overwashed.

As shown in Figure 1.1, all the three fields and the thirty plots are within the Goodwater Creek watershed. Goodwater Creek watershed is covered with 5-10 feet of loess (wind-blown soil) overlying 10-40 feet of glacial till (Blanchard et al., 1995). The modern soil, which developed from the loess, is subdivided to Ap, Bt and C horizons. The Ap horizon is on the surface and has a thickness of about 0-24 cm. The Bt horizon is under the Ap horizon and has a thickness of about 0-45 cm. The Bt horizon is a horizon which contains the highest clay content among the three horizons. The C horizon is under the Bt horizon and consists of the original wind-blown loess with a thickness of 150-300 cm.

The Ap horizon consists of silt loam whereas the Bt horizon consists of clay or silty clay and the C horizon consists of silty clay or silty clay loam (See Table 3.1, 3.2). In the field it is easy to distinguish the Ap horizon from the Bt horizon by color or by feeling

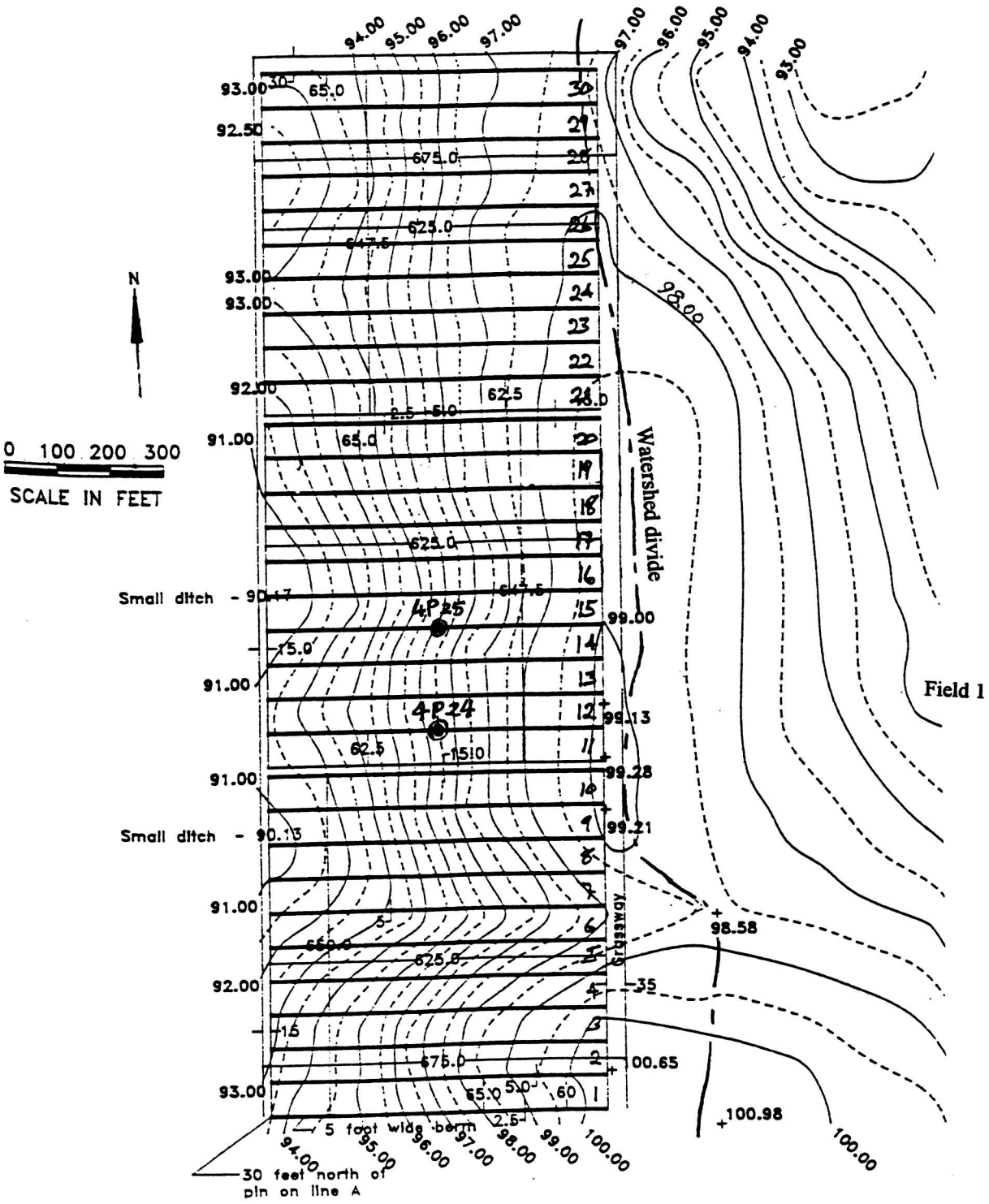

Figure 3.1 Research plots and Field 1 (Map drawn 2/12/91 by Robert L. Mahurin).

Table 3.1 Soil textural analysis results of Plot 13 (Baer, 1995)

SAPLE #	DEPTH	TOTAL			SILT		SAND						TEXT
	cm	CLAY	SILT	SAND	FINE	COARSE	VF	F	M	C	VC	>VF	CLASS
		<.002	.002-.05	.05-2	.002-.02	.02-.05	.05-.10	0.1-.25	.25-.50	.5-1	1.-2	.10-2	
13.01.01	0-15	22.8	66.3	10.9	33.9	32.4	1.4	0.9	1.8	4.1	2.7	9.5	SIL
13.01.02	15-30	64	34.9	1.1	23.6	11.3	0.4	0.2	0.2	0.3	0	0.7	C
13.01.03	30-45	47.6	50	2.5	33.9	16.1	0.9	0.6	0.4	0.4	0.2	1.6	SIC
13.01.04	45-60	37.6	59.4	2.9	39.9	19.5	0.9	0.7	0.4	0.6	0.4	2.1	SICL
13.01.05	60-75	35.4	63.8	0.8	43	20.8	0.4	0.2	0.1	0.1	0.1	0.5	SICL
13.01.06	75-90	34.5	64.5	1	44.4	20.1	0.6	0.2	0.1	0.1	0	0.4	SICL
13.02.01	0-15	26.5	60.3	13.2	33.7	26.6	1.4	1	2	5.3	3.4	11.7	SIL
13.02.02	15-30	59.3	39.5	1.3	28.2	11.3	0.4	0.3	0.2	0.2	0.1	0.8	C
13.02.03	30-45	41	56.1	2.9	38.2	17.9	0.8	0.7	0.5	0.7	0.2	2.1	SIC
13.02.04	45-60	39.2	57	3.8	41.2	15.9	1.1	1	0.4	0.6	0.6	2.7	SICL
13.02.05	60-75	36.1	61.3	2.6	43.4	17.9	0.8	0.8	0.4	0.4	0.2	1.8	SICL
13.02.06	75-90	31.6	67.3	1.1	48.1	19.2	0.5	0.2	0.1	0.2	0.1	0.6	SICL
13.03.01	0-15	27.8	63	9.2	34.3	28.7	0.9	0.8	1.5	3.5	2.5	8.3	SICL
13.03.02	15-30	53.5	42.7	3.7	27.5	15.2	0.4	0.4	0.6	1.6	0.7	3.4	SIC
13.03.03	30-45	55.7	42.8	1.5	29.3	13.5	0.4	0.3	0.3	0.4	0.1	1	SIC
13.03.04	45-60	42.1	56.7	1.2	41	15.7	0.4	0.3	0.2	0.2	0.1	0.7	SIC
13.03.05	60-75	35.6	62.8	1.6	43.3	19.5	0.6	0.5	0.2	0.2	0.1	1.1	SICL
13.03.06	75-90	32.3	59.6	8.1	37.4	22.2	2.3	2.9	1.5	0.9	0.4	5.8	SICL

*The fourth digit 1, 2, 3 in sample number represent summit, middle and foot position in Plot 13.

Table 3.2 Soil textural analysis results of Plot 19 (Baer, 1995)

SAMPLE #	DEPTH	TOTAL			SILT		SAND						TEXT
	cm	CLAY	SILT	SAND	FINE	COARSE	VF	F	M	C	VC	>VF	CLASS
		<.002	.002-.05	.05-2	.002-.02	.02-.05	.05-.10	0.1-.25	.25-.50	.5-1	1.-2	.10-2	
19.01.01	0-15	16.5	73.8	9.7	36.7	37.1	1.3	0.6	1.3	3.6	2.8	8.4	SIL
19.01.02	15-30	56.8	38.4	4.7	25.5	13.0	0.3	0.2	0.3	1.4	2.5	4.4	C
19.01.03	30-45	65.2	33.9	0.9	23.5	10.5	0.2	0.2	0.1	0.3	0.1	0.7	C
19.01.04	45-60	45.9	52.7	1.3	39.1	13.6	0.5	0.4	0.2	0.2	0.1	0.9	SIC
19.01.05	60-75	39.8	58.6	1.7	42.6	16.0	0.5	0.5	0.2	0.4	0.1	1.1	SICL
19.01.06	75-90	37.2	60.4	2.4	41.7	18.7	0.7	0.5	0.3	0.6	0.2	1.6	SICL
19.05.01	0-15	28.2	58.3	13.5	31.1	27.2	1.2	0.8	1.7	5.5	4.2	12.2	SICL
19.05.02	15-30	55.1	42.4	2.5	30.8	11.6	0.5	0.4	0.3	0.8	0.5	2.0	SIC
19.05.03	30-45	45.4	52.6	2.1	37.3	15.2	0.7	0.6	0.3	0.4	0.0	1.4	SIC
19.05.04	45-60	39.9	57.4	2.6	41.2	16.2	0.7	0.7	0.4	0.6	0.2	1.9	SICL
19.05.05	60-75	39.0	58.2	2.8	42.6	15.7	0.6	0.8	0.4	0.6	0.4	2.2	SICL
19.05.06	75-90	36.5	59.5	4.0	43.2	16.3	1.2	1.0	0.5	0.8	0.6	2.8	SICL
19.10.01	0-15	26.5	61.5	12.0	29.8	31.7	1.1	1.2	1.9	4.4	3.5	10.9	SIL
19.10.02	15-30	58.1	38.4	3.5	25.8	12.6	0.5	0.5	0.5	1.3	0.8	3.1	C
19.10.03	30-45	54.1	43.8	2.0	28.5	15.3	0.6	0.5	0.2	0.4	0.3	1.4	SIC
19.10.04	45-60	40.5	55.9	3.6	35.9	19.9	0.9	0.7	0.4	0.6	1.2	2.7	SIC
19.10.05	60-75	34.4	60.7	4.9	38.9	21.8	1.5	1.3	0.7	0.9	0.5	3.4	SICL
19.10.06	75-90	33.5	57.3	9.1	36.3	21.0	2.5	3.2	1.9	1.2	0.3	6.6	SICL

*The third and fourth digit 01, 05, 10 in sample number represent summit, middle and foot position in Plot 19.

the soil. The Ap horizon has a lighter soil color and a feeling of more silt and less clay. Also, it is easy to distinguish the Bt horizon from the C horizon by color or feel. The C horizon has some light green mineral such as kaolinite and chlorite and a more silty feeling.

3.2 Geometry of Soil Shrinkage

This section is taken from the work of Bronswijk (1991). A soil cube with sides z and volume $V=z^3$ undergoes isotropic shrinkage to form a soil cube with sides $z-\Delta z$ (Figure 3.2), where

$$V-\Delta V = (z-\Delta z)^3 \tag{3.1}$$

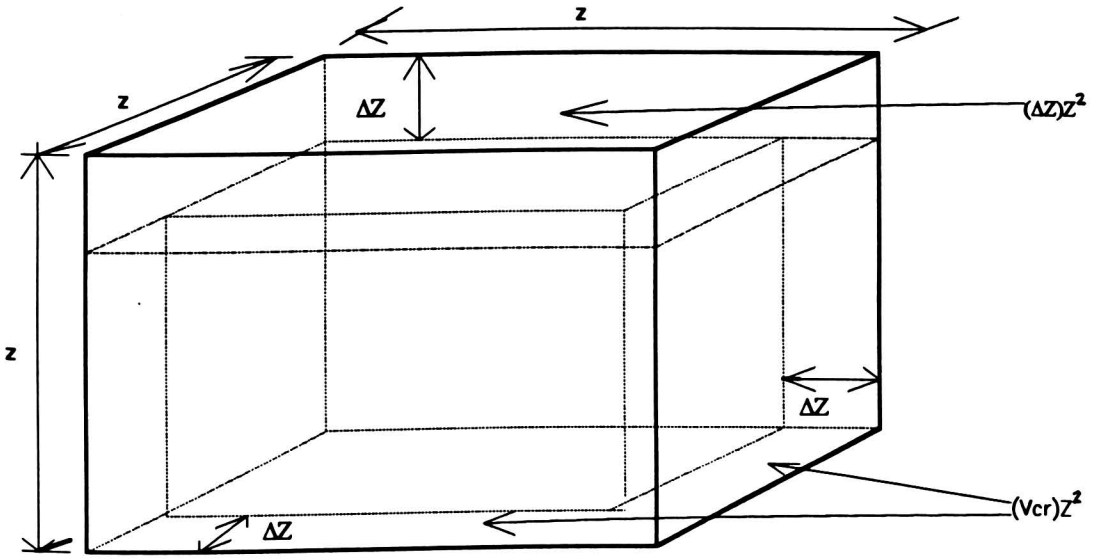

Figure 3.2 Isotropical soil cube shrinkage (after Bronswijk, 1991).

By dividing both sides of equation (3.1) by V, we have:

$$(1-\frac{\Delta V}{V}) = (1-\frac{\Delta z}{z})^3 \tag{3.2}$$

In general shrinkage, we have:

$$(1-\frac{\Delta V}{V}) = (1-\frac{\Delta z}{z})^{r_s} \tag{3.3}$$

where r_s is a dimensionless geometry factor. When r_s equals three, it is assumed that shrinkage occurs in all three directions, and isotropic shrinkage occurs; when r_s equals one, it is assumed that shrinkage only occurs in vertical direction, and subsidence without cracking happens; when r_s is between one and three, subsidence dominates cracking.

Solving equation (3.2) for ΔV, we have:

$$\Delta V = \{1-(1-\frac{\Delta z}{z})^{r_s}\}\cdot z^3 \tag{3.4}$$

The shrinkage volume per unit area, ΔV_a, is obtained by dividing both sides of equation (3.3) by z^2:

$$\Delta V_a = \frac{\Delta V}{z^2} = \{1-(1-\frac{\Delta z}{z})^{r_s}\}\cdot z \tag{3.5}$$

In isotropic shrinkage, ΔV_a is:

$$\Delta V_a = \{1-(1-\frac{\Delta z}{z})^{3}\}\cdot z \tag{3.6}$$

The shrinkage volume per unit area, ΔV_a, includes the volume decrease of soil matrix per unit area and the crack volume per unit area. The volume decrease of soil matrix per unit area can be represented by Δz. Therefore, the crack volume per unit area is:

$$V_{cr} = \Delta V_a - \Delta z \tag{3.7}$$

The shrinkage volume in Figure 3.2 is represented as follows. The shrinkage due to subsidence at the top of Figure 3.2 is $z^2\Delta z$. The shrinkage on the right side of Figure 3.2 due to cracking is $z\Delta z(z-\Delta z)$. The shrinkage on the front face due to cracking is $\Delta z(z-\Delta z)^2$. The sum of these two shrinkage vulumes due to cracking can be represented as $V_{cr}z^2$.

3.3 Measurements and Calculations

A single soil layer with saturated thickness z at time i undergoes isotropic shrinkage to produce a soil layer with thickness z-Δz at time t. Δz can be determined by monitoring the elevation changes of two discs, one positioned at the top (disc 1) and the other at the bottom (disc 2) of the soil layer (Figure 3.3).

Δz is calculated as:

$$\Delta z = (elev_{1,i} - elev_{1,t}) + (elev_{2,t} - elev_{2,i}) \qquad (3.8)$$

Δz calculated by equation (3.8) is positive when the layer thickness decreases, and the change in soil matrix volume (ΔV) will also be positive if matrix volume decreases.

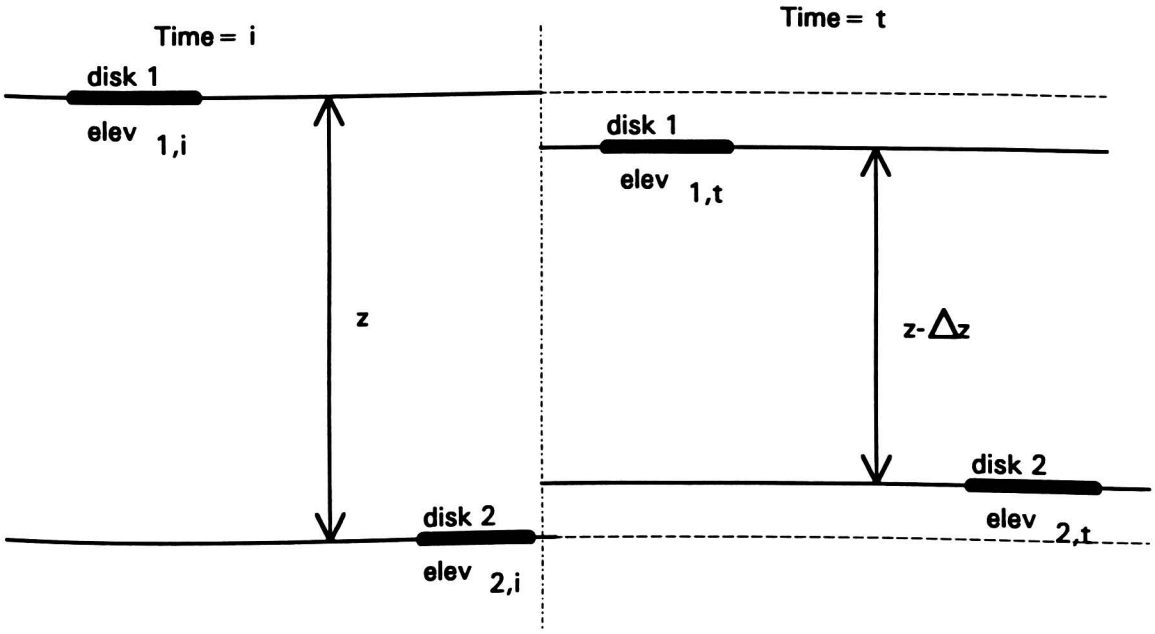

Figure 3.3 The isotropic shrinkage of a soil layer (after Baer, 1995).

For a soil profile with six layers, the calculation is the same, but summation is needed (Figure 3.4). Each layer is monitored separately and then combined. The profile totals for Δz, ΔV and V_{cr} are obtained as follows:

$$\Delta z_{profile} = \sum_{k=1}^{6} \Delta z_{layer\ k} \tag{3.9}$$

$$\Delta V_{profile} = \sum_{k=1}^{6} \Delta V_{layer\ k} \tag{3.10}$$

$$V_{CT_{profile}} = \sum_{k=1}^{6} V_{CT_{layer\ k}} \tag{3.11}$$

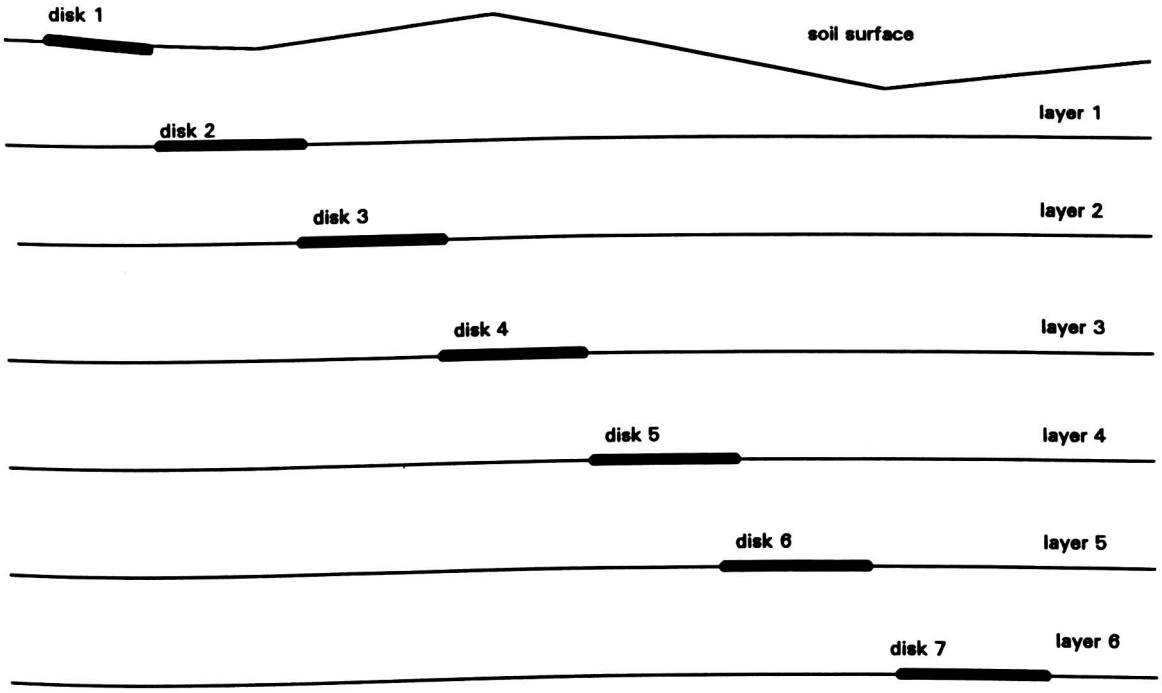

Figure 3.4 A soil profile with six layers (after Baer, 1995).

Values obtained by layers are more accurate compared to values obtained by monitoring the profile as a whole because soil does not shrink uniformly at every depth.

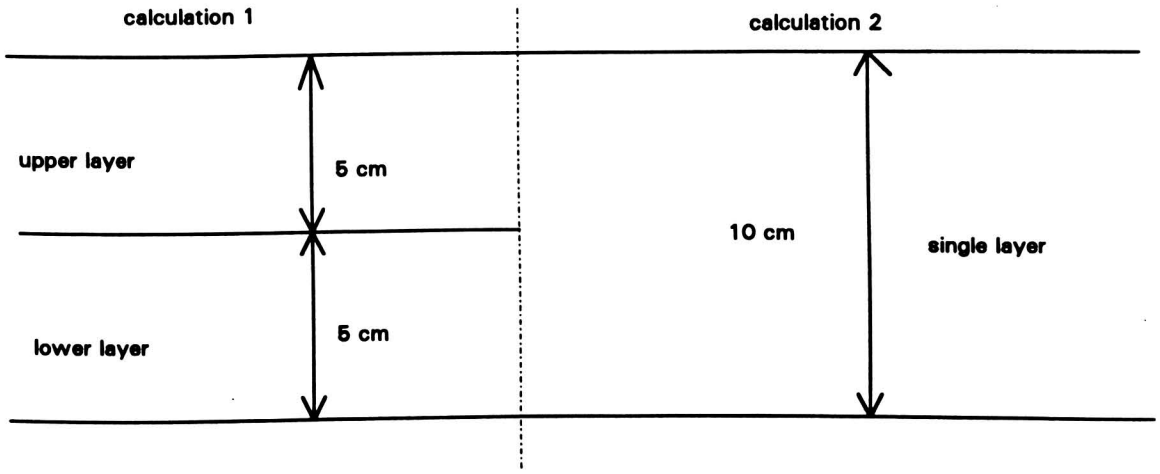

Figure 3.5 A soil profile of 10 cm thickness (after Baer, 1995).

For example, consider a soil profile of 10 cm thickness. First, calculate crack volume by dividing the profile into two 5 cm layers. Then, calculate crack volume by considering the profile as a single 10 cm layer (Figure 3.5).

Suppose the upper 5cm layer of the profile undergoes a 0.5 cm decrease in thickness (Figure 3.6).

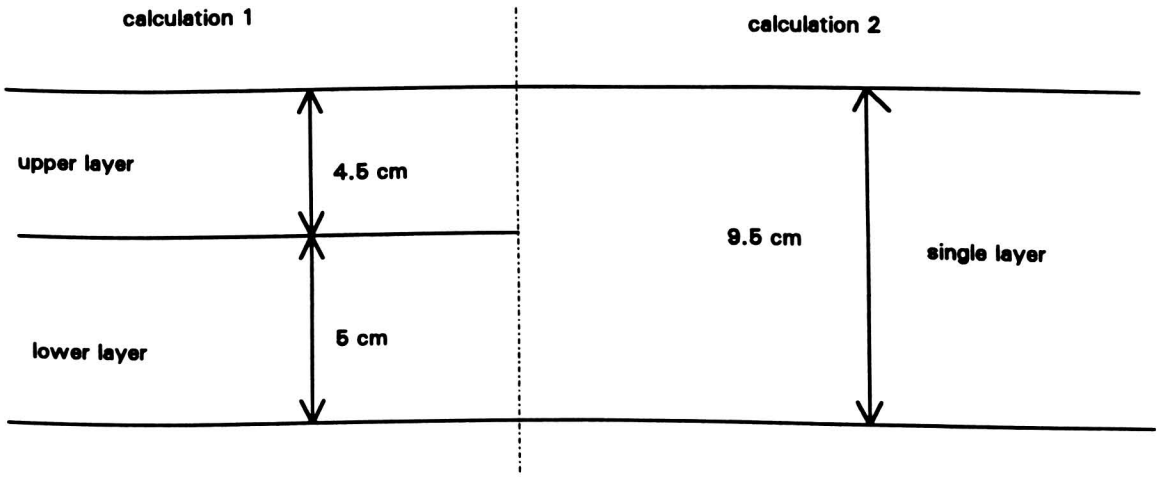

Figure 3.6 The soil profile after a 0.5 cm shrinkage of the upper layer (after Baer, 1995).

Crack volume is calculated using equations (3.5) and (3.6). In the first case, we have:

$$\Delta V = \{1-(1-\frac{0.5}{5})^3\}\cdot 5+\{1-(1-\frac{0}{5})^3\}\cdot 5 = 1.355$$

$$V_{cr} = (1.355-0.5)+(0-0) = 0.855$$

In the second case, we have:

$$\Delta V = \{1-(1-\frac{0.5}{10})^3\}\cdot 5 = 1.426$$

$$V_{cr} = 1.426-0.5 = 0.926$$

The results show that with the same thickness decrease, the second calculation gives a bigger ΔV and V_{cr} which are less accurate.

3.4 Experimental Arrangement

Installation of disk apparatus and disk readings that are described in this section were conducted by others as part of the USDA MSEA project (Baer, 1995).

3.4.1 Disk Apparatus

Earth anchors (AB Chance #4345) were used for the subsurface disks (Figure 3.7). An earth anchor is consisted of a four-inch diameter inverted single helix and a 3/4 inch diameter rod of sufficient length to reach 8 inches above the soil surface from the depth in the soil profile at which the helix was placed. In addition, the rod was sleeved from just above the helix to six inches above the soil surface. Sleeve material was two inch diameter schedule 40 PVC. Rubber caps with center holes allowing free rod passage were placed on the sleeve ends. Sleeving isolated the rod from the surrounding soil, minimizing the influence of this soil on vertical movement of the earth anchor. This arrangement allowed for seating the disks to the desired depth and for monitoring elevation changes of the disks.

Plexiglass plates, six inches in diameter, were used for the surface disks. The plates were pinned to the soil with eight inch aluminum gutter spikes.

3.4.2 Disk Location

A set of seven disks were installed at six locations at the Missouri MSEA site, at three landscape positions on Plot 13 and Plot 19, each having an area of 18.29 m x 190.5 m (Figure 3.1). At each site, the disks were seated at 15cm depth increments in the soil profile (Figure 3.4). Disks were positioned 50cm apart, horizontally, between adjacent crop rows. It is assumed that the net horizontal movement of the anchors was negligible. However, no observations were conducted on the monitoring of horizontal movement of anchors.

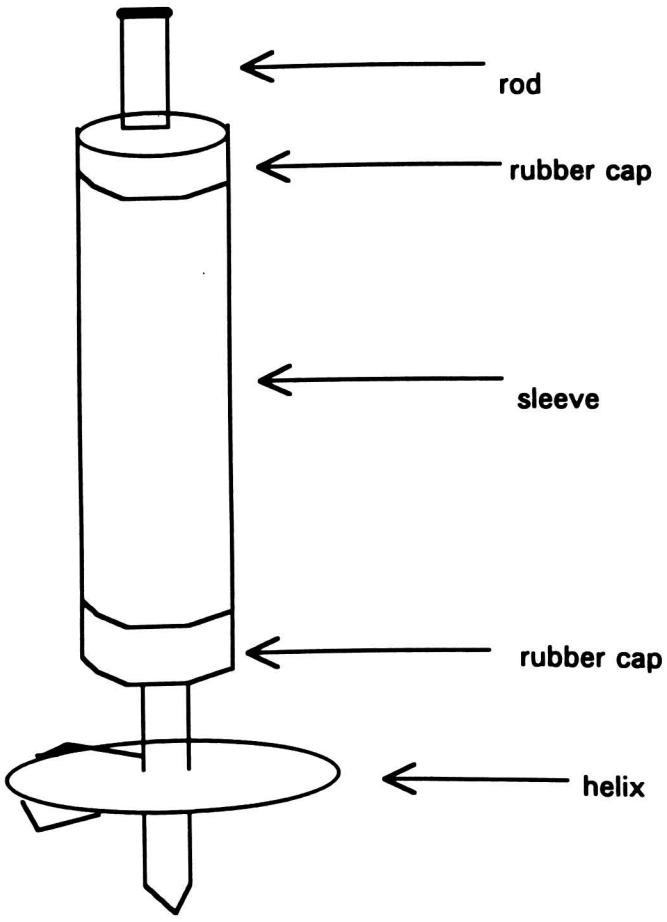

Figure 3.7 Earth anchor (after Baer, 1995).

3.4.3 Disk Installation

Disks were installed at approximately fully swollen soil conditions between December 1991 and February 1992.

3.4.4 Disk Readings

Disk elevations were read relative to a benchmark, using an engineer's level and a Philadelphia rod marked in 0.01ft. Reading resolution was ± 0.005ft (± 1.5mm). Weekly readings began April 2, 1992 and lasted to October 1, 1992. Biweekly readings began October 1, 1992. Table 3.3 and 3.4 show the results of cracking volume per unit area at Plot 13 in 1992 and 1993.

Figures 3.8 and 3.9 show values for Vcr versus time based on equation (3.7). These two figures show that the Bt horizon has the highest value of V_{cr} which is reasonable because the Bt horizon has highest clay content among the three horizons.

Table 3.3 The results of crack volume per unit area at Plot 13, nest 2 in 1992 (Baer, 1995)

Horizon	2-Apr	8-Apr	14-Apr	28-Apr	5-May	13-May	20-May	27-May	3-Jun	11-Jun	18-Jun	24-Jun	30-Jun	9-Jul
C,55-90cm	0.00	0.00	0.00	0.00	0.00	0.00	0.00	0.00	0.00	0.00	0.00	0.59	0.00	0.59
Bt,10-55cm	0.00	0.00	0.00	0.00	0.00	0.59	0.59	0.59	0.59	0.59	0.59	0.59	1.18	1.74
Ap,0-10cm	0.00	0.59	0.59	0.59	0.59	0.59	0.59	0.59	0.59	1.15	0.59	0.59	0.59	0.00
Horizon	16-Jul	23-Jul	30-Jul	6-Aug	13-Aug	20-Aug	3-Sep	10-Sep	17-Sep	24-Sep	1-Oct	15-Oct	29-Oct	17-Nov
C,55-90cm	0.00	0.00	0.00	0.30	0.28	0.28	0.87	0.89	0.59	0.59	0.89	0.59	0.89	0.59
Bt,10-55cm	2.33	2.05	2.33	2.88	2.88	2.86	2.86	2.86	2.86	2.32	2.05	2.04	1.74	0.59
Ap,0-10cm	0.00	0.30	0.59	0.30	0.30	0.87	1.15	0.87	1.15	0.87	1.15	1.15	0.87	-0.31

* The C horizon is not 35 cm thick. Because the deepest depth at which the anchors were placed was 90 cm deep, the V_{cr} in the C horizon is only from the depth 55 cm to 90 cm. Actually, the V_{cr} deeper than 90 cm is very small and can be neglected because below 90 cm the soil is near saturation.

Table 3.4 The results of crack volume per unit area at Plot 13, nest 2 in 1993 (Baer, 1995)

Horizon	17-Jun	24-Jun	8-Jul	5-Aug	26-Aug	10-Sep	17-Sep	1-Oct	15-Oct	29-Oct	19-Nov
C,55-90cm	0.00	0.00	0.00	0.00	0.30	0.30	0.30	0.30	0.00	0.30	0.00
Bt,10-55cm	0.00	0.60	0.30	2.33	2.89	2.89	1.45	0.88	0.58	0.29	0.58
Ap,0-10cm	0.00	0.00	0.00	0.30	0.87	0.59	0.87	0.59	0.87	0.59	0.59

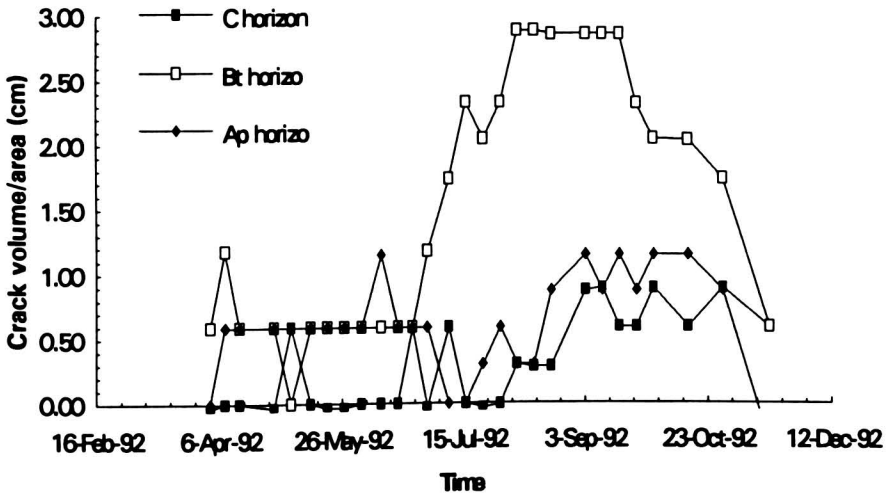

Figure 3.8 V_{cr} vs time at the middle position of Plot 13 in 1992.

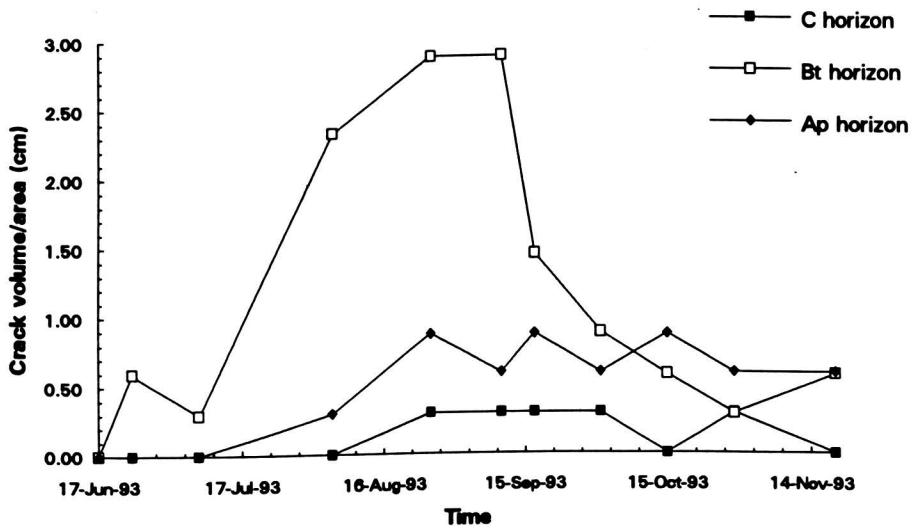

Figure 3.9 V_{cr} vs time at the middle position of Plot 13 in 1993.

3.5 Soil Moisture Cracking Model

It is believed that there is a relation between crack volume per unit area and water content (Figure 3.10). With the decrease of water content, crack volume per unit area

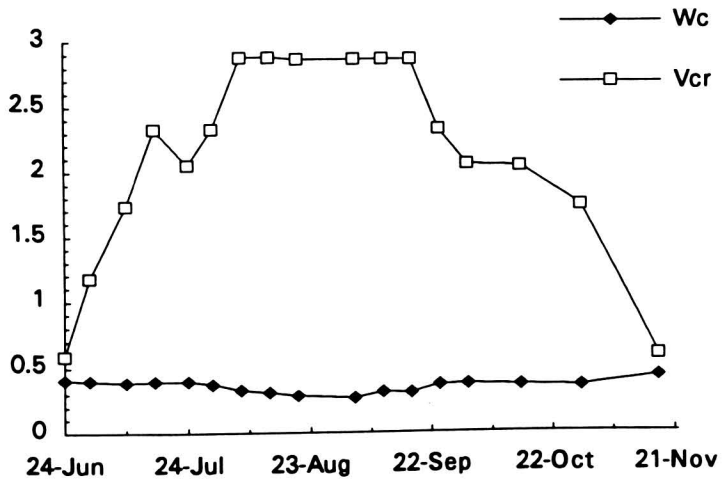

Figure 3.10 θ and V_{cr} at Plot 13, Nest 2, the Bt horizon vs time.
*Wc represents water content; Vcr represents crack volume per unit area.

increases and vice versa. Since water content and soil subsidence at different depth were measured from 1992 to 1994 at Plot 13 and 19, regression method can be used to develop soil moisture cracking model (Figure 3.11, 3.12, 3.13). Linear and 2nd order polynomial regressions were conducted on the data of the Ap, Bt and C horizons in 1992 and three linear and three 2nd order polynomial soil moisture cracking models were developed.

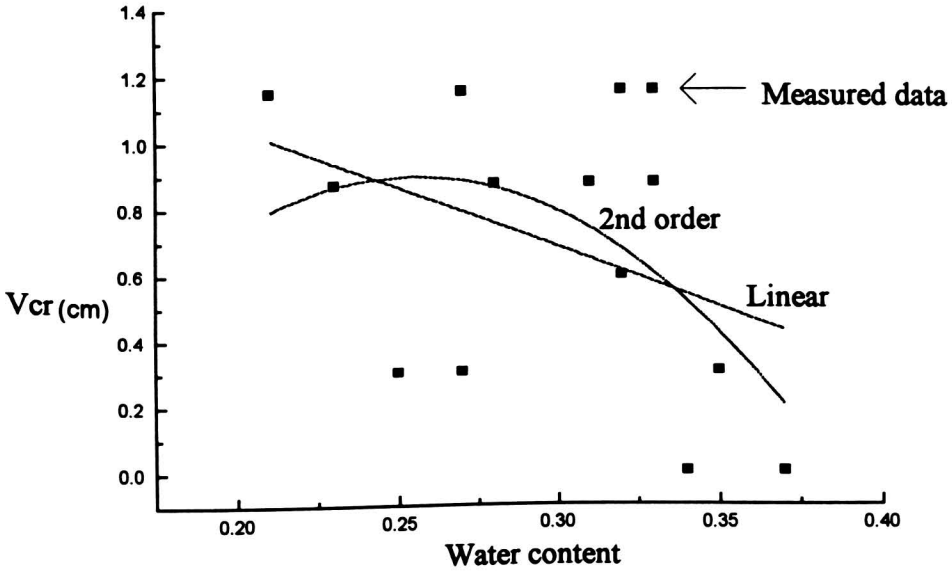

Figure 3.11 Soil moisture cracking model of the Ap horizon with 1992 data.

The linear and second order polynomial soil moisture cracking models and the R^2 of each model for the Ap horizon are:

$$V_{cr} = 1.777\text{-}3.661\theta \quad (3.12)$$

$$R^2 = 0.164$$

$$V_{cr} = -2.477\text{+}26.501\theta\text{-}52.085\theta^2 \quad (3.13)$$

$$R^2 = 0.230$$

The R^2 value of Ap layer is very small. The reason for this could be that the anchors were placed 15 cm apart, not at the interface of Ap and Bt horizon. Another reason could be that the water content measured at 15 cm is an average water content within a sphere of soil with a diameter of about 15 cm because neutron method was used to measure water content. The measured water content did not represent the real water content in the Ap horizon.

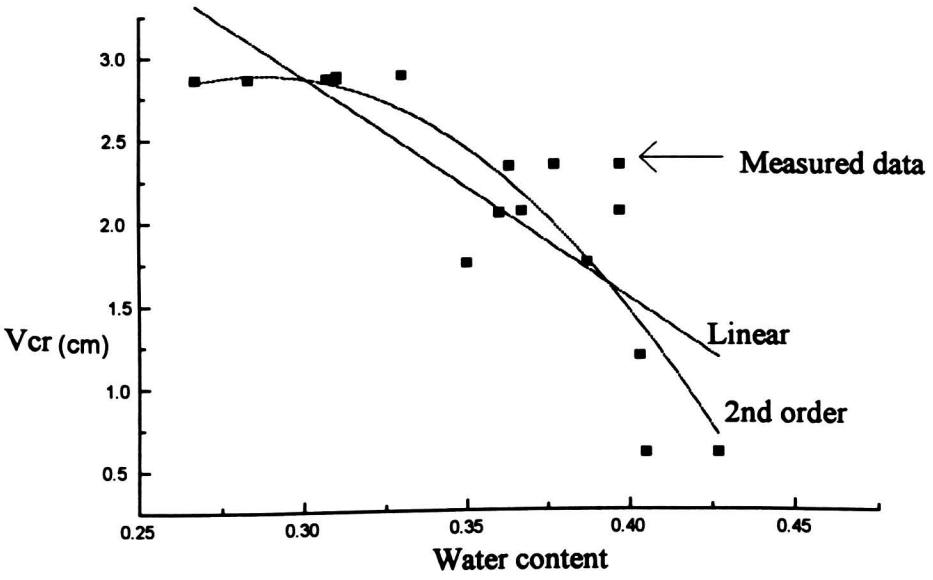

Figure 3.12 Soil moisture cracking model of the Bt horizon with 1992 data.

The linear and second order polynomial soil moisture cracking models and the R^2 of each model for the Bt horizon are:

$$V_{cr} = 6.889\text{-}13.403\theta \quad (3.14)$$

$$R^2 = 0.677$$

$$V_{cr} = -6.076\text{+}62.703\theta\text{-}109.699\theta^2 \quad (3.15)$$

$$R^2 = 0.760$$

The linear and second order polynomial soil moisture cracking models and the R^2 of each model for the C horizon are:

$$V_{cr} = 30536\text{-}80529\theta \quad (3.16)$$

$$R^2 = 0.489$$

$$V_{cr} = -4.639\text{+}37.623\theta\text{-}64.831\theta^2 \quad (3.17)$$

$$R^2 = 0.505$$

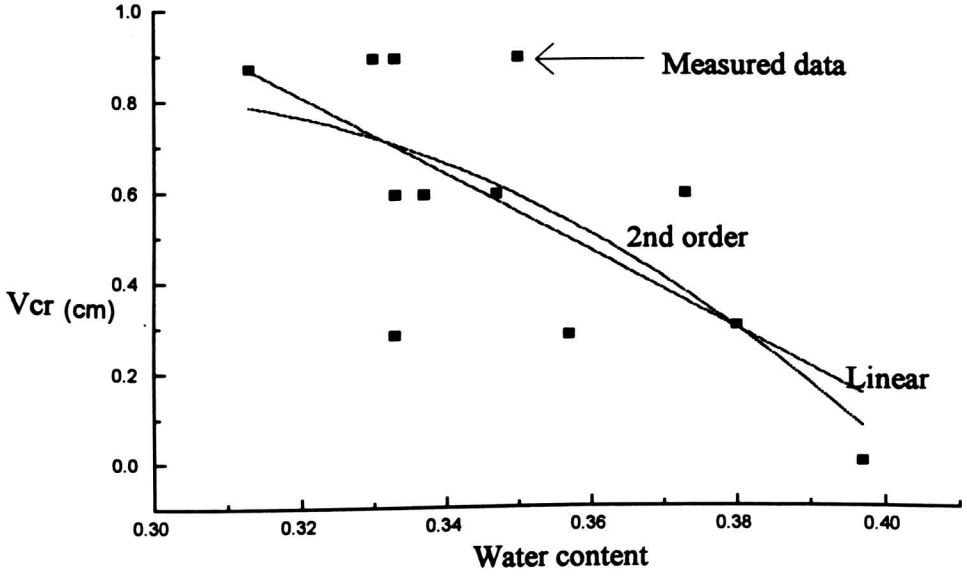

Figure 3.13 Soil moisture cracking model of the C horizon with 1992 data.

In the above soil moisture cracking models, 2nd degree polynomial models will be used in running the revised RZWQM because they have higher R^2 values. Also, it is more reasonable to use second order soil moisture cracking models than to use linear soil

moisture cracking models because in second order soil moisture cracking models V_{cr}'s approach zero more rapidly than linear soil moisture cracking models when water content becomes high.

The 1993 cracking data are not used to develop a soil moisture cracking model because it was too wet in 1993. Also, it should be mentioned here that efforts have been spent in trying to find reasonable soil moisture cracking models for the Ap, Bt and C horizons using all disk reading data from six locations which are the summit , middle and foot positions of Plot 13 and the summit, middle and foot positions of Plot 19. The efforts failed because the R^2 is much smaller than the method for individual position. The reason may be that the disks should be placed at the interface of each horizon rather than at a fifteen interval because the thicknesses of the the Ap, Bt and C horizons at each location are different. Also, a more accurate engineering level should be used.

3.6 Macroporosity and Crack Width

From the disk readings V_{cr}, which is crack volume per unit area and has the unit of cm^3/cm^2 can be developed. Also, as defined in Chapter two, P_{mac} is the macroporosity as a fraction of soil volume. If all macropores are cracks and there are no root holes and worm holes in soil, P_{mac} is:

$$\begin{aligned} P_{mac} &= \text{crack volume/total volume in a layer with thickness M} \\ &= (\text{crack volume/unit area})\cdot(1/M) \\ &= V_{cr}\cdot(1/M) \end{aligned} \qquad (3.12)$$

It was assumed that all the cracks were vertical, which is a fair assumption because at the Missouri MSEA site most cracks are vertical from field observation, and extend down to the bottom of a layer, and crack width at the top of a layer is equal to the width

at the bottom of the layer, and all the cracks in one square meter have equal length, then P_{mac} is:

$$P_{mac} = \frac{N \cdot d \cdot L \cdot M}{(100cm) \cdot (100cm) \cdot M} = V_{cr} \cdot (\frac{1}{M}) \tag{3.13}$$

and

$$d = \frac{10^4 \cdot V_{cr}}{N \cdot L \cdot M} \tag{3.14}$$

where L = the length of one crack [L]

N = the number of cracks on one square meter,

and other terms are as defined before.

Let

$$R = \frac{d}{L} \tag{3.15}$$

then

$$d = 100 \cdot \sqrt{\frac{V_{cr} \cdot R}{N \cdot M}} \tag{3.16}$$

In later simulations R is assumed to be a constant and is obtained from image analysis.

3.7 Excavation of Cracked Soil

In order to quantify crack porosity, excavation of cracked soil was conducted during the summer of 1994 when cracking was at the most developed stage. Pictures were taken at ground surface, 5 cm depth, the top of the claypan and the bottom of the claypan after plants and soil were removed. After developing the pictures, image analysis methods were used to find the crack porosity. When pictures were taken, a meter stick was placed on the soil surface so that the resolution of the pictures could be determined during image analysis. Table 3.5, 3.6, 3.7 show the image analysis results (Raw data are

from Baer, 1995). In these tables, "point" means the center of a picture element (pixel); "crack width in point" equals to total points in crack area divided by crack length in point; "crack width in cm" equals to crack width in point divided by points per centimeter; "crack length in image (cm)" equals to crack length in point divided by points per centimeter; "crack length in 1 m^2 (cm)" equals to crack length in image times one hundred then divide by image length in centimeter; "P_{mac}"equals to total point in crack area divided by total point in image; and "crack length" equals to crack length in 1 m^2 divided by the number of cracks.

Table 3.5 The image analysis results at the summit of Plot 18 (after Baer, 1995)

Image file name	e1.asc	e2.asc	e3.asc	e4.asc
position	surface	5 cm	top of claypan	bottom of claypan
Total points in image*	619369	622521	622521	617796
Total points in crack area*	9261	17477	60829	34764
Crack length in point*	1067	2151	5074	5225
Points in each image side*	787	789	789	786
Crack width in point	8.679	8.125	11.988	6.653
Crack width in cm	0.824	0.867	1.064	0.575
Crack length in image (cm)	101.253	229.577	450.282	451.338
Crack length in 1 m^2 (cm)	135.578	272.624	643.093	664.758
Points/cm*	10.538	9.369	11.269	11.577
Image length (cm)	74.682	84.210	70.018	67.895
P_{mac}	0.015	0.028	0.098	0.056
No. of cracks	2	3	7	7
Crack length	67.789	90.875	91.870	94.965
Crack width/crack length	0.01216	0.00954	0.01158	0.00605

*Raw data

Table 3.6 The image analysis results at the summit of Plot 13 (after Baer, 1995)

Image file name	e9.asc	e10.asc	e11.asc	e12.asc
position	surface	5 cm	top of claypan	bottom of claypan
Total points in image*	609961	622521	622521	625681
Total points in crack area*	15441	14905	12123	10811
Crack length in point*	1932	1066	1296	1865
Points in each image side*	781	789	789	791
Crack width in point	7.992	13.982	9.354	5.797
Crack width in cm	0.721	1.245	0.816	0.563
Crack length in image (cm)	174.341	94.915	113.074	181.015
Crack length in 1 m^2 (cm)	247.375	135.108	164.259	235.777
Points/cm*	11.082	11.231	11.462	10.303
Image length (cm)	70.477	70.251	68.839	76.774
P_{mac}	0.025	0.024	0.019	0.017
No. of cracks	3	2	2	3
Crack length	82.46	67.554	82.13	78.59
Crack width/crack length	0.00874	0.01843	0.00994	0.00716

*Raw data

Table 3.7 The image analysis results at the middle of Plot 13 (after Baer, 1995)

Image file name	e5.asc	e6.asc	e7.asc	e8.asc
position	surface	5 cm	top of claypan	bottom of claypan
Total points in image*	619369	614656	609961	622521
Total points in crack area*	20252	16554	49205	14025
Crack length in point*	2523	2088	6670	2398
Points in each image side*	787	784	781	789
Crack width in point	8.027	7.928	7.377	5.849
Crack width in cm	0.713	0.694	0.668	0.522
Crack length in image (cm)	223.962	182.791	604.117	214.033
Crack length in 1 m^2 (cm)	320.584	266.327	854.033	303.929
Points/cm*	11.265	11.423	11.041	11.204
Image length (cm)	69.861	68.634	70.737	70.422
P_{mac}	0.033	0.027	0.081	0.023
No. of cracks	4	3	9	4
Crack length	80.15	88.78	94.89	75.98
Crack width/crack length	0.00890	0.00782	0.00704	0.00687

*Raw data

The number of cracks is obtained by assuming that single crack is straight, its length is less than one meter, all single cracks are of equal length, and the number of

cracks is an integer. In obtaining crack width, it is assumed that cracks are straight and have equal width.

Under the above assumptions, it can seen that the number of cracks at each site is different. Because spatial variability is not considered in RZWQM, it is necessary to chose a representative location. The site where most data required are available is the middle position of Plot 13, and it is near the center of all plots. Therefore, it is chosen as a representative point (unit area) to simulate the movement of water, nutrients, and pesticides hereafter.

CHAPTER 4

THE HYDRAULIC PROPERTIES AT THE MISSOURI MSEA

4.1 The Theory of Hydraulic Properties

The unsaturated effective hydraulic conductivity function is defined by Darcy's Law:

$$q = -K_e(\theta)\frac{\partial H}{\partial z} \tag{4.1}$$

where q is the flux density (L/t) and $\partial H/\partial z$ is the hydraulic head gradient.

The fraction of the total pore space occupied by water is defined as saturation S:

$$S = \frac{\Delta v_w}{\Delta v_p} \tag{4.2}$$

where Δv_w = the volume of water occupying a portion of the pore volume [L^3]

Δv_p = the volume of pores in a small volume element, V, of soil [L^3].

The effective saturation is defined by Brooks and Corey (1964) as:

$$S_e = \frac{S - S_r}{1 - S_r} \tag{4.3}$$

where S_r = the residual saturation, sometimes called irreducible saturation.

Also, according to Brooks and Corey (1964), the following relationship exists:

$$S_e = (\frac{\tau_b}{p_c})^{\lambda} \qquad \text{for } p_c \geq \tau_b \tag{4.4}$$

where p_c = capillary pressure [F/L^2]

τ_b = bubbling pressure [F/L^2]

λ = pore-size distribution index.

Relative hydraulic conductivity is defined as:

$$K_r = \frac{K_e}{K_s} \tag{4.5}$$

where K_e is unsaturated hydraulic conductivity of a soil to water when soil is partially occupied by water and K_s is saturated hydraulic conductivity.

Muelam (1976) developed the following equation for predicting the relative hydraulic conductivity, K_r, from knowledge of the soil water characteristic:

$$K_r = \Theta^{1/2}\left[\frac{\int_0^{\Theta}\frac{1}{h(x)}dx}{\int_0^{1}\frac{1}{h(x)}dx}\right]^2 \tag{4.6}$$

where Θ is the dimensionless water content given as:

$$\Theta = \frac{\theta - \theta_r}{\theta_s - \theta_r} \tag{4.7}$$

where θ_r is the residual water content and θ_s is the saturated water content.

In order to solve Equation 4.6, van Genuchten introduced (1980):

$$\Theta = \left[\frac{1}{1+(\alpha h)^n}\right]^m \tag{4.8}$$

where α, m, and n are fitted parameters. In order to simplify Equation 4.8, assume that m=1-1/n. Solving equation 4.8 for $h(\theta)$ and substituting it into Equation 4.6 yields:

$$K_r(h) = \frac{\left[1-(\alpha h)^{n-1}\left[1+(\alpha h)^n\right]^{-m}\right]^2}{\left[1+(\alpha h)^n\right]^{m/2}} \tag{4.9}$$

The soil water content (θ) vs. the matric suction (τ, τ = -h) relationship is expressed by two equations (USDA-ARS, 1992):

$$\theta(\tau) = \theta_s - A_1 \cdot \tau \qquad 0 \le \tau \le \tau_b \qquad (4.10)$$

$$\theta(\tau) = \theta_r + B \cdot \tau^{-\lambda} \qquad \tau \ge \tau_b \qquad (4.11)$$

where $B = (\theta_s - \theta_r - A_1 \cdot \tau_b) \cdot \tau_b^{\lambda}$ and A_1 is a constant. All other parameters are as defined before.

The hydraulic conductivity (K) vs. matric suction (τ) relations are represented by two piecemeal sections as:

$$K(\tau) = K_s \tau^{-N_1} \qquad 0 \le \tau \le \tau_{bK} \qquad (4.12)$$

$$K(\tau) = C_2 \tau^{-N_2} \qquad \tau \ge \tau_{bK} \qquad (4.13)$$

where τ_{bK} is the air-entry of bubbling suction for the above function (which may equal to τ_b introduced above) and N_1 ,N_2, and C_2 are constants.

4.2 Method of Determining Residual Saturation

The following steps to find S_r are adopted from Brooks and Corey (Brooks and Corey, 1964). In order to determine the pore-size distribution index λ and bubbling pressure τ_b, first calculate S_e using Equation 4.3. In doing so, it is necessary to have

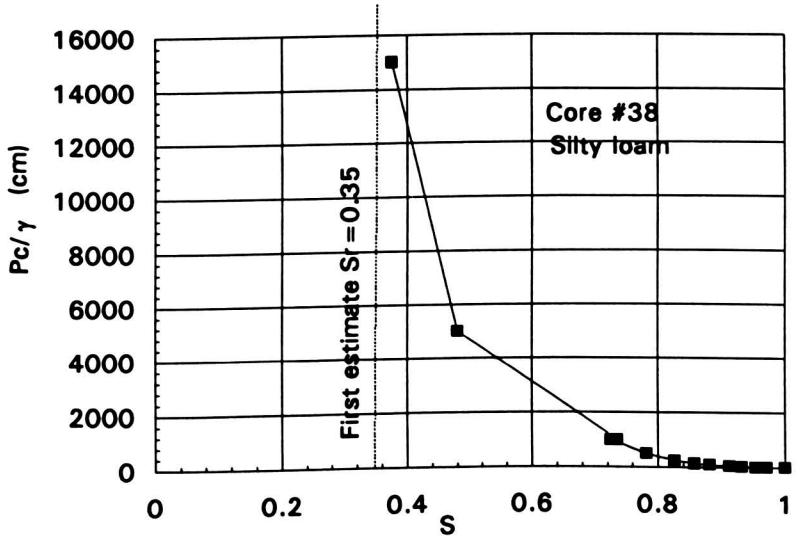

Figure 4.1 Capillary pressure head as a function of saturation.

measured values of saturation, S as a function of P_c/γ to determine S_r.

An approximate value of S_r is obtained by selecting a value of S at which the curve P_c/γ versus S appears to approach a vertical asymptote as shown in Figure 4.1. With this estimate of S_r, tentative values of log S_e are computed and plotted as a function of log P_c/γ. Usually, the plot will not be a straight line, but an intermediate portion of the computed values will fall on a straight line as shown in Figure 4.2.

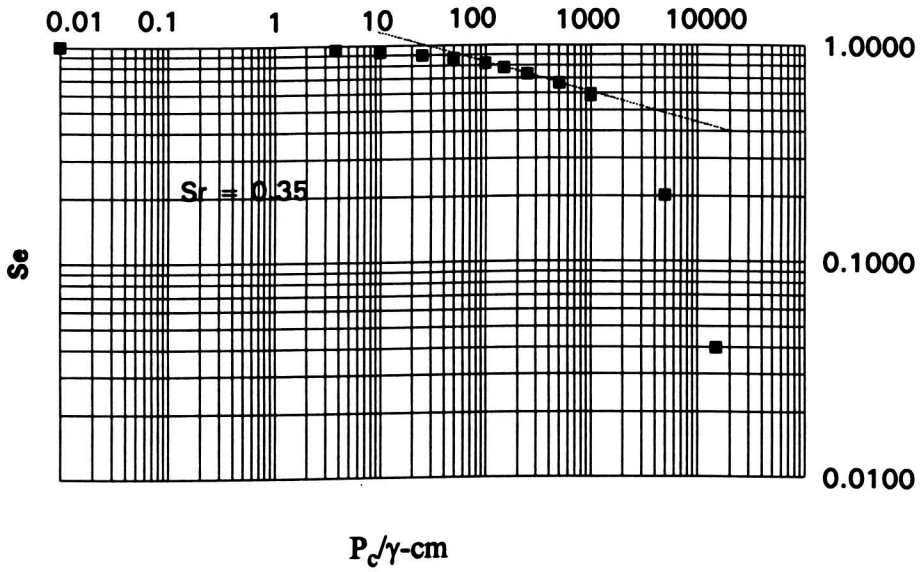

Figure 4.2 Effective saturation as a function of capillary pressure head.

A second estimate of S_r is then obtained such that a value of S_e, in the high capillary pressure range which does not lie on the straight line, will fall on the straight line. In this case, by looking at Figure 4.2, if the last S_e falls on the straight line, S_r should be:

$$S_r = \frac{S - S_e}{1 - S_e} = \frac{0.3758 - 0.4}{1 - 0.4} = -0.04$$

If S_r is less than zero, it is meaningless. By using this negative S_r value, S_e still can be calculated , and new results are shown in Figure 4.3.

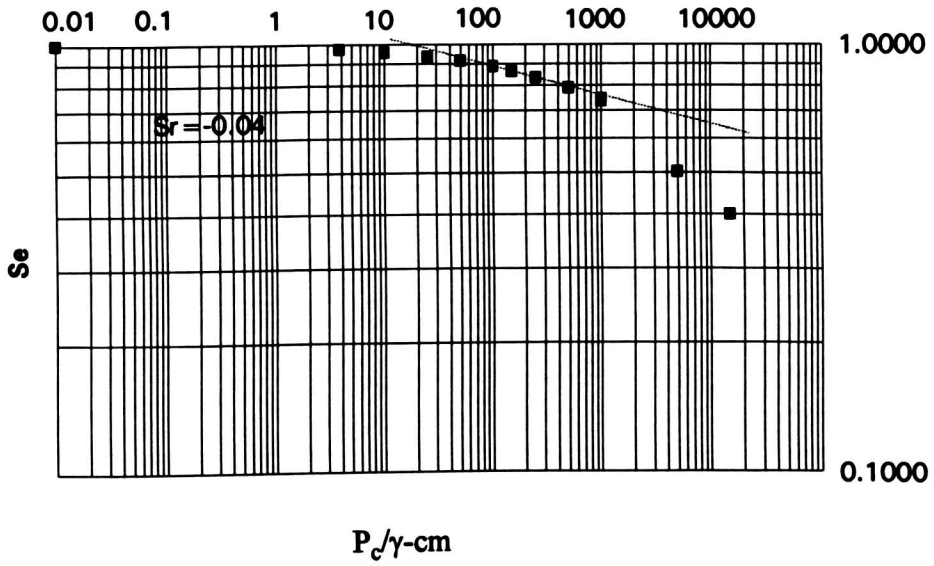

Figure 4.3 Second trial to get S_r

Table 4.1 shows the two sets of S_e values for the two S_r estimates and S values used in the above three figures. The data are from Core #38, and the porosity of the soil in Core #38 is 0.44. There are two values at 1000 cm of P_c/γ because at that value the methods used to measure water content changed.

The above steps are exactly what Brooks and Corey described in their paper (1964). However, a negative S_r value was determined using these steps. The reason a negative S_r value was determined is that the P_c/γ values are too large in the high capillary pressure range(higher than 1000 cm). Actually, there is no need to consider the values of S_e when P_c/γ is bigger than 1000 cm if considering the figures presented in Brooks and Corey's paper. Therefore, S at 15000 cm of P_c/γ is used as S_r which is a fairly good estimation because by using this value, the intermediate portion of the computed values of S_e will fall on a straight line as shown in Figure 4.4 (Anderson, 1995).

Table 4.1 The data used in the above three figures

Pc/γ*	outflow*	theta*	S	Se	Se
cm	(mL)	(mL/mL)		Sr=0.35	Sr=-0.04
0.01	0	0.438	1.000	1.000	1.000
3.81	5.7	0.425	0.970	0.954	0.971
10.00	8.9	0.417	0.954	0.929	0.955
25.00	13.2	0.408	0.931	0.894	0.934
50.00	16.8	0.399	0.912	0.865	0.916
100.00	22.8	0.386	0.881	0.817	0.886
150.00	27.5	0.375	0.857	0.780	0.862
250.00	33.4	0.362	0.826	0.732	0.833
500.00	41.80	0.342	0.782	0.665	0.791
1000.00	52.60	0.318	0.726	0.578	0.737
1000.00		0.322	0.735	0.593	0.746
5000.00		0.210	0.481	0.201	0.501
15000.00		0.165	0.376	0.040	0.400

*Raw data provided by Baer, 1995.

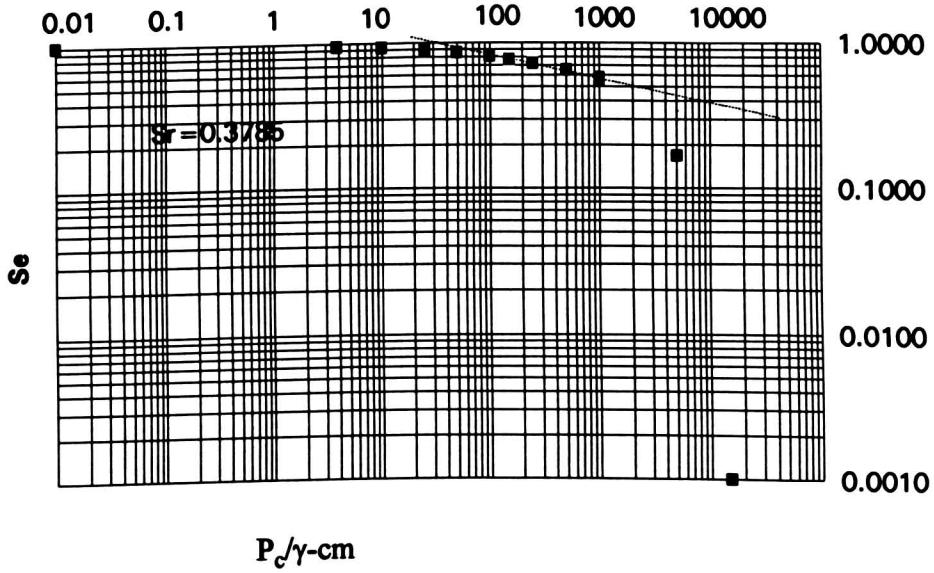

Figure 4.4 Effective saturation when S_r equals to S at 15000 cm.

4.3 The Method of Determining λ and τ_b

Equation 4.4 is used to determine λ and τ_b (Raw data from Baer, 1995). The values of S_e at different P_c/γ ranging from 50 to 1000 are chosen to do non-linear regression. Figure 4.5 is an example of the regression of Core #38 to determine λ and P_b which are 0.1341 and 19.3945 with the standard deviation of 0.1126 and 3.7722 respectively while χ^2 equals to 0.00037.

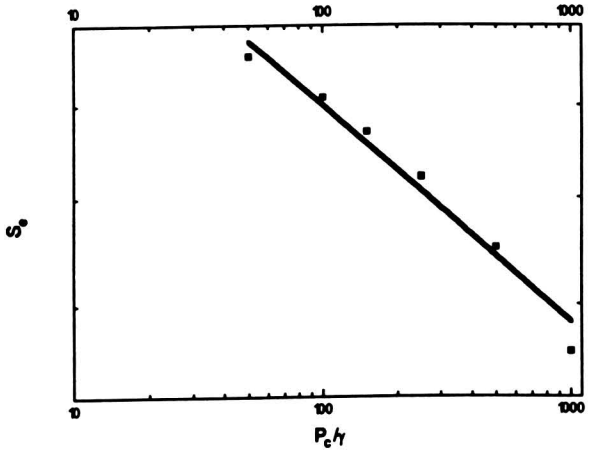

Figure 4.5 An example of regression to determine λ and τ_b.

Table 4.2 The results of τ_b and λ at the A_p horizon (after Baer, 1995)

core #	location	horizon	τ_b (cm)	S_d	λ	S_d
38	13.01	Ap	19.3945	3.7722	0.1341	0.1126
39	13.01	Ap	19.1042	1.7373	0.1272	0.0049
40	13.01	Ap	23.7156	3.57415	0.152	0.0108
41	13.02	Ap	18.7514	3.01649	0.133080	0.0090
42	13.02	Ap	13.8153	2.60927	0.15112	0.0109
43	13.02	Ap	18.7130	4.60947	0.10059	0.0102
44	13.03	Ap	19.6907	5.61395	0.08715	0.0103
45	13.03	Ap	22.8463	4.77604	0.12012	0.0113
46	13.03	Ap	20.5401	3.139460	0.136750	0.0091
47	19.01	Ap	17.8268	10.25171	0.08786	0.0229
48	19.01	Ap	36.9409	14.72348	0.14787	0.0398
50	19.01	Ap	27.9762	13.125	0.11634	0.0310
54	19.05	Ap	14.2481	2.32186	0.145140	0.0101
55	19.10	Ap	22.4358	8.42941	0.172020	0.0302
56	19.10	Ap	4.2937	1.77462	0.04471	0.0051
57	19.10	Ap	18.9666	4.10169	0.041880	0.0041

The rest of the results are shown in Table 4.2, 4.3 and 4.4. In these tables, Sd is the standard deviation of a parameter.

Table 4.3 The results of τ_b and λ at the Bt horizon (after Baer, 1995)

core #	location	horizon	depth (cm)	τ_b (cm)	s_d	λ	s_d
11	13.01	Bt	13	11.2318	2.43542	0.21031	0.01825
12	13.01	Bt	18	13.6222	3.82967	0.24048	0.02963
13	13.01	Bt	14	13.2566	2.79900	0.21689	0.01962
14	13.02	Bt	13	10.3191	3.43093	0.18982	0.02424
17	13.02	Bt	13	13.1466	2.49492	0.23376	0.01910
18	13.03	Bt	19	16.4564	2.50016	0.33056	0.02507
19	13.03	Bt	23	13.7743	1.89116	0.28926	0.01664
20	13.03	Bt	20	12.7821	3.46828	0.18885	0.02134
22	19.01	Bt	27	12.5062	1.57846	0.23685	0.01165
24	19.01	Bt	26	12.4934	2.22261	0.52068	0.04478
26	19.01	Bt	26	12.2318	0.86827	0.217	0.00589
27	19.02	Bt	17	21.9479	6.9231	0.18156	0.02669
29	19.02	Bt	15	16.1044	2.13487	0.32821	0.02147
31	19.02	Bt	15	6.0233	1.3982	0.19375	0.01442
35	19.10	Bt	24	19.3857	2.16807	0.81092	0.06601
37	19.10	Bt	25	6.9871	0.45426	0.19972	0.00438

Table 4.4 The results of τ_b and λ at the C horizon (after Baer, 1995)

core #	location	horizon	depth (cm)	τ_b (cm)	s_d	λ	s_d
3	13.01	C	75	24.720	4.92903	0.037	0.00381
5	13.03	C	72	55.88622	13.51316	0.0927	0.01866
6	13.02	C	78	37.04978	14.63887	0.08217	0.02095
7	13.03	C	72	16.43966	9.39301	0.09213	0.02312
9	13.02	C	82	38.94966	16.48242	0.63509	0.31207
10	13.03	C	68	36.76376	11.42988	0.72037	0.26102

4.4 The Method to Determine K_e

From Equation 4.7 and 4.8 water content θ can be calculated:

$$\theta = \theta_r + \frac{\theta_s - \theta_r}{[1+(\alpha h)^n]^m} \tag{4.14}$$

where h, θ, and θ_s are known measured values. Also, θ at 15000 cm can be used as θ_r. Again, regression was performed to obtain parameters such as α and n under the simplified assumption of $m = 1 - \frac{1}{n}$. One of the regressions for Core #38 is shown in Figure 4.6 and the rest of the results are shown in Table 4.5, 4.6 and 4.7.

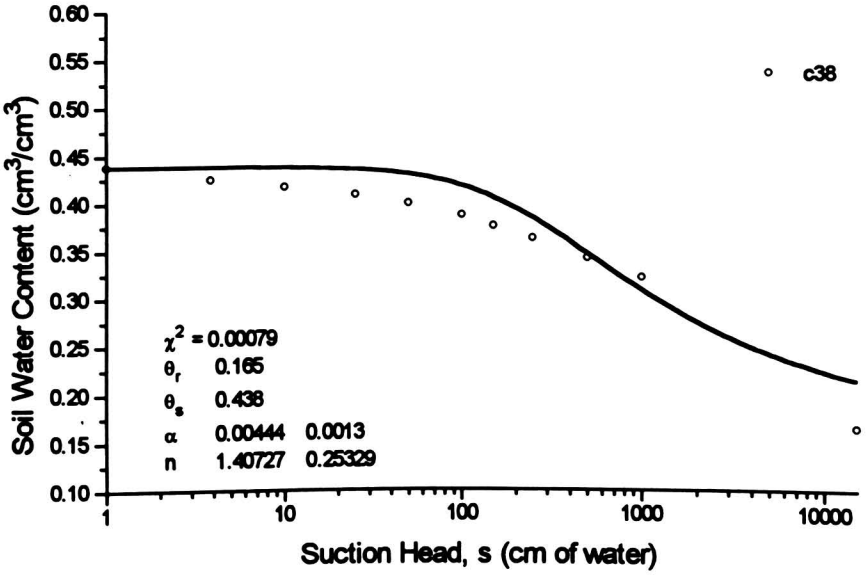

Figure 4.6 The regression to determine α and n (after Baer, 1995)

Table 4.5 α, n, m and other parameters at the Ap horizon

core #	α^*	n^*	m^*	K_s^*	N_1	C_2	N_2	θ_r^*	θ_s^*	A_1	$\theta_{1/3}$	$\theta_{1/10}$	θ_{15}
				cm/hr		cm/hr		ml/ml	ml/ml		ml/ml	ml/ml	ml/ml
38	0.0079	1.3683	0.2692	0.589	0.4704	5.684	1.17999	0.165	0.438	0.00136	0.355	0.385	0.163
39	0.0070	1.3931	0.2822	0.834	0.4120	7.918	1.11614	0.157	0.442	0.00105	0.355	0.389	0.156
40	0.0076	1.4102	1.2909	0.379	0.4234	4.082	1.15803	0.169	0.442	0.00106	0.356	0.390	0.167
41	0.0079	1.3785	0.2746	0.684	0.4545	6.804	1.17556	0.171	0.430	0.00136	0.350	0.381	0.171
42	0.0187	1.2885	0.2239	0.780	0.8319	8.812	1.61909	0.175	0.449	0.00237	0.348	0.380	0.176
43	0.0037	1.4872	0.3276	0.217	0.2241	1.561	0.83385	0.172	0.419	0.00094	0.362	0.381	0.172
44	0.0033	1.5841	0.3687	0.379	0.1558	2.718	0.75856	0.185	0.431	0.00060	0.372	0.401	0.185
45	0.0045	1.5065	0.3362	0.304	0.2447	2.604	0.90389	0.186	0.412	0.00088	0.353	0.377	0.187
46	0.0073	1.4180	0.2948	0.726	0.4003	7.754	1.13891	0.179	0.421	0.00118	0.347	0.375	0.179
47	0.0031	1.7736	0.4362	0.024	0.0828	0.175	0.68823	0.126	0.421	0.00135	0.356	0.382	0.123
48	0.0024	2.0402	0.5099	0.044	0.0385	0.254	0.5459	0.126	0.402	0.00033	0.346	0.378	0.123
50	0.0032	1.7732	0.4360	0.155	0.0988	1.190	0.70678	0.129	0.425	0.00094	0.353	0.388	0.127
54	0.0128	1.2731	0.2145	0.163	0.7371	1.334	1.40622	0.209	0.420	0.00172	0.344	0.370	0.205
55	0.0102	1.3780	0.2743	0.116	0.5307	1.429	1.31158	0.189	0.409	0.00136	0.336	0.361	0.187
56	0.0023	1.7210	0.4189	0.005	0.0069	0.029	0.60421	0.201	0.390	0.00321	0.357	0.366	0.199
57	0.0014	2.3903	0.5816	0.379	0.0051	0.063	0.35644	0.200	0.434	0.00044	0.408	0.419	0.197

*Data from Baer, 1995.

Table 4.6 α, n, m and other parameters at the B_t horizon

core #	α^*	n^*	m^*	K_s^*	N_1	C_2	N_2	θ_r^*	θ_s^*	A_1	$\theta_{1/3}$	$\theta_{1/10}$	θ_{15}
				cm/hr		cm/hr		ml/ml	ml/ml		ml/ml	ml/ml	ml/ml
11	0.0210	1.3328	0.2497	0.840	0.771	14.065	1.7225	0.366	0.585	0.00391	0.475	0.499	0.363
12	0.0520	1.2958	0.2283	0.630	1.305	8.959	2.1973	0.386	0.586	0.00272	0.481	0.503	0.383
13	0.0470	1.2876	0.2234	0.202	1.257	2.726	2.1311	0.366	0.565	0.00270	0.467	0.489	0.363
14	0.0506	1.2728	0.2143	0.732	1.298	8.263	2.1405	0.370	0.563	0.00355	0.472	0.490	0.367
17	0.0576	1.2822	0.2201	0.348	1.388	4.080	2.2185	0.383	0.588	0.00315	0.481	0.506	0.381
18	0.0834	1.3024	0.2322	0.091	1.629	0.968	2.4091	0.410	0.575	0.00232	0.473	0.496	0.408
19	0.0850	1.2911	0.2255	0.183	1.637	1.702	2.3929	0.427	0.581	0.00245	0.489	0.510	0.426
20	0.0287	1.2946	0.2276	0.275	0.988	3.937	1.8726	0.397	0.588	0.00211	0.502	0.521	0.395
22	0.0466	1.3105	0.2369	1.728	1.200	29.537	2.1681	0.414	0.596	0.00243	0.498	0.527	0.413
24	0.1880	1.3846	0.2778	1.932	2.182	11.601	2.8257	0.461	0.606	0.00435	0.486	0.512	0.459
26	0.0390	1.3191	0.2419	0.182	1.084	3.446	2.0851	0.426	0.571	0.00197	0.497	0.518	0.425
27	0.0088	1.3709	0.2706	0.295	0.498	3.118	1.2316	0.378	0.558	0.00091	0.494	0.515	0.376
29	0.0491	1.3699	0.2700	0.059	1.183	1.750	2.3058	0.450	0.572	0.00102	0.496	0.518	0.448
31	0.1014	1.2493	0.1995	0.535	1.765	2.495	2.3492	0.418	0.599	0.00763	0.502	0.522	0.416
35	0.0981	1.2464	0.1977	N/A	N/A	N/A	N/A	N/A	0.580	0.00210	0.468	0.492	N/A
37	0.0672	1.2832	0.2207	2.040	1.376	21.749	2.2864	0.372	0.542	0.00457	0.451	0.471	0.369

*Data from Baer, 1995.

Table 4.7 α, n, m and other parameters at the C horizon

Core #	α^*	n^*	m^*	K_s^*	N_1	C_2	N_2	θ_r^*	θ_s^*	A_1	$\theta_{1/3}$	$\theta_{1/10}$	θ_{15}
				cm/hr		cm/hr		ml/ml	ml/ml		ml/ml	ml/ml	ml/ml
3	N/A	N/A	N/A	N/A	N/A	N/A	N/A	0.288	0.445	0.00001	0.439	0.444	0.284
5	0.0018	2.0287	0.5071	N/A	N/A	N/A	N/A	N/A	0.444	0.00045	0.402	0.424	N/A
6	0.0019	1.9532	0.4880	0.0395	0.0314	0.182	0.46304	0.285	0.414	0.00003	0.394	0.410	0.282
7	0.0037	1.5611	0.3594	0.0122	0.0385	0.060	0.49342	0.267	0.430	0.00023	0.404	0.420	0.264
9	N/A	N/A	N/A	0.0247	0.1733	0.192	0.80947	0.309	0.412	0.00050	0.388	0.398	0.306
10	N/A	N/A	N/A	0.0255	N/A	N/A	N/A	N/A	0.439	0.00018	0.404	0.428	N/A

*Data from Baer, 1995. In the above three tables, A_1, N_1, N_2, C_2 are constants in Equation 4.10, 4.12, 4.13; $\theta_{1/3}$, $\theta_{1/10}$, θ_{15} are water contents at suction head of 1/3 bar, 1/10 bar and 15 bar.

After α and n are obtained, Equation 4.9 is used to calculate K_r. Then Equation 4.5 is used to calculate K_e. One set of sample calculation results of Core #38 is shown in Table 4.8.

Table 4.8 The K_e calculation results of Core #38 (after Baer, 1995)

τ	θ	K_r	K_e	K_e
			(cm/min)	(mm/hr)
0	0.438	1	0.00982	5.892
3.81	0.437391	0.525136	0.005157	3.0941
10	0.435753	0.37067	0.00364	2.183986
25	0.430487	0.212481	0.002087	1.251937
50	0.420341	0.108383	0.001064	0.638595
100	0.400621	0.040035	0.000393	0.235886
150	0.383991	0.018801	0.000185	0.110776
250	0.359097	0.006119	6.01E-05	0.036053
500	0.323227	0.001061	1.04E-05	0.006254
1000	0.290384	0.000158	1.55E-06	0.000931
15000	0.211941	6.27E-08	6.16E-10	3.7E-07

4.5 The method to Determine N_1, C_2, N_2 and A_1

After having determined K_e at different suction heads (τ), Equation 4.12 is used to determine N_1 through non-linear regression. In doing so, K_e values which are at suction head less than p_b are used.

C_2 and N_2 are obtained by using Equation 4.13 with the same method of getting N_1. The difference between the two steps is that K_e values which are at suction heads

greater than p_b are used. The values of N_1, C_2 and N_2 at different layers are listed in Table 4.5, 4.6 and 4.7 already.

Since τ_b is known, Equation 4.10 is used to determine A_1. This time linear-regression is used. The values of A_1 are also listed in Table 4.5, 4.6 and 4.7. The θ values at one-third, one-tenth, and fifteen bar suction heads in Table 4.5, 4.6 and 4.7 are obtained by linear interpolation method from the known measured water content versus suction data.

CHAPTER 5

CALIBRATION OF THE ROOT ZONE WATER QUALITY MODEL

In this chapter, focus will be on the calibration of the RZWQM first. Then, calibration results will be presented.

The calibration precedures are: (1) try to match the predicted water table with the measured water table by adjusting the depth of the soil profile; (2) adjust hydraulic parameters and try to match the predicted water content with the measured water content. For example, at last the residual water content from Rawls was used because the residual water content obtained using laboratory values are too large to be used.

Doing the calibration without cracks in the soil profile is the strategy of the calibration. The calibration would be not perfect because of the lack of cracks in the soil profile. However, constant cracks cannot be considered in the calibration because they would transfer too much water.

5.1 Main Input Data File: RZWQM.DAT

As mentioned in Chapter 2, there are seven data files that have to be fed into the RZWQM. In this chapter, only three data files are going to be discussed. The rest of the files are not site specific and therefore could be read in the user manual of the Root Zone Water Quality Model (USDA-ARS, 1992). RZWQM.DAT is the main parameter input file used by the simulation program. The data in this file include parameters relating to: physiography, soil horizons, layer discretization, physical and hydraulic properties, soil heat, macroporosity, potential evaporation, residue, water chemistry, pesticides, plant growth, nutrient cycling, management of fertilizers, manures, planting operations, Best Management Practices (BMP's), tillage, and irrigation. This chapter will address those

parameters which are specific to the Missouri MSEA site, and other general parameters can be found in the user's manual (USDA-ARS, 1995).

5.1.1 Physiographic Parameters

Data in the physiographic section describe the field where the simulation will take place. Table 1 shows the information on area of the field [ha], elevation [m], aspect from true north [rad], latitude placement on the earth surface [rad], and slope of the field [rad] at the Missouri MSEA site.

Table 5.1. Physiographic parameters of the Missouri MSEA site

area of the field (ha)	0.3484
elevation of the field (m)	29.57
aspect measured clockwise from true north (radians)	4.71239
latitude of field (radians)	0.7
slope of field (radians)	0.015

5.1.2 Soil Physical System Configuration

The soil horizons are divided as shown in Table 5.2. Layer discretization is important because layer dependent input data are required for each layer. The soil profile is divided into six layers. The total thickness of the soil profile is 208 cm.

Table 5.2 The soil layer description

Layer No.	Depth (cm)
1	3
2	10
3	55
4	90
5	150
6	208

In the above table, the first layer is a synthetic one with the same layer dependent input data as that of the second layer. The reason for this synthetic layer can be found in Chapter 2 of this thesis. The second layer is the A_p horizon with a thickness of 7 cm. The actual A_p horizon is 10 cm at Plot 13, Nest #2. Because a 3 cm synthetic layer has to be put on top of the A_p horizon, the A_p horizon is adjusted to 7 cm. The third layer is the B_t horizon with a thickness of 45 cm and the fourth layer is the C horizon with a thickness of 45 cm also. The thicknesses of the A_p, B_t and C horizons are from field observation (see Table 3.3). The fifth and sixth layers are synthetic layers with the same layer dependent input data as the C horizon. The reason for having these two layers is that a certain profile thickness is required to simulate water table fluctuation. In water table simulation the last layer of the profile has to be set to saturation. A very thin last layer is not suitable because the RZWQM needs enough water to be redistributed at the beginning of a simulation. If there is not enough water to be redistributed, the water table might fall down beyond the bottom of the profile. At this time, the RZWQM assumes that the profile be 999 cm, and the predicted water table will fluctuate based on the profile of 999 cm. Therefore, the predicted water table will never reach the bottom of the profile specified before. The thicker the last layer is, the more likely that the water table can stay within the expected range of depth. Therefore, the thicknesses of the last two layers are adjustable according to the need of the water table simulation. Different thicknesses have been tried, and the best match between the measured water table and the predicted water table appears when the soil profile is specified as shown in Table 5.2.

5.1.3. Numerical System Configuration

To simulate root zone water quality, soil profile has to be discretized into numerical nodes. All these numerical nodes consist a numerical node system. The values

for this discretization should come from the grid generation program supplied by the developer of the RZWQM. One can not change the node system arbitrarily because layer boundaries must match a set of rules on thickness and node placement (USDA-ARS, 1992a). Table 5.3 shows the numerical node system used in simulations.

Table 5.3 Numerical system configuration used in simulations

Node No.	1	2	3	4	5	6	7	8	9	10	11	12
Depth (cm)	1	2	3	4	6	10	14	18	25	34	44	55
Node No.	13	14	15	16	17	18	19	20	21	22	23	
Depth (cm)	66	78	90	102	117	134	150	166	183	197	208	

Table 5.3 shows that there are 23 numerical nodes in the soil profile, and the depth from the soil surface to the last node is 208 cm.

5.1.4 Soil Layer Physical Properties

This section specifies the physical make up of each soil layer including: soil type, particle density [g/cm^3], bulk density [g/cm^3], porosity, % sand, % silt, and % clay. Table 5.4 gives the values used for all simulations at the MSEA site.

Table 5.4 Soil layer physical property

Layer No.	Texture class name	Texture code	Particle density (g/cm^3)	Bulk density (g/cm^3)*	Porosity	Fraction of sand	Fraction of silt	Fraction of clay
1	Mexico	0	2.65	1.496	0.435472	0.132	0.603	0.265
2	Mexico	0	2.65	1.496	0.435472	0.132	0.603	0.265
3	Mexico	0	2.65	1.194	0.549434	0.013	0.395	0.593
4	Mexico	0	2.65	1.524	0.424906	0.026	0.613	0.361
5	Mexico	0	2.65	1.524	0.424906	0.026	0.613	0.361
6	Mexico	0	2.65	1.524	0.424906	0.026	0.613	0.361

* Data from Baer.

The texture code is the number corresponding to the index number for each soil type and can be found in Table 5.5 (USDA-ARS, 1992b).

In Table 5.4, texture code is set to zero for all layers. This is important because if this value is anything other than zero, the program will automatically generate hydraulic properties to adhere to the physical characteristics. This was not clearly stated until version 3.0 of User's Manual came out. If on-site measured hydraulic properties are going to be used, texture codes have to be set to zero. On the other hand, there is a need to compare the results with the texture code being zero to the results using non-zero texture code, the correct texture codes have to be chosen from Table 5.5 for the right soil type.

Table 5.5 Representative values of soil physical properties

Texture code	Soil type	Particle density	Bulk density	Porosity	% sand	% silt	% clay
1	sand	2.65	1.492	0.437	1	0	0
2	loamy sand	2.65	1.492	0.437	0.85	0.1	0.05
3	sandy loam	2.65	1.45	0.453	0.65	0.25	0.1
4	loam	2.65	1.423	0.463	0.45	0.4	0.15
5	silt loam	2.65	1.322	0.501	0.2	0.6	0.2
6	silt	2.65	1.322	0.501	0	1	0
7	sandy clay loam	2.65	1.595	0.398	0.5	0.15	0.35
8	clay loam	2.65	1.42	0.464	0.28	0.37	0.35
9	silty clay loam	2.65	1.402	0.471	0.15	0.55	0.3
10	sandy clay	2.65	1.511	0.43	0.5	0.05	0.45
11	silty clay	2.65	1.381	0.479	0.25	0.45	0.3
12	clay	2.65	1.391	0.475	0.25	0.3	0.45

The bulk densities of the A_p, B_t and C horizons are the measured mean values of multiple samples from MSEA site research plots and Field 1. The numbers of samples from the A_p, B_t and C horizons are 31, 29 and 21, respectively. The porosity of each layer is gained by using the following equation:

$$n = 1 - \frac{\rho_b}{\rho_m} \tag{5.1}$$

where ρ_b = bulk density [g/cm^3],

ρ_m = particle density [g/cm^3].

Values of the fraction of sand, silt and clay can be found in Table 3.1.

5.1.5 Soil Layer Hydraulic Properties

This section defines the water flow parameters of the soil profile. These parameters describe modified Brooks-Corey water retention curves (Equation 4.10 and 4.11), hydraulic conductivity functions (Equation 4.12 and 4.13), and the saturated lateral conductivity. Table 5.6 shows all the hydraulic parameters used in simulations.

In Table 5.6, A_1 is a constant corresponding to line (3) for $\theta(h)$ curve represented by Equation 4.10 (Figure 5.1) (USDA-ARS, 1992b). The A_2 values are the average values of λ, which is called pore size distribution index, in Table 4.2, 4.3 and 4.4. The C_2 values, the second intercept on K(h) curve, for each layer are obtained by using Equation 4.12 and 4.13 together. The K_{sat} values for the A_p and B_t horizons are from the geometric mean of K_s in Table 4.5 and 4.6 respectively, and the K_{sat} values for the C horizon is from the mean of K_s in Table 4.7. The reason for using geometric means for the A_p and B_t horizons is that K_{sat} varies in a very large range. The $K_{lateral}$ values, which is called lateral saturated conductivity, are set to zero because there were no drains in field at the MSEA site. By default, if zero is input for lateral saturated conductivity, the RZWQM will assume that the lateral conductivity is equal to the vertical saturated conductivity (Ks). The N_1 and N_2, first and second exponent for K(h) curve, are from the average values of equivalent variables in Table 4.5, 4.6 and 4.7. The S_1 and S_2 are bubbling pressure on K(h) curve and $\theta(h)$ curve respectively (Figure 5.1), and they are set to equal. Their

values for each layer are from the average values of τ_b in Table 4.2, 4.3 and 4.4. Also, θ_s, $\theta_{1/3}$, $\theta_{1/10}$, θ_{15}, which are called saturation water content and field capacities at one-third, one-tenth and 15 bars, are from the average values of equivalent variables in Table 4.5, 4.6 and 4.7. The θ_r values for each layer are from Rawls (Rawls, 1982). The reason for using Rawls' values is that the values of θ_r obtained by using the method described in Chapter 4 of this thesis are too large to use.

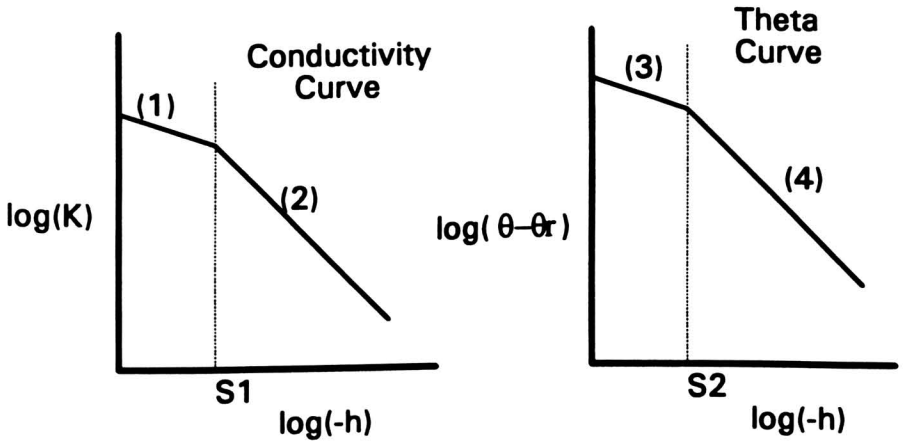

Figure 5.1 Modified Brooks-Corey soil hydraulic functions.

Table 5.6 Soil layer hydraulic properties (after Baer, 1995)

Layer No.	1	2	3	4	5	6
A_1	0.0013	0.0013	0.003	0.00022	0.00022	0.00022
A_2	0.119	0.119	0.2868	0.2767	0.2767	0.2767
C_2 (cm/hr)	1.4397	1.4397	3.69	0.1549	0.1549	0.1549
K_{sat} (cm/hr)	0.2062	0.2062	0.40799	0.0255	0.0255	0.0255
N_1	0.3198	0.3198	1.304	0.0811	0.0811	0.0811
N_2	0.969	0.969	2.1558	0.5886	0.5886	0.5886
S_1 (cm)	19.954	19.954	13.267	34.968	34.968	34.968
S_2 (cm)	19.954	19.954	13.267	34.968	34.968	34.968
$\theta_{1/3}$ (ml/ml)	0.356	0.356	0.4834	0.4026	0.4026	0.4026
$\theta_{1/10}$ (ml/ml)	0.38	0.38	0.5056	0.4178	0.4178	0.4178
θ_{15} (ml/ml)	0.17	0.17	0.3994	0.2839	0.2839	0.2839
θ_r (ml/ml)	0.015	0.015	0.09	0.04	0.04	0.04
θ_s (ml/ml)	0.424	0.424	0.5783	0.4276	0.4276	0.4276

Here it should be pointed out that if all the values are unknown, the model still can be run. In this case, set all the parameters to zero except layer sequence number. Then the model will use average textural-class values (USDA-ARS, 1992b) based on bulk density and the fraction of sand, silt and clay specified in the last section. Nevertheless, the texture code for each layer in last section has to be set to non- zero values.

If either the 1/3-bar or 1/10-bar soil water content is known and supplied to the model, the model will estimate other parameters from knowledge of soil bulk density, texture and given water content (USDA-ARS, 1992a). In this case, all the parameters except the given water content should be set to zero and the texture code in the last section must be non-zero.

In the above two cases, if saturated hydraulic conductivity (C_1 in the K(h) function) is known and supplied to the model, the model will scale the conductivity curve to this given value.

5.1.6 Hydraulic Control Information

Switches for controlling the hydraulics of the simulation program are described in this section. All the switches as shown in Table 5.7 act either upon the infiltration model or the redistribution model.

The data in Table 5.7 are practically used in the 1992 simulation at the Missouri MSEA site. If there is soil crust on the soil surface, 1 should be used. Since there is no soil crust on the soil surface at the MSEA site, zero is selected for the surface crust switch. Therefore, the conductivity of the crust is zero. One is entered for the macropore switch which means that macropores are present in the soil. If zero is entered for this switch, the data entered in Section 5.1.8 will not effect the simulation, even though the

data still must be entered. For comparison, simulation was conducted assuming that there are no macropores present in the soil, i.e., zero being entered for macropore switch.

Table 5.7 Hydraulic control switches

Surface crust switch	0
Crust hydraulic conductivity	0
Macropores switch	1
Bottom boundary condition switch	1
Value of leakage rate	0
Field saturation fraction for θ_s	0.9
Management cutoff threshold for θ	0.95
Water table switch	1
Depth from surface to drains	0
Drain space	0
Radius of drain	0
Unit gradient flow switch	1
Pan evaperation coefficient	1

The bottom condition switch specifies how the model treats the soil profile bottom boundary for soil water redistribution. This switch could be equal to 1, 2 or 3. If 1 is chosen, it means that constant head boundary exists. If 2 is chosen, it means that unit gradient boundary exists. If 3 is chosen, constant flux boundary exists. In the MSEA site simulations, constant head boundary is chosen because water table is needed in the calibration process. If there is a water table in the soil profile, the bottom node is in saturation. Therefore, constant head boundary has to be chosen. The value of leakage rate is set to zero because constant flux boundary is not chosen for the simulations.

A typical value for the field saturation fraction for θ_s which provides an estimate of the maximum degree of saturation which can occur when the soil is near total saturation, is 0.9. The field saturation fraction for θ_s modifies θ_s in the redistribution and infiltration processes to account for the effects of air entrapment. The next item is management

cutoff threshold for soil moisture content and a typical value of 0.95 is chosen for this item.

Water table switch specifies if a high water table is present in the soil. In the MSEA site, water table fluctuates within the C horizon and sometime reaches the B_t horizon. Therefore, one is used for the simulations.

The three drain items in Table 5.7 are set to zero in the simulations because there are no drains in field at the MSEA site. However, there is a creek about 250 meter from the toe of Plot 13. This creek may have an effect on the water table on Plot 13, but it was not considered because no data about this creek was available. The unit gradient flow switch is set to 1, meaning that unit gradient flow occurs during infiltration events. The pan evaperation coefficient is set to 1 and this will discussed in the section 5.3.2.

5.1.7 Micropore Information

This section contains the microporosity of the system and the rainfall-runoff soil mixing parameters for chemical transfer to runoff or macropores as shown in Table 5.8.

Table 5.8 Micropore information data

Microporosity data switch	0
Constant A of nonuniform mixing equation: mixing=Ae^{-Bx}	1
Constant B of nonuniform mixing equation: mixing=Ae^{-Bx}	4.4
Microporosity of layer 1	0.42
Microporosity of layer 2	0.42
Microporosity of layer 3	0.56
Microporosity of layer 4	0.41
Microporosity of layer 5	0.41
Microporosity of layer 6	0.41

The microporosity data switch is to specify if the model is going to use the given microporosity values or to calculate microporosity at 2-bar suction. Since the microporosities of all layers are not known exactly, zero is entered for this switch. Otherwise, 1 could be entered for this switch.

Next, parameter A and B are entered. Values for A and B of 1.0 and 4.4 respectively, are borrowed from the experimental determination of A and B of some representative soils in Oklahoma and Iowa.

Finally, the microporosities for each layer have to be supplied to the model even if the model is to recalculate these values as indicated by the microporosity data switch. The microporosity values listed in Table 5.7 are slightly smaller than the porosities provided in Table 5.4.

5.1.8 Macropore Information

Macropore information of the soil profile is entered in this section. The sorptivity factor is used to limit the amount of water that can be absorbed from the macropores into the soil matrix. The sorptivity factor value of 1.0 means full Green-Ampt lateral infiltration, while the sorptivity factor of zero implies no lateral infiltration. In simulations, 1.0 is used for the sorptivity factor. Table 5.9 specifies other macropore information used in simulations.

The macropore system is divided into two sections: 1) upper layers with cylindrical holes (e.g., worm holes, root channels, etc.); and 2) lower layers with cracks. Cylindrical holes can be specified in the upper several layers. Once a lower layer is specified with cracks, no holes can be specified in the layers below this layer.

Table 5.9 Macropore information data

Layer No.	Total macroporosity (cm^3/cm^3)	Average radius of cylindrical pores (cm)	Width of rectangular cracks in lower layers (cm)	Length of cracks in lower layers (cm)	Average length of aggregate in lower layers (cm)	Fraction of dead end pores
1	0.1	0	0	0	10	0.5
2	0.02	0	0	88.78	10	0.5
3	0.02	0	0	94.89	10	0.5
4	0.02	0	0	75.98	10	0.5
5	0.02	0	0	75.98	10	0.5
6	0.02	0	0	75.98	10	0.5

For cylindrical holes, the total macroporosity [cm^3/cm^3] is entered first. Then the average radius of the cylindrical holes is entered [cm]. In simulations of this thesis, total macroporosity and the average radius are going to be changed with water content or crack volume divided by area during simulation. In calibration simulations, no macropores are specified in the soil profile. Hence, the values of these two parameters are not important now. The next three parameters are for cracks. Therefore, zero values are entered for them. The fraction of dead end pores of the total macropore volume is an estimation since no practical value can be found. Right now 0.5 is used. The deadend macropores are branching off laterally from the continuous macropores in each layer. They can store water and chemical solution which is then available for late radial infiltration.

In layers with cracks, enter the total macroporosity first as before. Then place a zero for hole radius. The third parameter is crack width and the fourth is crack length in cm. The fifth is the length of an average aggregate. Finally, give an estimate of the fraction of dead end pores. Within the crack parameters to be entered, none of them are important during simulation, because most of them except the fraction of dead end pores are changed by the revised program according to the changing water content or input crack volume divided by area.

5.1.9 Pesticides Information

Pesticides are parameterized in this section. Alachlor and atrazine are used at the Missouri MSEA site and therefore used in simulations (Table 5.10).

Table 5.10 Pesticides parameters used in simulations

Name of pesticides	Alachlor	Atrazine
Dissipation method to use	1	1
Molecular weight (g/mole)	269.77	215.69
Lumped half-life (days)	15	60
Temperature half-life was measured at (C^0)	25	25
Oxygen content during anaerobic conditions (%)	15	15
Water solubility (μg/L)	240000	33000
Daughter product formation percentage (%)	50	50
Sorption constant for soil OM (K_{oc})	170	100

The data listed in Table 5.10 are used by many users. Therefore, they were used in the simulations of this thesis. Those parameters listed in the pesticide section of the data file RZWQM.DAT but not listed in Table 5.10 are zeros and out of the range of discussion of this thesis. In Table 5.10, two pesticides, alachlor and atrazine, have been specified. The simulation model has six alternative dissipation methods to choose and each has a specific dissipation pathway. These pathways are listed in Table 5.11. The 1-compartment model is a simple single term exponential and is the general case dissipation method. In Table 5.10, the 1-compartment model is chosen for both alachlor and atrazine. The 2-compartment is used primarily to simulate chemicals that have a high volatilization rate immediately after application. Independent parameterization through specific pathways is allowed by the individual pathway method. If daughter products are formed, the daughter product formulation method can be used.

Table 5.11 Dissipation method

dissipation code	dissipation method description
1	Lumped dissipation by a one-compartment model.
2	Lumped dissipation using a 2-compartment model for highly volatile chemicals.
3	Individual pathways dissipation where each degradation rate is specifically identified.
4	Parent chemical for daughter product (metabolite) formulation, where this parent chemical gives rise to one or more metabolites.
5	Daughter product 1st generation. The user can specify a maximum of two of these.
6	Daughter product 2nd generation. The user specify this daughter only if a 1st generation daughter is set concurrently.

In order to adjust the dissipation rate, the molecular weight has to be used. Also, if the lumped half-life in not known, molecular weight can be used to determine the lumped dissipation rate. The lumped half-life is used to determine the long term degradation rate. The temperature at which the laboratory lumped half-life is determined is used to adjust lumped half-life to different temperatures. The dissipation rate under anaerobic conditions deep in the soil profile is adjusted by oxygen content. The daughter product formation percentage is a multiplier to partition chemical amounts into parent-daughter or daughter-daughter pools.

Comparison between the lumped half-lives of alachlor and atrazine shows that the lumped half-life of atrazine is three times long than that of alachlor. In opposite, the water solubility of alachor is six times larger than that of atrazine, and the K_{oc} value of alachlor is 0.7 time larger than that of atrazine. Therefore, atrazine is more environmental resistant.

5.1.10 Plant Growth Parameters

Plant model control parameters are described in this section. The number of plants the model can parameterize is five. Two plants, soybeans and corn, are parameterized in the RZWQM.DAT data file for the Missouri MSEA site simulation. In Plot 13, soybean was planted in 1992, and corn was planted in 1993. Therefore, in the 1992 simulation, soybean should be listed first in the plant growth section of the RZWQM.DAT data file. In 1993 simulation, corn should by listed first.

5.1.11 Site Specific Parameters of Plant Growth Model

This section includes nine parameters which effect how plants grow. These parameters are site specific and should be calibrated for the Missouri MSEA site. Table 5.12 displays these parameters used in all simulations.

Table 5.12 Site specific plant parameters used in the Missouri MSEA site simulations

Name of plant	Soybeans	Corn
Maximum nitrogen uptake rate (g/plant/day)	3	6.5
Proportion of photosynthate to respire (0...1)	0.05	0.4
Amount of biomass needed to obtain leaf area index of 1.0 (g)	1.65	12.5
Plant density (plants/ha)	395000*	54000*
Age effect for propagules as prop. of photo. (0...1)	0.4	0.8
Age effect for seeds as prop. of photo. (0...1)	0.3	0.5
Normal maximum root system depth (m)	0.8	0.95
Potential min leaf stomatal resistance (S/M) (100...400)	200	200
Nitrogen sufficiency index threshold (0...1)	0.9	0.9

* Data from Newell Kitchen, 1995.

In Table 5.12, the maximum nitrogen uptake rate is adjustable. The increase of this rate will result in an increased yield. The parameter the proportion of photosynthate to respire maintains nitrogen uptake while decreasing biomass accumulation. Increasing this parameter results in a decrease in biomass. The parameter the amount of biomass needed

to obtain leaf area index of 1.0 affects the conversion between leaf area and biomass. Increasing this parameter causes a decrease in total plant production. The parameter the age effect for propagules as proportion of photosynthesis keeps the total production constant while decreasing the yield by decreasing photosynthesis efficiency during propagate development. The parameter the age effect of seeds as proportion of photosynthesis effect photosynthesis during yield development period. The parameter the normal maximum root system depth allows more root development, and therefore increase in root depth generally increases total plant production. The parameter nitrogen sufficiency index threshold will trigger fertilizer applications if calculated nitrogen sufficiency index is lower than the given number. Among the parameters in Table 5.12, the most important one is the third one, the amount of biomass needed to obtain leaf area index of 1.0. The numbers 1.65 for soybean and 12.5 for corn are calibrated numbers for the Missouri MSEA site. The calibrations were conducted so that the maximum leaf index would not exceed 2.5 for soybean and 4.0 for corn (Seaki, 1959). The normal maximum root system depth for soybean is 0.8 meter and for corn is 0.95 (measured data). The plant density for soybeans in 1992 was 395,000 and for corn in 1993 was 54,000 plants per hectare (measured data). The rest of the parameters are used by other users and remain unchanged in the calibration of this thesis.

5.1.12 Plant Management

This section includes the data controlling the planting and harvesting of crops during the simulation. Table 5.13 shows the planting and harvesting times and methods selected for each crop.

Table 5.13 Plant management data

Name of plant	Soybeans	Corn
Date of planting (dd/mm/yy)	8/5/92*	17/5/93*
Row spacing for planting operation (cm)	76*	90*
Planting depth (layer index number)	2	2
Planting density (#seeds/ha)	395000	54000
Growth stage of harvest (0...1)	0.95	0.95
Julian date for harvest (day)	273*	284*

* Data from Newell Kitchen, 1995.

5.1.13 Fertilizer Management

The data in Table 5.14 describes the fertilizer used in 1992 and 1993. Table 5.14 shows that there was not any fertilizer applications in 1992. In 1993, 140 pounds of UAN which consists of 25% of nitrate, 25% of ammonium and 50% of urea was applied on the same day when corn was planted.

Table 5.14 Fertilizer application data

Name of plant	Soybeans	Corn
Application date	7/5/92	17/5/93
Time to apply fertilizer	preplant	preplant
Method to apply fertilizer	leave on surface	leave on surface
Amount of NO_3 applied	0	35*
Amount of NH_4 applied	0	35*
Amount of urea applied	0	70*

* Data from Newell Kitchen, 1995.

5.1.14 Pesticide Management

The pesticide applications are described in this section. Table 5.15 shows that only alachlor was applied on the same date when soybeans were planted in Plot 13 in 1992 and the amount applied was 3.472 kg/ha. In 1993, both alachlor and atrazine were applied.

Table 5.15 Pesticide application data

Name of pesticide	Alachlor	Alachlor	Atrazine
Application date (dd/mm/yy)	8/5/92	17/5/93	17/5/93
Method of application	Leave on soil surface	Leave on soil surface	Leave on soil surface
Amount applied (Kg/ha)	3.472*	3.02*	2.24*

* Data from Newell Kitchen, 1995.

5.2 Initial Condition Data File: RZINIT.DAT

The initial condition data file RZINIT.DAT contains the initial state of the soil layer system at the start of the simulation program. This file initializes both the physical and chemical variables. There are four sections in this file: physical processes section, soil chemistry section, nutrient section and pesticide section. Because soil chemistry is not a concern in this study, soil chemistry initial section is skipped in the following discussions.

5.2.1 Physical Processes Section

The physical processes section initializes the soil moisture and temperature profiles in the layer grid. Table 5.16 shows the data used in 1992 and 1993 runs.

Table 5.16 Physical processes section data

Layer No.	92 run	93 run
	Water content	Water content
1	0.37	0.3633
2	0.37	0.3669
3	0.413	0.4237
4	0.367	0.3416
5	0.427	0.3887
6	1	1

If the water content for a layer is 1, it means that the layer is in saturation. Table 5.16 shows that the last layer is saturated. Also, the fifth layer is near saturation for 1992 run (the porosity of the fifth layer is 0.4276). The purpose of doing this is to maintain the

water table in a shallower position. The water content at the other layers are the water content at the date the simulation begins for 1992 run. The initial water contents of layer one to five for the 93 run are the output water contents at the end of 1992 simulation.

5.2.2 Nutrient Section

The nutrient section initializes the soil profile state of the nutrient chemistry model. Table 5.17 only lists initial nitrogen, urea and ammonium concentration states, and other nutrient items, such as humus, carbon, etc., are not listed because they are out of the range of this research.

Table 5.17 shows the initial nitrate nitrogen concentration for each layer according to measured data on April 29, 1992. The initial urea and ammonium concentrations for all the layers are zeros because no measured data are available.

Table 5.17 Nutrient initial section

Layer No.	Nitrate concentration* (μg-N/g-soil)	Urea concentration (μg-N/g-soil)	ammonium concentration (μg-N/g-soil)
1	4.3	0	0
2	4.3	0	0
3	5.3	0	0
4	3.6	0	0
5	3.6	0	0
6	1.2	0	0

* Data from Newell Kitchen, 1995.

5.2.3 Pesticide Section

The initial alachlor and atrazine concentrations for all layers are zeros because no measured data are available at the beginning of simulations.

5.3 Daily Meteorology Data File: DAYMET.DAT

Included in data file DAYMET.DAT are simulation timing control and daily values for minimum and maximum air temperature (^{0}C), wind run (km/day), incoming short wave solar radiation (MJ/m^2/day), pan evaporation (cm), and relative humidity (percentage).

5.3.1 Simulation Timing Control Section

In this section the beginning and ending times of the simulation are set (Table 5.18). Time control can be entered in two formats, Julian or calendar. Calendar format dates are used in the simulations of this study.

Table 5.18 Simulation timing control data

1992 run		1993 run	
Beginning date	Ending date	Beginning date	Ending date
8/4/1992	30/12/1992	1/1/1993	12/30/1993

5.3.2 Meteorology Data Section

Meteorology data are entered in this section (Table 5.19).

Table 5.19 Daily meteorology data

Day	Year	T_{min} (^{0}C)	T_{max} (^{0}C)	Wind run (km/day)	Solar radiation (MJ/m^2/day)	Pan evaporation (cm H_2O/day)	Relative humidity (%)
1	1992	-1	3	316.65	0	0.083	89
2	1992	1	7	193.08	0	0.079	88.5
3	1992	-2	10	185.36	0	0.112	78.5

When the RZWQM is supplied with certain available data, it can estimate the rest. However, the minimum data needed are the daily air temperatures, T_{min} and T_{max} because

the RZWQM can not estimate those data. If wind run is set to zero, the model assumes a calm, mild breeze at 100 km/day. Short wave radiation, pan evaporation, and relative humidity are used to estimate evaporation potentials. In most cases, either short wave radiation or pan evaporation is available, and in rare cases, both are available. There are three ways to handle energy input into the model.

1 If incoming short wave radiation is not available, and pan evaporation is available, the model can use pan evaporation as the best estimate of potential evaporation. The model will calculate the potential rates for evaporation and transpiration by using pan evaporation coupled with the pan coefficient from the data file RZWQM.DAT.

2 If incoming short wave radiation is supplied to the model, the model can use this radiation as the energy input into the evaporation algorithm, regardless of whether or not pan evaporation is supplied.

3 When neither short wave radiation nor pan evaporation is known, the model will estimate incoming short wave radiation based on site location on the earth surface, time of year and cloudy day percentage.

If relative humidity is unknown, the model can estimate this from supplied minimum and maximum air temperature.

The situation at the Missouri MSEA site is more complicated than the cases described above. In the simulation area, pan evaporation data are available from April to October. For the first three months and last two months, neither incoming short wave radiation nor pan evaporation data is available. Relative humidity and wind speed data of year 1992 and 1993 at Columbia Regional Airport, which is about thirty miles south of the Missouri MSEA site, are available (Raw data provided by Guinan, 1995). In order to get better simulation results, a C language program (Appendix D) is developed to calculate evaporation potential for the two years during the period when neither incoming short wave radiation nor pan evaporation is known. For the period when the pan evaporation is

known, the C language program converts it to evaporation potential directly based on the wind speed and relative humidity. The basis of this C program is from the book "Guidelines for prediction of crop water requirements" (Doorenbos and Pruitt, 1977). After using the C program, the pan coefficient in the data file RZWQM.DAT is set to 1 because the C program has considered the factors that affect pan evaporation.

5.4 The Calibration Results

After the calibration of the Root Zone Water Quality Model, the next task is to apply the calibrated model. The calibration simulation was conducted without macropores in all layers.

5.4.1 Calibration Results for 1992

A. Water Table Calibration Result. Water table is the first consideration in calibration because the water table affects the soil water content above the water table. Figure 5.2 shows both the measured water table (Paul Blanchard, 1995) and the predicted water table in 1992. The beginning date of the calibration period is day 99 (April 8, 1992) because from this day on the measured water content is available and because the water content is needed to initialize the soil moisture in the initial data file RZINIT.DAT. Also, by doing so, comparison between the predicted water content and the measured water content is possible.

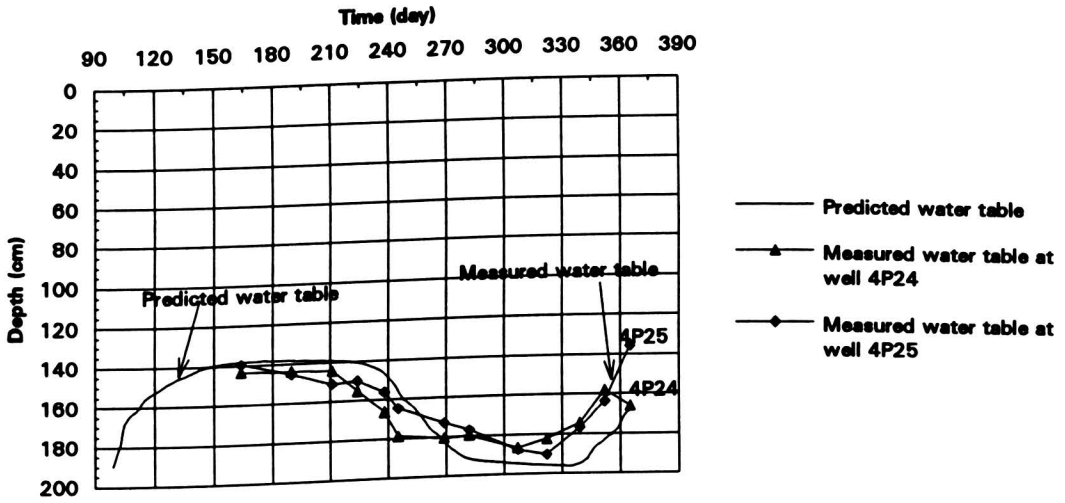

Figure 5.2 Measured and predicted water tables in 1992.

Figure 5.2 shows the comparison between the predicted water table and the measured water table represented by 4P24 and 4P25, two monitoring wells nearest to the middle position of Plot 13. The two monitoring wells can be found in Figure 3.1. From Figure 5.2 it can be seen that the predicted water table coincides with measured water table. Before day 255, the predicted water table is higher than the measured water table, and on day 224 the predicted water table is 9.3 cm higher than the measured water table at the well 4P25. After day 270, the predicted water table is lower than the measured water table, and on day 352 the predicted water table is 19.1 cm lower than the measured water table at the well 4P25.

B. Water Content Calibration Results. Water content is important in the calibration because it affects chemical movement. Figures 5.3 through Figure 5.8 show comparisons of the predicted water content with the measured water content (measured water content from Baer) at different depths in 1992, and Figure 5.9 shows the predicted water content at 150 cm and 208 cm depth. No measured water content beyond the 90 cm depth is available. Figure 5.3 shows that in April (day 99 to day 123) the predicted water content is higher than the measured water content and in May through early July (day 124 to day 195) the predicted water content is much lower than the measured water content. From middle July to the beginning of September (day 196 to day 244) the predicted water table coincides with measured water content while the predicted water content fluctuates more than the measured water content. From the beginning of September to the beginning of November (day 244 to day 305) the predicted water content is lower than measured water content and in November and December (day 305 to day 366) the predicted water is higher than the measured water content.

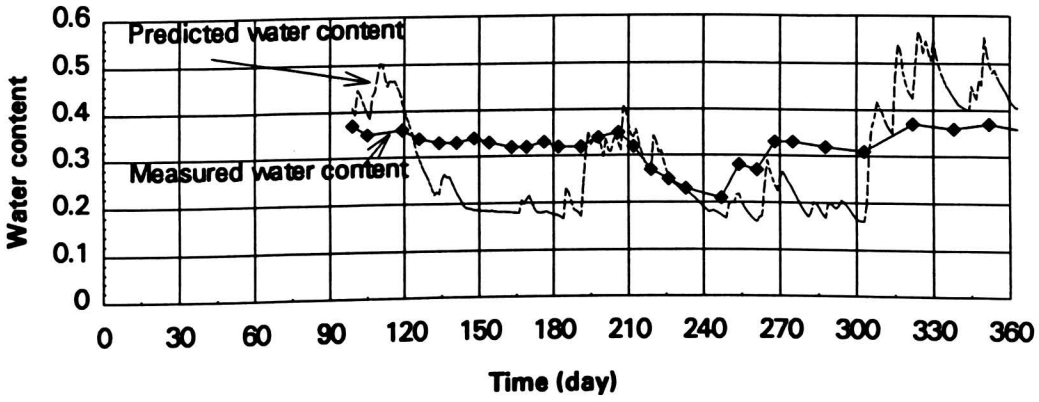

Figure 5.3 Comparison of water content at 15 cm in 1992.

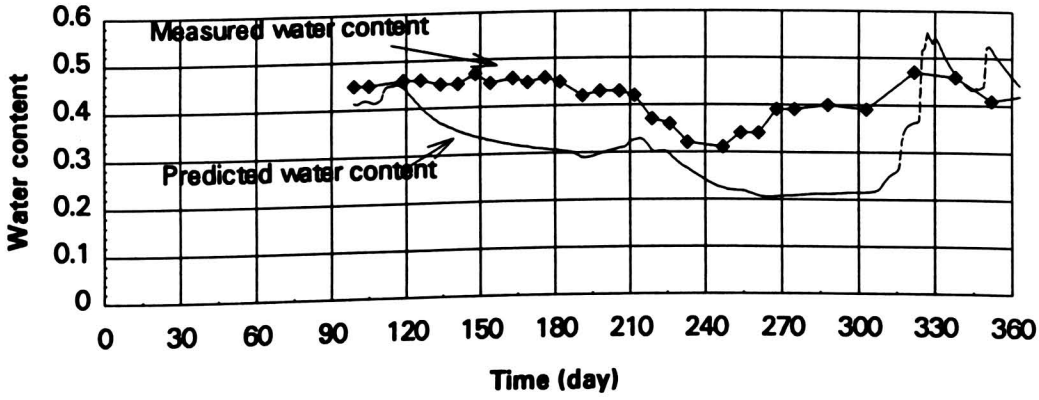

Figure 5.4 Comparison of water content at 30 cm in 1992.

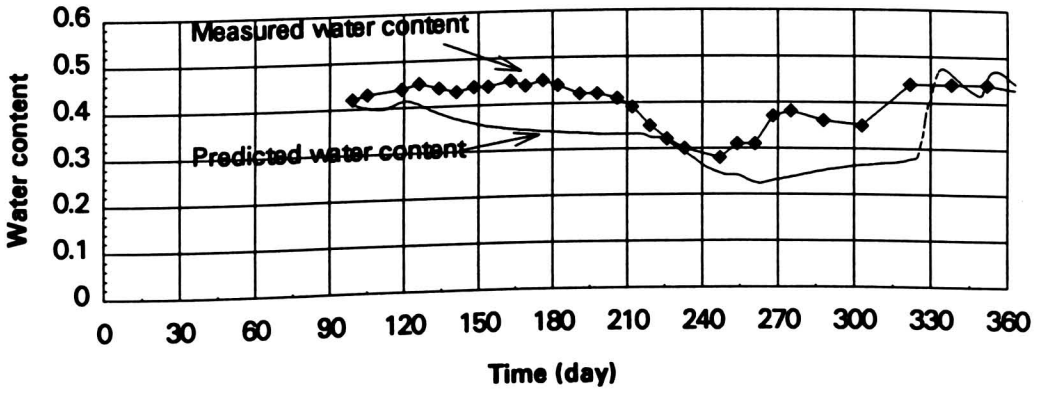

Figure 5.5 Comparison of water content at 45 cm in 1992.

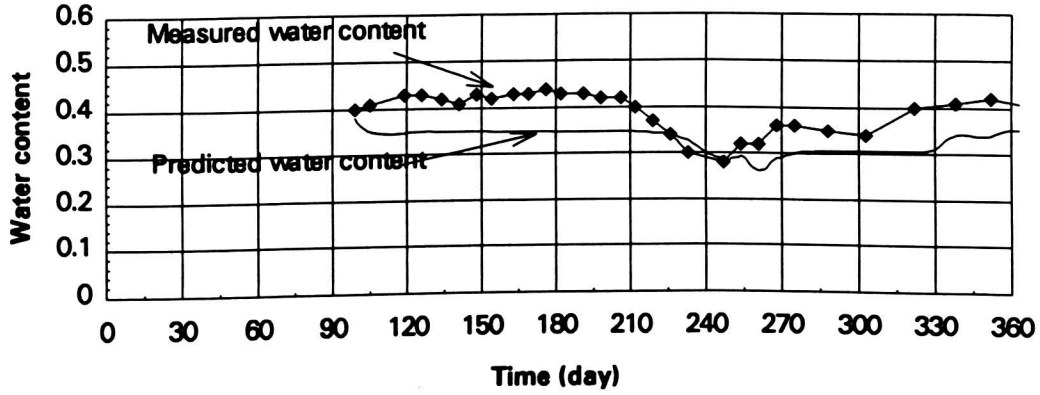

Figure 5.6 Comparison of water content at 60 cm in 1992.

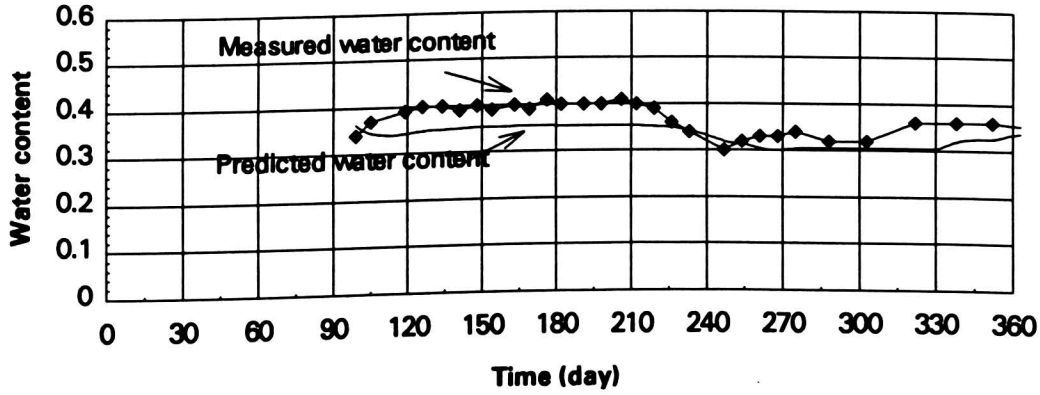

Figure 5.7 Comparison of water content at 75 cm in 1992.

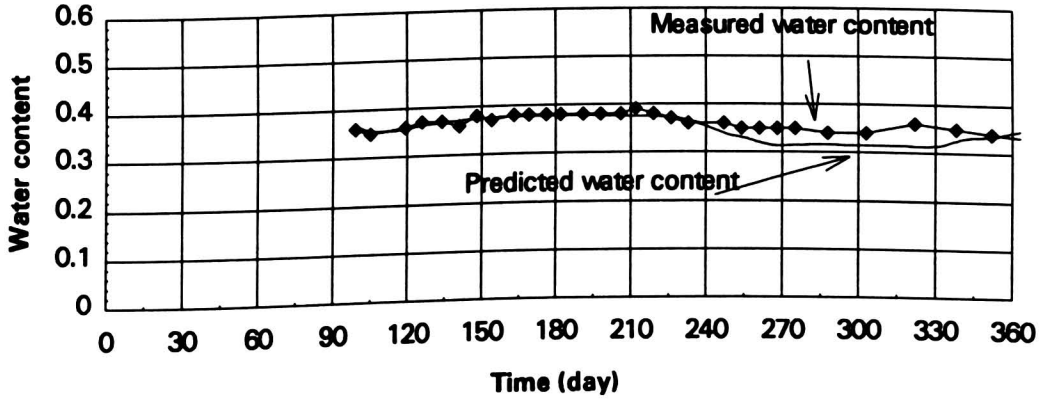

Figure 5.8 Comparison of water content at 90 cm in 1992.

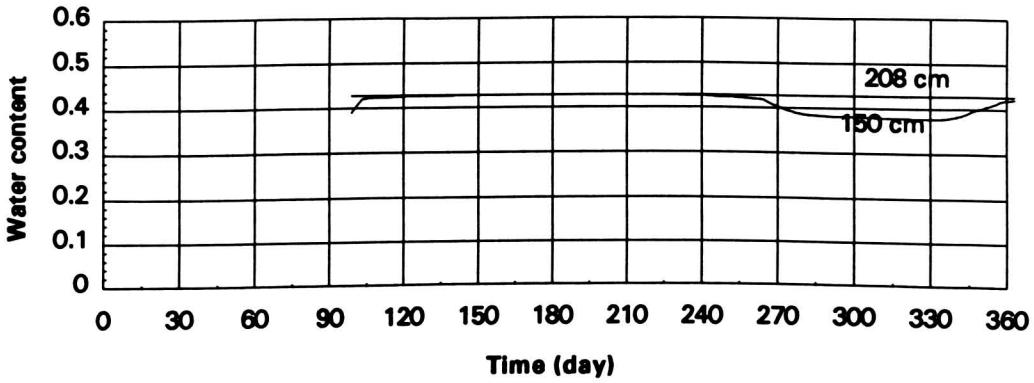

Figure 5.9 Predicted water content at 150 and 208 cm in 1992.

At 30 and 45 cm depth, the predicted water content is lower than the measured water content for most of the year except latter November and the whole December. At 60 and 75 cm depth, the predicted water content is lower than the measured water content for most of the year except latter August and early September (day 225 to day 245). At 90 cm depth, before day 240 the predicted water content coincides with the measured water content while after day 240 the predicted water content is lower than the measured water content. From Figure 5.9 it can be seen that at 150 cm depth, the predicted water content is still fluctuating during the fourth quarter of the year and at the bottom of the profile the predicted water content remains constant (saturated) during the whole simulation.

Why does the predicted water content match the measured water content so poorly while the predicted water table does match the measured water table? One possible explanation is that the plant (soybeans were planted in Plot 13 in 1992 and the maximum root depth of soybean is 0.8 m) took too much water from the profile. Now it is time to look at the result without plant at all.

C. Calibration without Planting. When there was no plant, the predicted water table does not match the measured water table very well (Figure 5.10).

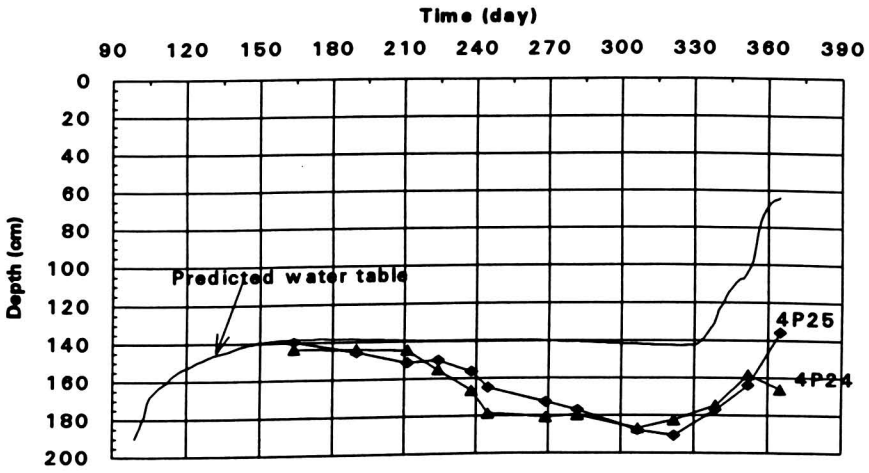

Figure 5.10 Measured and predicted water table without planting in 1992.

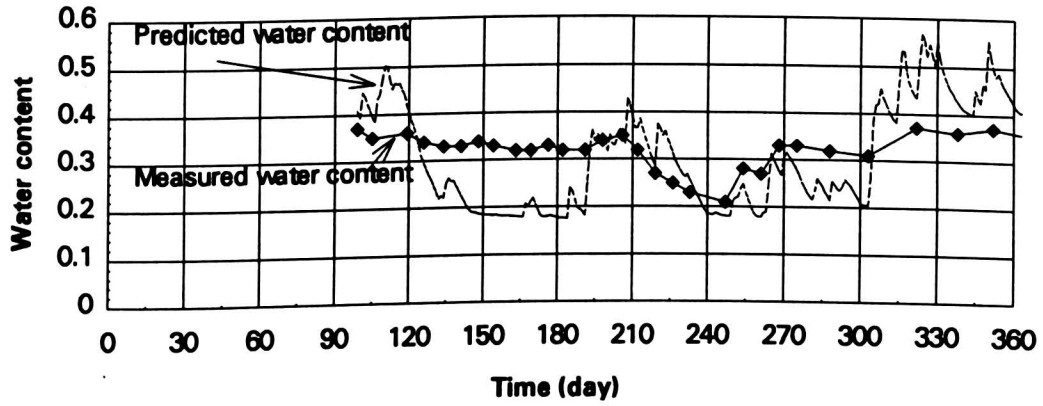

Figure 5.11 Comparison of water content at 15 cm without planting in 1992.

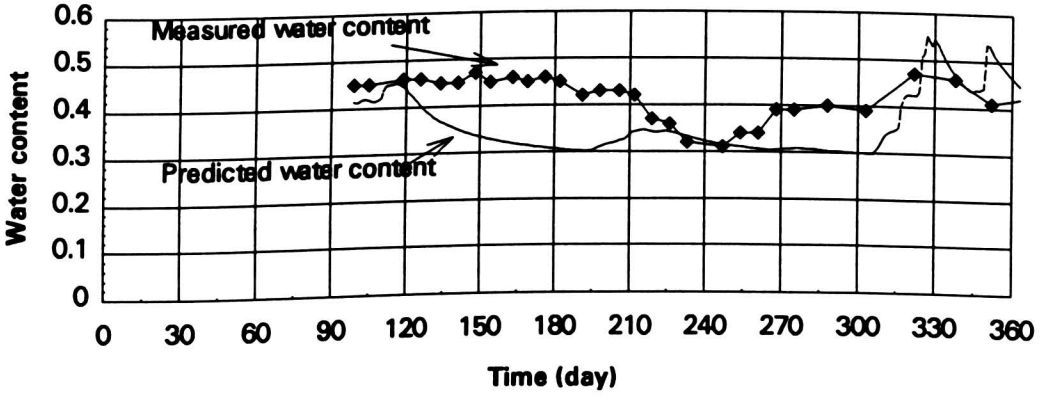

Figure 5.12 Comparison of water content at 30 cm without planting in 1992.

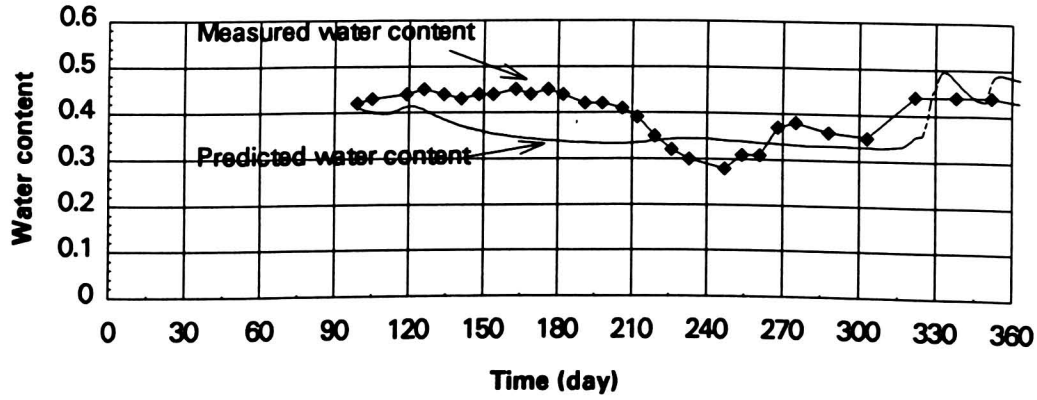

Figure 5.13 Comparison of water content at 45 cm without planting in 1992.

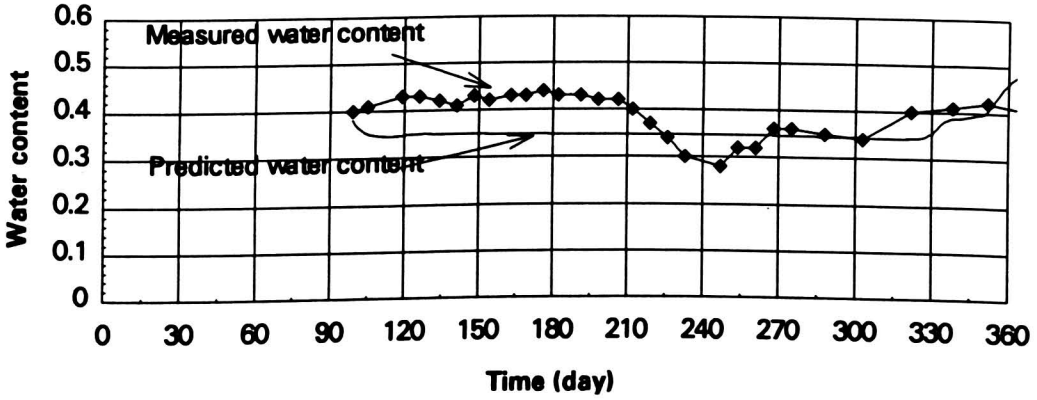

Figure 5.14 Comparison of water content at 60 cm without planting in 1992.

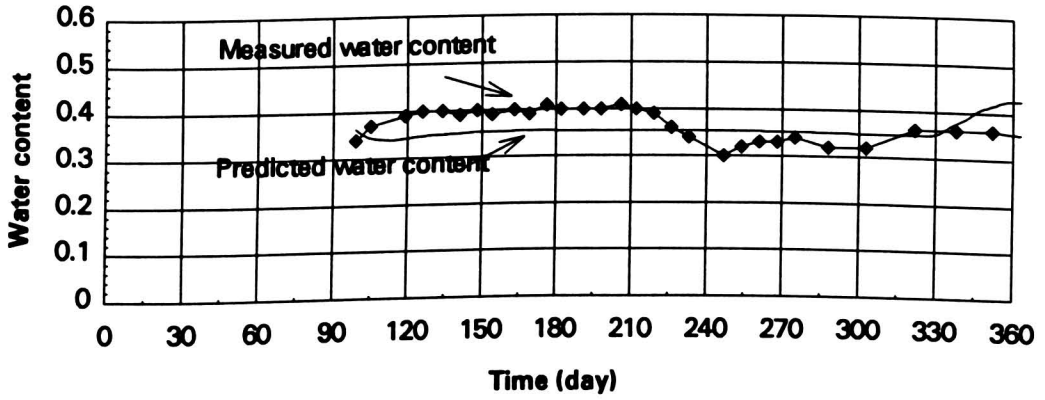

Figure 5.15 Comparison of water content at 75 cm without planting in 1992.

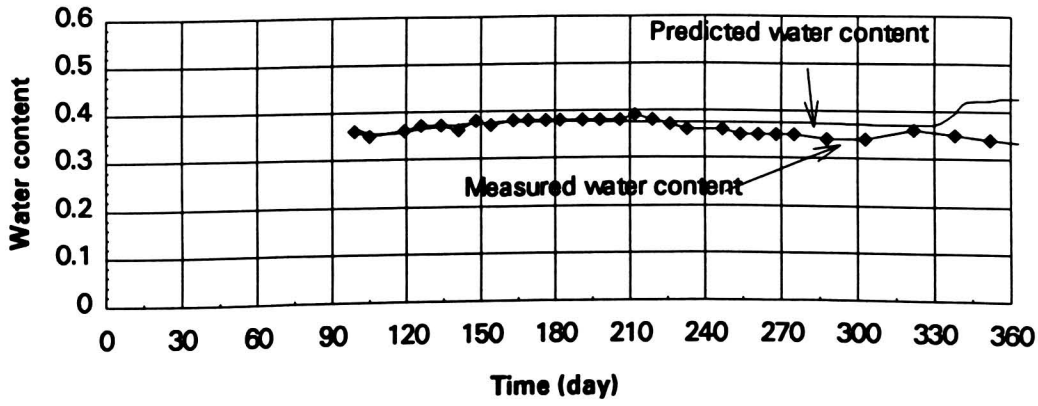

Figure 5.16 Comparison of water content at 90 cm without planting in 1992.

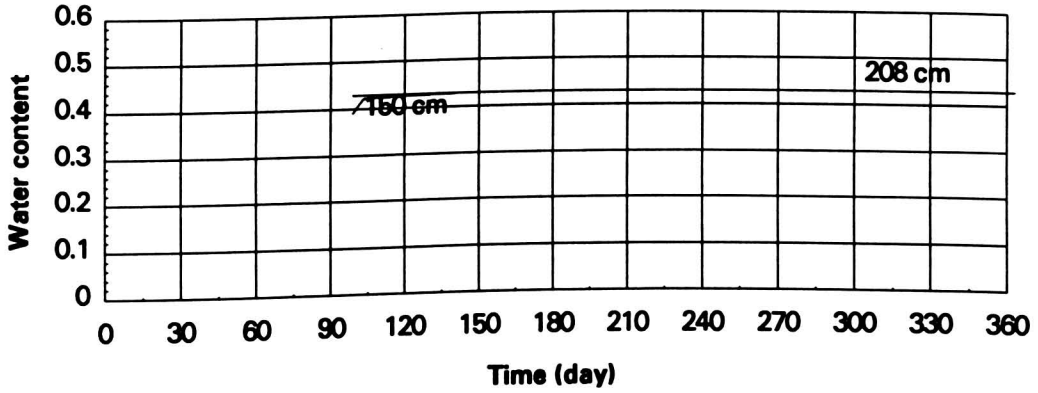

Figure 5.17 Predicted water content at 150 and 208 cm without planting in 1992.

The comparison between Figure 5.3 and Figure 5.11 shows that there is not any improving match between predicted water content and measured water content. The comparisons among Figure 5.4 through 5.8 and Figure 5.12 through 5.16 show that there are some improved matches, but the water content at Figure 5.12 through 5.16 do not fluctuate with measured water content between day 220 and 270. Figure 5.17 shows that predicted water content remains constant at 150 cm while Figure 5.9 shows that predicted water content still fluctuates at 150 cm depth.

Another possible explanation of the poor match between the predicted water content and the measured water content is that the soil hydraulic properties were not

accurate. An alternative is to use Rawls' mean values for those hydraulic properties (Rawls, et al., 1982).

D. Calibration by Using Rawls' Mean Hydraulic Properties. Rawls researched 1323 soils with about 5350 layers from 32 states in 1981 and came up with a set of hydraulic properties values (Rawls, 1982). Runs have been made by forcing the RZWQM to use Rawls' hydraulic properties values. The results showed that with a 208 cm deep profile, the water table could not remain in the profile, i. e., it fell down to 999 cm depth and never came up within the 208 cm range. Also, a lot of effort was spent in trying to keep the water table within the 208 cm range while varying the known soil hydraulic parameters supplied to the model. First, saturated hydraulic conductivities of all six layers used in the calibrations before were supplied to the model in order to let the model scale the conductivity curve to those given values. Second, one-third-bar soil water contents of all layers were supplied to the model. Third, instead of giving one-third-bar soil water contents, one-tenth-bar soil water contents were supplied to the model. Fourth, the measured soil hydraulic parameters in the fifth and sixth layers were supplied to the model. Finally, the measured soil hydraulic parameters in all layers except the third layer (B_t layer) were supplied to the model. All these efforts failed because the water table could not be retained within the 208 cm range.

In conclusion, the soil hydraulic properties used in the calibrations before the calibration using Rawls' mean hydraulic properties are reasonably correct, and no other hydraulic property values were found to improve the calibration.

5.4.2 Calibration Results for 1993

A. Water Table Calibration Result. Figure 5.18 shows that the predicted water

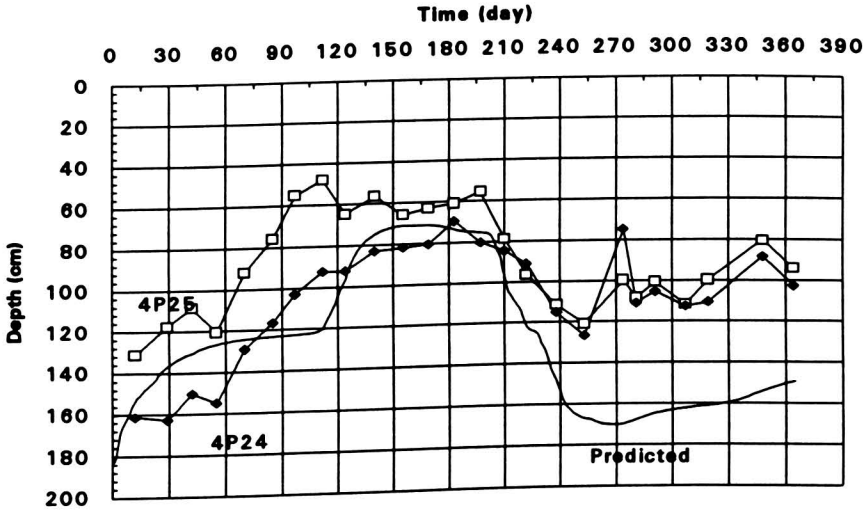

Figure 5.18 Measured and predicted water tables in 1993.

table coincides with the measured water table before day 210. After day 210 the predicted water table is lower than the measured water table. Since 1993 was a wet year, it seems that the model can not fit a wet year very well.

B. Water Content Simulation Results. Figure 5.19 shows that at the 15 cm depth the predicted water content fluctuates around the measured water content while the measured water content remains relatively stable. Figure 5.20 shows that at the 30 cm depth during most of the year the predicted water content is lower than the measured water content. Figure 5.21 shows that at the 45 cm depth the predicted water content coincides with the measured water content during January (day 1 to day 27), May, June and July (day 122 to day 205) while for the rest of the year the model under-predicts water content. Figure 5.22 shows that during May, June and July (day 122 to day 208) the model over-predicts water content while for the rest of the year the model under-predicted water content. Figure 5.23 shows that before day 115 predicted water content

coincides with measured water content while during the summer the model over-predicts water content and after summer the model under-predicts water content. Figure 5.24 shows that before day 228 the model over-predicts water content while after day 228 the model under-predicts water content. Figure 5.25 shows that at the 150 cm depth after day 240 water content is not constant. Overall, the model does not predicts water content in 1993 very well. The reason for the poor matches between the predicted water contents and the measured water contents is that the soil hydraulic properties used in the calibrations are reasonably correct, but they do not exactly represent the real soil hydraulic properties. In other word, the true soil hydraulic properties are not found yet.

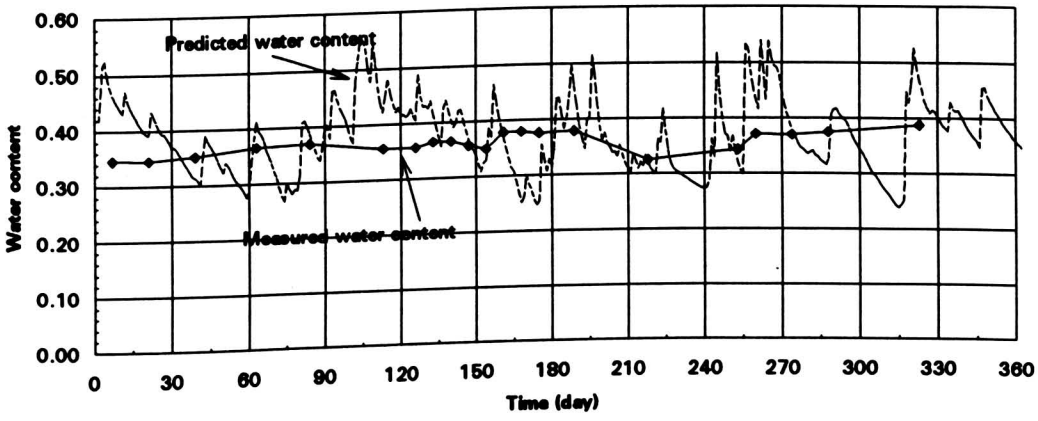

Figure 5.19 Comparison of water content at 15 cm in 1993.

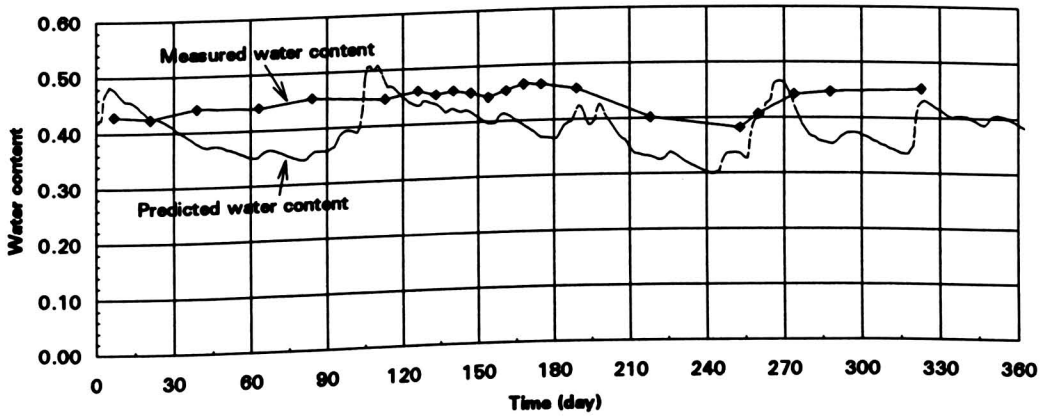

Figure 5.20 Comparison of water content at 30 cm in 1993.

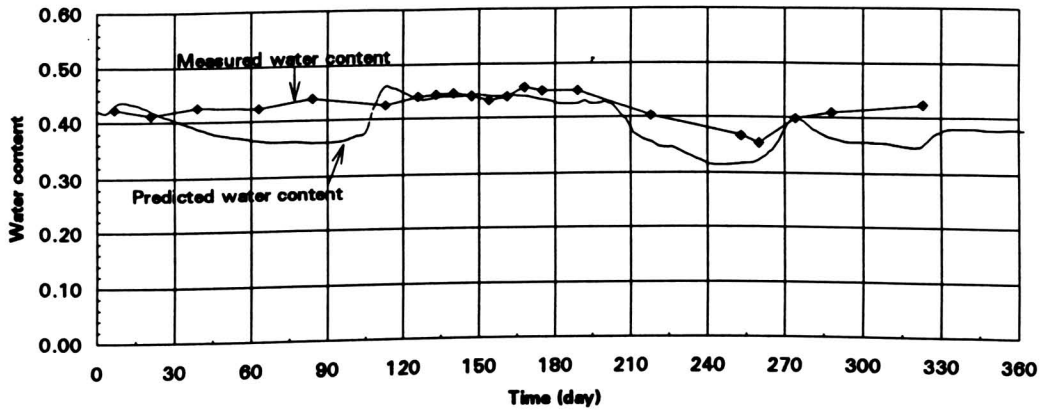

Figure 5.21 Comparison of water content at 45 cm in 1993.

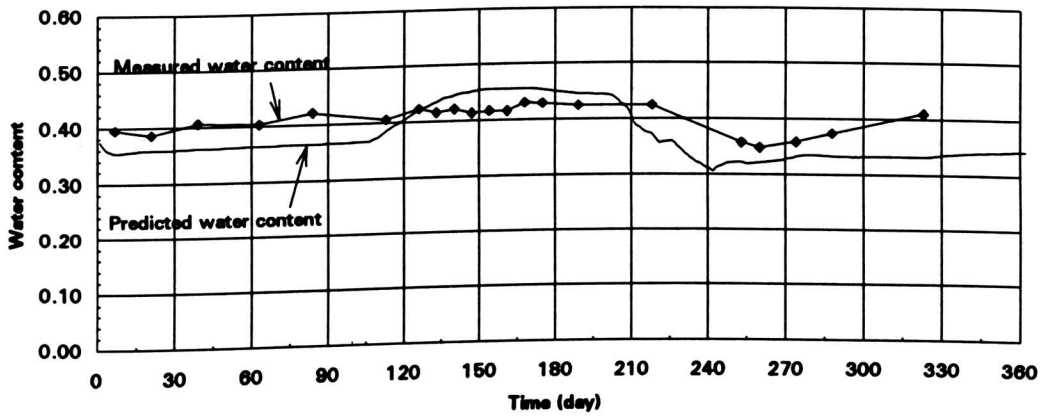

Figure 5.22 Comparison of water content at 60 cm in 1993.

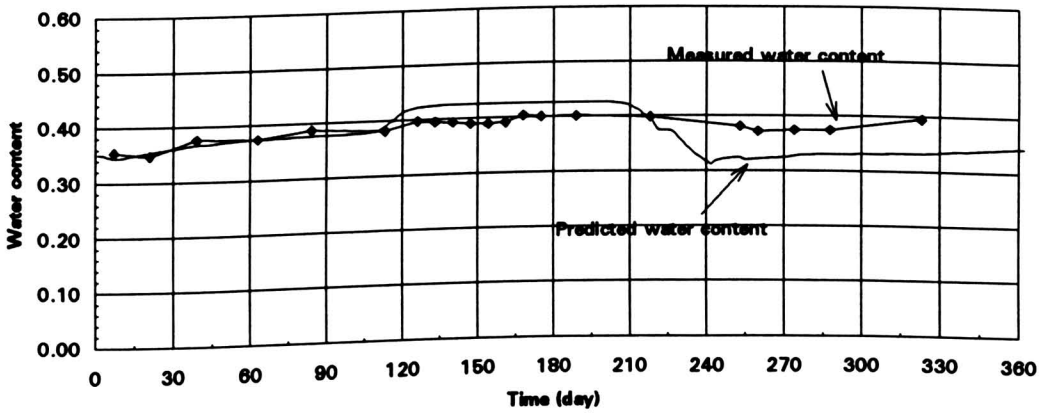

Figure 5.23 Comparison of water content at 75 cm in 1993.

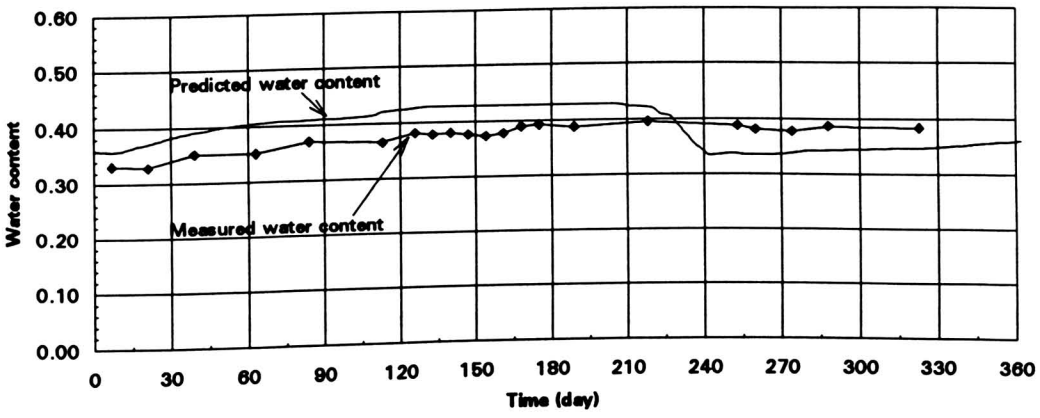

Figure 5.24 Comparison of water content at 90 cm in 1993.

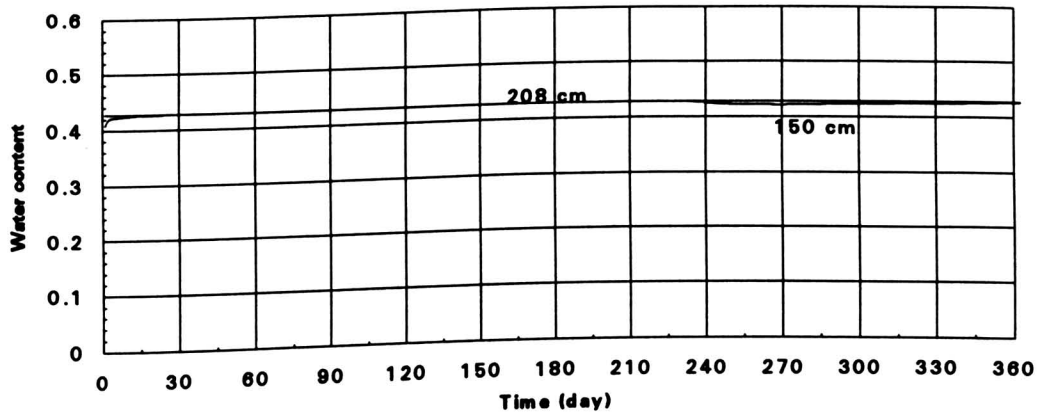

Figure 5.25 Predicted water content at 150 cm and 208 cm in 1993.

CHAPTER 6

SIMULATION RESULTS

In Chapter 5, the RZWQM was calibrated and applied for the situation when there are no cracks in the soil profile. In this chapter, the calibrated RZWQM is applied to simulate the situations when there are cracks in the soil profile. The simulations were conducted in the following ways: (1) run the model with input crack volume per unit area (V_{cr} cracking model) versus time; (2) run the model with crack width and length calculated from the cracking model using the water content calculated from the RZWQM (soil moisture cracking model); (3) run the model with constant crack width and length (constant cracking model). The revised RZWQM was used in the simulations with V_{cr} cracking model and with soil moisture cracking model. Since calibration is a kind of simulation, the nitrogen, alachlor, and atrazine simulation results from the calibration run in Chapter 5 are presented first. Another reason to present these results is that comparisons between the simulations with cracks and without cracks can be made.

6.1 Nitrogen and Alachlor Simulation Results without Macropores

6.1.1 Simulation Results for 1992

1. Nitrogen Simulation Results. In 1992 there was no nitrogen application because soybeans can fix nitrogen. However, an initial nitrogen concentration profile was specified in the initial data file RZINIT.DAT according to the measured values on April 29, 1992 at the summit position of Plot 13. Figure 6.1 and 6.2 show simulated nitrogen concentration at different depths. Figure 6.1 shows that at first the nitrogen concentrations at shallower depths (7.6 to 38.1 cm) fluctuate at a relatively high level, and then go to zero or near zero very quickly around day 195. Then, after day 270, the

concentrations go above zero gradually. After day 330, the concentrations begin to decrease again. The nitrogen concentration at 53.3 cm and 68.6 cm depths fluctuates following the type of shallower nitrogen concentration, but around day 200 the decrease of nitrogen concentration is smaller and the time to decrease is later. At deeper depths from 83.8 cm to 144.8 cm, the nitrogen concentrations increase first, then decrease and after day 330 increase again. At the depth deeper than 160 cm, nitrogen concentration remains almost constant near 1.10 ppm.

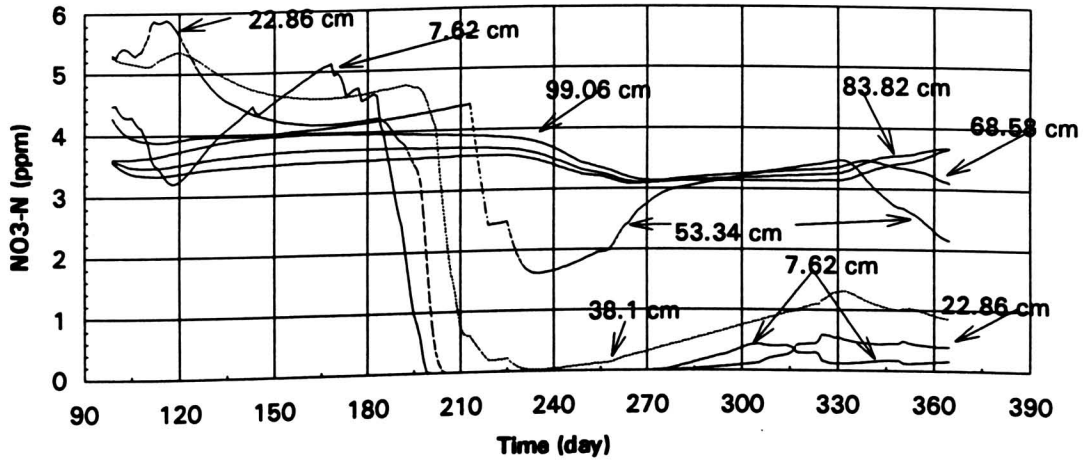

Figure 6.1 Nitrogen concentration at different depth (7-84 cm) in 1992.

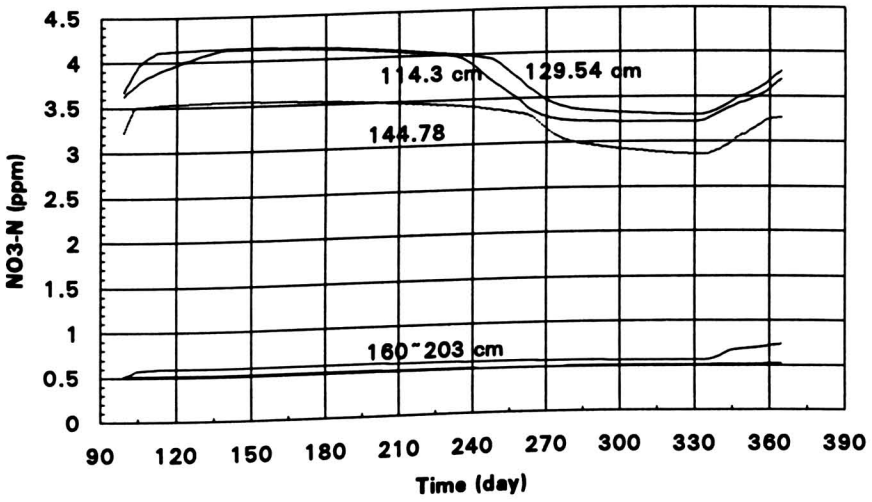

Figure 6.2 Nitrogen concentration at different depth (114-208 cm) in 1992.

It seems that the nitrogen concentration variation in 1992 run is reasonable. Nitrate nitrogen has four sources in the soil profile. The first source is the initial nitrogen concentration. The second one is from the production of plants, like soybeans. The third one is nitrification and the fourth one is fertilizer application. On the other hand, the nitrate nitrogen has three ways to dissipate. The first one is plant uptake. The second one is to move away with water movement. The third one is denitrification.

First, consider the nitrogen concentrations at 7.6 cm and 22.8 cm depths. At the beginning of the simulation the nitrogen concentration at 7.6 cm depth decreases sharply while the nitrogen concentration at 22.8 cm depth increases quickly. These two variations might be caused by water movement due to the rainfall between day 102 and day 117 (Figure 6.3). When it is day 118, the nitrogen concentration at 7.6 cm begins to increase and this increase may be caused first by nitrification of residue on the soil surface and then by the production of soybeans (in 1992, soybeans were planted on day 129). Around day 183, the nitrogen concentration at 7.6 cm begins to decrease sharply and reaches zero. This might be caused also by water movement due to the large rainfall between day 183 and day 212 (Figure 6.3). Another possibility is that nitrogen is taken up by soybeans

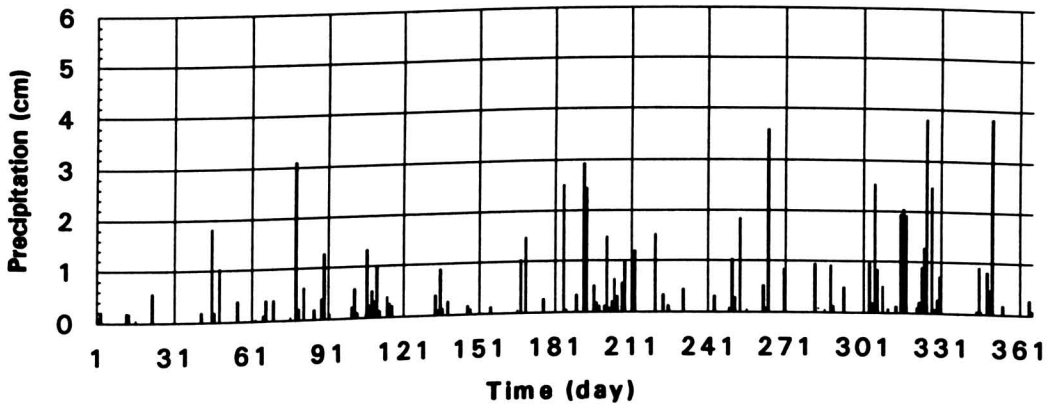

Figure 6.3 Precipitation in 1992.

because soybeans are in a fast growing stage. After day 275, the nitrogen concentration at 7.6 cm begins to increase gradually again and this is due to the decay of residue (soybeans were harvested on day 273 in 1992). The decrease after day 330 is due to precipitation. The reason for the nitrogen concentration change between 38.1 cm and 68.6 cm depth is the same as that of the nitrogen concentration at 7.6 cm depth. Next, consider the nitrogen concentration between 99.1 cm and 144.8 cm depth. At first it increases because water movement transports nitrate nitrogen from shallower depths to deeper depths. Then, around day 240, because there is a large amount of passing water with a near-zero nitrogen concentration (Figure 6.1) caused by the rainfall between day 183 and day 212, nitrogen is diluted at the depth between 99.1 cm and 114.8 cm. And around day 330, it increases again caused by the cumulative of nitrogen from shallower depth (Figure 6.1).

Last, consider the nitrogen concentration between 160 cm and 203 cm depth. The nitrogen concentration at this depth remains constant because of denitrification.

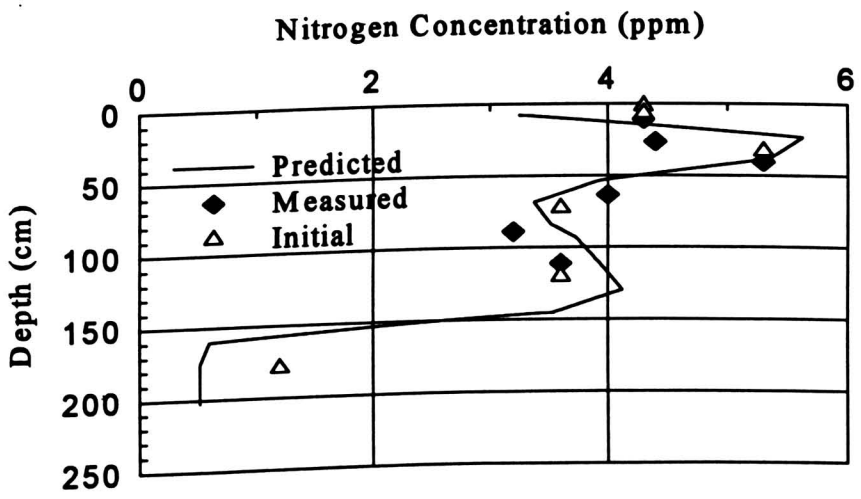

Figure 6.4 Nitrogen concentration profile on April 29, 1992.

The comparison between the predicted nitrogen concentration and the measured nitrogen concentration can show that the nitrogen concentration simulation is meaningful. On April 29, 1992 (day 120) and October 28, 1992 (day 302) nitrogen concentration in the soil profile were measured. As mentioned before, the initial nitrogen concentration was given according to the measured values on April 29, 1992. The RZWQM was run from April 8, 1992 (day 99) because the measured water content is available from that day on. After 21 days running, the predicted nitrogen concentration coincides with both measured and initial nitrogen concentrations (Figure 6.4).

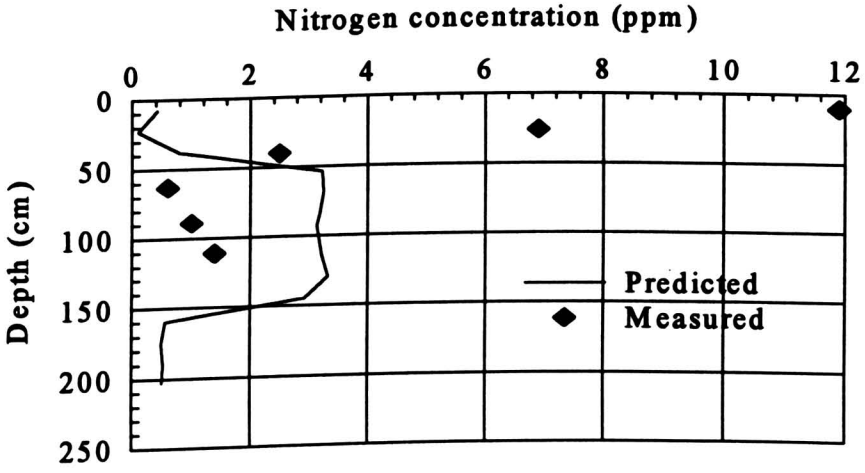

Figure 6.5 Nitrogen concentration profile on October 28, 1992.

The comparison of predicted nitrogen concentration and measured nitrogen concentration on October 28, 1992 shows that the model under-predicts the nitrogen concentration at shallow depth (Figure 6.5). At deeper depth (50-150) the model over-predicts nitrogen concentration. It is clear that the model puts too much weight on nitrogen movement with water so more nitrogen accumulates at depth 50 cm to 150 cm.

Another possibility for the under-prediction of nitrogen concentration at shallower depth is that the model may under-predict the production of nitrogen by soybean.

2. Alachlor Simulation Results. In 1992 alachlor was applied on Plot 13 on day 129 (when soybeans were planted) at a rate of 3.47 kg/ha. Figure 6.6 shows that on day 129 alachlor concentration is higher than 780 ppb and it decreases very quickly. Figure 6.7 shows that the down-movement of alachlor is very slow and alachlor appears at 22.8 cm depth from day 194 on (Figure 6.8). It seems that it takes 64 days for alachlor to move from depth 7.6 cm to depth 22.8 cm, about 0.24 cm/day. When alachlor appears at 22.8 cm depth, its concentration is very low also (about 0.001 ppb). The alachlor concentration deeper than 38.2 cm is zero. The measured alachlor concentration one moment before the application of alachlor on day 129 (April 29, 1992) and on day 302 (October 28, 1992) is less than 5.0 ppb (detection limit) in all soil cores from different depths. Because on day 128 (April 28) the predicted alachlor concentration for the whole profile is zero (initial value is zero also) and on day 302 (October 28) it is less than 5.0 ppb for the whole profile, it is safe to say that the model does not over-predict alachlor concentration.

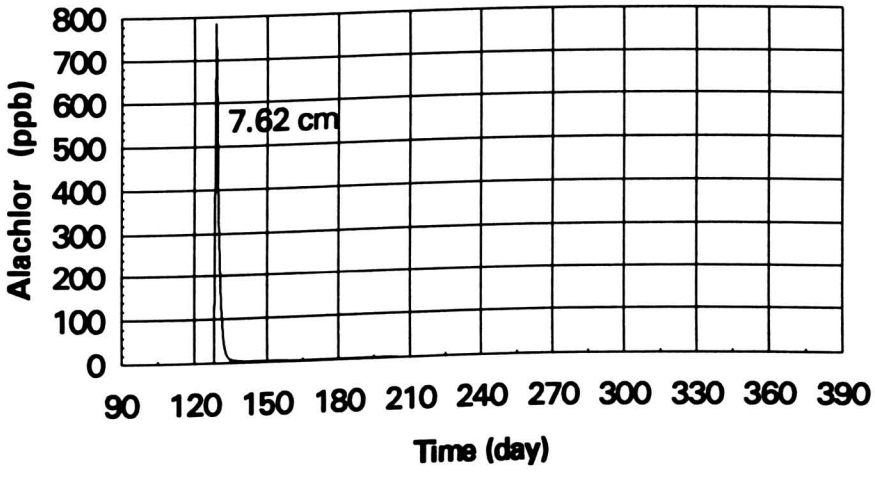

Figure 6.6 Predicted alachlor concentration at depth 7.6 cm in 1992.

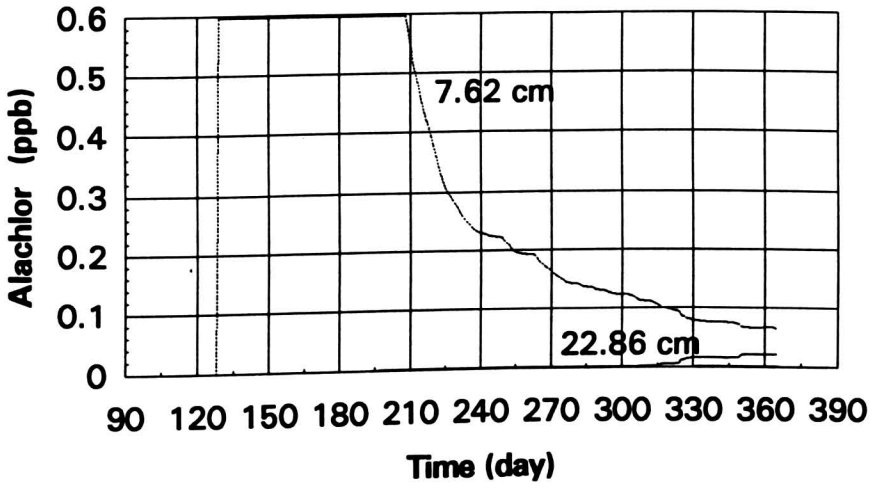

Figure 6.7 Predicted alachlor concentration at depth 7.6 cm and 22.8 cm in 1992.

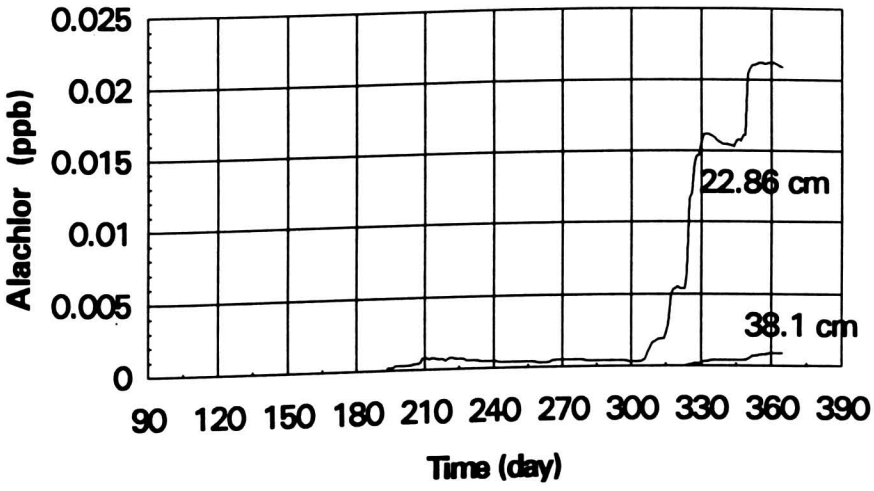

Figure 6.8 Predicted alachlor concentration at depth 22.8 cm and 38.1 cm in 1992.

6.1.2 Simulation Results for 1993

1. Nitrogen Simulation Results. In 1993 nitrogen was applied since corn was planted on Plot 13. The amounts of nitrate nitrogen, ammonium nitrogen and urea nitrogen applied were 35 kg/ha, 35 kg/ha and 70 kg/ha, respectively. The nitrogen application date was May 17 (day 137). Figure 6.9 shows that right after the nitrogen

application, the nitrate nitrogen concentration goes up sharply at the 7.6 cm depth. The nitrogen concentration at the 7.6 cm depth during this peak period is higher than 35 ppm. From day 1 to day 136 and from day 225 to day 365 the nitrogen concentration at the 22.8 cm depth is higher than the nitrogen concentration at the 7.6 cm depth. The nitrogen concentration at 22.8 cm is interesting (Figure 6.10). It has four main peaks (marked with the Roman numerals). The first peak is caused by the downward nitrogen movement above 22.8 cm depth since there were rains on day 2 and day 3 (Figure 6.12). The second peak seems unbelievable at first glance because there was no nitrogen application around day 105. Again, the peak is caused by the downward nitrogen movement above depth 22.8 cm due to several rainfalls around day 105 (Figure 6.12). Figure 6.9 also shows that around 105 the nitrogen concentration at depth 7.6 cm goes down while the nitrogen concentration at depth 22.8 cm goes up. Because the B_t horizon (10 to 55 cm) is a clay horizon, water and nutrients can accumulate at the top portion of the B_t horizon. The third peak is much later and lower than the peak at depth 7.6 cm. The peak delay time is about 18 days. The fourth peak is 25 days later than the third peak but is higher than the later. The comparison between the nitrogen concentration at depth 22.8 cm and precipitation in 1993 will reveal that the four peaks are related to rainfall events which cause nitrogen to move downward. The nitrogen concentration decrease around day 210 is caused by corn uptake for at that time corn is in a rapid growth stage. Because root distribution decreases with the increase in depth, the nitrogen concentration increases with an increase in depth (Figure 6.10). Although the maximum root system depth is specified to 0.95 meter, the effect of the root zone on nitrogen concentration still can be seen down to the depth of about 130 cm (Figure 6.11). The nitrogen concentration between the 160 and 203 cm depths remains constant but at a lower value compared to that in 1992 (Figure 6.2). The reason for this could be that there is more rain in 1993 than in 1992. Rain causes nitrogen dilution and washes away nitrogen as runoff.

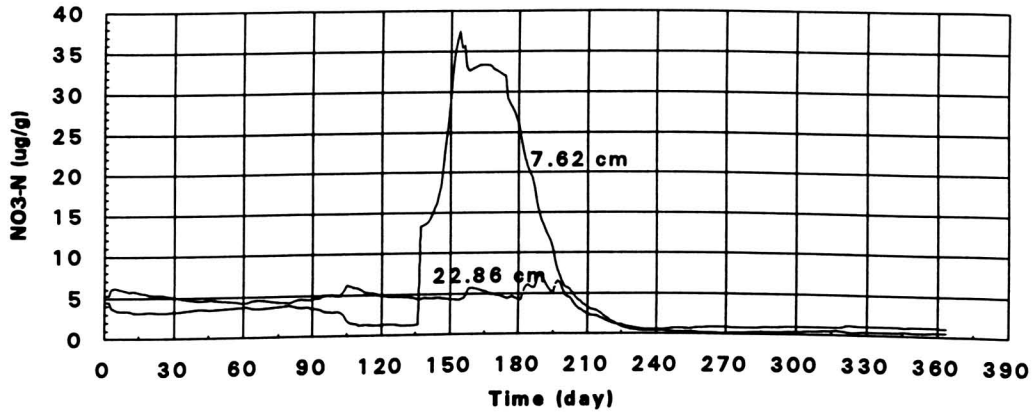

Figure 6.9 Nitrogen concentration at 7.62 cm and 22.86 cm in 1993.

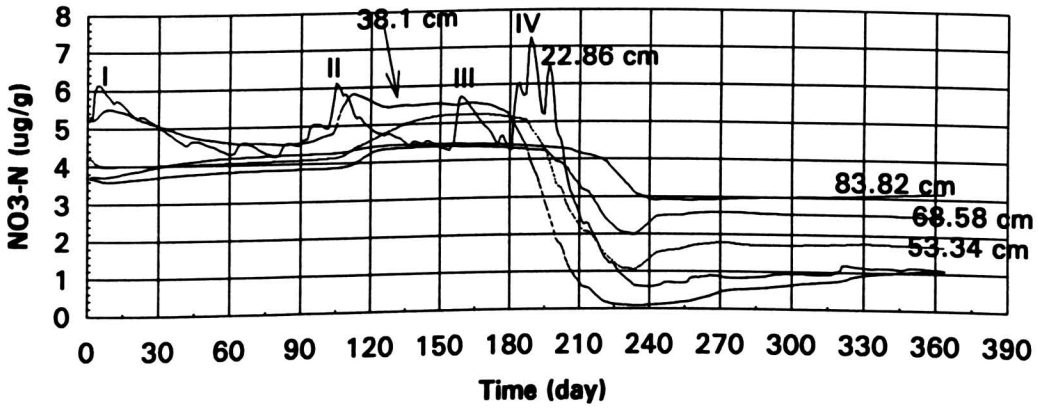

Figure 6.10 Nitrogen concentration at different depths (22-84 cm).

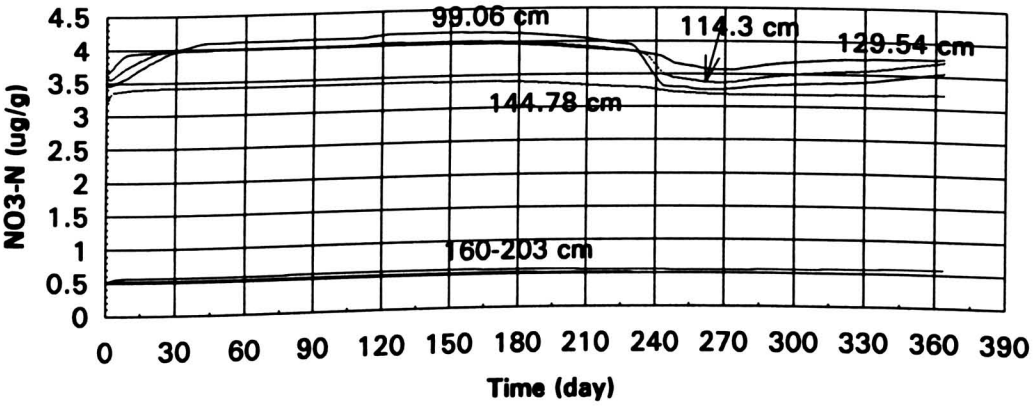

Figure 6.11 Nitrogen concentration at different depths (99-203 cm).

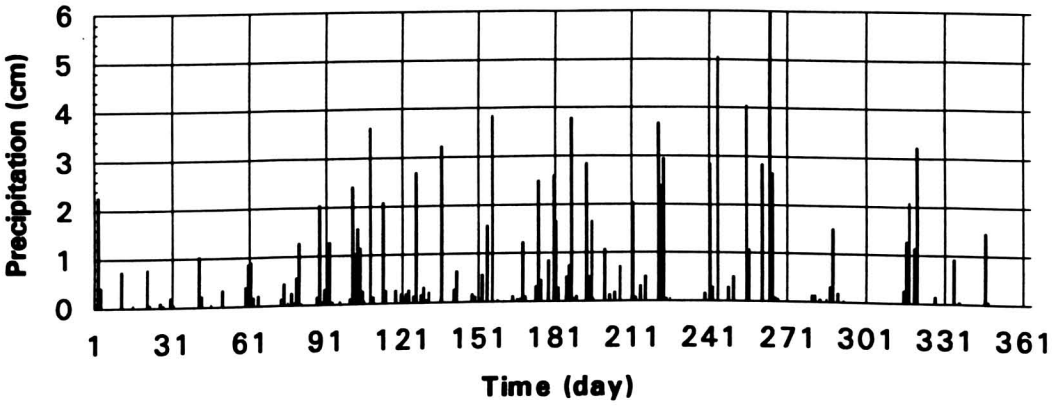

Figure 6.12 Precipitation in 1993.

* For comparison with Figure 6.3, Figure 6.12 is scaled to 6 cm on precipitation. Therefore, the rainfall data on day 265 which is 15.164 cm can not be plotted correctly.

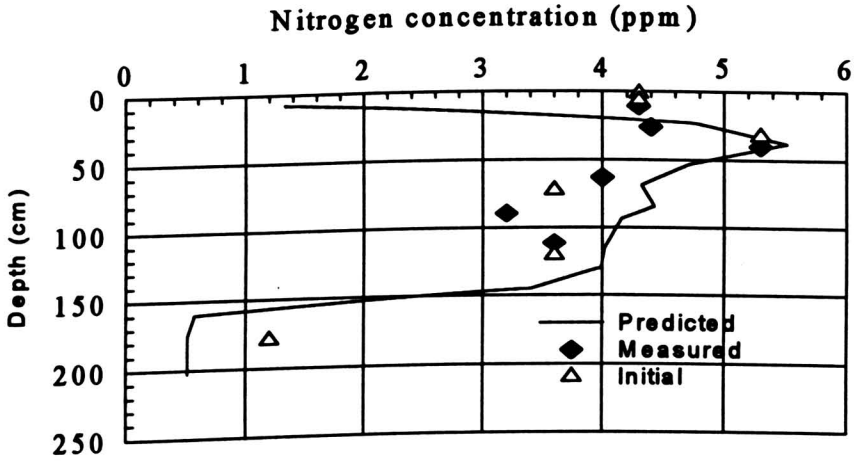

Figure 6.13 Nitrogen concentration profile on May 4, 1993.

Figure 6.13 shows the measured nitrogen concentration and predicted nitrogen concentration on May 4, 1993. The initial nitrogen concentration is the same as used in the 1992 run because there was no measured nitrogen concentration on January 1, 1993. The comparison of measured nitrogen concentrations on October 28, 1992 (Figure 6.5) and on May 4, 1993 shows that the initial concentration used is reasonable. Figure 6.13 shows that at shallower depths (0-22 cm) the model under-predicts nitrogen concentration

while the difference between measured and predicted nitrogen concentration between depths 22 cm and 68 cm is small. The model over-predicts nitrogen concentration at depths 70 cm to 123 cm. Overall, the predicted nitrogen concentration is meaningful.

2. Alachlor Simulation Results. In 1993 alachlor was applied on Plot 13 on the day 137 (when corn was planted) and the amount applied was 3.02 kg/ha. Figure 6.14 shows that on day 137 alachlor concentration is very high (about 800 ppb) and it decreases very quickly. Figure 6.38 shows that the alachlor concentration at the 22.86 cm depth is very low (less than 0.11 ppb) compared to the alachlor concentration at the 7.6 cm depth. Alachlor first appears at a concentration of 0.0006 ppb at depth 22.8 cm on day 155 (Figure 6.15). It only takes eighteen day for alachlor to move from 7.6 cm to 22.8 cm and the speed is about 0.85 cm/day. Compared to the result from Figure 6.7 it can be seen that alachlor moves faster in 1993 than in 1992. The reason for this is that in 1993 there is more rain than in 1992 (the total rainfall in 1992 is 76.962 cm while the total rainfall in 1993 is 125.171 cm). So, the more rain, the more soil water movement, the faster alachlor can move. Figure 6.16 shows that alachlor concentration at depth 38.1 cm is very low (less than 0.001 ppb) and can be neglected.

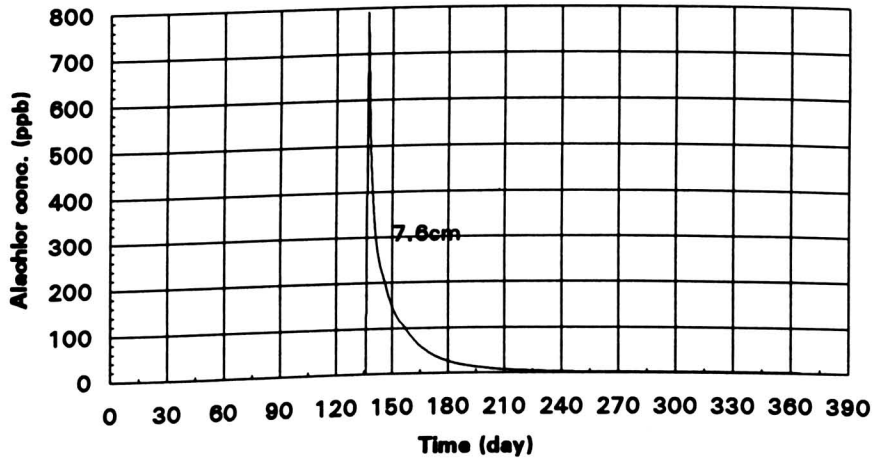

Figure 6.14 Predicted alachlor concentration at depth 7.6 cm in 1993.

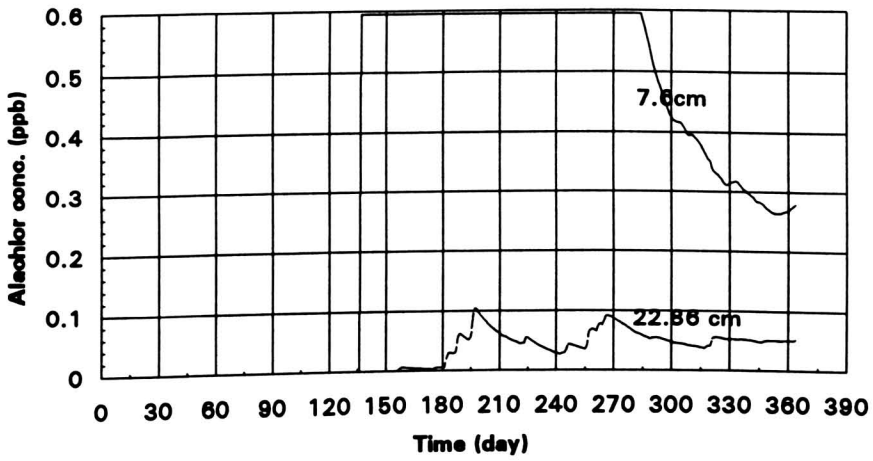

Figure 6.15 Predicted alachlor concentration at depth 7.6 cm and 22.8 cm.

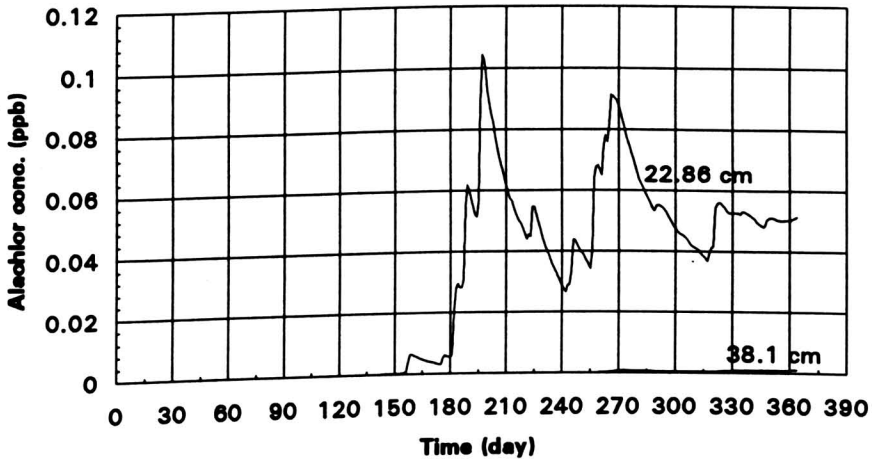

Figure 6.16 Predicted alachlor concentration at depth 22.8 cm and 38.1 cm.

3. Atrazine Simulation Results. In 1993 atrazine was applied on Plot 13 on the day 137 (when corn was planted) and the amount applied was 2.24 kg/ha. Figure 6.17 shows that on day 137 atrazine concentration is very high (about 900 ppb) and it decreases very quickly. Figure 6.18 shows that the atrazine concentration at the 22.86 cm depth is not too low, about 20 ppb. Figure 6.19 shows that atrazine can reach as deep as 68.6 cm although atrazine concentration at that depth is low.

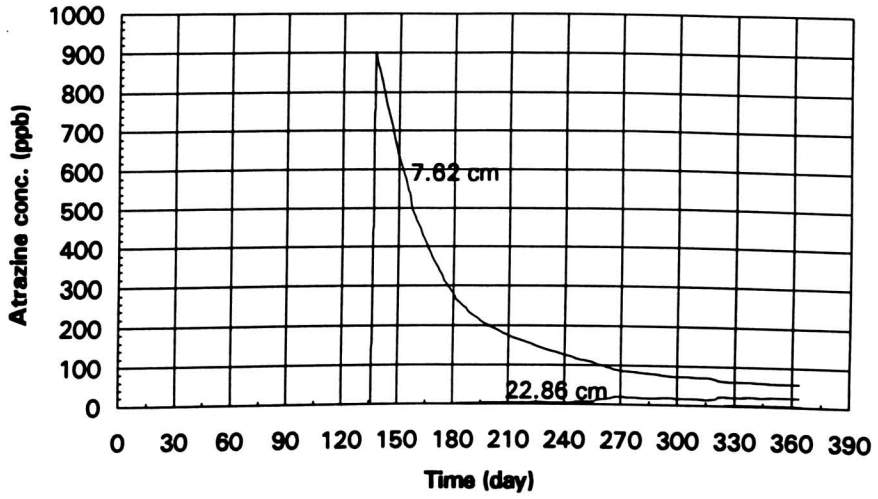

Figure 6.17 Predicted atrazine concentration at depth 7.6 cm and 22.8 cm.

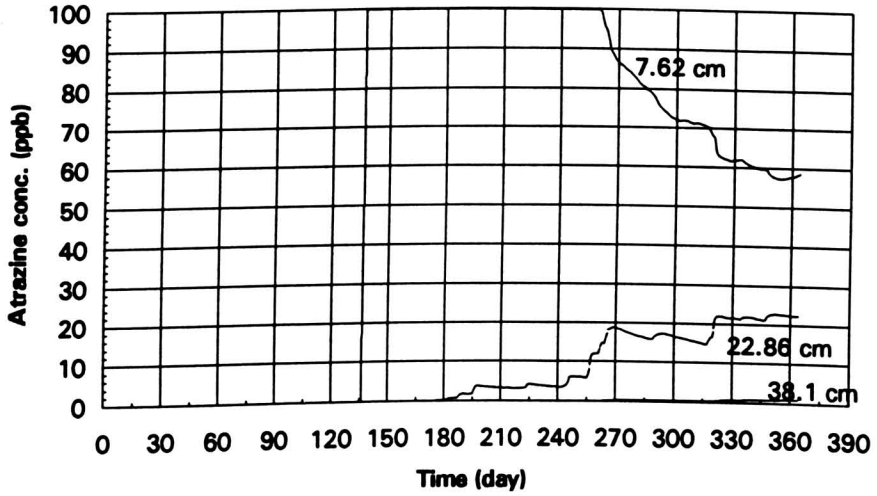

Figure 6.18 Predicted atrazine concentration at depth 22.8 cm and 38.1 cm.

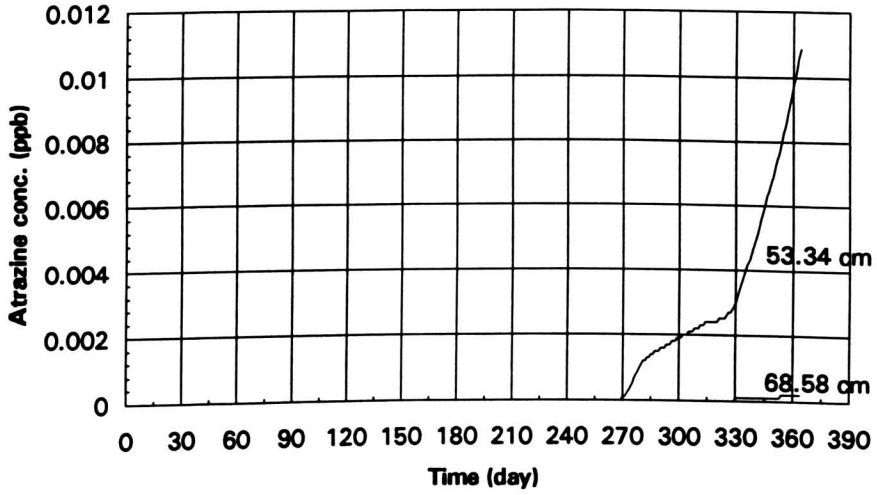

Figure 6.19 Predicted atrazine concentration at depth 53.3 cm and 68.6 cm.

Comparison between Figure 6.14 and 6.17 shows that atrazine has a higher concentration at the same depth than alachlor although the applied amount of atrazine is lower than that of alachlor (2.24 kg/ha to 3.02). Therefore, atrazine lasts longer than alachlor in the environment.

6.2 Simulation Results Using V_{cr} Cracking Model

As discussed in Chapter 3, disk elevation data were collected and used to calculate V_{cr} (cack volume per unit area). In this section, discussion will be focused on the simulation results using V_{cr} cracking model.

6.2.1 Simulation Results of 1992

The data on Table 3.3 and 3.4 are not on daily base while the RZWQM needs daily V_{cr} data. Therefore, interpolation was used to obtain the daily data of V_{cr}. Figure 6.20 shows the output crack width after inputting daily V_{cr} into the revised RZWQM. In the simulation, it was assumed that there were no cracks below 90 cm where water content was relatively high and near saturation. If input V_{cr} data are not zero for a horizon, the revised RZWQM will have cracks for that horizon. Since the model does not allow cracks in the top horizon, holes were assumed to exist in this top horizon (see Section 2.6). Therefore, if there were cracks in the Ap horizon, holes appeared in the top horizon also.

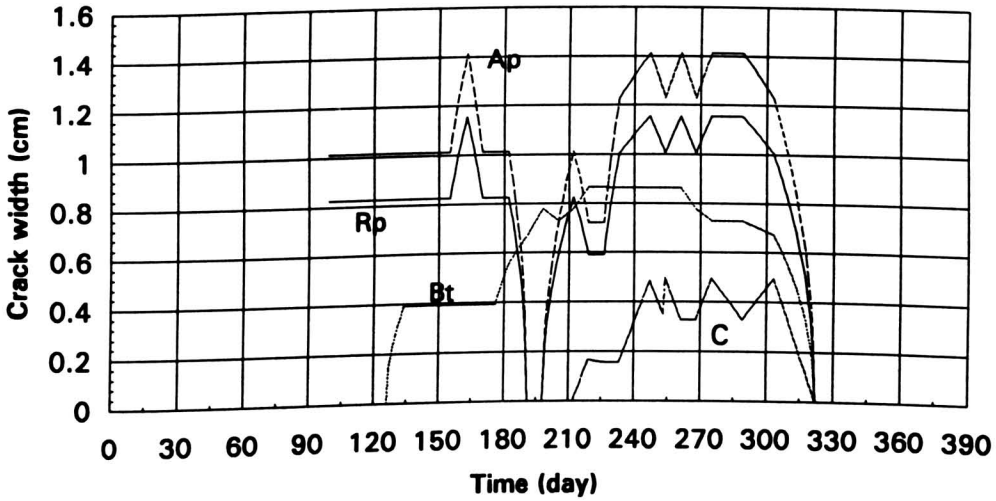

Figure 6.20 Crack widths in 1992 simulation using V_{cr} cracking model.
* R_p is the radius of the cylindrical hole in the synthetic horizon on the top of the soil profile.

A. Water Table Simulation Result. The match between the predicted and measured water talbe in Figure 6.21 is approximately the same as that in Figure 5.2, except for an improvement in Figure 6.21 between day 300 and 366. The reason for this better match is that cracks can transport more water to deeper locations than the case when there are no cracks in the soil profile. Figure 6.3 shows that after day 300 there were several heavy rains and before day 300 there were less and lighter rains. Figure 6.20 shows that there are cracks in the soil profile after day 300. Cracks plus rainfall result in the rise of the water table.

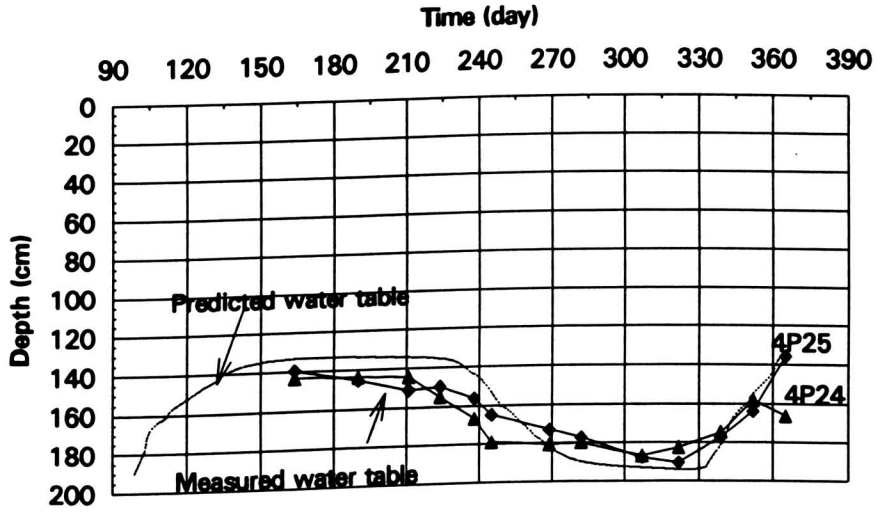

Figure 6.21 Measured and predicted water tables using V_{cr} cracking model in 1992.

B. Water Content Simulation Results. The comparisons between Figure 5.3 through 5.8 and Figure 6.22 through 6.27 show that there are some small improvements among Figure 6.22 through 6.27. Figure 6.28 shows the same thing as Figure 5.9.

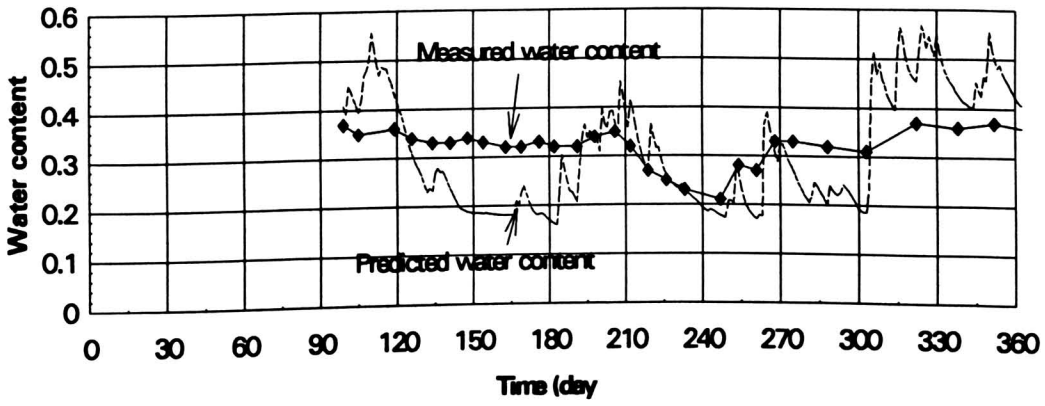

Figure 6.22 Comparison of water content at 15 cm using V_{cr} cracking model in 1992.

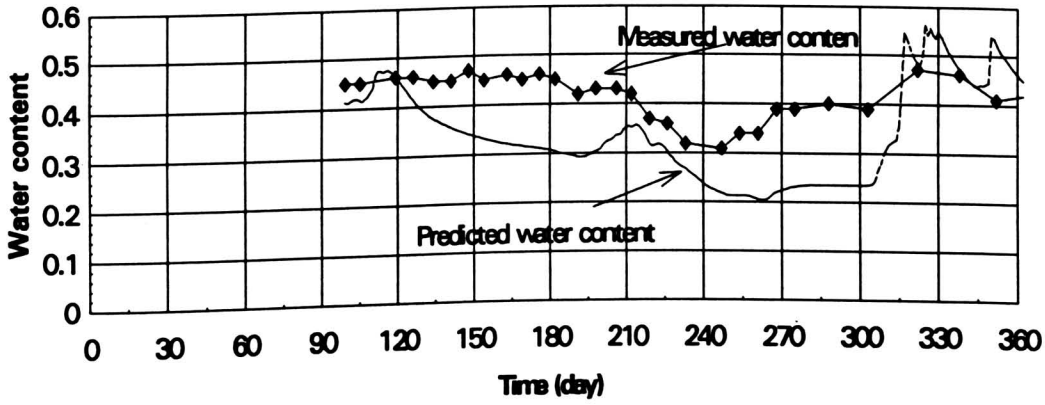

Figure 6.23 Comparison of water content at 30 cm using V_{cr} cracking model in 1992.

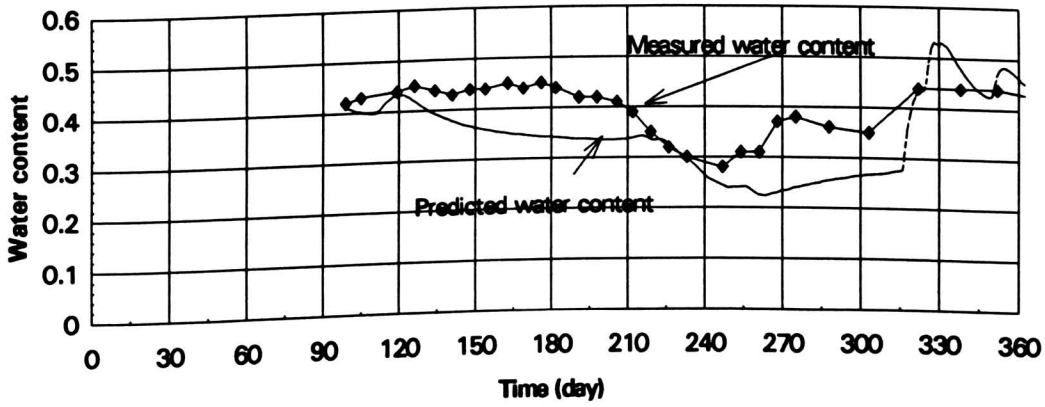

Figure 6.24 Comparison of water content at 45 cm using V_{cr} cracking model in 1992.

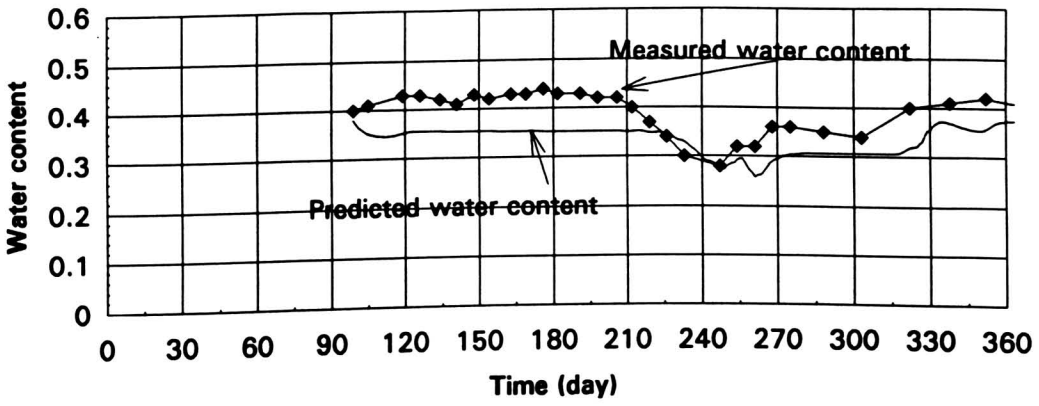

Figure 6.25 Comparison of water content at 60 cm using V_{cr} cracking model in 1992.

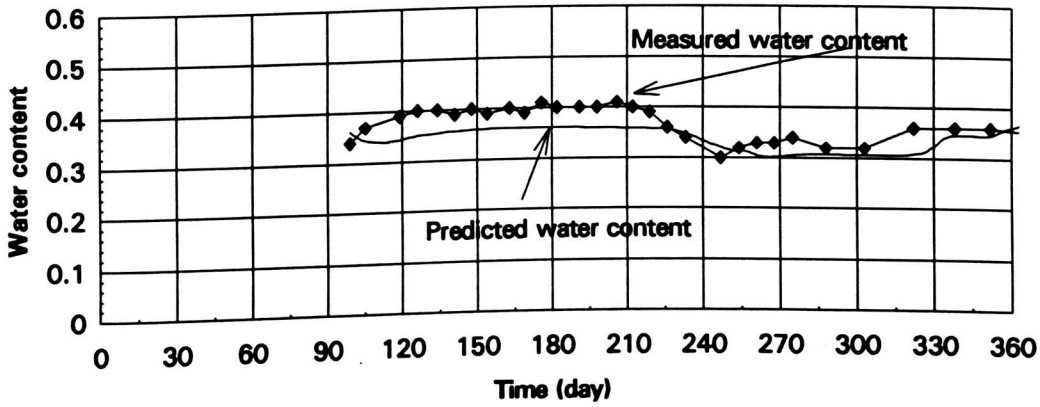

Figure 6.26 Comparison of water content at 75 cm using V_{cr} cracking model in 1992.

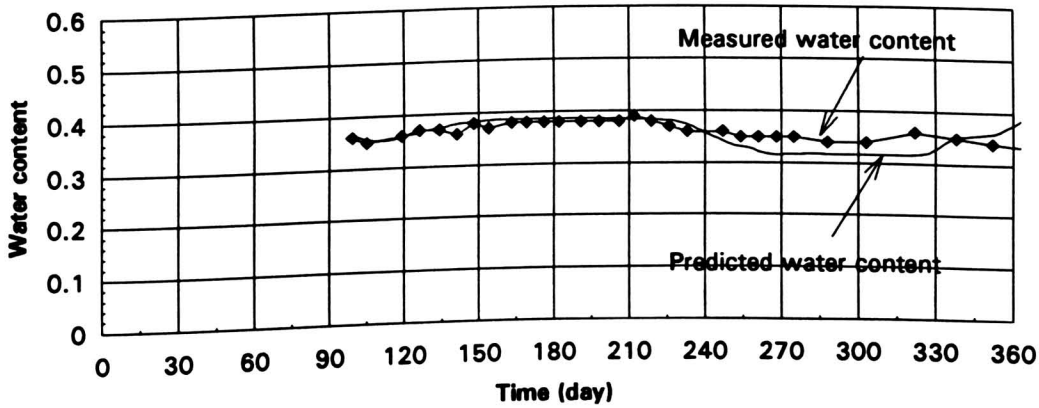

Figure 6.27 Comparison of water content at 90 cm using V_{cr} cracking model in 1992.

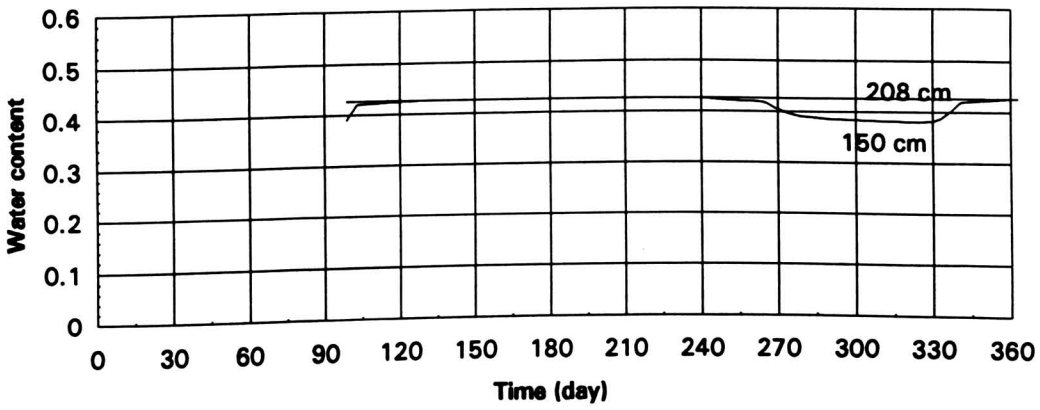

Figure 6.28 Predicted water content at 150 and 208 cm using V_{cr} cracking model in 1992.

C. Nitrogen and Alachlor Simulation Results

1. Nitrogen Simulation Results. Comparison between Figure 6.1 and Figure 6.29 shows that because of the existence of cracks, the nitrogen concentration at 7.6 cm from day 99 to day 180 in Figure 6.29 is lower than that in Figure 6.1 while the nitrogen concentration at 22.8 cm around day 120 in Figure 6.29 is higher than in Figure 6.1. Also, the nitrogen concentration from depth 38 cm to about 80 cm in the second half of the year in Figure 6.29 is lower than that in Figure 6.1, while the nitrogen concentration from depth 90 cm to 145 cm in Figure 6.29 and 6.30 is higher than that in Figure 6.1 and 6.2.

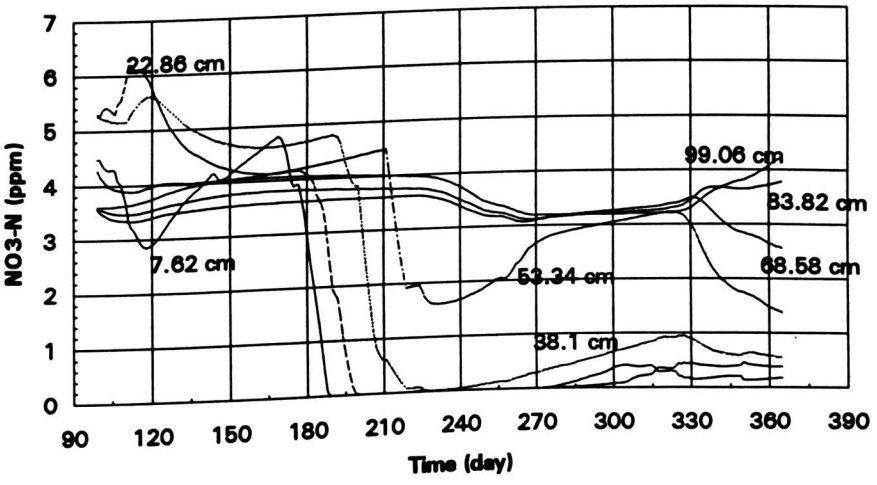

Figure 6.29 Nitrogen concentration at depth 7-100 cm using V_{cr} cracking model.

What this means is that cracks transport some nitrogen to deeper depth and some amount of nitrogen accumulates in the depth where there are no cracks (depth deeper than 90 cm). Figure 6.31 and 6.32 show the same trend as Figure 6.4 and 6.5.

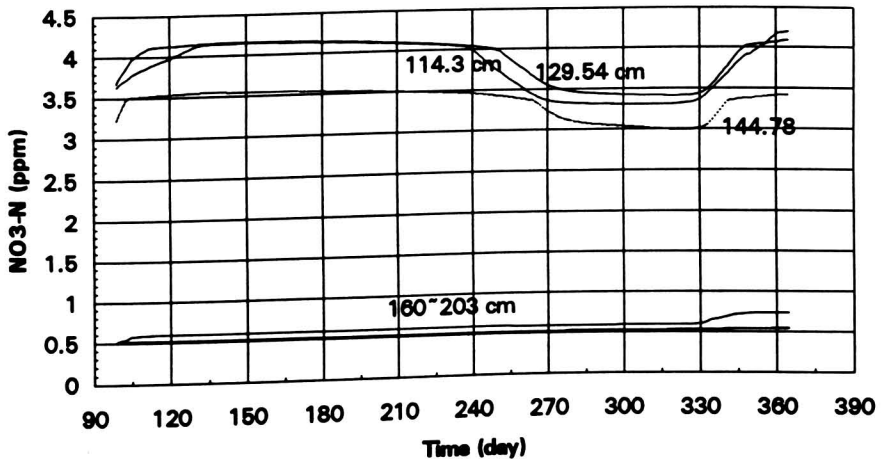

Figure 6.30 Nitrogen concentration at depth 114-203 cm using V_{cr} cracking model.

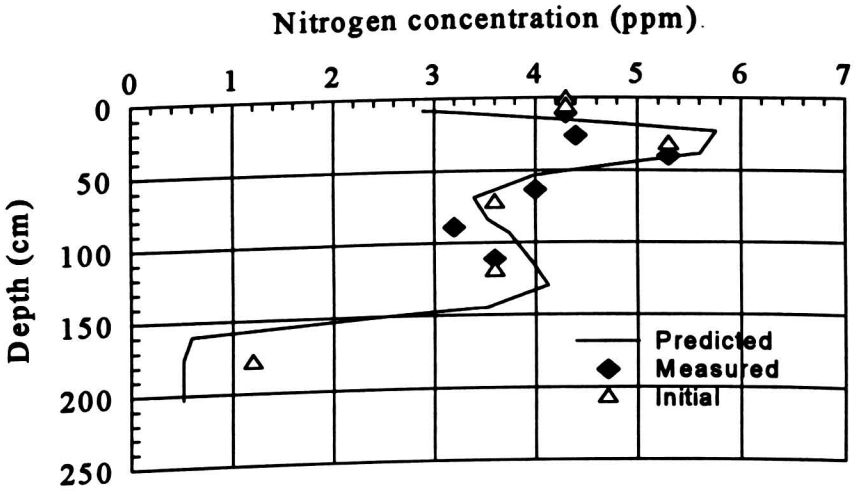

Figure 6.31 Nitrogen concentration profile on April 29, 1992 using V_{cr} cracking model.

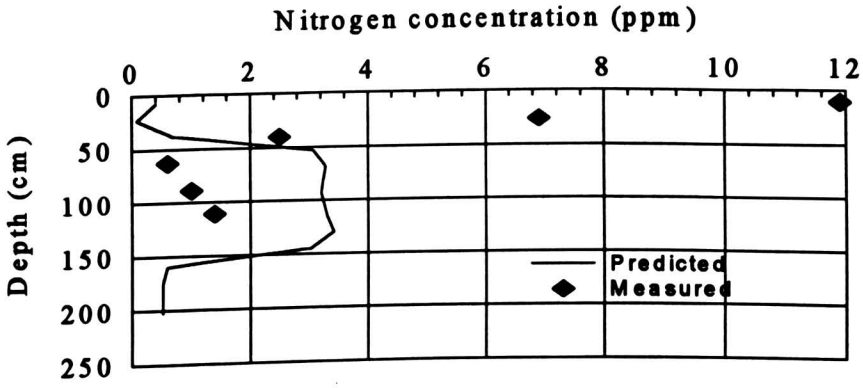

Figure 6.32 Nitrogen concentration profile on Oct. 28, 1992 using V_{cr} cracking model.

2. Alachlor Simulation Results. Comparison between Figure 6.6 and 6.33 shows that the peak alachlor concentration at depth 7.6 cm in Figure 6.6 is almost the same as that in Figure 6.33. However, the comparison between Figure 6.7 and Figure 6.34 shows that the alachlor concentration at depth 7.6 in Figure 6.34 is lower than that in Figure 6.7. The comparison between 6.8 and Figure 6.35 shows that the alachlor concentrations at the 22.8 cm and 38.1 cm depths in Figure 6.35 are lower than that in Figure 6.8, but the appearance of alachlor at depth 22.8 cm in Figure 6.35 is nine days earlier than that in Figure 6.8. All these mean that cracks play an important role in the transportation of pesticides.

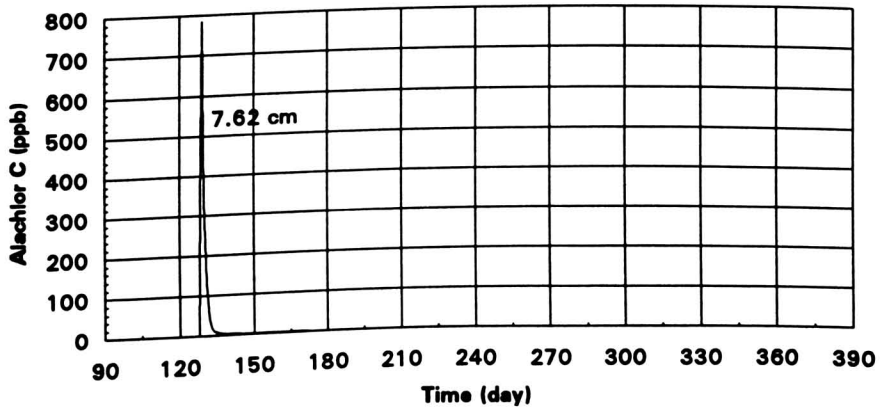

Figure 6.33 Predicted alachlor concentration at depth 7.6 cm using V_{cr} cracking mode.

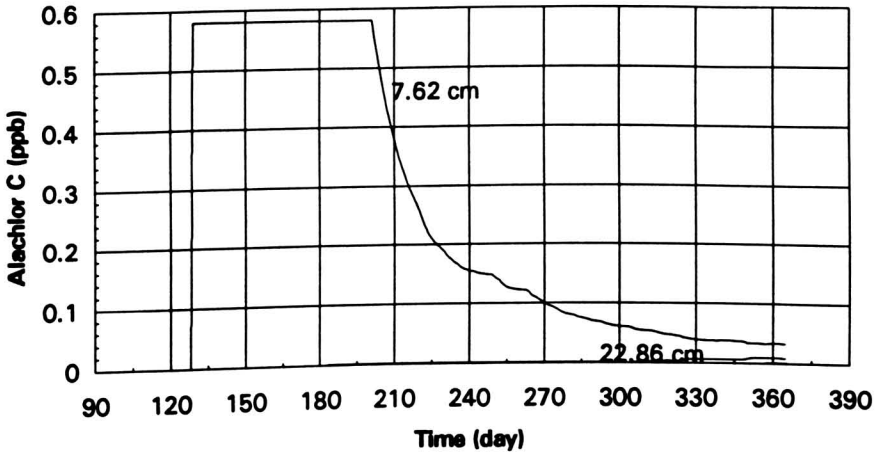

Figure 6.34 Predicted alachlor concentration at depth 7.6 cm and 22.8 cm using V_{cr} cracking model.

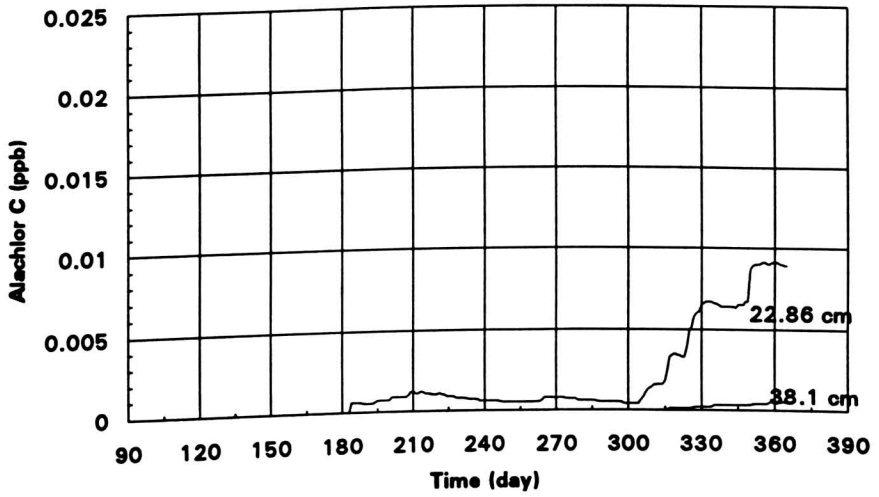

Figure 6.35 Predicted alachlor concentration at depth 22.8 cm and 38.1 cm using V_{cr} cracking model.

6.2.2 The Simulation Results of 1993

Figure 6.36 shows the resulting crack width after inputting V_{cr} data into the model. The comparison between Figure 6.20 and Figure 6.36 shows that the resulting crack width in Figure 6.36 is smaller than that in Figure 6.20 and the appearance of cracking in 1993 is later than in 1992.

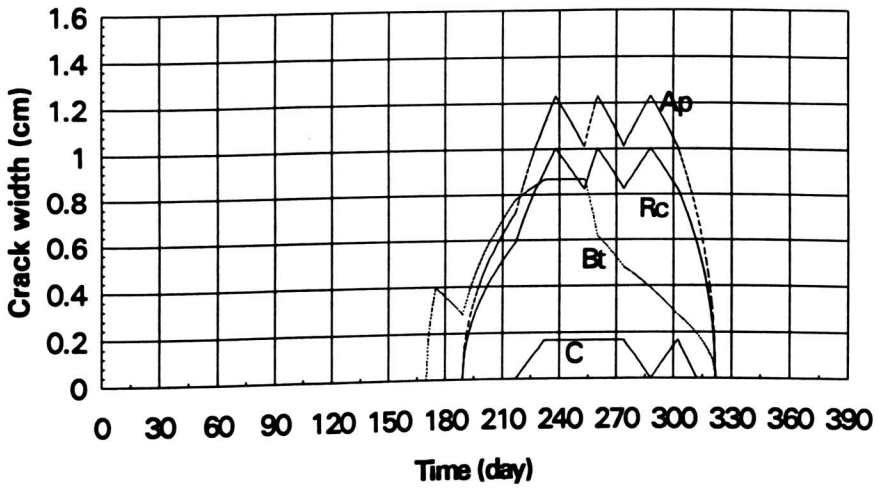

Figure 6.36 Crack width in 1993 simulation using V_{cr} cracking model.

A. Water Table Simulation Result. Figure 6.37 shows both the measured water table at 4P24 and 4P25 and the predicted water table using V_{cr} cracking model. In Figure 6.37 the predicted water table coincides with the measured water table before day 210. After day 210 the predicted water table is higher than measured water table. It is interesting to compare Figure 5.18 with Figure 6.37. If there are not any cracks in soil profile, the model under-predicts water table after day 210. In opposite, if V_{cr} data are input into the model, it over-predicts water table after day 210. The only possibility that makes the model over-predict water table is that the input V_{cr} data of 1993 are bigger than the true data. Since those data are measured data, there is no way to change them. Considering that the V_{cr} data of 1992 are good, the V_{cr} data of 1993 are still acceptable.

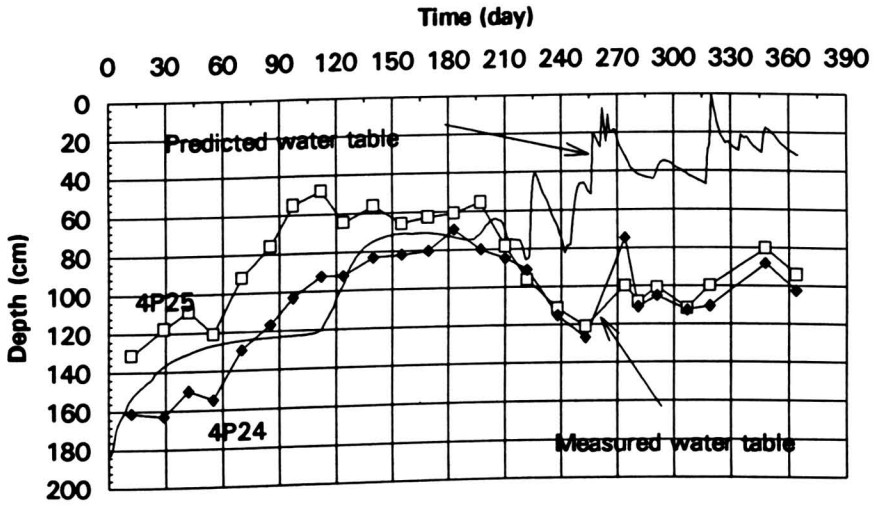

Figure 6.37 Measured and predicted water tables in 1993 using V_{cr} cracking model.

B. Water Content Simulation Results. Comparisons between Figure 5.19 through 5.24 and Figure 6.38 through 6.43 show that after day 210 the predicted water contents in Figure 6.38 through 6.43 go up resulting in a worse match. The reason for a poorer match is that the input V_{cr} data of 1993 are too large resulting in too much water to be transported through those cracks generated from the input data. Figure 6.44 shows that below 150 cm depth the predicted water content remains constant and is in saturation.

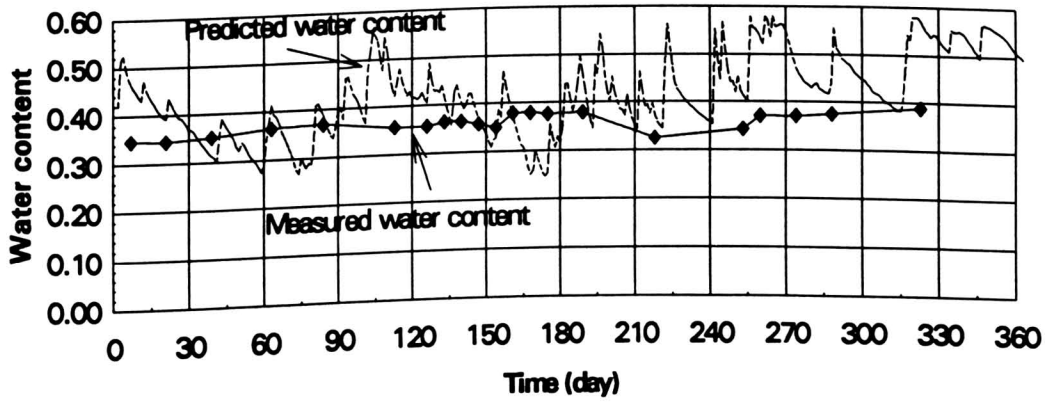

Figure 6.38 Comparison of water content at 15 cm using V_{cr} cracking model in 1993.

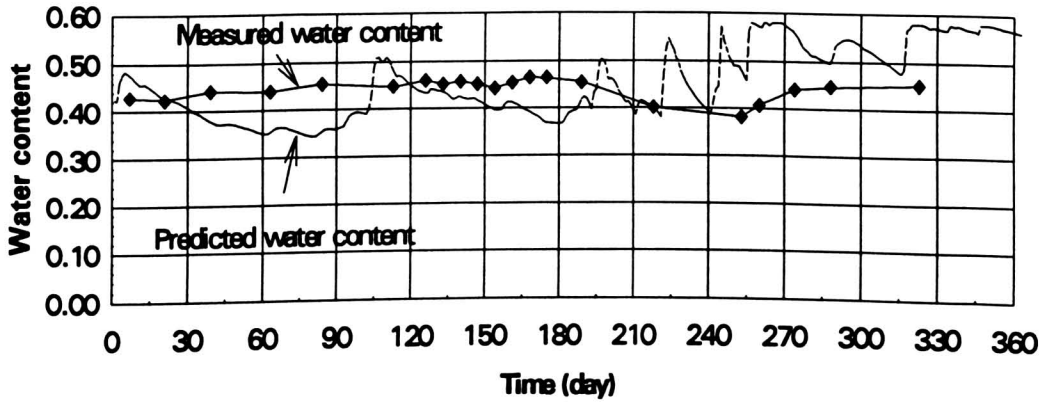

Figure 6.39 Comparison of water content at 30 cm using V_{cr} cracking model in 1993.

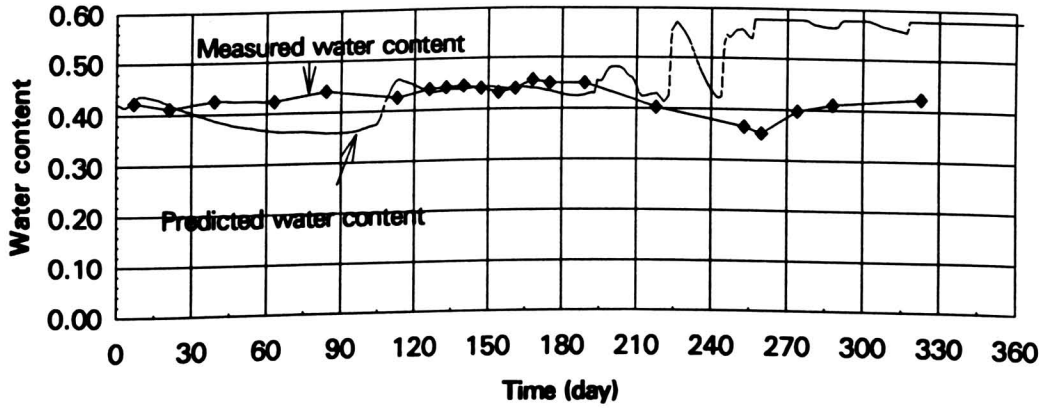

Figure 6.40 Comparison of water content at 45 cm using V_{cr} cracking model in 1993.

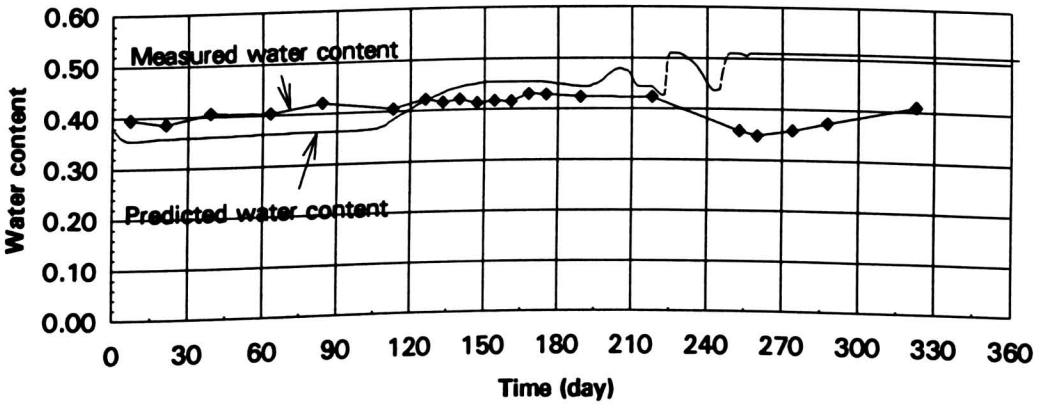

Figure 6.41 Comparison of water content at 60 cm using V_{cr} cracking model in 1993.

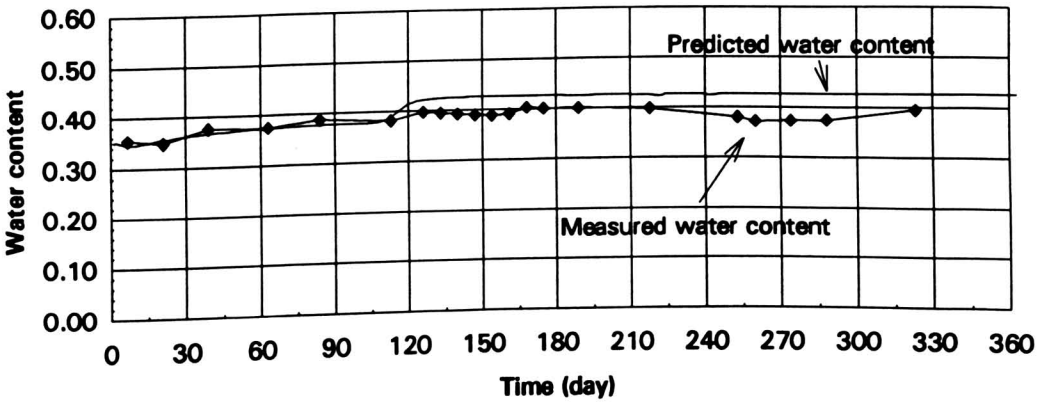

Figure 6.42 Comparison of water content at 75 cm using V_{cr} cracking model in 1993.

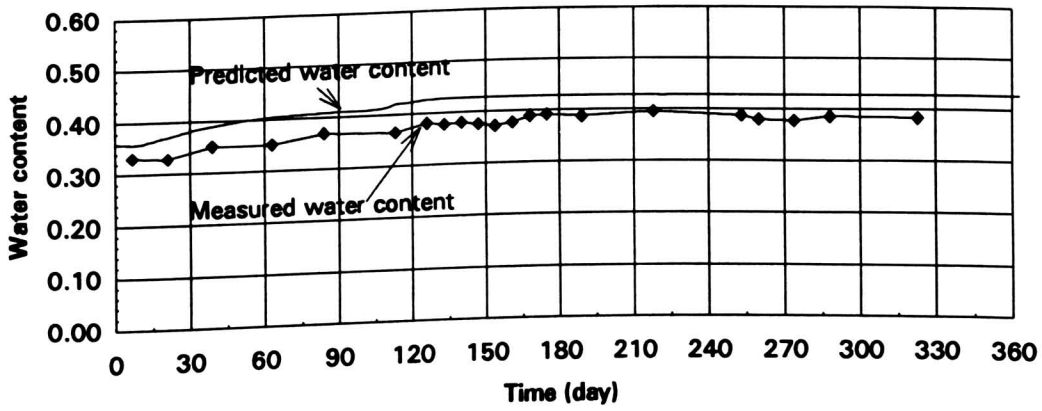

Figure 6.43 Comparison of water content at 90 cm using V_{cr} cracking model in 1993.

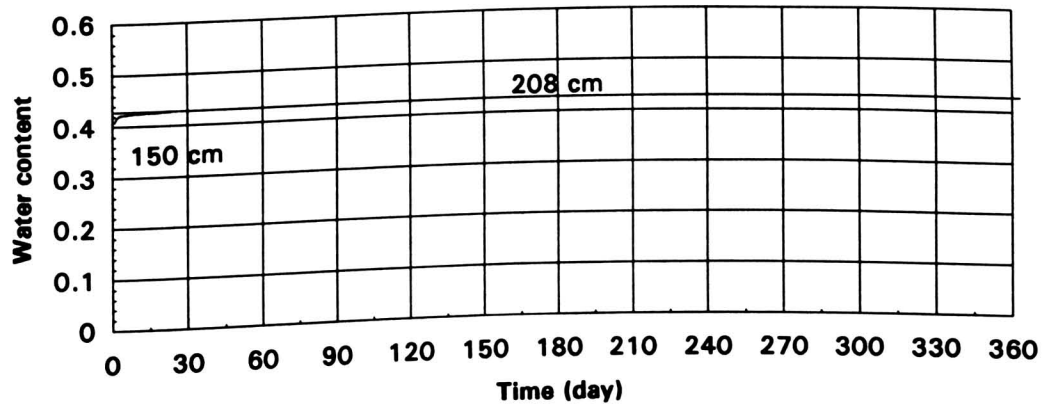

Figure 6.44 Predicted water content at 150 cm and 208 cm using V_{cr} cracking model in 1993.

C. Nitrogen, Alachlor and Atrazine Simulation Results

1. Nitrogen Simulation Results. Comparison between Figure 6.9 and Figure 6.45 shows that because of the existence of cracks, the peak value of nitrogen concentration at depth 7.6 cm in Figure 6.45 is lower than that in Figure 6.9. Figure 6.46 shows that because more water in 1993 is transported through cracks after day 210, nitrogen is flushed down to a deeper depth resulting in the deficiency of nitrogen in shallower depths after day 210. Figure 6.47 shows that at the 160 cm depth nitrogen concentration goes up after day 265, an accumulation of nitrogen at deeper depths.

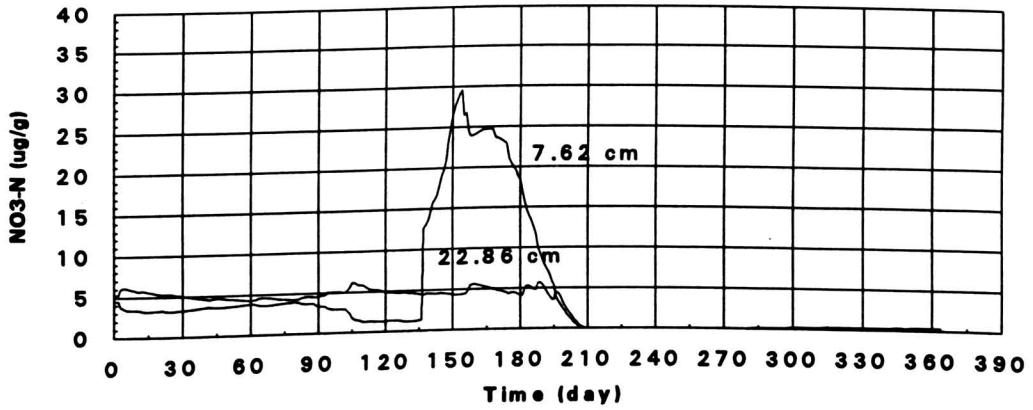

Figure 6.45 Nitrogen concentration at 7.62 cm and 22.86 cm using V_{cr} cracking model in 1993.

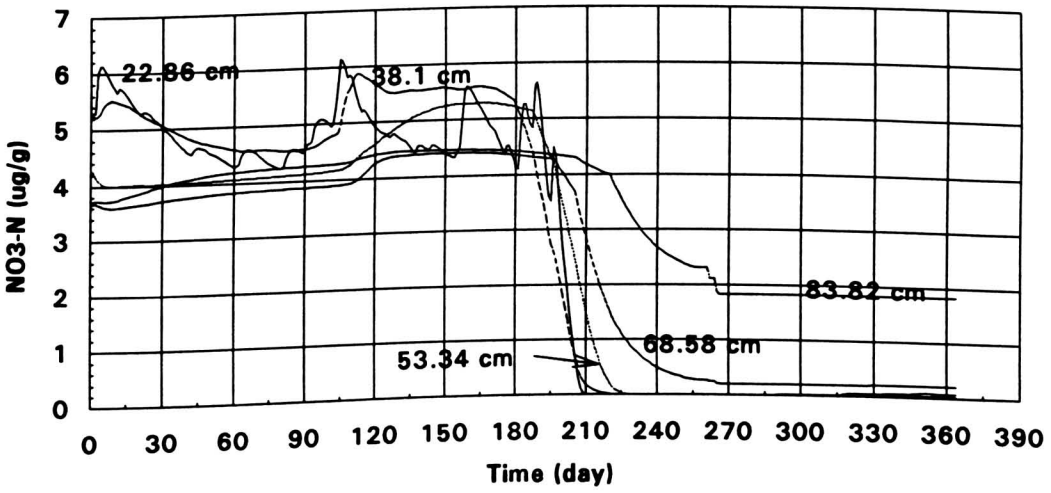

Figure 6.46 Nitrogen concentration at 22-84 cm using V_{cr} cracking model in 1993.

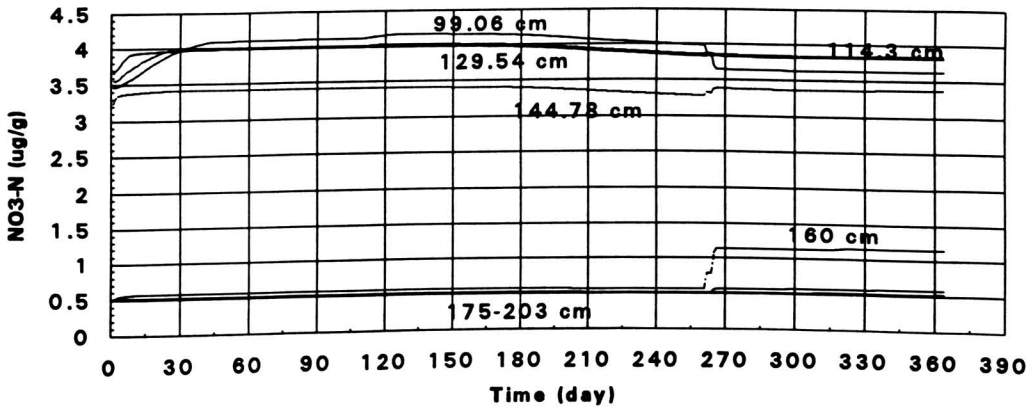

Figure 6.47 Nitrogen concentration at 99-203 cm using V_{cr} cracking model in 1993.

2. Alachlor Simulation Results. Comparison between Figure 6.14 and Figure 6.48 shows that the peak alachlor concentration in Figure 6.48 is lower than that in Figure 6.14. However, comparisons between Figure 6.15, 6.16 and Figure 6.49, 6.50 show that the alachlor concentrations at depth 22.8 cm and 38.1 cm in Figure 6.49 and 6.50 are higher than that in Figure 6.15 and 6.16. In Figure 6.50, alachlor even appears at depth 53.3 cm. All these differences are caused by the effects of cracks.

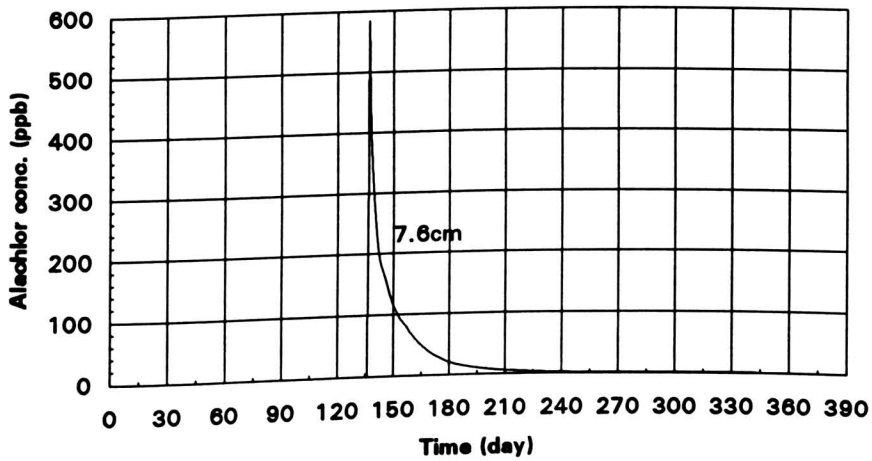

Figure 6.48 Predicted alachlor concentration at 7.6 cm using V_{cr} cracking model in 1993.

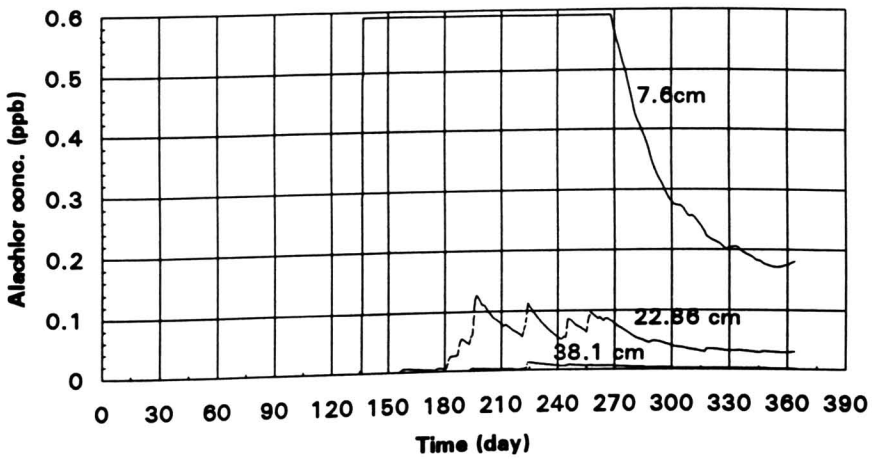

Figure 6.49 Predicted alachlor concentration at 7.6-38.1 cm using V_{cr} cracking model in 1993.

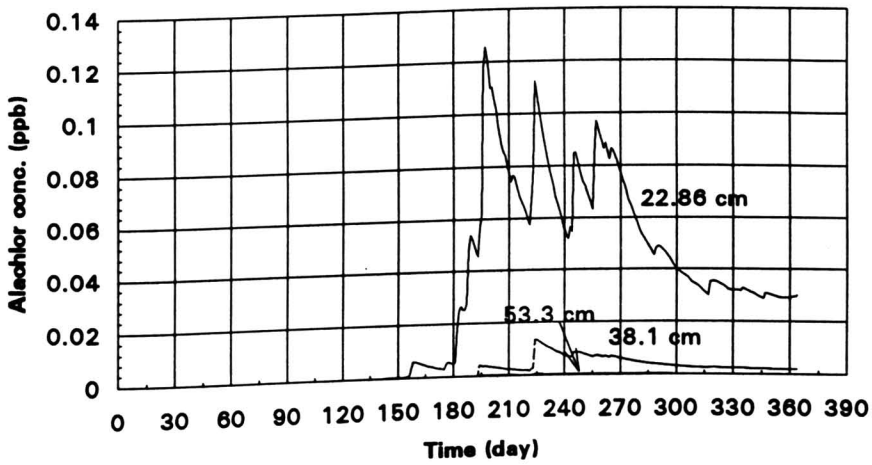

Figure 6.50 Predicted alachlor concentration at 22.8-53.3 cm using V_{cr} cracking model in 1993.

3. Atrazine Simulation Results. Comparisons between Figure 6.17, 6.18 and Figure 6.51, 6.52 show that the peak atrazine concentrations at depth 7.6 cm and 22.8 cm in Figure 6.51 and 6.52 are lower than that in Figure 6.17 and 6.18. In contrast, the atrazine concentrations at depth 53.3 cm and 68.8 cm in Figure 6.53 are higher than that in Figure 6.19 while the atrazine concentration at depth 38.1 cm in Figure 6.52 remains

almost the same as that in Figure 6.18. This means that atrazine is moved deeper in the soil above 38 cm while below 38 cm atrazine accumulates. The differences between Figure 6.17 through 6.19 and Figure 6.51 through 6.53 are, of course, caused by the existence of cracks.

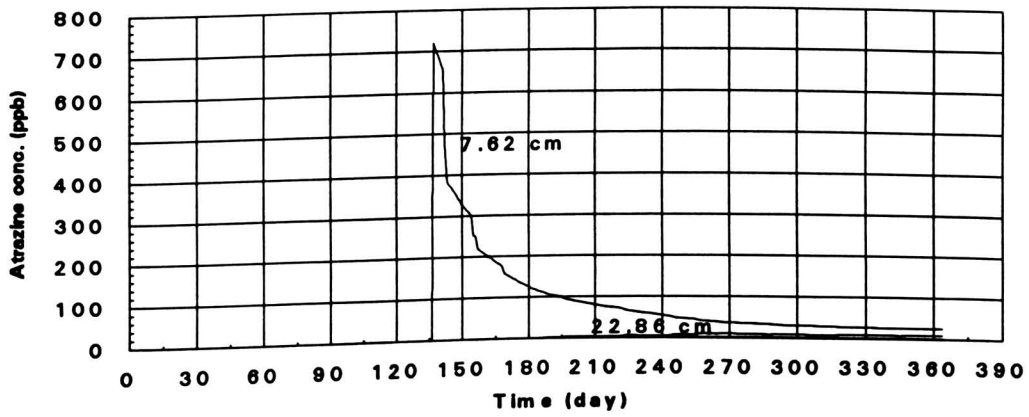

Figure 6.51 Predicted atrazine concentration at 7.6-22.8 cm using V_{cr} cracking model in 1993.

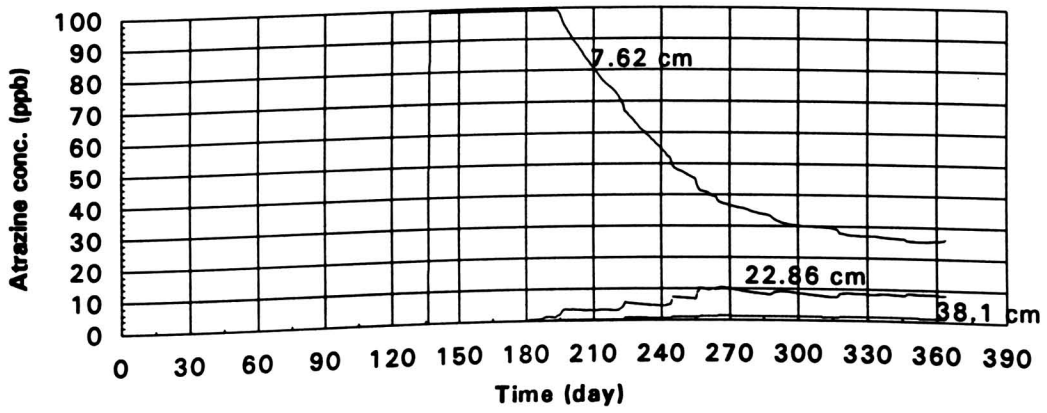

Figure 6.52 Predicted atrazine concentration at 22.8-38.1 cm using V_{cr} cracking model in 1993.

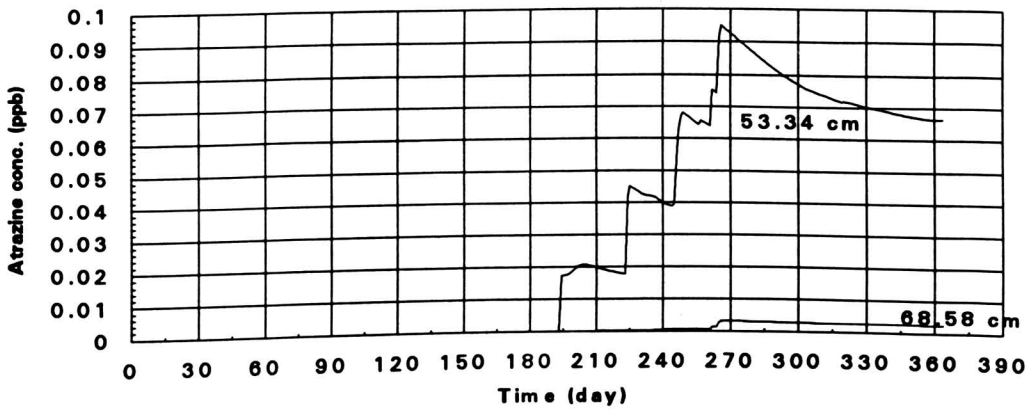

Figure 6.53 Predicted atrazine concentration at 53.3-68.6 cm using V_{cr} cracking model in 1993.

6.3 The Simulation Results Using Soil Moisture Cracking Model (SMCM)

In this section, discussion will be focused on the effects of cracks generated by using the soil moisture cracking models developed in Chapter 3. The revised RZWQM used the calculated water content to calculate V_{cr} using the soil moisture cracking model described in Figure 3.12, 3.13 and 3.14. Then the revised RZWQM used the generated V_{cr} to calculate crack width and length in each horizon (also the cylindrical radius of the top synthetic horizon). The revised RZWQM began to use the cracking model for each horizon when the input V_{cr} for that horizon in the simulation of V_{cr} cracking model was greater than zero and stopped using the soil moisture cracking model when the input V_{cr} for this horizon was zero. The reason is because the revised RZWQM cannot predict water content very accurately, and the cracking model is not perfect either. The resulting crack widths of each horizon and the cylindrical radius are shown in Figure 6.54 and Figure 6.55. The comparison between Figure 6.20 and Figure 6.54 shows that the crack widths of each horizon in Figure 6.54 are larger than that in Figure 6.20. The comparison between Figure 6.36 and Figure 6.55 shows that the crack widths of each horizon in

Figure 6.55 are larger than that in Figure 6.36. Also, the shapes of crack width versus time of each horizon in the two figures are different. In Figure 6.55, the crack width in the

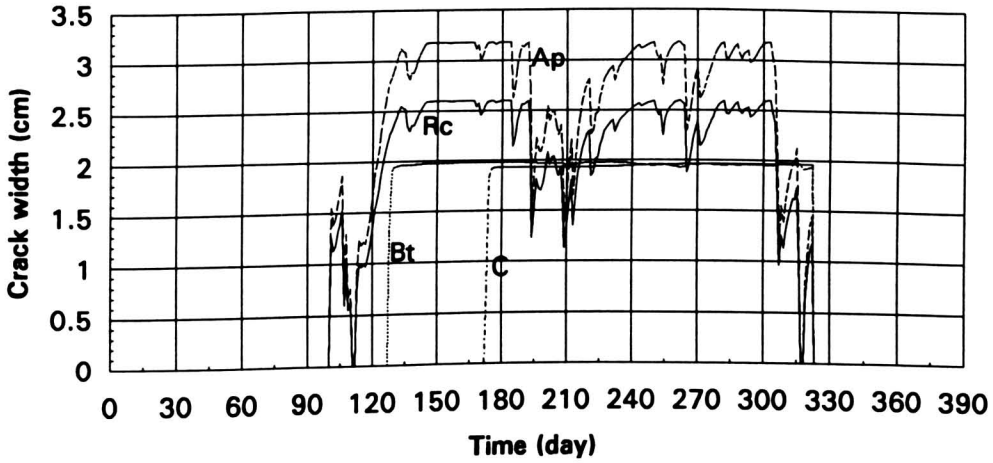

Figure 6.54 Crack width generated using soil moisture cracking model in 1992.

Ap horizon reaches zero five times between day 240 and day 290. This means that the water content in the Ap horizon significantly fluctuates during that time period.

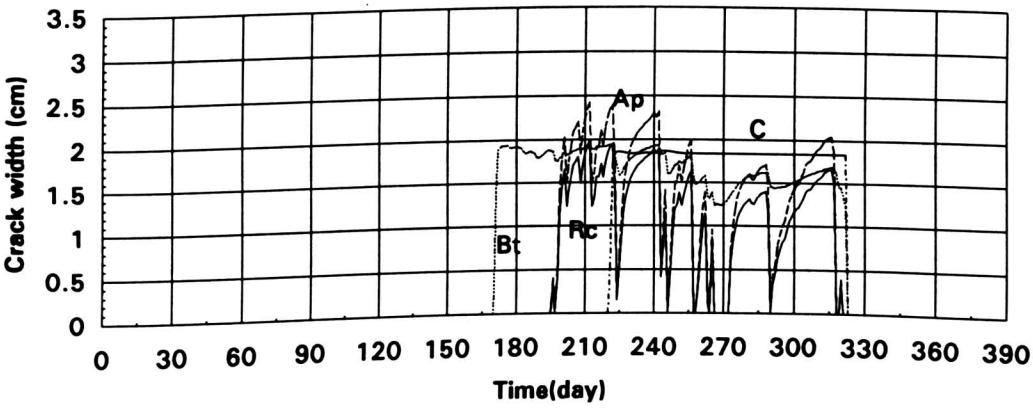

Figure 6.55 Crack width generated using soil moisture cracking model in 1993.

After the revised RZWQM had this macropore information, it used the macropore information in the simulation of water, nutrient and pesticides movement.

6.3.1 The Simulation Results of 1992

A. Water Table Simulation Result. Comparison of Figure 6.56 with Figure 6.21 shows that the predicted water table in Figure 6.56 is a little shallower than that in Figure 6.21. This is understandable because the crack widths in Figure 6.54 are larger than that in Figure 6.20. The predicted water table in Figure 6.56 is still reasonable.

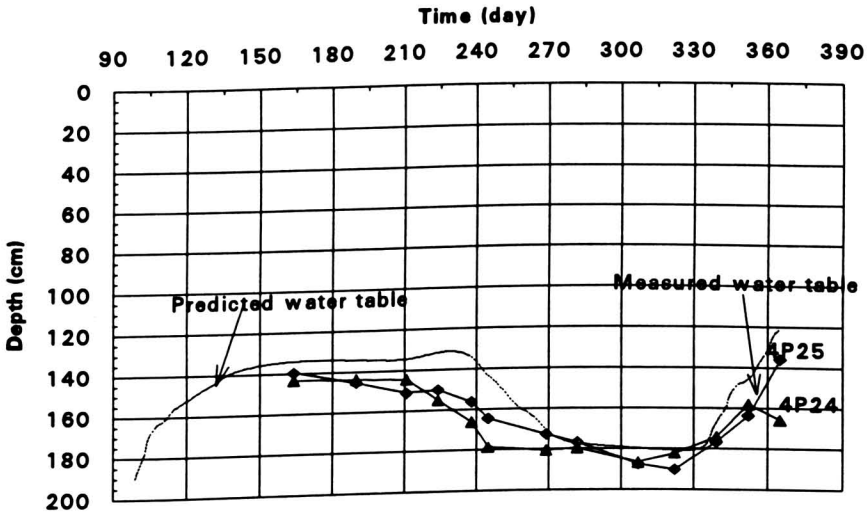

Figure 6.56 Measured and predicted water tables in 1992 using SMCM.

The goodness of fit can be quantified by calculation of the R^2 (sample coefficient of determination) value according to the following (Walpole, 1989):

$$R^2 = \frac{S_{xy}^2}{S_{xx} S_{yy}} \tag{6.1}$$

Table 6.1 The R^2 values for 1992 simulations

Water table simulation in 1992	r^2 (day 164-245)	r^2 (day 269-365)	r^2 (day 164-365)
Non cracking	0.945331	0.798311	0.742888
Vcr	0.942307	0.969559	0.910031
SMCM	0.545021	0.958087	0.825799

Table 6.1 shows that the simulation using Vcr cracking model gives the best fit amoung all the simulations.

B. Water Content Simulation Results. The comparisons between Figure 6.22 through 6.27 and Figure 6.57 through 6.62 show that around day 210 there are some small improvements among Figure 6.57 through 6.62 although the match between the predicted water content and the measured water content is still poor. The predicted water content at depth 150 cm in Figure 6.63 is higher than that in Figure 6.28, meaning that more water is transported down to deeper depth in the simulation using the soil moisture cracking model.

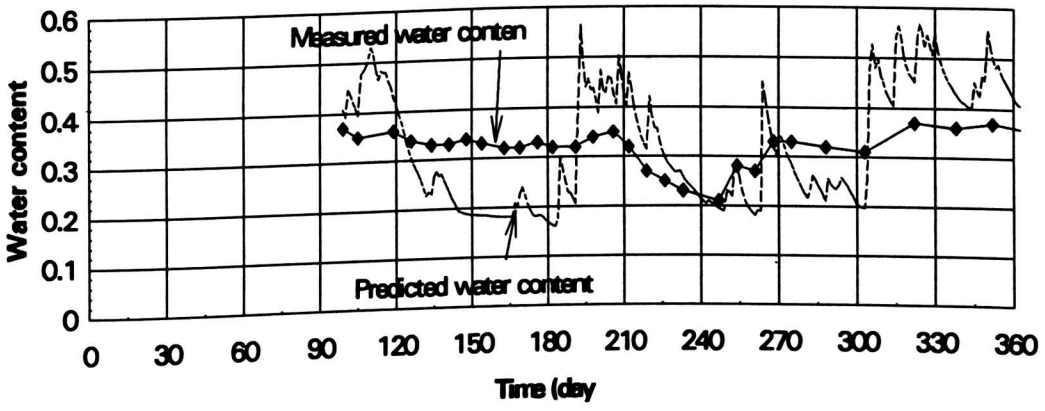

Figure 6.57 Comparison of water content at 15 cm in 1992 using SMCM.

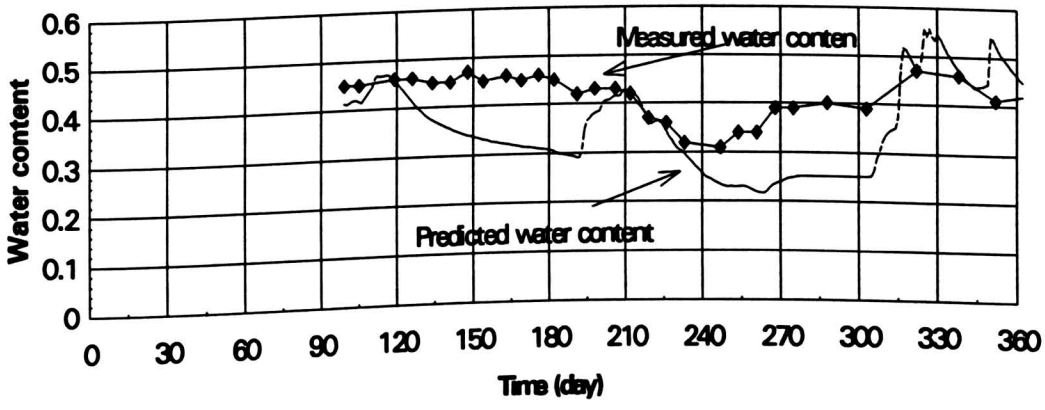

Figure 6.58 Comparison of water content at 30 cm in 1992 using SMCM.

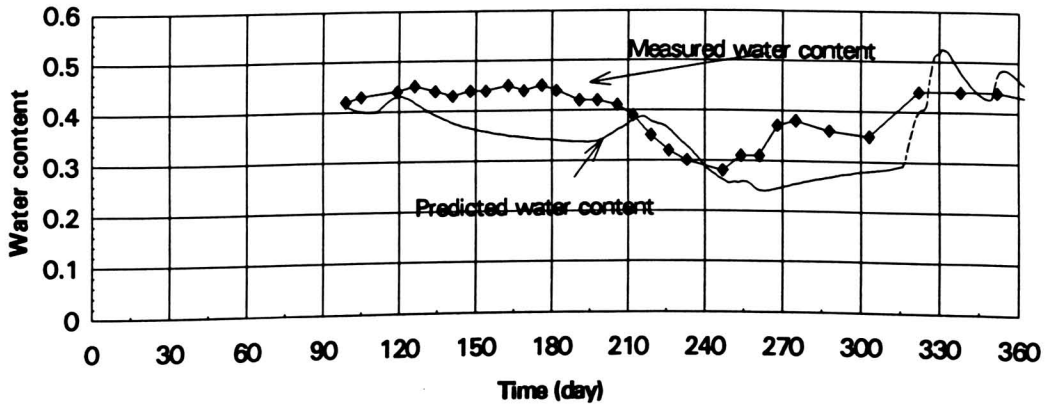

Figure 6.59 Comparison of water content at 45 cm in 1992 using SMCM.

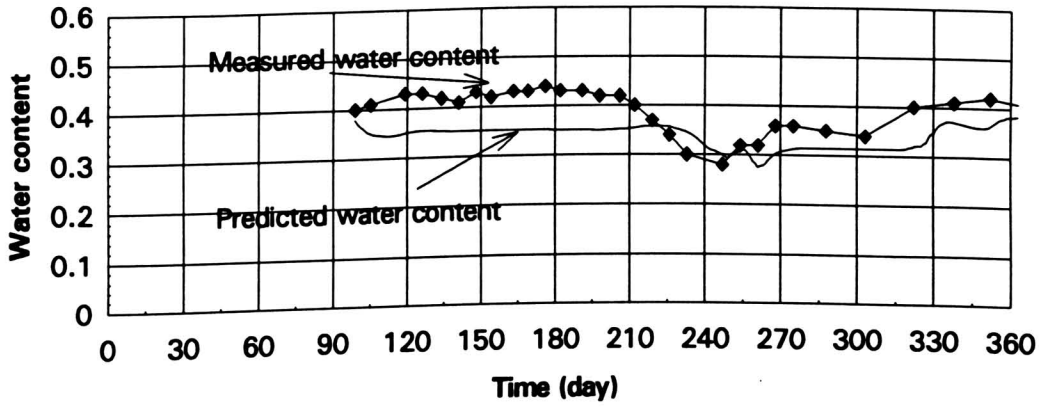

Figure 6.60 Comparison of water content at 60 cm in 1992 using SMCM.

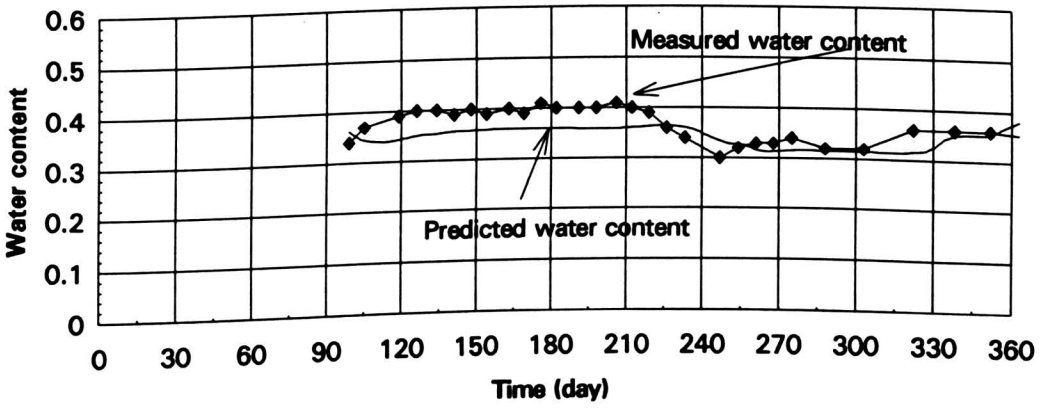

Figure 6.61 Comparison of water content at 75 cm in 1992 using SMCM.

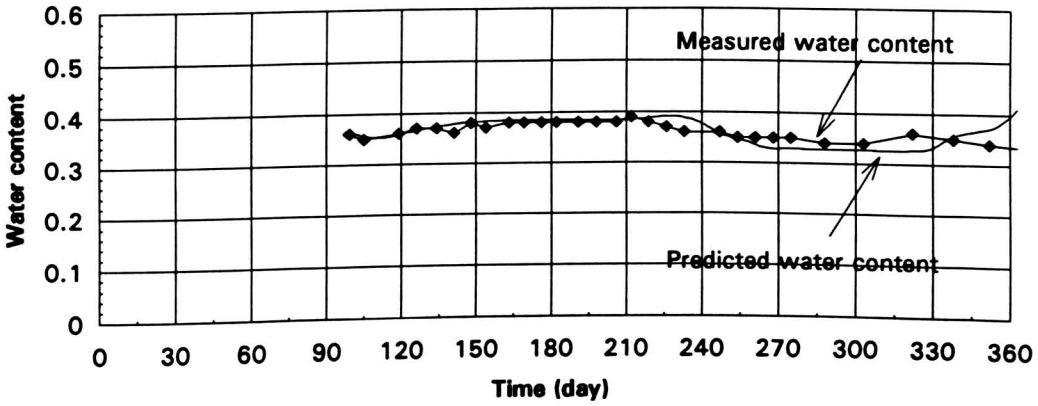

Figure 6.62 Comparison of water content at 90 cm in 1992 using SMCM.

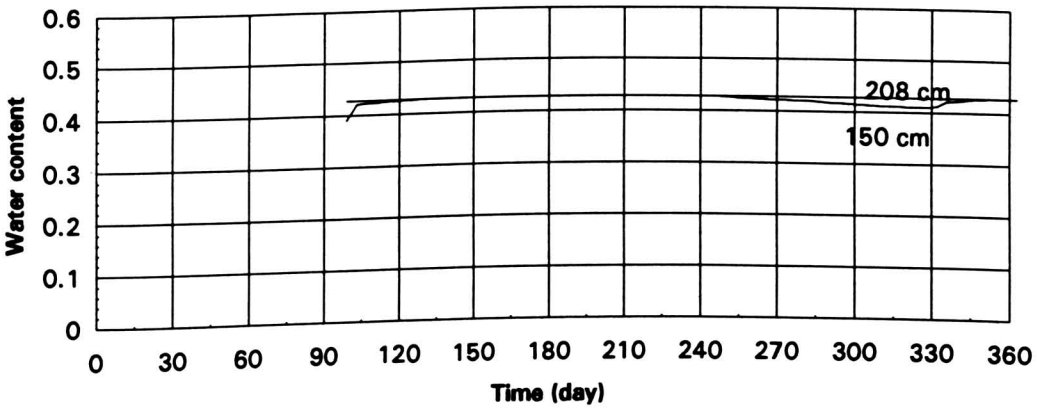

Figure 6.63 Predicted water content at 150 and 208 cm in 1992 using SMCM.

C. Nitrogen and Alachlor Simulation Results

1. Nitrogen Simulation Results. The comparison between Figure 6.29 and Figure 6.64 shows that there are some differences between the two figures. For example, the nitrogen concentration at depth 83.8 cm at the end of 1992 in Figure 6.64 is higher than that in Figure 6.29 while at depth 99.1 cm the situation is reversed. This is, of cause, caused by larger cracks.

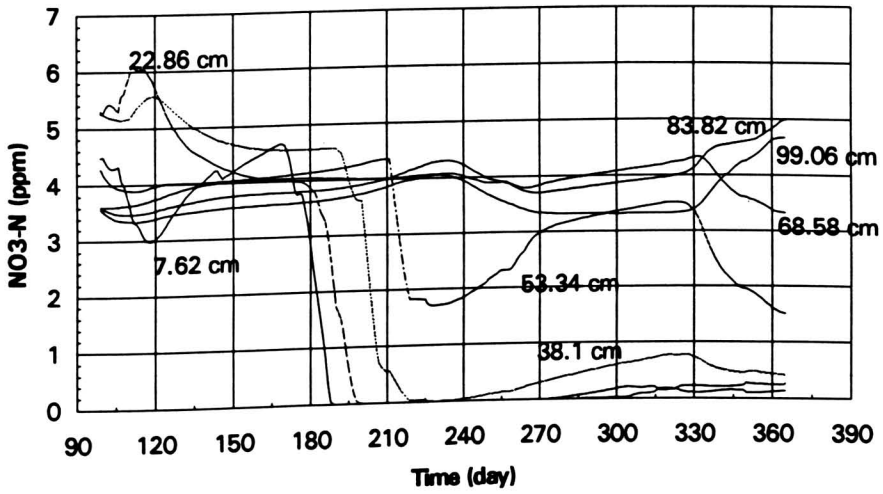

Figure 6.64 Nitrogen concentration at depth 7-100 cm in 1992 using SMCM.

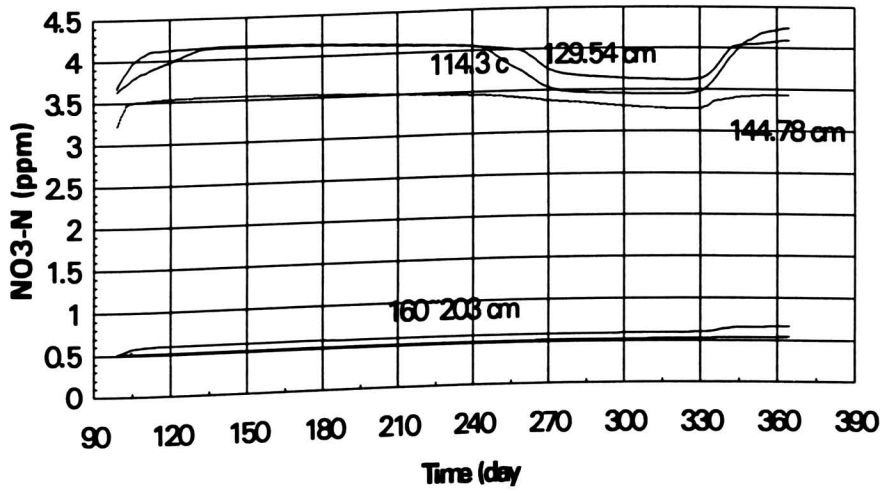

Figure 6.65 Nitrogen concentration at depth 114-203 cm in 1992 using SMCM.

The comparison between Figure 6.30 and Figure 6.65 shows that the nitrogen concentration from depth 114.3 cm to depth 144.7 cm between day 240 and day 340 in Figure 6.65 is higher than that in Figure 6.30, meaning that more nitrogen is transported down to this depth because of larger cracks.

Since there is not a large difference between the nitrogen concentration of the V_{cr} cracking model simulation and the nitrogen concentration using the soil moisture cracking

model simulation, there is no need to plot nitrogen concentration profile on April 29 and October 28, 1992.

2. Alachlor Simulation Results. The comparison between Figure 6.33 and Figure 6.66 shows no difference because during peak time there are no cracks in the two simulations. The comparison between Figure 6.34 and Figure 6.67 shows that at the end of 1992 the alachlor concentration in Figure 6.67 is lower than that in Figure 6.34. The comparison between Figure 6.35 and Figure 6.68 shows that the alachlor concentration at depth 22.8 cm in Figure 6.68 is higher than that in Figure 6.35 during the period from day 194 to day 300 although the difference is small.

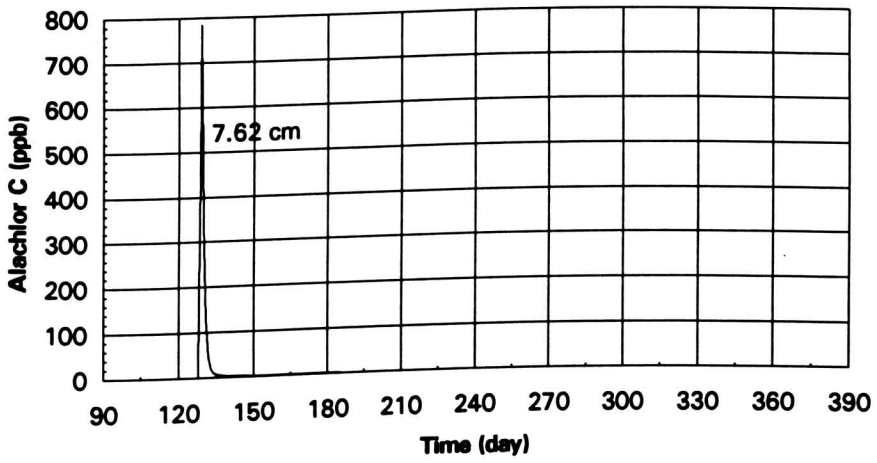

Figure 6.66 Predicted alachlor conc. at depth 7.6 cm in 1992 using SMCM.

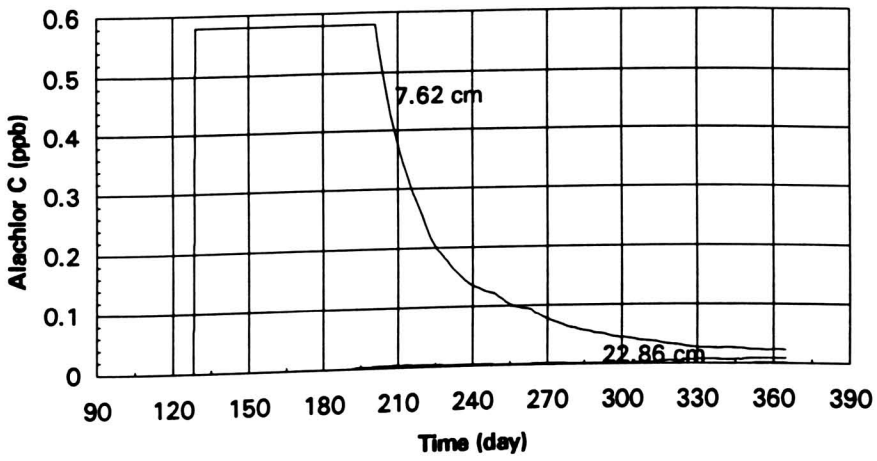

Figure 6.67 Predicted alachlor conc. at depth 7.6 cm and 22.8 in 1992 using SMCM.

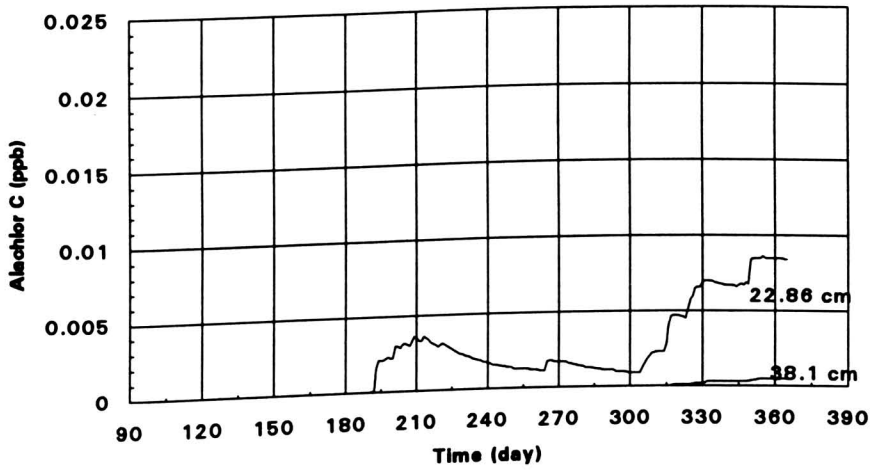

Figure 6.68 Predicted alachlor conc. at depth 22.8 cm and 38.1 cm in 1992 using SMCM.

6.3.2 The Simulation Results of 1993

A. Water Table Simulation Result. Figure 6.69 shows both the measured and the predicted water tables in 1993 using SMCM. Notice that even though the crack widths of each horizon using the soil moisture cracking model are larger than using the V_{cr} cracking model, the predicted water table using the soil moisture cracking model is lower than that using the V_{cr} cracking model. The reason is that the crack width in the Ap horizon and

the radius of the cylindrical hole in the top synthetic layer reach zero five times between day 240 and day 290 because of rains. It seems more reasonable that if it rains, the top soil gets wet. After the top soil gets wet, it closes its cracks. Therefore, the top soil restricts the amount of rain allowed into the soil profile.

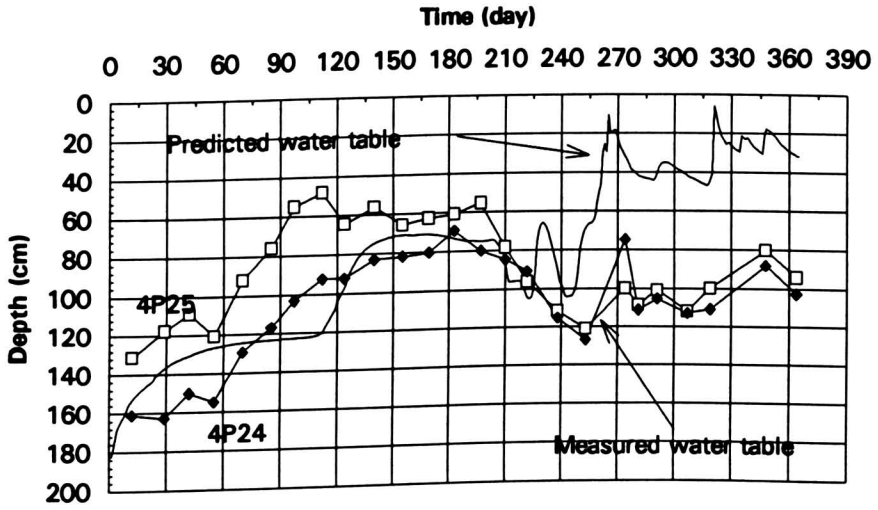

Figure 6.69 Measured and predicted water tables in 1993 using SMCM.

B. Water Content Simulation Results. The comparison between Figure 6.38 through 6.44 and Figure 6.70 through 6.76 shows that there are only small differences around day 210 to day 240 between the figure pairs of the same depths. These differences are caused by the closed holes in the top layer and cracks in the Ap horizon.

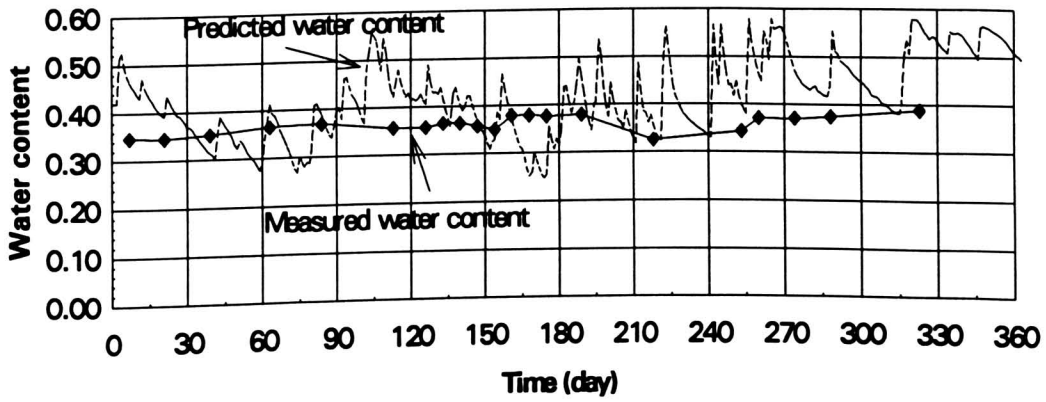

Figure 6.70 Comparison of water content at 15 cm in 1993 using SMCM.

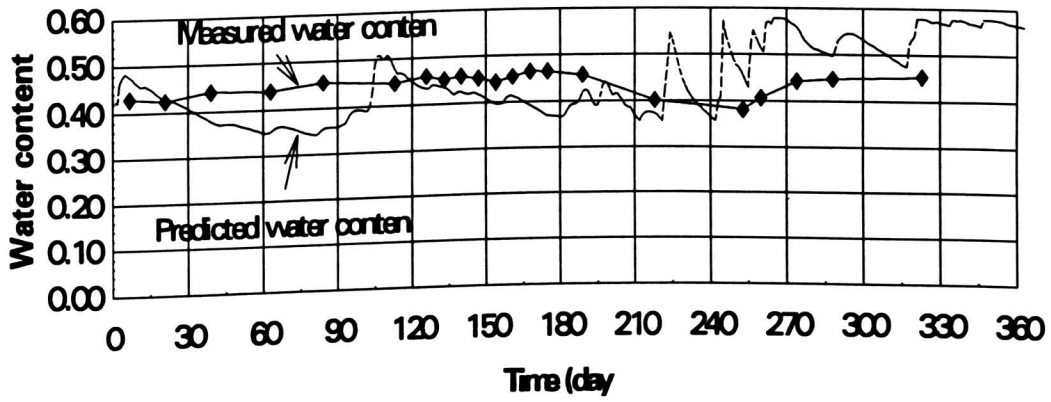

Figure 6.71 Comparison of water content at 30 cm in 1993 using SMCM.

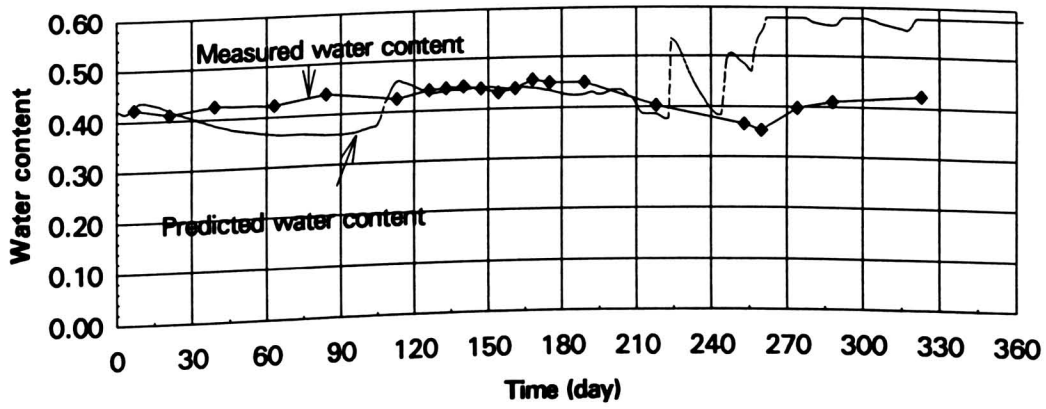

Figure 6.72 Comparison of water content at 45 cm in 1993 using SMCM.

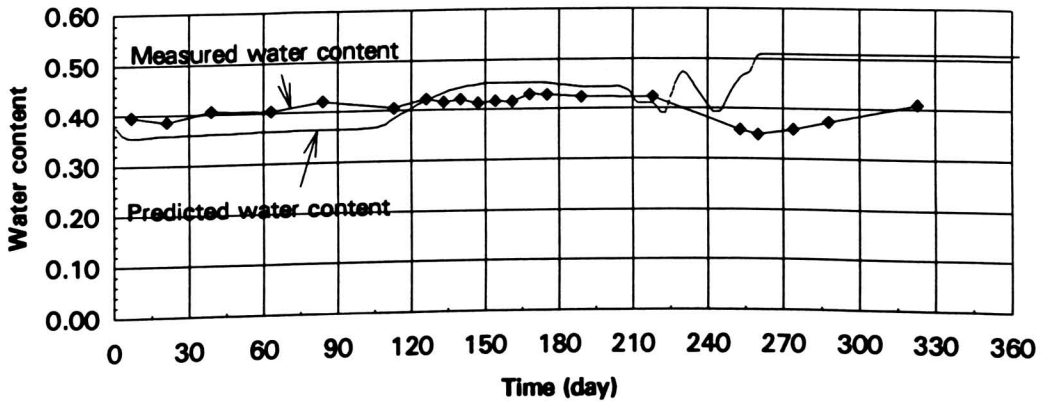

Figure 6.73 Comparison of water content at 60 cm in 1993 using SMCM.

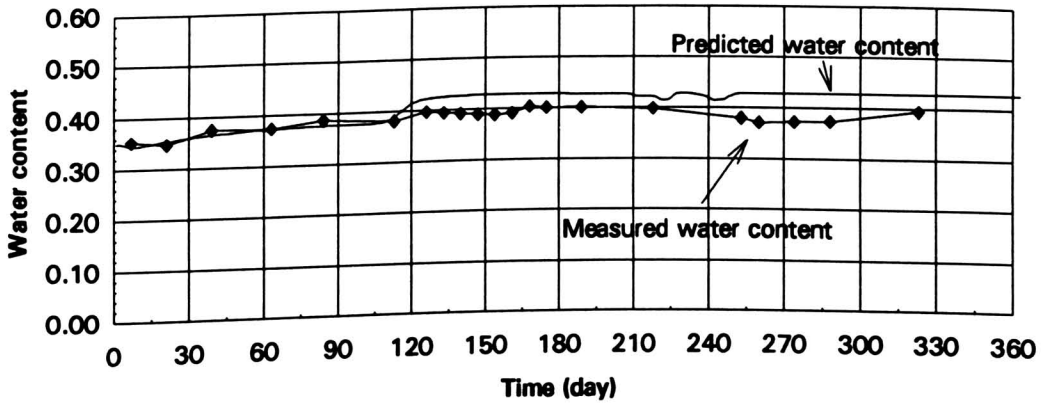

Figure 6.74 Comparison of water content at 75 cm in 1993 using SMCM.

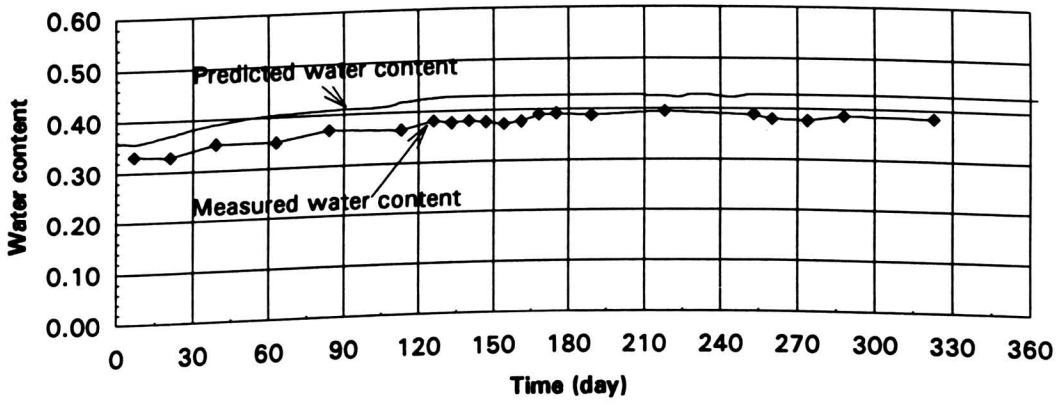

Figure 6.75 Comparison of water content at 90 cm in 1993 using SMCM.

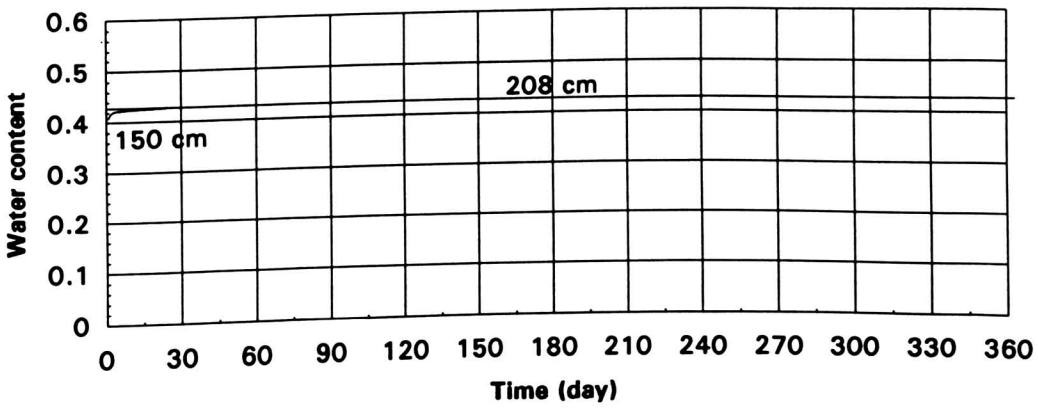

Figure 6.76 Predicted water content at 150 and 208 cm in 1993 using SMCM.

C. Nitrogen, Alachlor and Atrazine Simulation Results

1. Nitrogen Simulation Results. The comparison between Figure 6.45 and Figure 6.77 shows that the nitrogen concentration in Figure 6.77 is slightly lower than in Figure 6.45. This is caused by different cracking behavior (Figure 6.36 and Figure 6.55). The comparison between Figure 6.46, 6.47 and Figure 6.78, 6.79 shows that there are some small differences between the two pairs of figures and this is also caused by the cracking behavior.

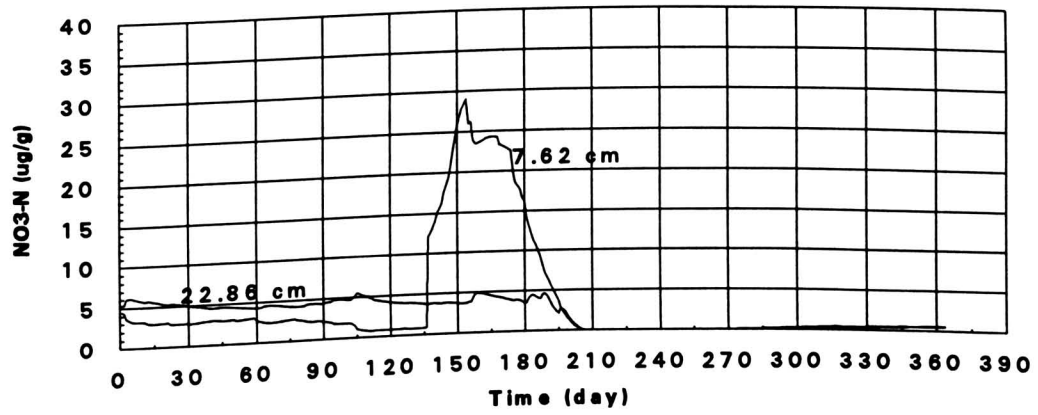

Figure 6.77 Nitrogen concentration at 7.6 cm and 22.8 cm in 1993 using SMCM.

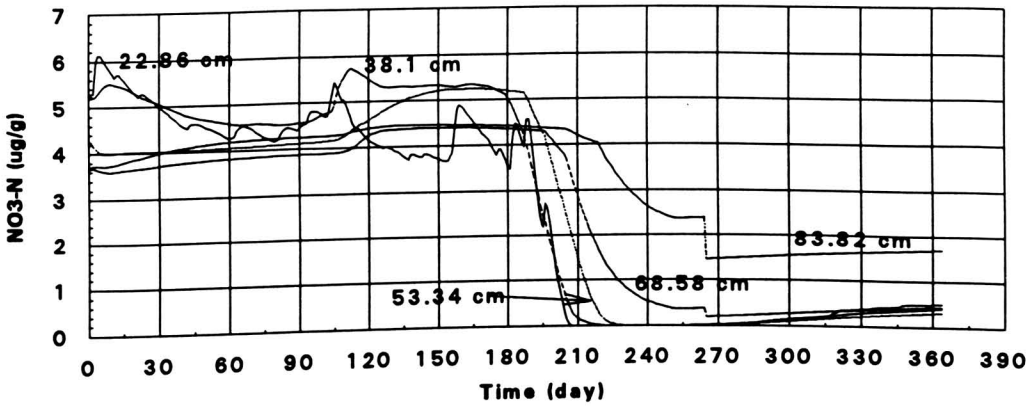

Figure 6.78 Nitrogen concentration at 22-84 cm in 1993 using SMCM.

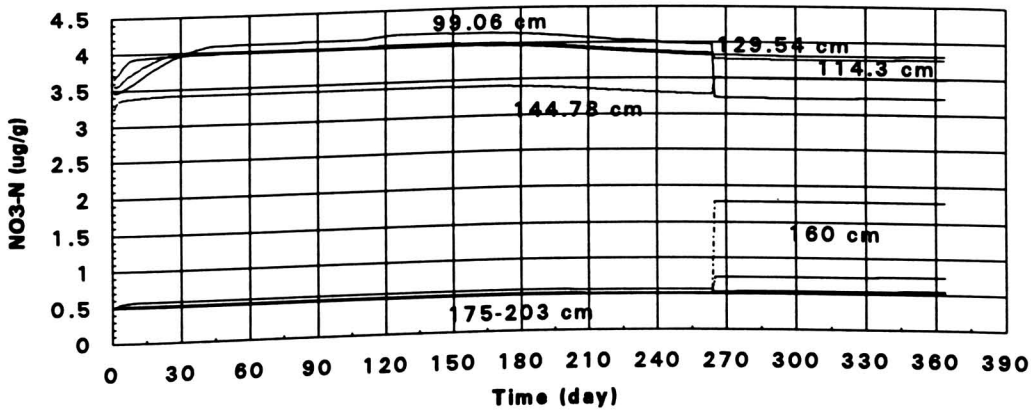

Figure 6.79 Nitrogen concentration at 99-203 cm in 1993 using SMCM.

2. Alachlor Simulation Results. The comparison between Figure 6.48 and Figure 6.80 shows that there is no large difference between the two figures. However, the comparison between Figure 6.49 and Figure 6.81 does show that the alachlor concentration at depth 22.8 cm in the second half of 1993 is higher than in Figure 6.49. The comparison between Figure 6.50 and Figure 6.82 shows the same result as the above comparison. This means that if less water flushes down, alachlor will accumulate at shallower depths.

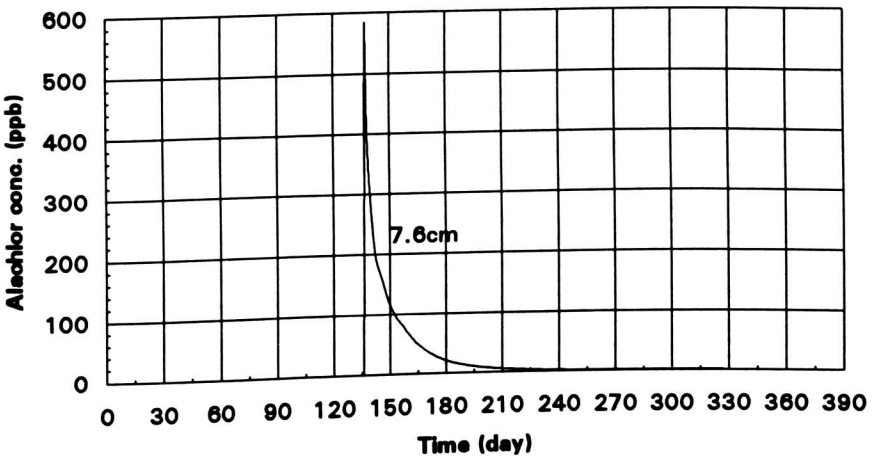

Figure 6.80 Alachlor concentration at 7.6 cm in 1993 using SMCM.

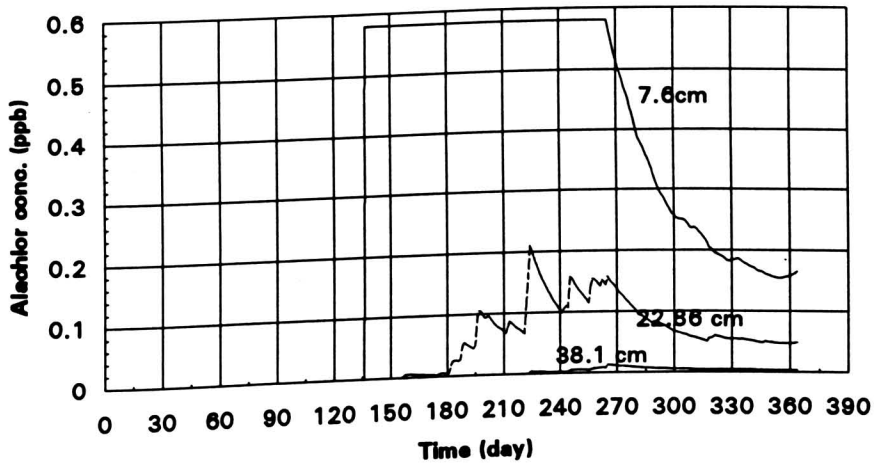

Figure 6.81 Alachlor concentration at depth 7.6-38.1 cm in 1993 using SMCM.

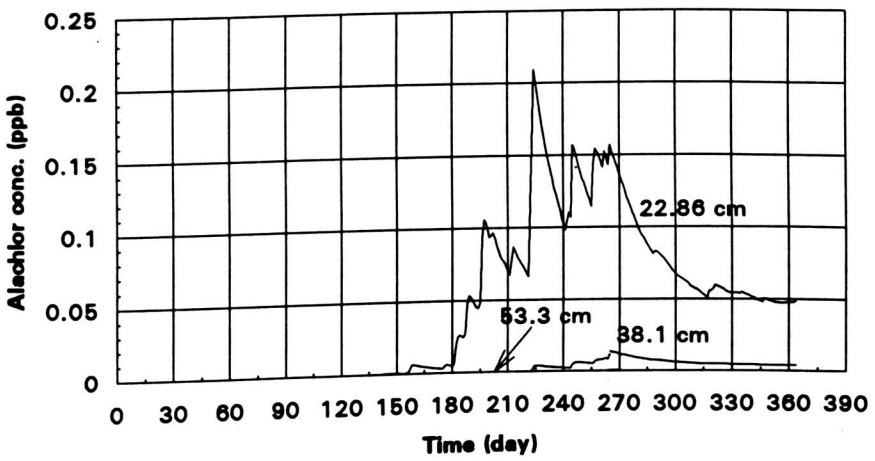

Figure 6.82 Alachlor concentration at 22.8-53.3 cm in 1993 using SMCM.

3. Atrazine Simulation Results. The comparison between Figure 6.51 and Figure 6.83 shows that there is no large difference between the two figures. The comparison between Figure 6.52, 6.53 and Figure 6.84, 6.85 shows that the atrazine concentration at 22.8 cm and 53.3 cm in Figure 6.84 and 6.85 is higher than that in Figure 6.52 and 6.53. This also simply means that atrazine will accumulate at shallower depth if infiltration water is less. However, it is not obvious why the atrazine concentration at 7.6 cm in Figure 6.84 is lower than that in Figure 6.52. The reason is that if infiltration water is less, then runoff water is more. The runoff water takes more atrazine away in the simulation of V_{cr} cracking model.

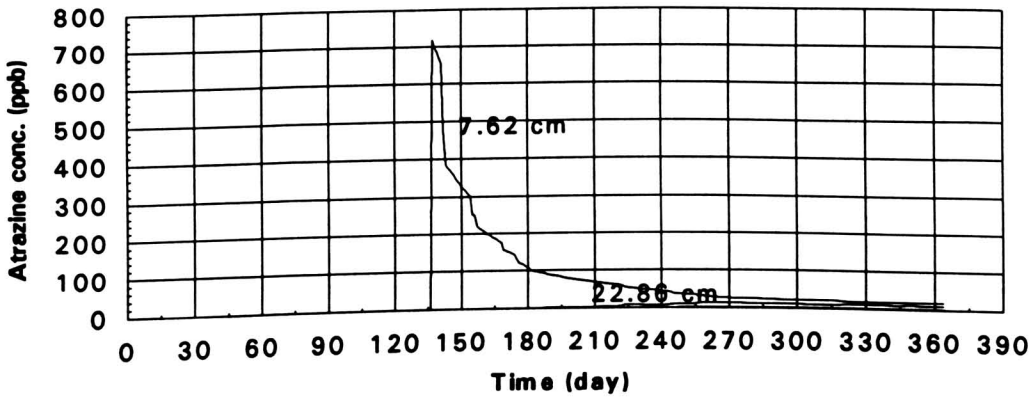

Figure 6.83 Atrazine conc. at depth 7.6 cm and 22.8 cm in 1993 using SMCM.

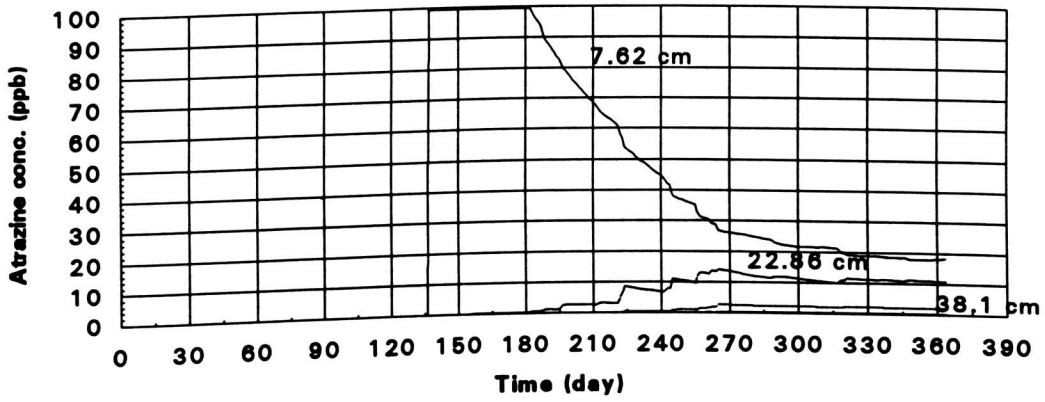

Figure 6.84 Atrazine conc. at depth 22.8 cm and 38.1 cm in 1993 using SMCM.

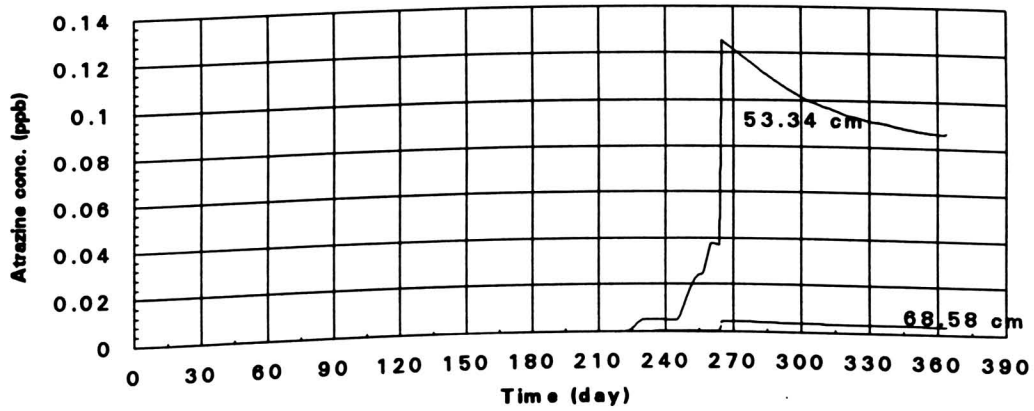

Figure 6.85 Atrazine conc. at depth 53.3 cm and 68.6 cm in 1993 using SMCM.

6.4 The Simulation Results Using Constant Cracking Model

6.4.1 The Determination of Constant Crack Width and Length

From previous simulations it can be seen that the computed crack widths in the Ap, Bt and C horizons in the simulations using the V_{cr} cracking model are smaller than those in the simulations using the soil moisture cracking models. In the simulations using constant crack model, the determination of constant crack width and length is very important. In some site, it may be true that constant cracks stay in the field for all the time, like the cracks caused by geological faults. However, most cracks appeared in soils are caused by the shrinkage of clay soils. This is the case for the Missouri MSEA site. If constant cracks are going to be used in the RZWQM simulations of the Missouri MSEA site, the crack width observed in field could be used. However, to make reasonable comparisons between the simulations using variable cracking models and the simulations using constant cracking model, it is better to use small crack width and length in the constant cracking model simulation because if by using small constant crack width and length, the RZWQM predicts much worse results than the revised RZWQM using variable cracking model, then there is no need to try to use even larger constant crack width and length. Therefore, the crack widths produced by the simulations using the V_{cr} cracking model will be used in the determination of constant crack widths and lengths of the Ap, Bt and C horizons for the simulations hereafter. Because the crack widths and lengths of the Ap, Bt and C horizons are not constant during the simulations, an average method has to be used to determine the reasonable crack widths and lengths. Table 6.2 shows the crack widths, lengths and macroporosities which are used in the constant crack and length simulations.

The widths in Table 6.2 are obtained from the averages of the crack widths in the output of the simulations using the V_{cr} cracking model. Those days when crack width is

zero are not used in the averages. The radius of the holes of the top synthetic horizon is obtained by the same way. The lengths of the cracks at each horizon are obtained by using Equation 3.14, and R in Equation 3.14 is listed in Table 3.7. By using Equation 3.15, V_{cr} can be calculated by using the N value from Table 3.7 and M values of 15 cm, 30 cm and 45 cm for the Ap, Bt and C horizons, respectively. The M values are different from the thicknesses of the Ap, Bt and C horizons because the anchors were installed 15 cm apart vertically and V_{cr}'s which were input in the former simulations are calculated by using those values.

Table 6.2 The parameters used in the constant cracking model simulation

Year	Layer	Top		Ap	Bt	C
	Radius (cm)	0.845	Width (cm)	1.035	0.637	0.316
1992			Length (cm)	132.35	90.48	46
	P_{mac}	0.0411	P_{mac}	0.0411	0.0519	0.00581
	Radius (cm)	0.747	Width (cm)	0.915	0.526	0.12
1993			Length (cm)	117.01	74.72	17.5
	P_{mac}	0.0321	P_{mac}	0.0321	0.0354	0.000841

6.4.2 The Simulation Results of 1992

A. Water Table Simulation Result. Figure 6.86 shows that the predicted water table significantly deviates from the measured water table after day 330. Figure 6.3 shows that from day 300 to day 330 there were some heavy rains. These rains cause the predicted water table to rise up very quickly because of the existence of constant cracks in those horizons.

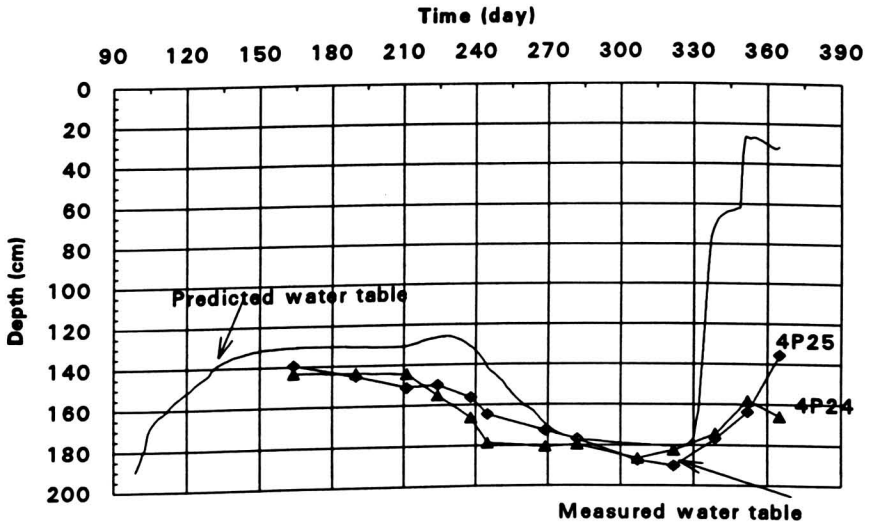

Figure 6.86 Measured water tables at 4P24 and 4P25, and predicted water table using constant cracking model in 1992.

B. Water Content Simulation Results. The comparison between Figure 6.87 and Figure 6.22 shows that the predicted water content in Figure 6.87 is higher than that in Figure 6.22 from day 193 to day 225. The comparisons between Figure 6.88 through 6.92 and Figure 6.23 through 6.27 show that the predicted water contents in Figure 6.88 through 6.92 are higher than that at equal depths in Figure 6.23 through 6.27 from day 200 to day

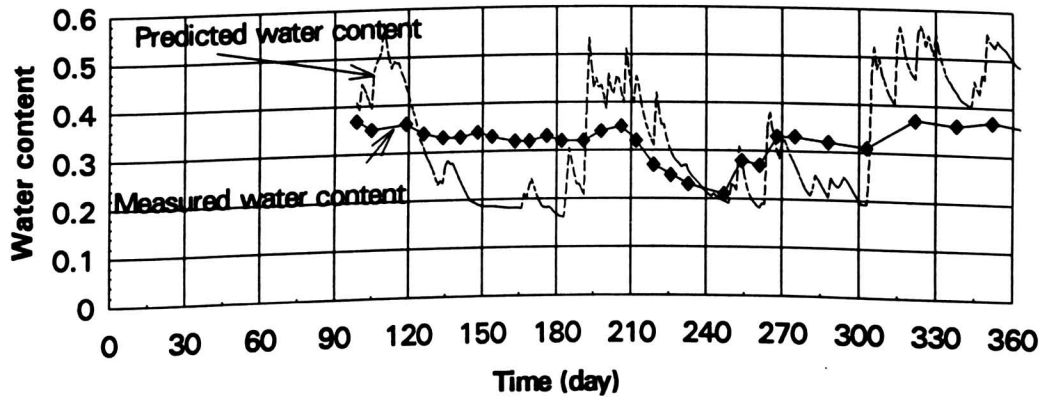

Figure 6.87 Comparison of water content at 15 cm in 1992 using constant cracking model.

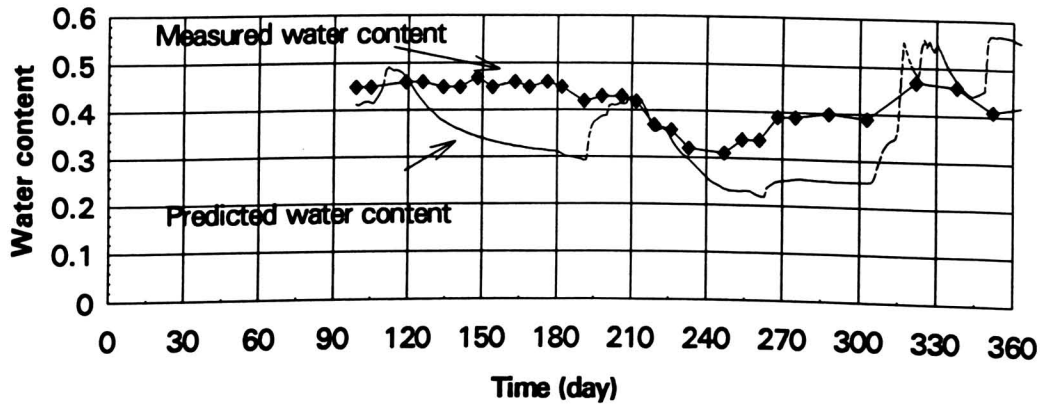

Figure 6.88 Comparison of water content at 30 cm in 1992 using constant cracking model.

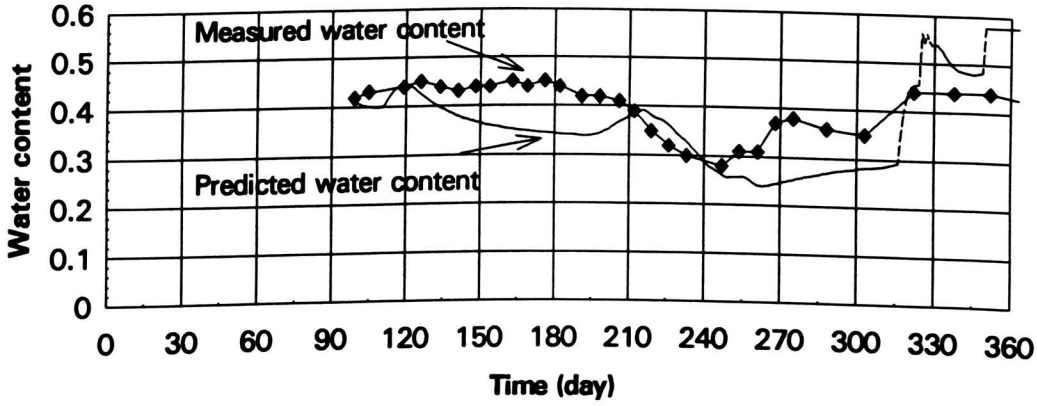

Figure 6.89 Comparison of water content at 45 cm in 1992 using constant cracking model.

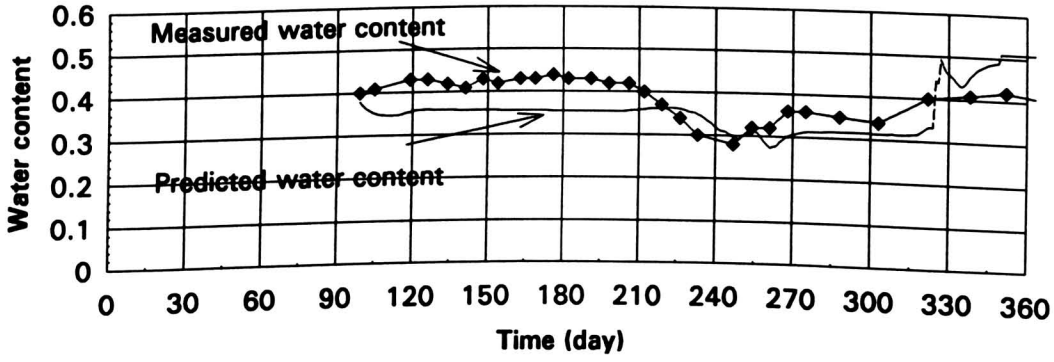

Figure 6.90 Comparison of water content at 60 cm in 1992 using constant cracking model.

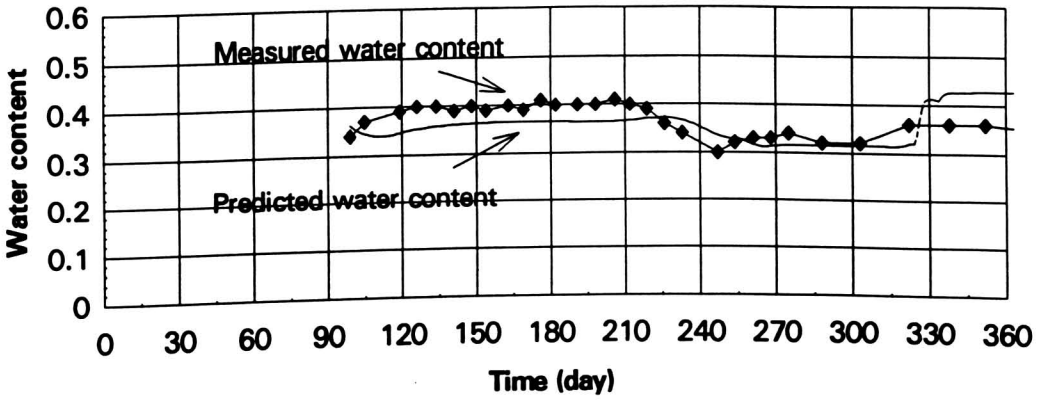

Figure 6.91 Comparison of water content at 75 cm in 1992 using constant cracking model.

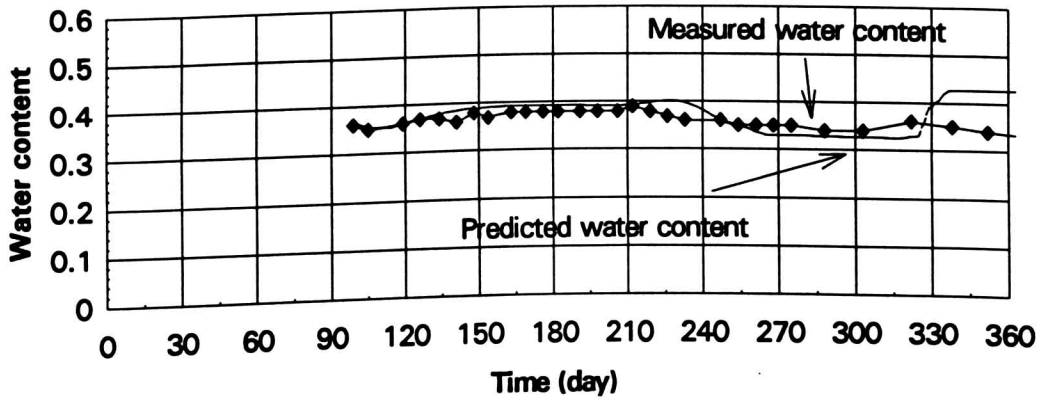

Figure 6.92 Comparison of water content at 90 cm in 1992 using constant cracking model.

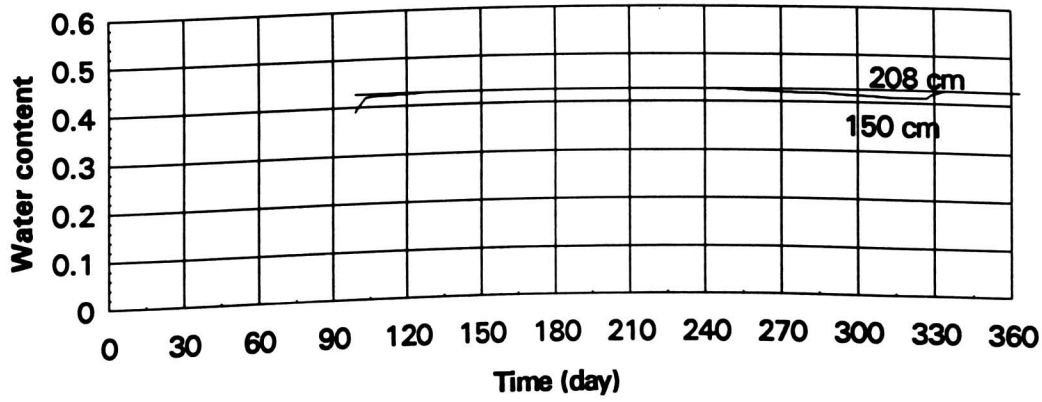

Figure 6.93 Predicted water content at 150 and 208 cm in 1992 using constant cracking model.

240. Also, the predicted water contents at the end of 1992 in Figure 6.88 through 6.92 go up and are much higher than the measured water content.

Figure 6.93 shows that the predicted water content at the 150 cm depth is higher than in Figure 6.28, meaning that more water was transported down to this depth if there were constant cracks in the field.

C. Nitrogen and Alachlor Simulation Results

1. Nitrogen Simulation Results. Comparison between Figure 6.94 and Figure 6.29 shows that the nitrogen concentration at depth 7.6 cm in Figure 6.94 is lower than that in Figure 6.29. Also, the nitrogen concentrations from depth 53.3 cm to 99.06 cm in Figure 6.94 remain almost constant after day 335 while the equivalents in Figure 6.29 go up or down. The comparison between Figure 6.95 and Figure 6.30 also shows that the nitrogen concentrations from depth 114.3 cm to 144.8 after day 270 in Figure 6.95 are higher than that in Figure 6.30, while the nitrogen concentration at depth 160 cm at the end of the year in Figure 6.95 is lower than that in Figure 6.30. All of these results are because there are more flushed-down water than that in the V_{cr} cracking model simulation.

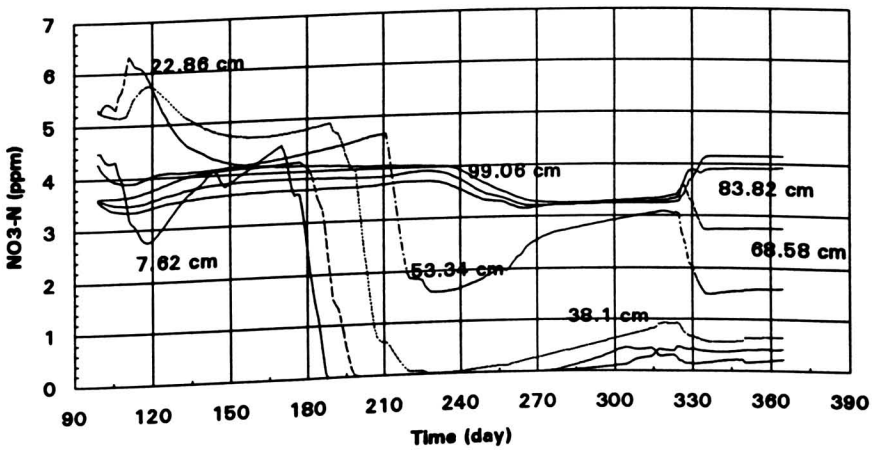

Figure 6.94 Predicted nitrogen concentration at 7-100 cm in 1992 using constant cracking model.

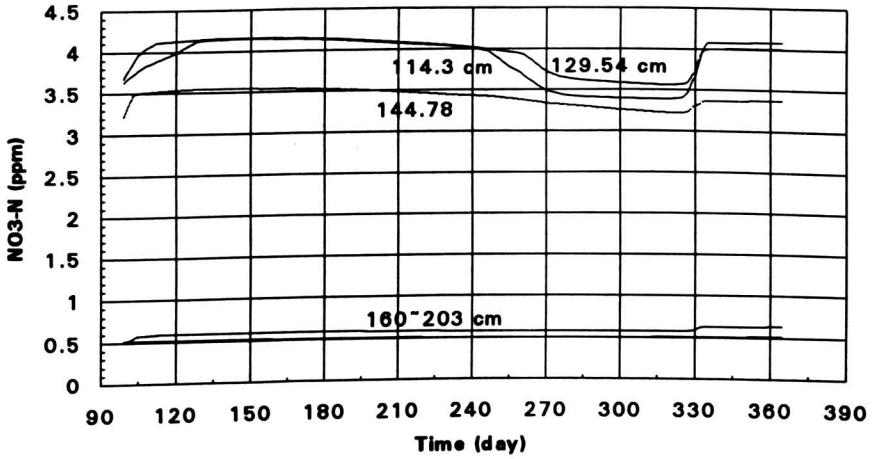

Figure 6.95 Predicted nitrogen concentration at 114-203 cm in 1992 using constant cracking model,

2. Alachlor Simulation Results. The comparison between Figure 6.96 and Figure 6.33 shows that there is no difference between the peak concentrations in the two figures. However, the comparison between Figure 6.97 and Figure 6.34 shows that the alachlor concentration at the 7.6 cm depth in Figure 6.97 is lower than that in Figure 34 for most of the year. The comparison between Figure 6.98 and Figure 6.35 shows that the alachlor concentration at depth 22.8 cm around day 210 in Figure 6.98 is higher than that in Figure

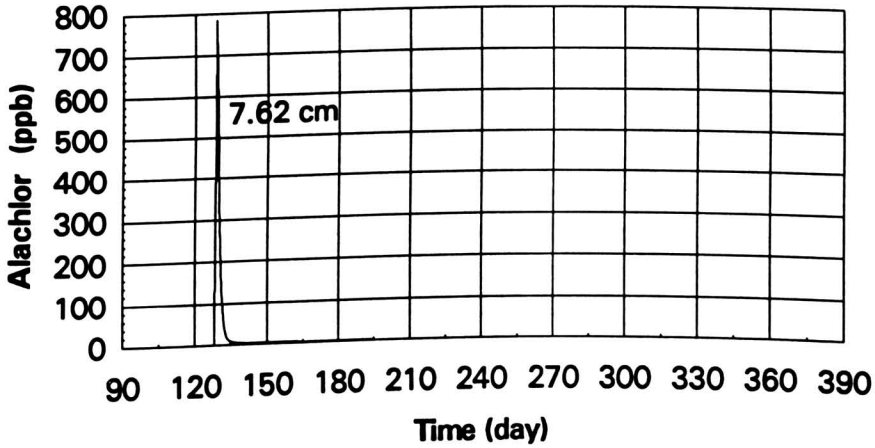

Figure 6.96 Predicted alachlor concentration at depth 7.6 cm in 1992 using constant cracking model.

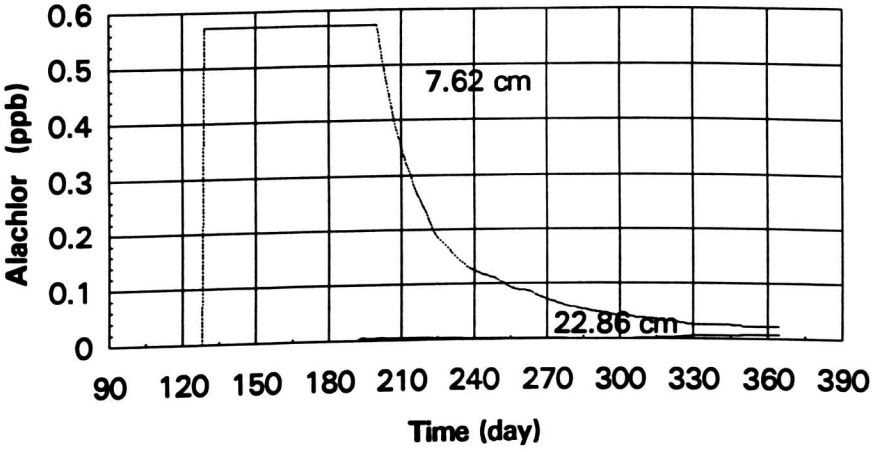

Figure 6.97 Predicted alachlor concentration at depth 7.6 and 22.8 cm in 1992 using constant cracking model.

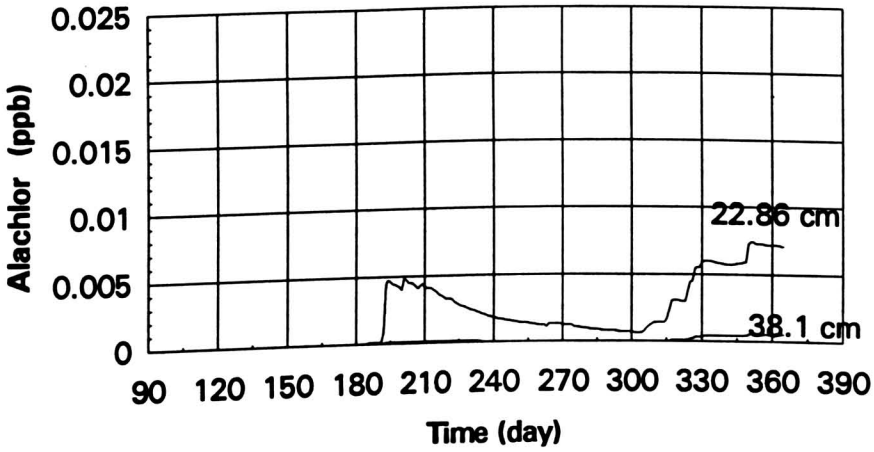

Figure 6.98 Predicted alachlor concentration at depth 22.8 and 38.1 cm in 1992 using constant cracking model.

6.35 while the alachlor concentration at the same depth at the end of the year in Figure 6.98 is lower than that in Figure 6.35. The reason is that when there are constant cracks in the soil profile, more alachlor can be transported by the water flowing in the constant cracks than the case of the Vcr cracking model simulation. At the end of the year, because more alachlor was transported to the depth below 22.8 cm than in the Vcr

cracking model simulation, the alachlor concentration at depth 22.8 cm in the constant cracking model simulation is lower than that in the Vcr cracking model simulation.

6.4.3 The Simulation Results of 1993

A. Water Table Simulation Result. Figure 6.99 shows that the predicted water table is much higher than the measured water table after day 120 and sometimes it almost reaches the ground surface. The predicted water table using constant cracking model is the worst prediction among all the predicted water tables.

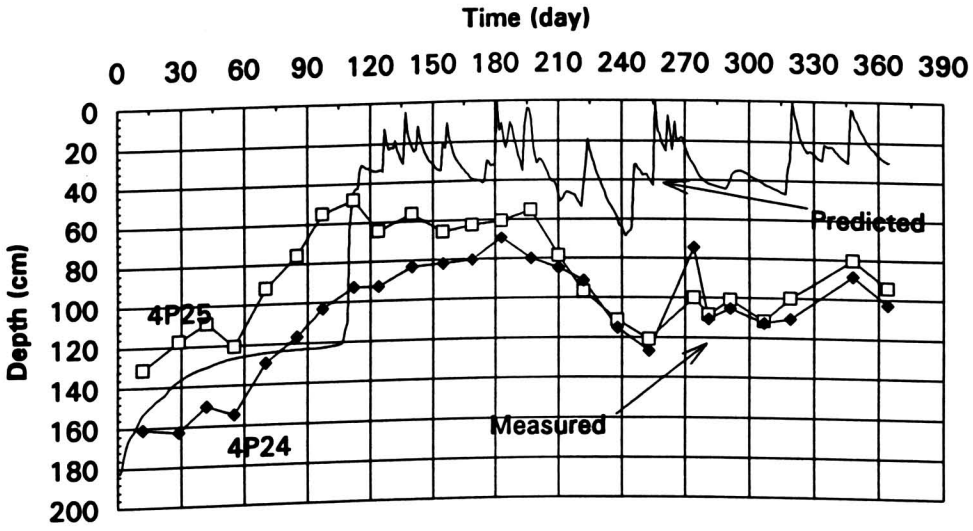

Figure 6.99 Measured and predicted water tables in 1993 using constant cracking model.

B. Water Content Simulation Results. Comparing Figures 6.100 through 6.105 to Figures 6.38 through 6.43 and Figures 6.70 through 6.75, it is obvious that the predicted water contents in Figures 6.100 through 6.105 are the worst among all the predicted water contents in 1993.

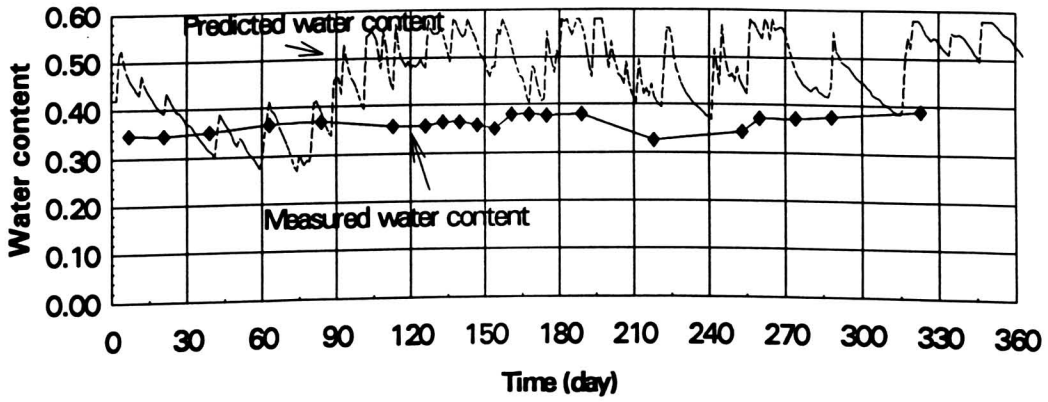

Figure 6.100 Comparison of water content at 15 cm in 1993 using constant cracking model.

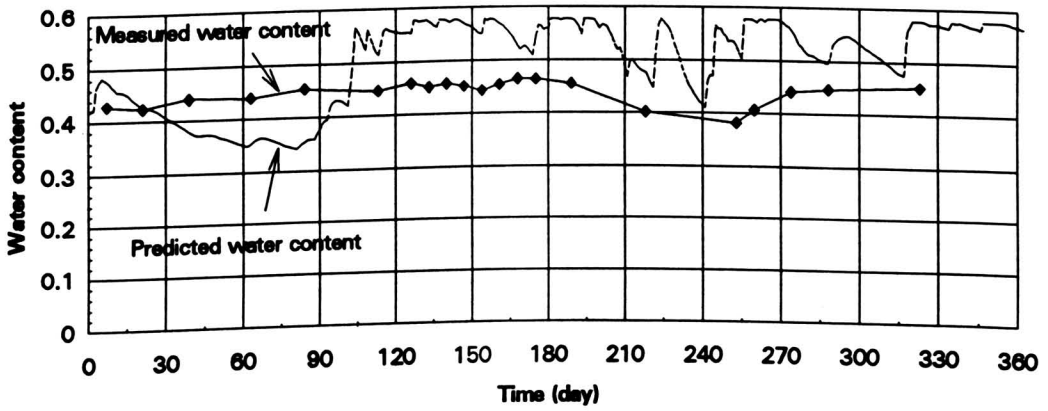

Figure 6.101 Comparison of water content at 30 cm in 1993 using constant cracking model.

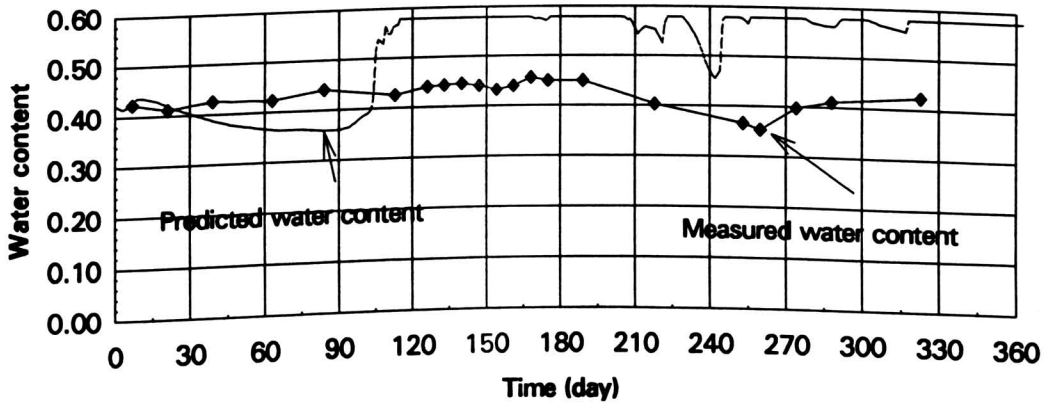

Figure 6.102 Comparison of water content at 45 cm in 1993 using constant cracking model.

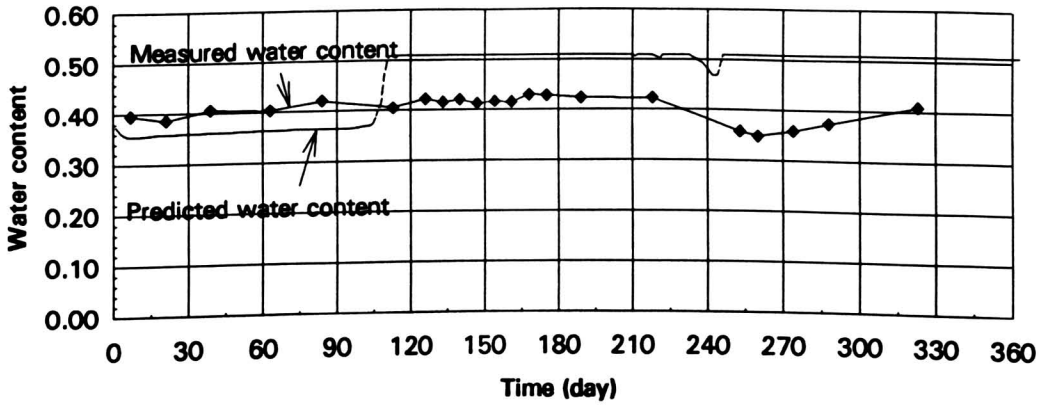

Figure 6.103 Comparison of water content at 60 cm in 1993 using constant cracking model.

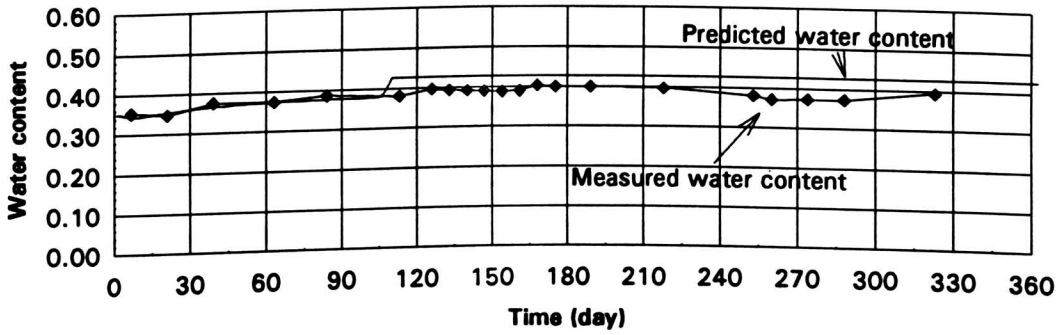

Figure 6.104 Comparison of water content at 75 cm in 1993 using constant cracking model.

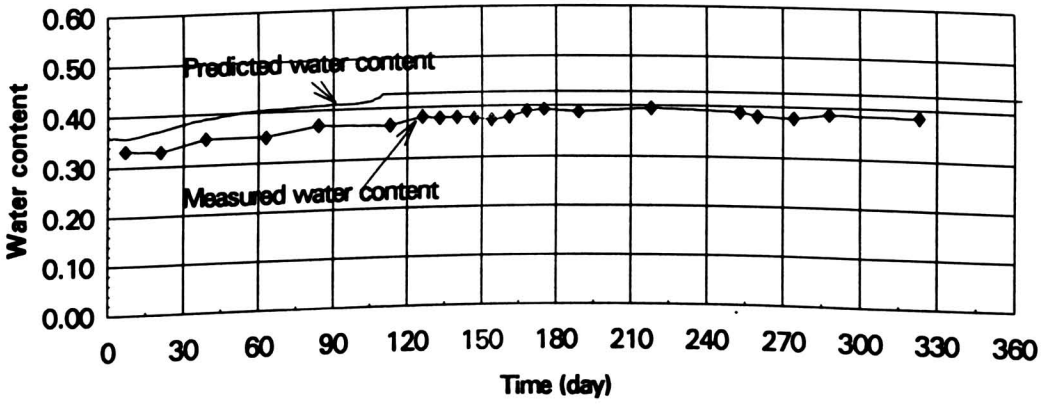

Figure 6.105 Comparison of water content at 90 cm in 1993 using constant cracking model.

C. Nitrogen, Alachlor and Atrazine Simulation Results

1. Nitrogen Simulation Results. The comparison between Figure 6.106 and Figure 6.45 shows that the nitrogen concentration in Figure 6.106 is much higher than that in Figure 6.45. The reason is that when there are constant cracks in the soil profile, less nitrogen is washed away by runoff and more nitrogen is carried down to the soil profile by water flowing in the constant cracks than the case in the Vcr cracking model simulation. Figure 6.107 shows that the nitrogen concentration from depth 22.8 cm to 83.8 cm remains above 1 ug/g, while in Figure 6.46 the nitrogen concentration above depth 53.3 is almost zero after day 210. Figure 6.130 shows that the nitrogen concentration from depth 160 cm to 190 cm goes up in the later half of 1993. Again, this is caused by more flushed-down nitrogen than the case in the Vcr cracking model simulation. The nitrogen profile in 1993 using constant cracking model is different from that in 1992. The reason is that 1993 is a flood year and in 1993 there was a nitrogen application. More nitrogen was flushed down because there was more transporting water in soil profile in 1993 and because there was more nitrogen in the field than in 1992.

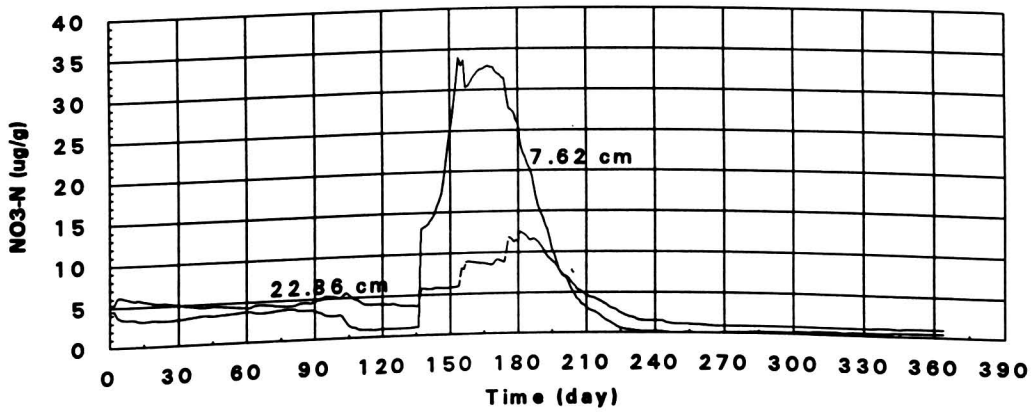

Figure 6.106 Predicted nitrogen concentration at 7.6 cm and 22.8 cm in 1993 using constant cracking model.

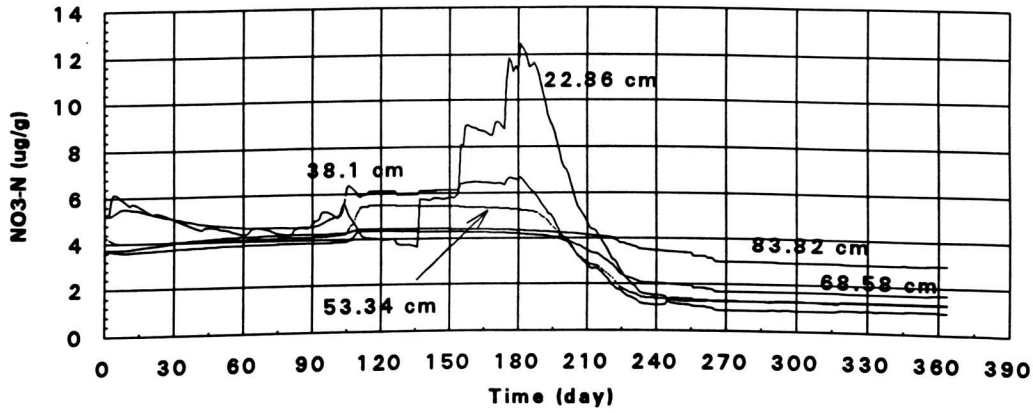

Figure 6.107 Predicted nitrogen concentration at 22-84 cm in 1993 using constant cracking model.

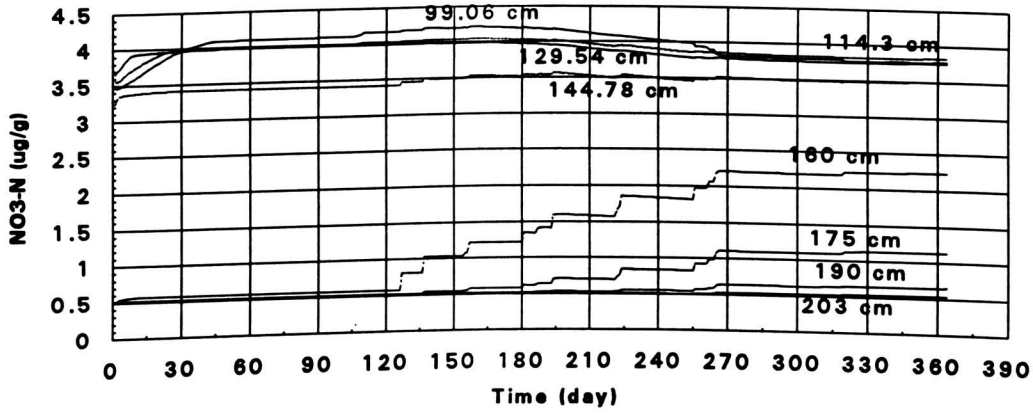

Figure 6.108 Predicted nitrogen concentration at 99-203 cm in 1993 using constant cracking model.

2. Alachlor Simulation Results. The comparison between Figure 6.109 and Figure 6.48 shows that the peak alachlor concentration at the 7.6 cm depth in Figure 6.109 is about 170 ppb higher than that in Figure 6.48. The comparison between Figure 6.110 and Figure 6.49 shows that the alachlor concentrations at depth 22.8 cm and 38.1 cm are much higher than that in Figure 6.49 also. Figure 6.111 shows that the alachlor concentration at depth 53.3 is much higher than that in Figure 6.73 and alachlor even appears at the depth 68.6 cm. All these mean that if there are constant cracks in the soil

profile, agriculture chemicals will move to a deeper depth and appear with a much higher concentration. The comparison between Figure 6.110 and Figure 6.97 show that alachlor concentration at depths 22.8 cm an 38.1 in 1993 is much higher than in 1992, meaning that more alachlor is transported to deep soil profile in 1993 than in 1992. The reason is that in 1993 there was more precipitation than in 1992.

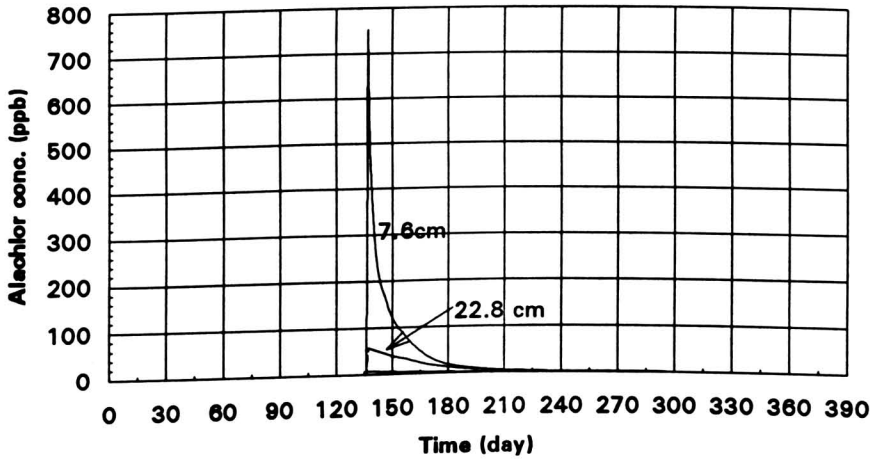

Figure 6.109 Predicted alachlor concentration at 7.6-22.8 cm in 1993 using constant cracking model.

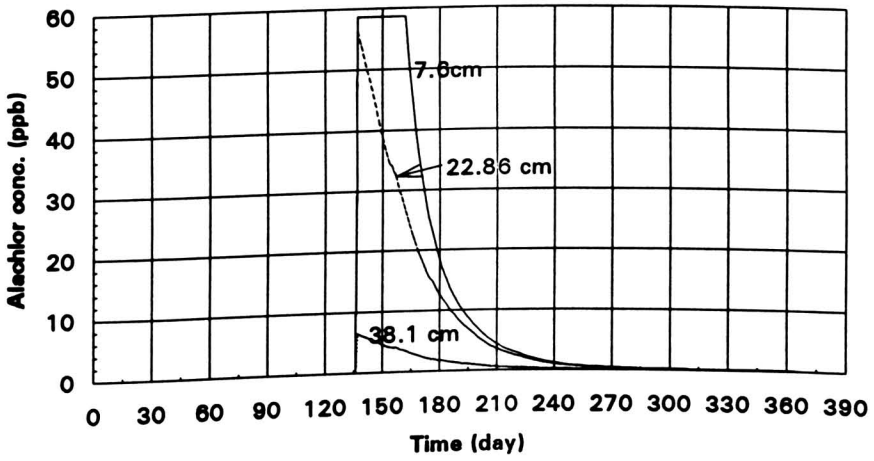

Figure 6.110 Predicted alachlor concentration at 7.6-38.1 cm in 1993 using constant cracking model.

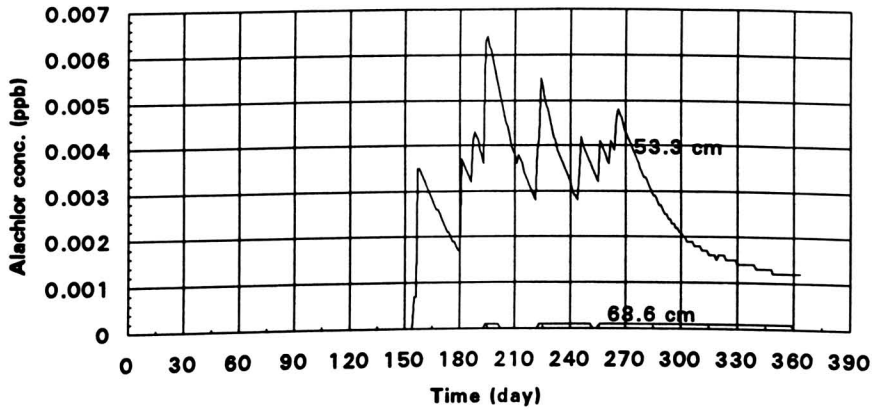

Figure 6.111 Predicted alachlor concentration at 53.3- 68.6 cm in 1993 using constant cracking model.

3. Atrazine Simulation Results. The comparison between Figure 6.112 and Figure 6.51 shows that the peak atrazine concentration at the depth 7.6 cm in Figure 6.112 is about 180 ppb higher than in Figure 6.51, and the atrazine concentration at the depth 22.8 cm in Figure 6.112 is much higher than that in Figure 6.51 also. The atrazine concentration at the depth 38.1 cm through 68.6 cm in Figure 6.113 and 6.114 is much higher than that in Figure 6.52 and 6.53. Figure 6.115 shows that atrazine even appears at the depth 99.1 cm. All above comparisons show the same meaning as alachlor comparisons.

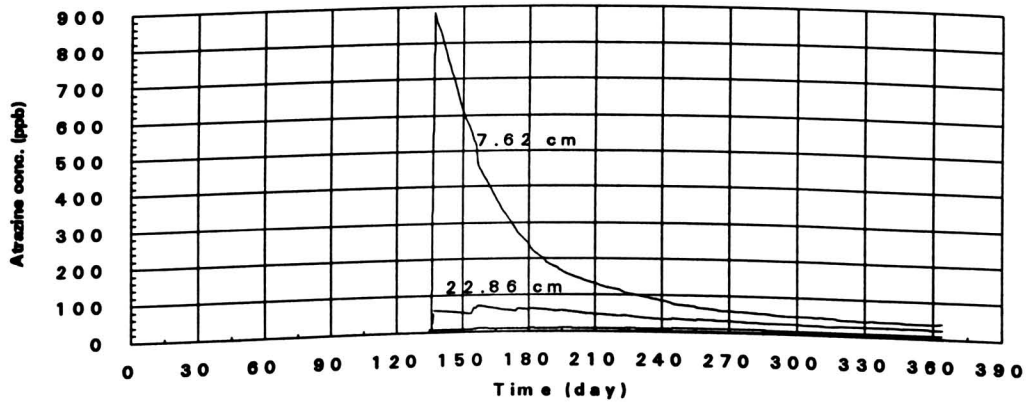

Figure 6.112 Predicted atrazine concentration at 7.6-22.8 cm in 1993 using constant cracking model.

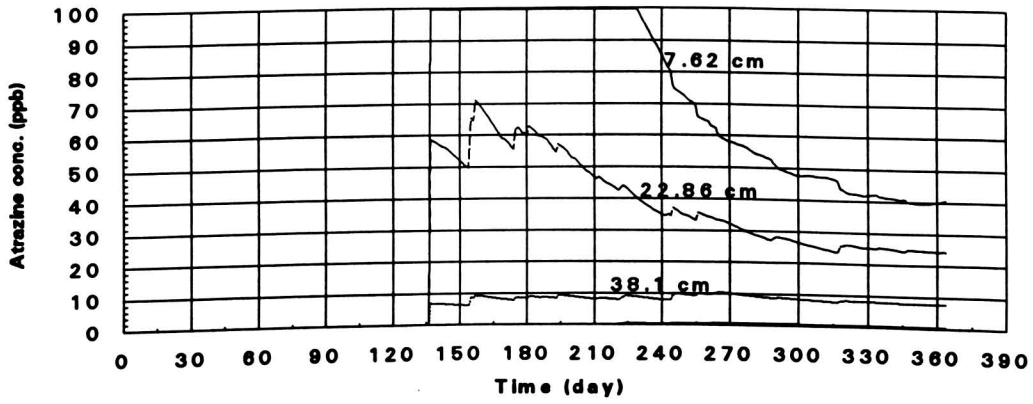

Figure 6.113 Predicted atrazine concentration at 22.8-38.1 cm in 1993 using constant cracking model.

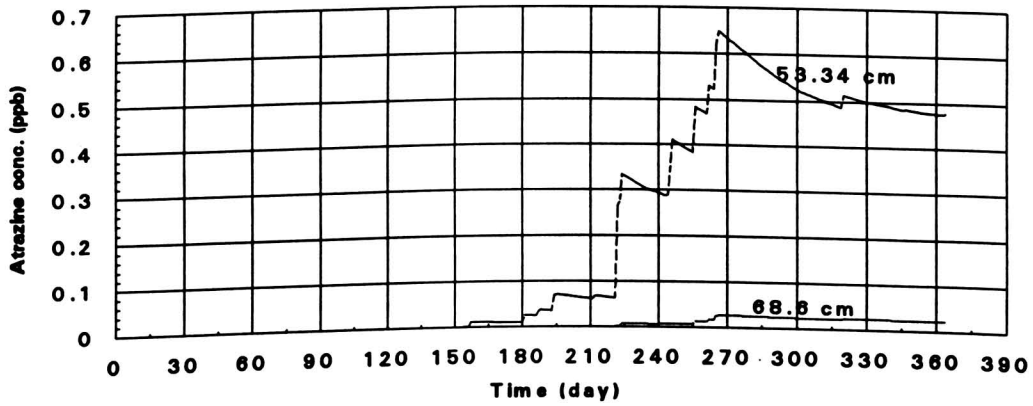

Figure 6.114 Predicted atrazine concentration at 53.3-68.6 cm in 1993 using constant cracking model.

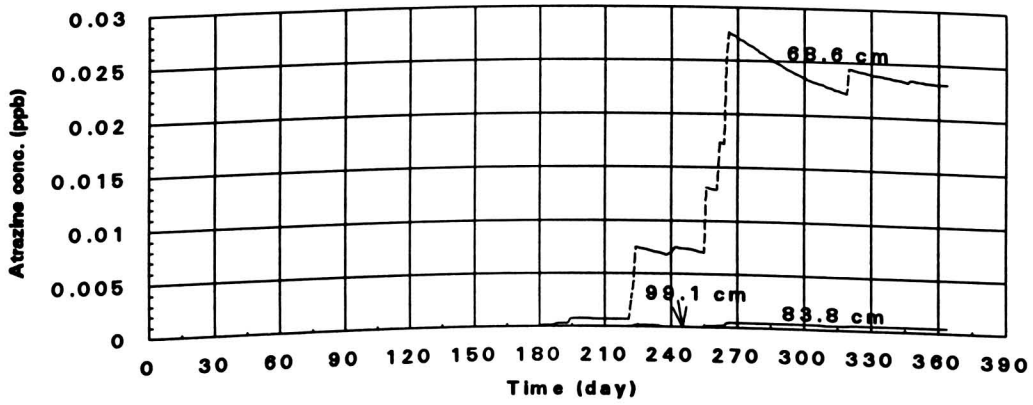

Figure 6.115 Predicted atrazine concentration at 68.6-99.1 cm in 1993 using constant cracking model.

CHAPTER 7

CONCLUSIONS AND RECOMMENDATIONS

7.1 Conclusions

The simulation results of constant cracking model show that it is unrealistic to assume constant cracks at the Missouri MSEA site. This thesis has overcome the limitations in the RZWQM of constant crack specification and non-existence cracks in the top horizon of a soil profile. The first limitation was solved by revising the original FORTRAN code and the second limitation was solved by the use of Equation 2.3 under the assumption that the macroporosity of the first horizon is equal to that of second horizon.

The two schemes to revise RZWQM are successful. In the first scheme, very accurate V_{cr} data are needed. In the second scheme, very accurate soil moisture cracking models are required. The simulations show that the first scheme works better than the second scheme. The keys of using the second scheme are accurate soil moisture cracking models and accurate water content. The predicted water content and the soil moisture cracking models are not accurate, which are the major obstacles in using the second scheme.

By introducing the ratio of crack width to crack length, crack width can be calculated by using Equation 3.15. The ratio of crack width to crack length can be obtained from image analysis data. Because image analysis data vary from place to place, it is arbitrary to use the data from only one image analysis. If there were three adjacent excavations at the same site, better estimates of the ratio of crack width to crack length and the number of cracks per unit area could be obtained. Unfortunately, there was only one excavation per site.

In chapter 4, the values for the thirteen hydraulic parameters were determined based on laboratory data measured by Baer (1995). Among the thirteen parameters, only residual water content can not be used in running the RZWQM because when the residual water content is input into the RZWQM, the RZWQM predicts unrealistic water content. Instead of using the residual water content obtained in this thesis, Rawls' mean values of residual water content for each horizon were used in the simulations (Rawls, 1982). The other twelve parameters obtained in this thesis were used in running the RZWQM and the revised RZWQM. However, the predicted water contents in all the simulations do not exactly coincide with the measured water content, meaning that some parameters need to be improved. Trying to find better values for these parameters, the mean values of the thirteen hydraulic properties from Rawls were used in running the RZWQM. Nevertheless, the water table could not be maintained within the range of measured water table using the mean values of hydraulic properties from Rawls. Overall, the twelve soil hydraulic property values determined in this thesis are reasonably correct, and no other hydraulic property values were found to improve the simulations.

In order to simulate the fluctuation of water table, the depth of the soil profile must be set to 208 cm. By using this depth, the predicted water tables in the simulations without macropores and the simulations of the V_{cr} cracking model and the soil moisture cracking model vary within the range of the measured water table. The water table simulation results without cracking in 1992 and 1993 show that the predicted water table is lower than the measured water table during the last one-third of these two years. This means that without cracking, less water is permitted to infiltrate to a deeper depth, and there must be variable cracks in the field. When the V_{cr} data were input into the revised RZWQM, the revised model produced better predicted water table in the 1992 run and over-predicted the water table in the latter one-third of the year in the 1993 run. This could mean that the V_{cr} data in 1992 are more accurate than those in 1993. Also, it could

mean that the model cannot fit a flood year. When the soil moisture cracking models developed in this thesis were used, the revised RZWQM gave better predicted water table again in the 1992 run and over-predicted the water table in the latter one-third of the year in the 1993 run too. However, the comparison between the water table simulation results of 1993 of the V_{cr} cracking model and the soil moisture cracking model shows that the water table simulation using the soil moisture cracking model is better than the simulation using the V_{cr} cracking model. The water table prediction in the simulation of the constant cracking model is the worst among all the water table predictions. It should be emphasized here that both the V_{cr} cracking model and the soil moisture cracking model are correct methods to solve variable cracking problem and the revised RZWQM should produce the same results if the V_{cr} data and the soil moisture cracking models are accurate.

None of the water content simulation results are perfect since some hydraulic property values still need to be improved. However, the simulations of the V_{cr} cracking model and the soil moisture cracking model predict water content better than the simulations without cracks and the simulations of constant cracking model.

In additon, it was possible that the water in the saturated zone below the water table moved laterally as well as vertically. The model simulations used in this thesis assumed that only vertical flow occurred.

The analysis of the predicted nitrogen concentration profile illustrates that the predicted nitrogen concentrations are meaningful. However, not enough measured nitrogen concentration data are available for comparison. The comparison between the measured nitrogen concentration and the predicted nitrogen concentration on April 29, 1992 shows that the predicted nitrogen concentration matches the measured nitrogen concentration while the comparison between the predicted nitrogen concentration and the measured nitrogen concentration on October 28, 1992 shows that the RZWQM under-

predicts the nitrogen concentration at shallow depth (0-40 cm) and over-predicts nitrogen concentration at deep depth (60-150 cm). Two possibilities may result in the poor match on October 28, 1992. One is that the model lets too much nitrogen move with leaching-down water. The other is that the model under-predicts the production of nitrogen by soybeans. The simulation results show that cracks transport some nitrogen to deep depths and some amount of nitrogen accumulates in the depth where there are no cracks (depths deeper than 90 cm). Among the three cracking model simulations, the constant cracking model simulation can transport more nitrogen to deeper depths than the other two cracking model simulations. The alachlor and atrazine simulation results of the three cracking model simulations show the same trends as the nitrogen simulation results. In the constant cracking model simulation, alachlor and atrazine can appear at deeper depths than in the simulations without macropores, in the simulations using the V_{cr} cracking model, and in the simulations using the soil moisture cracking model.

In conclusion, variable cracking plays an important role in the transport of agricultural chemicals. Based on the data and assumptions used in this thesis, the most successful method used in the prediction of water table and water content is the V_{cr} cracking model. However, it may be more practical to use the soil moisture cracking model because it may be more convenient to measure soil moisture than to install anchor plates and measure their elevation changs for the V_{cr} data.

7.2 Recommendations For Further Study

During the course of this study, many interesting and quite challenging questions have come to mind. The following briefly describe some of these differing ideas:

1) All the cracking data are calculated by assumption of isotropic shrinkage. It would be interesting to investigate the case when the geometry factor r_s is greater than three or less than three. It is possible to get better cracking data if a correct r_s is used.

2) More effort should be put to find reasonable θ_r instead of just to use the mean values of Rawls.

3) It could be interesting to investigate the reason why the model does not predict nitrogen concentration very well.

4) In the stead of running the RZWQM for one year, the version 3.2 of the RZWQM could be run for at least forty years. Multiple year operation can take care of the effects of plant, agricultural chemicals of last several years, and more reasonable results can be expected.

5) The right method to simulate variable cracking is to develop soil moisture cracking model for different soils. After a lot of soil moisture cracking models for different soils have been developed, a cracking model data system can be developed. Then, the future RZWQM can choose the relevant cracking model from the cracking model data system for a soil to simulate the effects of variable cracking on the movement of agricultural chemicals.

REFERENCES

Aitchison, G.D. and J.W. Holmes, 1953. Aspects of swelling in the soil profile. Aust. J. appl. Sci. 4: 244-259.

Anderson, S.H., J.U. Baer and K.S. McGinty, 1992. Quantifying crack features in Missouri claypan soils. *In*: Missouri MSEA project plan, Vol. 2, p. 101-117.

Anderson, S.H., 1995. Personal communication.

Baer, J.U., S.H. Anderson, and K.S. McGinty, 1993. Quantifying desiccation cracking in a Missouri claypan soil. p.26-31. *In* Proceedings of the 3rd annual Missouri water quality conference. Columbia, Missouri. 4-5 Feb. 1993.

Baer, J.U., 1994. Predicting Unsaturated Conductivity-special project for advanced soil physics, a course in the Department of Soil and Atmospheric Sciences (unpublished).

Baer, J.U., 1995. Personal communication.

Berteau, P.E., and D.P. Spath, 1986. The toxicological and epidemiological effects of pesticide contamination in California ground water. p. 423-435. *In*: W.Y. Garner, R.C. Honeycutt, and H.N. Nigg, eds. Evaluation of Pesticides in Ground Water. ACS Symp. Ser. 315. American Chemical Society, Washington, DC.

Blanchard, P. E., 1995. Personal communication.

Blanchard, P.E., W.W. Donald and E.E. Alberts, 1995. Herbicide concentrations in groundwater in claypan soil watershed. p. 21-24. In Clean water-clean environment-21st century conf. proc., Kansas City, Missouri. 5-8 March 1995. ASAE, St. Joseph, Michigan.

Bronswijk, J.J.B. 1991. Magnitude, modeling and significance of swelling and shrinkage processes in clay soils. Ph.D. thesis. Wageningen Agricultural University, Wageningen, The Netherlands. 145pp.

Brooks, R.H. and A.T. Corey, 1964. Hydraulic properties of porous media. Hydrology paper 3, Colo. State Univ., Fort Collings, CO, USA. 1-27.

Chan, K.Y., 1982. Shrinkage characteristics of soil clods from a gray clay under intensive calculation. Aust. J. Soil Res. 20:65-68.

Cohen, D.B. 1986. Ground water contamination by toxic substances. A California assessment. p. 499-529. *In*: W.Y. Garner, R.C. Honeycutt, and H.N. Nigg, eds. Evaluation of Pesticides in Ground Water. ACS Symp. Ser. 315. American Chemical Society, Washington, DC.

Dasog, G.S., D.F. Acton, A.R. Mermuth and E. de Jong., 1988. Shrink-swell potential and cracking in clay soils of Saskatchewan. Can. J. Soil Sci. 68: 251-260.

Doorenbos, J., and Pruitt, W.O., 1977. Guidelines for prediction crop water requirements. FAO Irrig. and Drain. Paper No. 24, 2nd ed., FAO Rome, Italy. 156pp.

Guinan, P. E., 1995. Personal communication.

Haines, W.B., 1923. The volume changes associated with variations of water content in soil. J. Agric. Sci. 13:296-311.

Hallberg, G.R., 1986. From hoes to herbicides: agriculture and groundwater quality. J. Soil Water Conserv. V. 41, p. 357-364.

Hance, R.J. 1987. Herbicide behavior in the soil, with particular reference to the potential for ground water contamination. *In*: D.H. Hutson and T.R. Roberts, eds. Herbicides. John Wiley and Sons, N.Y., p. 223-247.

Harris, C.I., E.A. Woolson, and B.E. Hummer, 1969. Dissipation of herbicides at three soil depths. Weed Sci. V. 17, p. 27-31.

Helling, C.S., and T.J. Gish, 1986. Soil characteristics affecting pesticide movement into ground water. *In*: W.Y. Garner, R.C. Honeycutt, and H.N. Nigg, eds. Evaluation of Pesticides in Ground Water. ACS Symp. Ser. 315. American Chemical Society, Washington, DC., p. 14-37.

Helling, C.S., W. Zhuang, T.J. Gish, C.B. Coffman, A.R. Isensee, P.C. Kearney, D.R. Hoagland, and M.D. Woodward, 1988. Persistence and leaching of atrazine, alachlor, and cyanazine under no-tillage practices. Chemosphere V. 17, p. 175-187.

Holmes, J.W., 1955. Water sorption and swelling of clay blocks. J. of Soil Sci. 6: 200-207.

Isensee, A.R., C.S. Helling, T.J. Gish, P.C. Kearney, C.B. Coffman, and W. Zhuang, 1988. Groundwater residues of atrazine, alachlor, and cyanazine under no-tillage practices. Chemosphere V. 17, p.165-174.

Jamison, V.C. and G.A. Thompson, 1967. Layer thickness changes in a clay-rich soil in relation to water content changes. Soil Science Society of America Proc. 31: 441-444.

Jayawardane, N.S. and E.L. Greachen., 1987. The nature of swelling in soils. Aust. J. Soil Res. 25: 107-113.

Johnston, J.R. and H.O. Hill, 1944. A study of the shrinking and swelling properties of rendzina soils. Soil Sci. Soc. Am. Proc. 9: 24-29.

Kelly, B.P., D.W. Blevins and A. C. Ziegler, 1992. The role of preferential flow in the transport of agricultural chemicals in claypan soils. *In*: Missouri MSEA project plan, Vol. 2, p. 119-128.

Kitchen, N. R., 1995. Personal communication.

Korvin, G, 1989. Fractured but not fractal: Fragmentation of the Gulf of Suez basement. PAGEOPH 131(1/2):289-305.

Lauritzen, C.W. and A.J.Stewart, 1941. Soil volume changes and accompanying moisture and pore-space relationships. Soil Sci. Soc. Am. Proc. 6: 113-116.

Lavy, T.L., F.W. Roeth, and C.R. Fenster, 1973. Degradation of 2,4-D and atrazine at three depths in the field. J. Environ. qual. V. 2, p. 132-137.

Moorman, T.B., and S.S. Harper, 1989. Transformation and mineralization of metribuzin in surface and subsurface horizons of a Mississippi delta soil. J. Environ. Qual. 18: 302-306.

Muelam, Y., 1976. A new model for predicting the hydraulic conductivity of unsaturated porous media. Water Resour. Res. 12: 513-522.

Newman, A.C.D. and A.J. Thomasson, 1979. Rothamsted studies of soil structure. III. Pore size distribution and shrinkage processes. J. Soil Sci. 30: 415-439.

Oostindie K. and J.J.B. Bronswijk, 1992. FLOCR - A simulation model for the calculation of water balance, cracking and surface subsidence of clay soils. Wageningen (The Netherlands), DLO The Winand Staring Centre. Report 47, 65 pp.

Rao, P.S.C., A.G. Hornsby, and R.E. Jessup, 1985. Indices for ranking the potential for pesticide contamination of ground water. Proc. Soil Crop Sci. Soc. Fla. 44:1-8.

Rawls, W.J., D.L. Brakensiek and K.E. Saxton, 1982. Estimation of soil water properties. Trans. ASAE 25: 1316-1320, 1328.

Reeve, M.J. and D.G.M. hall., 1978. Shrinkage of clayey subsoils. J. of Soil Sci. 29: 315-323.

Reeve, M.J., D.G.M. Hall and P. Bullock. 1980. The effect of soil composition and environmental factors on the shrinkage of some clayey British soils. J. of Sci. 31: 429-442.

Seaki, T., 1959. Interrelationships between leaf amount, light distribution and total photosynthesis in a plant community. Bot. Magazine, Tokyho 73:55-63.

Stirk, G.B., 1954. Some aspects of soil shrinkage and the effect of cracking upon water entry into the soil. Aust. J. Agric. Res. 5: 279-290.

Tempany, H.A., 1917. The shrinkage of soils. J. Agr. Sci. 8:312-330.

USDA-ARS, 1992a. Root Zone Water Quality Model (RZWQM). Technical documentation, version 1.0. GPSR Techinical Report No. 2. Fort Collins, CO.

USDA-ARS, 1992b. Root Zone Water Quality Model (RZWQM). User's manual, version 1.0. GPSR Techinical Report No. 3. Fort Collins, CO.

USDA-ARS, 1995. Root Zone Water Quality Model (RZWQM). User's manual, version 3.0. GPSR Techinical Report No. 5. Fort Collins, CO.

van Genuchten, M.Th., 1980. A closed-form equation for predicting the hydraulic conductivity of unsaturated soils. Soil Sci. Soc. Am. J. 44:892-898.

Walpole, R. E. and Myers, R. H., 1989. Probability and statistics for engineers and scientists. Macmillan Publishing Company, New York, NY.

Woodruff, C.M, 1936. Linear changes in the Selby loam profile as a function of soil moisture. Soil Sci. Soc. Am. Proc. 1: 65-69.

Yaalon, D.H. and D. Kalmar, 1984. Extent and dynamics of cracking in a heavy clay soil with xeric moisture regime. *In*: J. Bouma and P.A.C. Raats (eds.). Proceedings ISSS Symposium on water and solute movement in heavy clay soils. Publ. 37. International Institute for Land Reclamation and Improvement, Wageningen, the Netherlands:45-48.

Yule, D.F. and J.T. Ritchie, 1980a. Soil shrinkage relationships of Texas Vertisols. I. Small cores. Soil Sci. Soc. Am. J. 44:1285-1295.

Yule, D.F. and J.T. Ritchie, 1980b. Soil shrinkage relationships of Texas Vertisols. II. Large cores. Soil Sci. Soc. Am. J. 44: 1291-1295.

Appendix A Subroutines in the RZWQM Program

File name	Subroutine name	Line No.	Function name	Line No.	External Line No.
1 RZCHEM.FOR	1 ACDCOF	2			
	2 ACDEXC	360			
	3 ACDUPD	460			
	4 ACDVTR	608			
	5 ALKCOF	931			
	6 ALKEXC	1143			
	7 ALKUPD	1206			
	8 ALKVTR	1326			
	9 CHEM	1555			
	10 SCACD	1739			
	11 SCALK	1840			
	12 SCCON	1938			
	13 SCDBHK	2105			
	14 SCINIT	2179			
	15 SCMAIN	2315			
	16 SCSOLV	2495			
	17 SOLVSL	2634			
2 RZDAY.FOR	1 ADJDT	2			
	2 CHSPAN	92			
	3 PHYSCL	210			
	4 MASSBL	1226			
	5 RECON	1361			
	6 REDUCE	1521			
	7 SETTL	1578			
	8 STMINP	1637			
	9 DRAIN	1791			
	10 UPTAK	1939			
	11 TILEFLO	2142			
3 RZMAIN.FOR	1 INIT	1575			
	2 INPDAY	1941			
	3 INPUT	2064			
	4 TILADJ	3230			
	5 NITBAL	3662			
	6 NITBYR	3951			
	7 ECHO	4027			
	8 SIXAVG	4061			
	9 PESBAL	4150			
	10 PLREAD	4311			

4 RZMAN.FOR	1 CDATE	2	JDATE	374	
	2 MAIRR	67			
	3 MEQUE	435			
	4 MAQUE	488			
	5 BMPOPT	1013			
	6 BMPNIT	1117			
	7 MATILL	1271			
	8 MAFERT	1599			
	9 MAPEST	1751			
	10 MANURE	1994			
	11 MANOUY	2142			
	12 MAPLNT	2293			
	13 TMHARV	2931			
	14 HARVST	3069			
5 RZNUTR.FOR	*1 FCORR	2	FDCN	2156	NUTRTD 925
	2 NUTRI	74	CNEW	2330	DERIVS 1908
	*3 NUTRTD	571			
	*4 O2SOL	785			
	5 OMNI	883			
	*6 OMNIDC	944			
	*7 PRCRAT	1289			
	8 RK4	1882			
	9 RKDUMB	1994			
	*10 VOLAT	2074			
	11 RDECMP	2211			
	12 BIOTIL	2280			
6 RZOUT.FOR	1 CENTER	2	IFIRLT	529	
	2 CLOSER	46	ITRIM	570	
	3 CNTLRD	138			
	4 FAPEND	260			
	5 FIXLAB	295			
	6 HZPARO	361			
	7 OPENER	564			
	8 OUTIN1	668			
	9 OUTIN2	767			
	10 PLTHD	869			
	11 SGATE	1138			
	12 SWRITE	1298			
	13 TABHD	1339			
	14 VGATE	1419			
	15 VTAB	1611			
	16 VWRITE	1702			
7 RZSPUD.FOR	1 POTATO	5			
	2 INSIMP	456			

	3 PHENOL	582				
	4 OPHARV	901				
	5 PHASEI	958				
	6 GROSUB	1088				
	7 PRTTNVG	1519				
	8 PARTTN	1711				
	9 NFACTO	2014				
	10 ROOTGR	2085				
	11 DAYLTH	2158				
	12 PROGRI	2174				
8 RZPEST.FOR	1 PEMAIN	1				
	2 KDSTAR	282				
	3 KSBIO	364				
	4 KSSOIL	448				
	5 KSSURF	651				
	6 PASURF	770				
	7 PEDAUG	917				
	8 PEWASH	1008				
	*9 RTUPTK	1103				
	10 WASHOF	1198				
9 RZPET.FOR	1 ECONST	192	ALBSWS	2	FUNC	361
	2 MAXSW	464	CSRAD	69	CSRAD	549
	3 NETRAD	718	STRANS	131		
	4 POTEVP	788	GAUSS	300		
	5 RESIST	1136	SWSUM	1365		
			SNOWQE	1410		
10 RZPLNT.FOR	1 COLNIZ	127	AVEMOV	2		
	2 DCALC	441	BELL	64		
	3 ENVSTR	848	DLODG	627		
	4 ESTAB	988	EHERBP	683		
	5 FSDDTH	1070	ENDFND	720		
	6 GRSTAG	1204	ENITP	801		
	7 MORTAL	1314	EPHOP	951		
	8 PARTIT	1400	GROINT	1141		
	9 PGINIT	1542	HYP	1267		
	10 PGMAIN	1629	PHOPER	3320		
	11 PGNITE	2892	PHOTO	3376		
	12 DISTN	3144	PLPROD	3534		
	13 PLHGT	3469	SHTDET	3895		
	14 RTDIST	3633	THRESH	4039		
	15 SNSNC	3979	WPRESP	4084		
	16 CALCEVP	4145	CALCWAT	4197		
	17 VERNALIZ	4240				
11 RZRICH.FOR	1 CHKBC	2	POINTK	567		

	5 MZPHASEI	548	
	6 MZGROSUB	682	
	7 MZNFACTO	919	
	8 NUPTAK	948	
	9 MZROOTGR	970	
15 SNOWPRMS.FOR	1 SNOWCOMP_PRMS	2	
	2 SNOINIT	139	
	3 SNORUN	180	
	4 PPT_TO_PACK	452	
	5 CALOSS	566	
	6 CALIN	607	
	7 SNALBEDO	677	
	8 SNOWBAL	790	
	9 SNOWEVAP	895	
	10 SNOWCOV	947	
	11 READ_SNOW	1020	

* NOT BE CALLED IN VERSION 3.0 BUT STILL IN THE FILE

Appendix B Call Tree of the RZWQM

```
MAIN PROGRAM RZWQM
RZWQM→ INPUT→OUTIN1→OPENER
                   →SGATE→SWRITE
                          →TABHD→FIXLAB→CENTER(6 TIMES)
                          →SWRITE
                   →VGATE→VWRITE
                          →VTAB  →FIXLAB→CENTER(6 TIMES)
       →PLREAD
       →INDEXR
       →SOILPR
  → INIT  →VGATE →VWRITE
                 →VTAB  →FIXLAB →CENTER(6 TIMES)
       →SGATE  →SWRITE
                 →TABHD →FIXLAB →CENTER(6 TIMES)
                 →SWRITE
       →VGATE (7 TIMES)  →VWRITE
                          →VTAB→FIXLAB →CENTER(6 TIMES)
  → TILADJ→INDEXR
          →SOILPR
          →HZPARO
  → VGATE (23 TIMES)
  → SGATE
  → OUTIN2 →CNTLRD
           →CLOSER →FAPEND
           →OPENER
           →PLTHD
  → VGATE
  → SGATE
  → WATBL
  → HYDPAR
IF (ICHEM.EQ.1) THEN
  → CHEM   →SCMAIN→SCCON
                  →SCDBHK
                  →SCINIT →ALKEXC
                          →ACDEXC
                  →SCALK→ALKVTR
                          →ALKCOF
                          →SOLVSL
```

```
                                        →ALKUPD
                                  →ACDEXC
                                  →SCACD  →ACDVTR
                                          →ACDCOF
                                          →SOLVSL
                                          →ACDUPD
                                  →ALKEXC
                                  →SCDBHK
                                  →SCSOLV
ENDIF
        → NUTRI   →RDECMP
                  →BIOTIL
                  →OMNI →RKDUMB→DERIVS
                                  →RK4 →DERIVS
                  →SGATE(3 TIMES)
                  →VGATE(4 TIMES)
        → PESBAL
DO 500 MDAY=JBDAY,JEDAY
        → CDATE
 IF (NSC.GT.1)    →VGATE
        → INPDAY
        → KDSTAR
        → MAIRR   →CDATE
                  →MANOUT (3TIMES) →CDATE
        → MAQUE   →MANOUT →CDATE
        → MAFERT →MANOUT →CDATE
        → MAPEST →MANOUT →CDATE
        → MANURE→MANOUT →CDATE
        → MATILL  →MANOUT →CDATE
                  →SOILPR
        → HYDPAR
        → PHYSCL →POTEVP →ECONST
                         →MAXSW
                         →RESIST
                         →NETRAD
                  →RECON  →REDUCE
                         →SETTL
                  →SOILPR
                  →DRAIN
                  →WCHEAD
                  →WATBL
                  →STMINP
```

```
→SNOWCOMP_PRMS →READ_SNOW
                →SNOINIT
                →CDATE
                →SNORUN→PPT_TO_PACK→CALIN
                                    →CALOSS
                       →SNOWCOV
                       →SNALBEDO
                       →SSNOWBAL→CALIN
                                →CALOSS
                                →CALIN
                       →SSNOWBAL→CALIN
                                →CALOSS
                                →CALIN
                       →SNOWEVAP
→MANOUT
→CHSPAN
→MANOUT
→TILFLO
→EVNTRO→NTRPTR (4 TIMES)
       →CHEMBL
       →INFIL →UNSATFLO
              →MPFLOW
              →TILEFLO
              →SATFLO
              →FULFLO
              →UGFLOW
              →UNSATFLO →KNETIC
       →MOVE
       →MOVET
       →AVGRID (2 TIMES)
       →CHEMBL
       →SGATE
→WCHEAD
→WATBL
→MASSBL
→ADJDT
→SINK
→REDIST →RICHRD →REDGRD →INITCOND
                →CHKBC
                →CNHEAD →CHKBC
                →NODFLX
                →WCNODS
```

```
                                        →TRUGRD
                                →RETRAN →REROUT
                                        →REKNTC
                                →DRAIN
                                →WCHEAD
                                →WATBL
                        →HEATFX→HEATEQ →TBC
                                        →VMOVE
                                        →FACEC
                                        →TPROF →THCOND
                                               →HEATCO
                                               →TRIDAG
                                        →CHKCON
                                        →VMOVE
                        →UPTAKE
                        →RTUPTK
                        →MASSBL
                        →SGATE (26 TIMES)
                        →VGATE (4 TIMES)
DO 11 IP=1,NPEST
 IF (PACTIV(IP)) THEN
        → PEMAIN →KSBIO
                 →KSSURF
                 →KSSOIL
                 →PASURF (2 TIMES)
                 →KSSOIL
                 →PEDAUG (3 TIMES)
 ENDIF
 IF (NSC.GT.1) THEN
   →VGATE(2 TIMES)
   →SGATE (3 TIMES)
 ENDIF
11 CONTINUE
 IF (NSC.GT.1)
        → SGATE (2 TIMES)
        → VGATE (17 TIMES)
 ENDIF
 IF (ICHEM.EQ.1) THEN
        → CHEM   →SCMAIN→SCCON
                        →SCDBHK
                        →SCINIT →ALKEXC
                                →ACDEXC
```

```
                                    →SCALK →ALKVTR
                                           →ALKCOF
                                           →SOLVSL
                                           →ALKUPD
                                    →ACDEXC
                                    →SCACD →ACDVTR
                                           →ACDCOF
                                           →SOLVSL
                                           →ACDUPD
                                    →ALKEXC
                                    →SCDBHK
                                    →SCSOLV
ENDIF
        → NUTRI   →RDECMP
                  →BIOTIL
                  →OMNI→RKDUMB →DERIVS
                                →RK4 →DERIVS
                  →SGATE(4 TIMES)
                  →VGATE(4 TIMES)
        → SIXAVG
        → VGATE (19 TIMES)
        → MAPLNT→MANOUT
                  →POTATO →INSIMP
                          →PROGRI
                          →DAYLTH
                          →ROOTGR
                          →PHENOL
                          →PHASEI
                          →GROSUB →NFACTO
                                  →PRTTNVG
                                  →PARTTN
                          →OPHARV
                  →PGMAIN →PGINIT →FSDDTH
                          →ENVSTR
                          →GRSTAG
                          →COLNIZ →CALCEVP
                                  →VERNALIZ
                          →ESTAB
                          →PLHGT
                          →SNSNC
                          →MORTAL
                          →PARTIT
```

```
                                    →DCALC
                                    →RTDIST
                                    →PGNITE →DISTN
                                    →SGATE (13 TIMES)
                                    →VGATE (2 TIMES)
                          →SGATE (3 TIMES)
                          →TMHARV →HARVST →CDATE
                          →CERESMZ→INMAIZ
                                    →MZROOTGR
                                    →MZGROSUB →MZNFACTO
                                              →NUPTAK
                                    →MZPHENOL
                                    →MZOPHARV
                                    →MZPHASEI
                          →SGATE (18 TIMES)
                          →VGATE
                          →SGATE (3 TIMES)
                          →CDATE
                          →SGATE (4 TIMES)
                          →VGATE (2 TIMES)
          → MEQUE
          → NITBAL →NITBYR
                   →CDATE
                   →SGAGE (4 TIMES)
          → PESBAL →VGAGE
                   →CDATE
          → SGATE (4 TIMES)
          → VGATE
          → SGATE
500 CONTINUE
          → CLOSER →FAPEND
```

Appendix C Revised Program Part

1. The revised part for the simulation using the V_{cr} cracking model.

After the line 420 in the file RZMAIN.FOR

```
      OPEN(UNIT=10,FILE='CRK.TXT', STATUS='UNKNOWN',ERR=550)
      DO 11 I=1,153
      READ(10,*) IDA, YY1(I),YY2(I),YY3(I)
      PRINT*,IDA,YY1(I),YY2(I),YY3(I)
11    CONTINUE
      CLOSE (10)
      OPEN(UNIT=10,FILE='CRCKWH.OUT',STATUS='UNKNOWN',ERR=550)
      WRITE(10,12)
12    FORMAT(' DAY   LAYER 1   LATER 2   LAYER 3   LAYER 4 ')
```

After the line 458 in the file RZMAIN.FOR

```
      WRITE(*,551) WP
551   FORMAT(6F10.3)
      IF (JBDAY.GE.170.AND.JEDAY.LE.322) THEN
       JYY=JBDAY-169
       I=2
       YY=YY1(JYY)
       IF (YY.LT.0.0) YY=0.0D0
       MCPOR(I)=YY/15.0D0
       WP(I)=SQRT(YY*0.00782D0/3.0D0/15.0D0)*100.0D0
       IF (WP(I).LE.0.0) WP(I)=0.1D-50
       PL(I)=WP(I)/0.00782D0
       RP(1)=WP(I)*0.8165D0
       MCPOR(1)=MCPOR(I)
       I=3
       YY=YY2(JYY)
       IF (YY.LT.0.0) YY=0.0D0
       MCPOR(I)=YY/30.0D0
       WP(I)=SQRT(YY*0.00704D0/9.0D0/30.0D0)*100.0D0
       IF (WP(I).LE.0.0) WP(I)=0.1D-50
       PL(I)=WP(I)/0.00704D0
       I=4
       YY=YY3(JYY)
       IF (YY.LT.0.0) YY=0.0D0
       MCPOR(I)=YY/45.0D0
```

```
  WP(I)=SQRT(YY*0.00687D0/4.0D0/45.0D0)*100.0D0
  IF (WP(I).LE.0.0) WP(I)=0.1D-50
  PL(I)=WP(I)/0.00687D0
 ENDIF
 IF (JBDAY.LT.170) THEN
  RP(1)=0.1D-50
  WP(1)=0.1D-50
  WP(2)=0.1D-50
  WP(3)=0.1D-50
  WP(4)=0.1D-50
  WP(5)=0.1D-50
  WP(6)=0.1D-50
 ENDIF
```

After the line 571 in the file RZMAIN.FOR

```
 IF (MDAY.GE.170.AND.MDAY.LE.322) THEN
  JYY=MDAY-169
  I=2
  YY=YY1(JYY)
  IF (YY.LT.0.0) YY=0.0D0
  MCPOR(I)=YY/15.0D0
  WP(I)=SQRT(YY*0.00782D0/3.0D0/15.0D0)*100.0D0
  IF (WP(I).LE.0.0) WP(I)=0.1D-50
  PL(I)=WP(I)/0.00782D0
  RP(1)=WP(I)*0.8165D0
  MCPOR(1)=MCPOR(I)
  I=3
  YY=YY2(JYY)
  IF (YY.LT.0.0) YY=0.0D0
  MCPOR(I)=YY/30.0D0
  WP(I)=SQRT(YY*0.00704D0/9.0D0/30.0D0)*100.0D0
  IF (WP(I).LE.0.0) WP(I)=0.1D-50
  PL(I)=WP(I)/0.00704D0
  I=4
  YY=YY3(JYY)
  IF (YY.LT.0.0) YY=0.0D0
  MCPOR(I)=YY/45.0D0
  WP(I)=SQRT(YY*0.00687D0/4.0D0/45.0D0)*100.0D0
  WP(I)=MCPOR(I)/4.0D0*100.0D0
  IF (WP(I).LE.0.0) WP(I)=0.1D-50
  PL(I)=WP(I)/0.00687D0
 ENDIF
 IF (MDAY.GT.322) THEN
```

```
      RP(1)=0.1D-50
      WP(1)=0.1D-50
      WP(2)=0.1D-50
      WP(3)=0.1D-50
      WP(4)=0.1D-50
      WP(5)=0.1D-50
      WP(6)=0.1D-50
    ENDIF
C
      WRITE(10,559) JDAY,RP(1),(WP(I),I=2,6)
559    FORMAT(I4,6F10.4)
```

After the line 363 in the file RZTEST.FOR

```
c      FIRST = .FALSE.
```

2. The revised part for the simulation using the soil moisture cracking model.

After the line 420 in the file RZMAIN.FOR

```
    JN=1
    DO 401 IHH=1,NHOR
     DO 601 JHH=JN,NN
      IF (ZN(JHH).LE.HORTHK(IHH)) THEN
       THETAAV(IHH)=THETAAV(IHH)+THETA(JHH)
      ELSE
       JN=JHH
       GOTO 401
      ENDIF
601    CONTINUE
401   CONTINUE
    WRITE(*,551) WP
551   FORMAT(6F10.3)
    IF (JBDAY.GE.189.AND.JEDAY.LE.322) THEN
     I=2
     THETAAV(I)=THETAAV(I)/DEVID(I)
     YY=-52.085D0*THETAAV(I)*THETAAV(I)+26.501*THETAAV(I)+2.477
     IF (YY.LT.0.0) YY=0.0D0
     MCPOR(I)=YY/15.0D0
     WP(I)=SQRT(YY*0.00782D0/3.0D0/15.0D0)*100.0D0
     IF (WP(I).LE.0.0) WP(I)=0.1D-50
     PL(I)=WP(I)/0.00782D0
     RP(1)=WP(I)*0.8165D0
     MCPOR(1)=MCPOR(I)
```

```
ELSE
  RP(1)=0.1D-50
  WP(1)=0.1D-50
  WP(2)=0.1D-50
  PL(2)=0.1D-50
ENDIF
IF (JBDAY.GE.168.AND.JEDAY.LE.322) THEN
  I=3
  THETAAV(I)=THETAAV(I)/DEVID(I)
  YY=6.076D0+62.703D0*THETAAV(I)-109.699D0*THETAAV(I)*THETAAV(I)
  IF (YY.LT.0.0) YY=0.0D0
  MCPOR(I)=YY/30.0D0
  WP(I)=SQRT(YY*0.00704D0/9.0D0/30.0D0)*100.0D0
  IF (WP(I).LE.0.0) WP(I)=0.1D-50
  PL(I)=WP(I)/0.00704D0
ELSE
  WP(3)=0.1D-50
  PL(3)=0.1D-50
ENDIF
IF (JBDAY.GE.217.AND.JEDAY.LE.322) THEN
  I=4
  THETAAV(I)=THETAAV(I)/DEVID(I)
  YY=4.639D0+37.623D0*THETAAV(I)-64.831D0*THETAAV(I)*THETAAV(I)
  IF (YY.LT.0.0) YY=0.0D0
  MCPOR(I)=YY/45.0D0
  WP(I)=SQRT(YY*0.00687D0/4.0D0/45.0D0)*100.0D0
  IF (WP(I).LE.0.0) WP(I)=0.1D-50
  PL(I)=WP(I)/0.00687D0
ELSE
  WP(4)=0.1D-50
  PL(4)=0.1D-50
ENDIF
  WP(5)=0.1D-50
  WP(6)=0.1D-50
  PL(5)=0.1D-50
  PL(6)=0.1D-50
```

After the line 571 in the file RZMAIN.FOR

```
JN=1
DO 402 IHH=1,NHOR
  DO 602 JHH=JN,NN
    IF (ZN(JHH).LE.HORTHK(IHH)) THEN
      THETAAV(IHH)=THETAAV(IHH)+THETA(JHH)
```

```
        ELSE
          JN=JHH
          GOTO 402
        ENDIF
602     CONTINUE
402   CONTINUE
     WRITE(*,551) WP
552   FORMAT(6F10.3)
     IF (MDAY.GE.189.AND.MDAY.LE.322) THEN
      I=2
      THETAAV(I)=THETAAV(I)/DEVID(I)
      YY=-52.085D0*THETAAV(I)*THETAAV(I)+26.501*THETAAV(I)+2.477
      IF (YY.LT.0.0) YY=0.0D0
      MCPOR(I)=YY/15.0D0
      WP(I)=SQRT(YY*0.00782D0/3.0D0/15.0D0)*100.0D0
      IF (WP(I).LE.0.0) WP(I)=0.1D-50
      PL(I)=WP(I)/0.00782D0
      RP(1)=WP(I)*0.8165D0
      MCPOR(1)=MCPOR(I)
     ELSE
      RP(1)=0.1D-50
      WP(1)=0.1D-50
      WP(2)=0.1D-50
      PL(2)=0.1D-50
     ENDIF
     IF (MDAY.GE.168.AND.MDAY.LE.322) THEN
      I=3
      THETAAV(I)=THETAAV(I)/DEVID(I)
      YY=6.076D0+62.703D0*THETAAV(I)-109.699D0*THETAAV(I)*THETAAV(I)
      IF (YY.LT.0.0) YY=0.0D0
      MCPOR(I)=YY/30.0D0
      WP(I)=SQRT(YY*0.00704D0/9.0D0/30.0D0)*100.0D0
      IF (WP(I).LE.0.0) WP(I)=0.1D-50
      PL(I)=WP(I)/0.00704D0
     ELSE
      WP(3)=0.1D-50
      PL(3)=0.1D-50
     ENDIF
     IF (MDAY.GE.217.AND.MDAY.LE.322) THEN
      I=4
      THETAAV(I)=THETAAV(I)/DEVID(I)
      YY=4.639D0+37.623D0*THETAAV(I)-64.831D0*THETAAV(I)*THETAAV(I)
      IF (YY.LT.0.0) YY=0.0D0
      MCPOR(I)=YY/45.0D0
```

```
      WP(I)=SQRT(YY*0.00687D0/4.0D0/45.0D0)*100.0D0
      IF (WP(I).LE.0.0) WP(I)=0.1D-50
      PL(I)=WP(I)/0.00687D0
     ELSE
      WP(4)=0.1D-50
      PL(4)=0.1D-50
     ENDIF
      WP(5)=0.1D-50
      WP(6)=0.1D-50
      PL(5)=0.1D-50
      PL(6)=0.1D-50
558    continue
C
      WRITE(10,559) JDAY,RP(1),(WP(I),I=2,6)
559    FORMAT(I4,6F10.4)
```

After the line 363 in the file RZTEST.FOR

```
c      FIRST = .FALSE.
```

Appendix D The C language Program to calculate evaporation potential

```
#include <stdio.h>
#include <math.h>
#include <string.h>

/* declare variables */
 float Tmax[367],Tmin[367],U[367],Rad[367],Epan[367],relh[367],wind[367],c,c1,fed,
rec[367];
 float nN[367],uday[367],unight[367],hma[367],ea,w,w1,ra,uda,uni,ed,ead,fu,rs,ft,red,
fnN,Rn,ETo;
 int i,j,k,t1,t2;
void f(float humid);
void other(float tm);
float adjtpe( );
void main( )
{
 float humid,tm,kp;
 char word1[30],word2[30],word3[30];
 FILE *infp,*outfp1,*whhh;
 infp=fopen("daypg.dat","r");
 outfp1=fopen("daypsr1.dat","w");
 fprintf(outfp1,"========== MISSOURI MSEA (FIELD 1)
1992) ==========\n");
 fprintf(outfp1,"=\n");
 fprintf(outfp1,"=    DAILY METEOROLOGICAL DATA\n");
 fprintf(outfp1,"= record 1: indicates how beginning and ending dates are entered\n");
 fprintf(outfp1,"=          0 - julian date format  1 - calendar format [dd mm yyyy]\n");
 fprintf(outfp1,"= record 2: beginning & ending dates of record\n");
 fprintf(outfp1,"=\n");
 fprintf(outfp1,"= Beginning Date     Ending Date\n");

fprintf(outfp1,"==========
==========+\n");
 fprintf(outfp1,"1\n");
 fprintf(outfp1," 8 4 1992   30 12 1992\n");

fprintf(outfp1,"==========
==========+\n");
 fprintf(outfp1,"= Daily Data\n");
 fprintf(outfp1,"=\n");
 fprintf(outfp1,"= each record contains:\n");
```

```
 fprintf(outfp1,"=  Julian day counted from Jan 1st, year, Tmin [C], Tmax [C],\n");
 fprintf(outfp1,"=  wind run [km/day], sw rad [MJ/m^2/day], pan evap [cm
H2O/day],\n");
 fprintf(outfp1,"=  relative humidity [0..100]\n");
 fprintf(outfp1,"=\n");
 fprintf(outfp1,"= ...repeat record for each day\n");
 fprintf(outfp1,"=\n");
 fprintf(outfp1,"= Day  Year   Tmin    Tmax     U     Rad     E-pan  rel
humidity\n");

fprintf(outfp1,"==========================================================
==========\n");
 for(i=1;i<=18;++i)
 {
  fscanf(infp,"%30s %30s %30s",word1,word2,word3);
  printf("%30s %30s %30s\n",word1,word2,word3);
 }
  fscanf(infp,"%2d",&j);
  printf("%d\n",j);
  fscanf(infp,"%2d %2d %4d",&i,&j,&k);
  printf("%2d %2d %4d",i,j,k);
  fscanf(infp,"%2d %2d %4d",&i,&j,&k);
  printf("%2d %2d %4d\n",i,j,k);
 for(i=1;i<=19;++i)
 {
  fscanf(infp,"%30s %30s %30s",word1,word2,word3);
  printf("%30s %30s %30s\n",word1,word2,word3);
 }
  fscanf(infp,"%30s %30s",word1,word2);
  printf("%30s %30s\n",word1,word2);
 for(i=1;i<=365;++i)
 {
  fscanf(infp,"%3d %4d %f %f %f %f %f
%f\n",&j,&k,&Tmax[i],&Tmin[i],&U[i],&Rad[i],&Epan[i],&relh[i]);
 }
 fclose(infp);
 whhh=fopen("etw92.txt","r");
 for(i=1;i<=365;++i)
 {
  fscanf(whhh,"%f %10d %10d %f",&Epan[i],&t1,&t2,&wind[i]);
/*   fprintf(outfp1,"%5d %6d %8.2f %10.2f %10.2f %10.2f %9.3f
%9.2f\n",i,k,Tmax[i],Tmin[i],U[i],Rad[i],Epan[i],relh[i]);*/
 }
 fclose(whhh);
```

```
  whhh=fopen("wrhm.txt","r");
  printf(" Day    ETo      c        uda        Rn        hma[i]      tm      rs\n");
  for(i=1;i<=365;++i)
  {
   fscanf(whhh,"%f %f %f %f %f
%f",&U[i],&relh[i],&nN[i],&uday[i],&unight[i],&hma[i]);
  }
  fclose(whhh);
  for(i=1;i<=91;++i)
  {
   tm=(Tmax[i]+Tmin[i])/2.0;
   other(tm);
   humid=hma[i];
   f(humid);
   ETo=c*(w*Rn+w1*fu*ead)/10.0;
   rec[i]=c;
   fprintf(outfp1,"%5d %6d %8.2f %10.2f %10.2f %10.2f %9.3f
%9.2f\n",i,k,Tmax[i],Tmin[i],U[i],rs,ETo,relh[i]);
  }
  for(i=92;i<=305;++i)
  {
   kp=adjtpe( );
   rec[i]=kp;
   kp=kp*2.54;
   fprintf(outfp1,"%5d %6d %8.2f %10.2f %10.2f %10.2f %9.3f
%9.2f\n",i,k,Tmax[i],Tmin[i],U[i],Rad[i],Epan[i]*kp,relh[i]);
  }
  for(i=306;i<=365;++i)
  {
   tm=(Tmax[i]+Tmin[i])/2.0;
   other(tm);
   humid=hma[i];
   f(humid);
   ETo=c*(w*Rn+w1*fu*ead)/10.0;
   rec[i]=c;
   fprintf(outfp1,"%5d %6d %8.2f %10.2f %10.2f %10.2f %9.3f
%9.2f\n",i,k,Tmax[i],Tmin[i],U[i],rs,ETo,relh[i]);
  }
  fclose(outfp1);
  outfp1=fopen("rec.cpk","w");
  for(i=1;i<=365;++i)
  fprintf(outfp1,"%4d %10.3f\n",i,rec[i]);
}
void f(float humid)        /* a subroutine of calculating c value */
```

```
{
  if(humid<=45.0)
  {
   if(uda/uni<=1.0)
   {
       if(rs<=3.0)
       {
        c=0.862-0.081*uda+0.001667*uda*uda;   /* eq 37 */
       }
       else if(rs>3.0 && rs<=6.0)
       {
        c=0.862-0.081*uda+0.001667*uda*uda;
        c1=0.9025-0.0725*uda+0.001944*uda*uda;
        c=c+(rs-3.0)*(c1-c)/3.0;
       }
       else if(rs>6.0 && rs<=9.0)
       {
        c=0.9025-0.0725*uda+0.001944*uda*uda;    /* eq 38 */
        c1=1.0005-0.0671667*uda+0.0025*uda*uda;
        c=c+(rs-6.0)*(c1-c)/3.0;
       }
       else if(rs>9.0 && rs<=12.0)
       {
        c=1.0005-0.0671667*uda+0.0025*uda*uda;   /* eq 39 */
        c1=1.0-0.03833*uda+0.000556*uda*uda;
        c=c+(rs-9.0)*(c1-c)/3.0;
       }
       else
       {
        c=1.0-0.03833*uda+0.000556*uda*uda;      /*  eq 40 */
       }
  }
  else if(uda/uni<=2.0)
  {
       if(rs<=3.0)
       {
        c=0.8595-0.05683*uda+0.000278*uda*uda;    /* eq 25 */
       }
       else if(rs>3.0 && rs<=6.0)
       {
        c=0.8595-0.05683*uda+0.000278*uda*uda;
        c1=0.9015-0.0495*uda+0.0002778*uda*uda;
        c=c+(rs-3.0)*(c1-c)/3.0;
       }
```

```
    else if(rs>6.0 && rs<=9.0)
    {
     c=0.9015-0.0495*uda+0.0002778*uda*uda;    /* eq 26 */
     c1=0.999-0.053667*uda+0.001667*uda*uda;
     c=c+(rs-6.0)*(c1-c)/3.0;
    }
    else if(rs>9.0 && rs<=12.0)
    {
     c=0.999-0.053667*uda+0.001667*uda*uda;   /* eq 27 */
     c1=1.0-0.0266667*uda;
     c=c+(rs-9.0)*(c1-c)/3.0;
    }
    else
    {
     c=1.0-0.0266667*uda;                     /* eq 28 */
    }
}
else if(uda/uni<=3.0)
{
    if(rs<=3.0)
    {
     c=0.8625-0.0325*uda-0.001389*uda*uda;    /* eq 13 */
    }
    else if(rs>3.0 && rs<=6.0)
    {
     c=0.8625-0.0325*uda-0.001389*uda*uda;
     c1=0.9025-0.03083*uda-0.000833*uda*uda;
     c=c+(rs-3.0)*(c1-c)/3.0;
    }
    else if(rs>6.0 && rs<=9.0)
    {
     c=0.9025-0.03083*uda-0.000833*uda*uda;   /* eq 14 */
     c1=0.9965-0.03783*uda+0.000833*uda*uda;
     c=c+(rs-6.0)*(c1-c)/3.0;
    }
    else if(rs>9.0 && rs<=12.0)
    {
     c=0.9965-0.03783*uda+0.000833*uda*uda;   /* eq 15 */
     c1=1.0-0.02*uda;
     c=c+(rs-9.0)*(c1-c)/3.0;
    }
    else
    {
     c=1.0-0.02*uda;                          /* eq 16 */
```

```
        }
    }
    else
    {
        if(rs<=3.0)
        {
          c=0.861-0.01967*uda-0.001667*uda*uda;      /* eq 1 */
        }
        else if(rs>3.0 && rs<=6.0)
        {
          c=0.861-0.01967*uda-0.001667*uda*uda;
          c1=0.898-0.012333*uda-0.001667*uda*uda;    /* eq 2 */
          c=c+(rs-3.0)*(c1-c)/3.0;
        }
        else if(rs>6.0 && rs<=9.0)
        {
          c=0.898-0.012333*uda-0.001667*uda*uda;
          c1=0.9965-0.0211667*uda-0.0002778*uda*uda;
          c=c+(rs-6.0)*(c1-c)/3.0;
        }
        else if(rs>9.0 && rs<=12.0)
        {
          c=0.9965-0.0211667*uda-0.0002778*uda*uda;   /* eq 3 */
          c1=1.001-0.01133*uda;
          c=c+(rs-9.0)*(c1-c)/3.0;
        }
        else
        {
          c=1.001-0.01133*uda;                  /* eq 4 */
        }
    }
}
else if(humid<=75.0)
{
 if(uda/uni<=1.0)
 {
        if(rs<=3.0)
        {
          c=0.961-0.066333*uda+0.001667*uda*uda;      /* eq 41 */
        }
        else if(rs>3.0 && rs<=6.0)
        {
          c=0.961-0.066333*uda+0.001667*uda*uda;
          c1=0.985-0.04833*uda+0.000556*uda*uda;
```

```
      c=c+(rs-3.0)*(c1-c)/3.0;
    }
    else if(rs>6.0 && rs<=9.0)
    {
      c=0.985-0.04833*uda+0.000556*uda*uda;      /* eq 42 */
      c1=1.05-0.038333*uda+0.005556*uda*uda;
      c=c+(rs-6.0)*(c1-c)/3.0;
    }
    else if(rs>9.0 && rs<=12.0)
    {
      c=1.05-0.038333*uda+0.005556*uda*uda;      /* eq 43 */
      c1=1.05-0.02*uda;
      c=c+(rs-9.0)*(c1-c)/3.0;
    }
    else
    {
      c=1.05-0.02*uda;                    /* eq 44 */
    }
}
else if(uda/uni<=2.0)
{
    if(rs<=3.0)
    {
      c=0.961-0.04633*uda+0.0005556*uda*uda;      /* eq 29 */
    }
    else if(rs>3.0 && rs<=6.0)
    {
      c=0.961-0.04633*uda+0.0005556*uda*uda;
      c1=0.9825-0.024167*uda-0.000833*uda*uda;
      c=c+(rs-3.0)*(c1-c)/3.0;
    }
    else if(rs>6.0 && rs<=9.0)
    {
      c=0.9825-0.024167*uda-0.000833*uda*uda;      /* eq 30 */
      c1=1.047-0.012667*uda-0.001111*uda*uda;
      c=c+(rs-6.0)*(c1-c)/3.0;
    }
    else if(rs>9.0 && rs<=12.0)
    {
      c=1.047-0.012667*uda-0.001111*uda*uda;      /* eq 31 */
      c1=1.0495+0.0065*uda-0.001944*uda*uda;
      c=c+(rs-9.0)*(c1-c)/3.0;
    }
    else
```

```
    {
     c=1.0495+0.0065*uda-0.001944*uda*uda;     /* eq 32 */
    }
}
else if(uda/uni<=3.0)
{
    if(rs<=3.0)
    {
     c=0.9605-0.02983*uda-0.000278*uda*uda;     /* eq 17 */
    }
    else if(rs>3.0 && rs<=6.0)
    {
     c=0.9605-0.02983*uda-0.000278*uda*uda;
     c1=0.9825-0.004167*uda-0.001944*uda*uda;
     c=c+(rs-3.0)*(c1-c)/3.0;
    }
    else if(rs>6.0 && rs<=9.0)
    {
     c=0.9825-0.004167*uda-0.001944*uda*uda;     /* eq 18 */
     c1=1.0457+0.019167*uda-0.004167*uda*uda;
     c=c+(rs-6.0)*(c1-c)/3.0;
    }
    else if(rs>9.0 && rs<=12.0)
    {
     c=1.0457+0.019167*uda-0.004167*uda*uda;    /* eq 19 */
     c1=1.053+0.02933*uda-0.00333*uda*uda;
     c=c+(rs-9.0)*(c1-c)/3.0;
    }
    else
    {
     c=1.053+0.02933*uda-0.00333*uda*uda;     /* eq 20 */
    }
}
else
{
    if(rs<=3.0)
    {
     c=0.9605-0.009833*uda-0.0013889*uda*uda;     /* eq 5 */
    }
    else if(rs>3.0 && rs<=6.0)
    {
     c=0.9605-0.009833*uda-0.0013889*uda*uda;
     c1=0.981+0.013667*uda-0.002778*uda*uda;
     c=c+(rs-3.0)*(c1-c)/3.0;
```

```
      }
      else if(rs>6.0 && rs<=9.0)
      {
       c=0.981+0.013667*uda-0.002778*uda*uda;       /* eq 6 */
       c1=1.0485+0.0345*uda-0.0041667*uda*uda;
       c=c+(rs-6.0)*(c1-c)/3.0;
      }
      else if(rs>9.0 && rs<=12.0)
      {
       c=1.0485+0.0345*uda-0.0041667*uda*uda;       /* eq 7 */
       c1=1.0545+0.0565*uda-0.005278*uda*uda;
       c=c+(rs-9.0)*(c1-c)/3.0;
      }
      else
      {
       c=1.0545+0.0565*uda-0.005278*uda*uda;        /* eq 8 */
      }
  }
}
else
{
 if(uda/uni<=1.0)
 {
     if(rs<=3.0)
     {
      c=1.0195-0.061833*uda+0.0019444*uda*uda;     /* eq 45 */
     }
     else if(rs>3.0 && rs<=6.0)
     {
      c=1.0195-0.061833*uda+0.0019444*uda*uda;
      c1=1.058-0.047333*uda+0.001111*uda*uda;
      c=c+(rs-3.0)*(c1-c)/3.0;
     }
     else if(rs>6.0 && rs<=9.0)
     {
      c=1.058-0.047333*uda+0.001111*uda*uda;       /* eq 46 */
      c1=1.0975-0.0275*uda+0.00027778*uda*uda;
      c=c+(rs-6.0)*(c1-c)/3.0;
     }
     else if(rs>9.0 && rs<=12.0)
     {
      c=1.0975-0.0275*uda+0.00027778*uda*uda;      /* eq 47 */
      c1=1.1005-0.0181667*uda+0.0002778*uda*uda;
      c=c+(rs-9.0)*(c1-c)/3.0;
```

```
      }
      else
      {
       c=1.1005-0.0181667*uda+0.0002778*uda*uda;  /* eq 48 */
      }
  }
  else if(uda/uni<=2.0)
  {
      if(rs<=3.0)
      {
       c=1.0195-0.04863*uda+0.0013889*uda*uda;    /* eq 33 */
      }
      else if(rs>3.0 && rs<=6.0)
      {
       c=1.0195-0.04863*uda+0.0013889*uda*uda;
       c1=1.0565-0.0195*uda-0.0008333*uda*uda;
       c=c+(rs-3.0)*(c1-c)/3.0;
      }
      else if(rs>6.0 && rs<=9.0)
      {
       c=1.0565-0.0195*uda-0.0008333*uda*uda;    /* eq 34 */
       c1=1.1005+0.006833*uda-0.0025*uda*uda;
       c=c+(rs-6.0)*(c1-c)/3.0;
      }
      else if(rs>9.0 && rs<=12.0)
      {
       c=1.1005+0.006833*uda-0.0025*uda*uda;    /* eq 35 */
       c1=1.101+0.020333*uda-0.002788*uda*uda;
       c=c+(rs-9.0)*(c1-c)/3.0;
      }
      else
      {
       c=1.101+0.020333*uda-0.002788*uda*uda;   /* eq 36 */
      }
  }
  else if(uda/uni<=3.0)
  {
      if(rs<=3.0)
      {
       c=1.02-0.0266667*uda;                    /* eq 21 */
      }
      else if(rs>3.0 && rs<=6.0)
      {
       c=1.02-0.0266667*uda;
```

```
        c1=1.0575+0.0025*uda-0.001944*uda*uda;
        c=c+(rs-3.0)*(c1-c)/3.0;
       }
       else if(rs>6.0 && rs<=9.0)
       {
        c=1.0575+0.0025*uda-0.001944*uda*uda;    /* eq 22 */
        c1=1.1025+0.0375*uda-0.004722*uda*uda;
        c=c+(rs-6.0)*(c1-c)/3.0;
       }
       else if(rs>9.0 && rs<=12.0)
       {
        c=1.1025+0.0375*uda-0.004722*uda*uda;  /* eq 23 */
        c1=1.113+0.061*uda-0.006111*uda*uda;
        c=c+(rs-9.0)*(c1-c)/3.0;
       }
       else
       {
        c1=1.113+0.061*uda-0.006111*uda*uda;    /* eq 24 */
       }
}
else
{
    if(rs<=3.0)
    {
     c=1.0205-0.008167*uda-0.000833*uda*uda;  /* eq 9 */
    }
    else if(rs>3.0 && rs<=6.0)
    {
     c=1.0205-0.008167*uda-0.000833*uda*uda;
     c1=1.0575+0.0275*uda-0.00361*uda*uda;
     c=c+(rs-3.0)*(c1-c)/3.0;
    }
    else if(rs>6.0 && rs<=9.0)
    {
     c=1.0575+0.0275*uda-0.00361*uda*uda;    /* eq 10 */
     c1=1.1045+0.07317*uda-0.0075*uda*uda;
     c=c+(rs-6.0)*(c1-c)/3.0;
    }
    else if(rs>9.0 && rs<=12.0)
    {
     c=1.1045+0.07317*uda-0.0075*uda*uda;     /* eq 11 */
     c1=1.107+0.08733*uda-0.007778*uda*uda;
     c=c+(rs-9.0)*(c1-c)/3.0;
    }
```

```
        else
        {
         c=1.107+0.08733*uda-0.007778*uda*uda;   /* eq 12 */
        }
     }
    }
    printf("c = %10.3f\n",c);

}
void other(float tm)
{                              /* this function calculates all the other stuffs*/
   if(tm<=0.0)
   {
    ea=6.1;
    w=1.0-0.001053;
   }
   else
   {
    ea=7.60835-0.01441518*tm+0.040156*tm*tm;
    w1=0.6001053-0.0177064*tm+0.0001581*tm*tm;
    if(w1>1.0)
    {
        w1=1.0;
    }
    w=1.0-w1;
   }
  if(i<=31)
  {
   ra=6.525;
  }
  else if(i>=32 && i<=60)
  {
   ra=8.7;
  }
  else if(i>=61 && i<=91)
  {
   ra=11.5;
  }
  else if(i>=92 && i<=121)
  {
   ra=14.35;
  }
  else if(i>=122 && i<=152)
  {
```

```
 ra=16.4;
}
else if(i>=153 && i<=182)
{
 ra=17.275;
}
else if(i>=183 && i<=213)
{
 ra=16.7;
}
else if(i>=214 && i<=244)
{
 ra=15.225;
}
else if(i>=245 && i<=274)
{
 ra=12.575;
}
else if(i>=275 && i<=305)
{
 ra=9.7;
}
else if(i>=306 && i<=335)
{
 ra=7.1;
}
else
{
 ra=5.8;
}
ed=ea*relh[i]/100.0;
ead=ea-ed;
fu=0.27*(1.0+U[i]/100.0);
rs=(0.25+0.5*nN[i]/100.0)*ra;
if(tm<=0.0)
{
 ft=11.0;
}
else
{
 ft=11.04812+0.1554917*tm+0.0011388766*tm*tm;
}
fed=0.34-0.044*sqrt(ed);
fnN=0.1+0.9*nN[i]/100.0;
```

```
   Rn=rs*0.75-ft*fed*fnN;
   uda=uday[i]*1.15*1609.0/3600.0/4.0;  /* change unit from knots to m/sec */
   uni=unight[i]*1.15*1609.0/3600.0/4.0;
}
float adjtpe( )
{
 float kpe;
 if(wind[i]*1.609<175.0)
 {
  if(relh[i]<40.0)
  {
   kpe=0.65;
  }
  else if(relh[i]>=40.0 && relh[i]<=70.0)
  {
   kpe=0.75;
  }
  else
  {
   kpe=0.85;
  }
 }
 else if(wind[i]*1.609>=175.0 && wind[i]*1.609<425.0)
 {
  if(relh[i]<40.0)
  {
   kpe=0.6;
  }
  else if(relh[i]>=40.0 && relh[i]<=70.0)
  {
   kpe=0.7;
  }
  else
  {
   kpe=0.75;
  }
 }
 else if(wind[i]*1.609>=425.0 && wind[i]*1.609<700.0)
 {
  if(relh[i]<40.0)
  {
   kpe=0.55;
  }
  else if(relh[i]>=40.0 && relh[i]<=70.0)
```

```
    {
     kpe=0.6;
    }
    else
    {
     kpe=0.65;
    }
   }
   else
   {
    if(relh[i]<40.0)
    {
     kpe=0.45;
    }
    else if(relh[i]>=40.0 && relh[i]<=70.0)
    {
     kpe=0.55;
    }
    else
    {
     kpe=0.6;
    }
   }
  return kpe;
}
```

Appendix E List of symbols (variables)

ρ = density [FT^2/L^4]

g = gravitational constant [L/T^2]

r_p = the radius of cylindrical holes [L]

d = the width of planar cracks [L]

η = the dynamic viscosity of water [FT/L^2]

N = the number of pores per unit area

L = the total length of cracks per unit area [L]

P_{mac} = the macroporosity as fraction of soil volume [L^3/L^3]

K_{mac} = maximum flow-rate capacity [L/T]

V = volume of soil cube [L^3]

z = length of soil cube sides [L]

ΔV = volume change of a soil cube after shinkage [L^3]

Δz = length change of a soil cube sides [L]

r_s = a dimensionless geometry factor

ΔV_a, = shrinkage volume per unit area

V_{cr} = crack volume per unit area [L^3/L^2]

$elev_{1,i}$ = elevation of disk 1 at time = i [L]

$elev_{1,t}$ = elevation of disk 1 at time = t [L]

$elev_{2,i}$ = elevation of disk 2 at time = i [L]

$elev_{2,t}$ = elevation of disk 2 at time = t [L]